

THE UNIVERSITY OF ASTON IN BIRMINGHAM

(U.K.)

FAST NEUTRON ATTENUATION AND  
ENERGY LOSS IN EXTENDED SHIELDS

A Thesis Submitted for the Degree of

DOCTOR OF PHILOSOPHY

by

RIAD MOUSTAFA MEGAHID,

B.Sc (Hons), M.Sc.

621.039538

184904 = 9 AUG 1975

March, 1975

Department of Physics

ABSTRACT

This work is concerned with the investigation of the attenuation and energy degradation of fast neutrons passing through materials widely used in reactor shielding. Measurements and calculations have been performed for shields of iron and for homogeneous and heterogeneous media of iron-graphite and iron-polypropylene in the form of a cylinder having a monoenergetic point neutron source of energy 14.1 MeV produced by  $D(T,n)He$  reaction at its centre. All measurements were made with a proton recoil scintillation spectrometer using NE-213 liquid organic scintillator, and gamma ray background was discriminated by pulse shape discrimination using the zero crossing technique. Calibration of the spectrometer energy scale was made with monoenergetic neutrons of energies 2.48 MeV and 14.1 MeV from the  $D(d,n)He$  and  $D(T,n)He$  reactions respectively. These fixed points were used to scale the energy pulse height distribution determined by other workers for use in the conversion of integral pulse height distribution into neutron energy spectrum. This conversion was achieved by a method based on numerical differentiation.

Calculations have also been carried out with the multigroup diffusion and removal diffusion equations in one dimension by approximating the experimental assembly to a spherical geometry. These calculations provided a test for cross section data sets compiled by Abagyan and Yiftah and Sieger.

Measured and calculated spectra show reasonable agreement and shields containing hydrogen show stronger neutron attenuation than those containing graphite. Removal cross sections at 14 MeV have been experimentally determined for iron, carbon and hydrogen from the variation in transmitted neutron intensities with thickness for iron (steel) and double layers of iron and graphite or polypropylene. These have been compared with theoretical predictions by other workers and good agreement has been found.

ACKNOWLEDGEMENTS

I would like to thank Dr. P.N. Cooper for supervising and directing this work and for his continuous interest, help and guidance throughout the whole of the project.

I would also like to thank Professor S.E. Hunt, Head of the Department of Physics for his interest in the project.

I am also thankful to Messrs J. Phull and H. Biggs, the laboratory technical staff for their help in maintenance of the accelerator during the measurements.

Thanks are also due to the Physics Workshop Staff for their part in the construction of the various facilities. The staff of the Library of the University of Aston in Birmingham, who made a conscientious effort throughout the period to make available the literature and references necessary for the work from various sources. The staff of the Computer Centre should also be acknowledged for their consultation and for running the programmes and data preparation.

I am also grateful to the Government of A.R. of Egypt for the award of the financial assistance and to the Egypt Atomic Energy Establishment for granting me leave of absence for the period of this project.

Finally, I would like to thank my wife and my children for their patience during their absence from their country.

Riad M. Megahid.

Birmingham  
March, 1975.

TABLE OF CONTENTS

	<u>Page No.</u>
Abstract	i
Acknowledgements	ii
Table of Contents	iii
List of Figures	VII
List of Tables	VII
References	123
<u>CHAPTER 1</u>	<u>INTRODUCTION</u>
<u>CHAPTER 2</u>	<u>NEUTRON INTERACTION WITH MATTER</u>
2.1	Introduction 5
2.2	Elastic Scattering $X(n,n)X$ 6
2.3	Inelastic Scattering $X(n,n')X^*$ 7
2.4	Radiative Capture $X(n,\gamma)Y$ 9
2.5	Particle Reactions $X(n,p)Y$ , $X(n,\alpha)Z$ , (n,2n) and (n,3n)
<u>CHAPTER 3</u>	<u>FAST NEUTRON DETECTORS AND TECHNIQUES</u>
3.1	Introduction 13
3.2	The Main Parameters for Selecting a Neutron Detector 14
3.3	Reaction Used in Neutron Detection 15
3.3.1	(n.p) Scattering 15
3.3.2	Neutron Induced Reactions 16
3.3.2.1	Exoergic Reactions 17
3.3.2.2	Threshold Detectors 18
3.4	Different Detection Systems 20
3.4.1	Counter Telescopes 20
3.4.2	Proton Recoil Proportional Counters 21
3.4.3	Organic Scintillators 22

3.5	Detectors Based on Exoergic Reactions	23
3.5.1	${}^6\text{Li}$ (EU) Scintillator	23
3.5.2	The Long Counter	23
3.5.3	The Helium-3 Counter	24
3.6	Detectors Based on Fission and Threshold Reactions	25
3.6.1	Fission Counters	25
3.6.2	Fissionable Foils	26
3.6.3	Threshold Foils	26
3.7	Semiconductor Detectors	26
3.8	Time of Flight Technique	28

CHAPTER 4NEUTRON SPECTROMETER

4.1	Introduction	30
4.2	Scintillator	30
4.3	Discrimination Against Gamma Rays	31
4.4	Measuring and PSD systems	32
4.5	Calibration of the Spectrometer	34
4.5.1	Spectrometer Linearity	35
4.5.2	Relation Between Recoil Proton and Electron Pulses	36
4.5.3	Gain Standardization and Energy Scale	36
4.5.4	Discrimination Capability	37
4.6	Corrections for Losses in Electrons	37
4.7	Detector Efficiency	38
4.8	Corrections for Scintillator Size	39
4.9	Unfolding Methods	40
4.10	Smoothing of Data	43
4.11	Effect of Statistical Uncertainties in Counts	45
4.12	Test with ${}^{241}\text{Am}$ - $\alpha$ -Be Source	45

<u>CHAPTER 5</u>	<u>SHIELDING ASSEMBLIES AND NEUTRON SOURCE</u>	
5.1	Introduction	47
5.2	Shielding Assemblies	47
5.2.1	Iron Assembly	47
5.2.2	"Homogenous" Media Assemblies	48
5.2.3	Heterogeneous Shields Assemblies	48
5.3	Neutron Production	49
5.3.1	Neutrons From T(d,n)He Reaction	49
5.3.2	Target	50
5.4	Measurement of Neutron Yield by Associated Particle	50
5.4.1	Scintillator	53
5.4.2	Geometry Factor	53
<u>CHAPTER 6</u>	<u>METHODS AND COMPUTATIONAL TECHNIQUES USED FOR CALCULATIONS OF NEUTRON PENETRATION</u>	
6.1	Introduction	55
6.2	The Boltzmann Transport Equation	56
6.3	Methods Used for Solution of the Transport Equation	60
6.3.1	Spherical Harmonics Method	60
6.3.2	Discrete Ordinates Method	62
6.3.3	Moments Method	63
6.3.4	Diffusion Theory	64
6.3.5	Fermi Age Theory	66
6.4	Monte Carlo Method	68
6.5	Removal Diffusion Method	69
6.6	Comparison of the Computational Methods	70

<u>CHAPTER 7</u>	<u>SPECTRA CALCULATIONS BY MULTIGROUP DIFFUSION AND REMOVAL DIFFUSION METHODS</u>	
7.1	Introduction	73
7.2	Multigroup Methods of Calculation	73
7.3	Group Constants	74
7.3.1	Diffusion Coefficient	75
7.3.2	Group Cross Sections	76
7.3.3	Fission	79
7.4	Multigroup Equations	80
7.5	Solution of the Equations	81
7.6	Removal Diffusion Calculations	82
<u>CHAPTER 8</u>	<u>EXPERIMENTAL AND CALCULATED LEAKAGE SPECTRA AND THEIR ANALYSIS</u>	
8.1	Introduction	84
8.2	Deformation of Fast Neutron Spectra behind Iron Shields	85
8.3	Deformation of Fast Neutron Spectra behind a Homogenous and Heterogeneous Shields of Iron-Graphite	86
8.4	Deformation of Fast Neutrons Spectra behind Homogeneous and Heterogeneous Shields of Iron-polypropylene	87
8.5	Comparisons between the Leakage Spectra through Different Media of the Same Thickness	88
8.6	Determination of the Removal Cross Section	89
8.6.1	$\sigma_{rem}$ for Iron	90
8.6.2	$\sigma_{rem}$ for carbon	91
8.6.3	$\sigma_{rem}$ for hydrogen	92
<u>CHAPTER 9</u>	<u>GENERAL CONCLUSIONS</u>	94
APPENDIX 1	Numerical Scheme Used for Multigroup Flux Calculations	99
1.1	Boundary Conditions	101
1.1.1	Inner Boundary	102

	<u>Page No.</u>
1.1.2 Outer Boundary	103
1.1.3 Boundary at the Surface between Two Adjacent Materials	104
A1.2 Calculation Scheme	108
 <u>APPENDIX 2</u>	
Program FASTNFLUX: Multigroup Flux Calculations by Diffusion and Removal Diffusion Methods	110
 <u>APPENDIX 3</u>	
Program FASTNSPEC: Transformation of Pulse Amplitude Distribution into Neutron Energy Distribution by Differential Method	116
 <u>LIST OF REFERENCES</u>	123
 <u>LIST OF TABLES</u>	
Table 5.1 Variations of Angular Energy for Neutrons and Alpha Particles	52

LIST OF FIGURES

Figures are, in general, placed below the page where they are first mentioned and discussed).

CHAPTER 1INTRODUCTION

The studies of the spatial energy distribution of fast neutrons after passing through various thicknesses of different materials which are of interest in nuclear technology are certainly of major importance, not only from the point of view of the theory of neutron penetration through matter, but also from the point of view of designing of nuclear reactors and their associated equipments. A compilation of experimental work<sup>(3.6)</sup> has been carried out in developing analytical methods and techniques to handle shielding problems and in obtaining experimental data suitable to design procedures and against which to test the theoretical calculations, but there are still a lot of discrepancies between the experimental results and the data given by calculations.

It is obvious that a nuclear power station will be useless if it cannot operate for a long time without component failures. The life period of any power reactor is mainly decided by the radiation damage in the pressure vessel and the other constructional materials by the high energy component of fast neutrons. Such a problem is still an underdeveloped science, since the damage calculation is uncertain due to poor detailed cross section data. In a typical thermal power reactor it is estimated that about 60% of the damage to its pressure vessel is due to neutrons above 0.5 MeV<sup>(9)</sup>. Very little however is known about the deterioration of the structural materials in the long run in steel, due to accumulation of hydrogen and helium which will result from the interaction of fast neutrons with the emission of a charged particle.

Further, the knowledge of the spatial energy distributions of fast neutrons behind a shielding material is of primary importance,

since in most cases the flux of slowing down neutrons and secondary gamma radiations behind the shield are determined by the spatial distribution of fast neutron fluxes.

The attenuation of fast neutrons is affected by degrading the energy of the neutrons by inelastic and elastic scattering processes until they are absorbed. Unfortunately, the detailed cross sections for these interactions are less well known. The variation with energy is in some instances very rapid, and for those energy regions at which the cross sections are lowest and the penetration is highest, the data are the least well known.

Therefore, a study of the behaviour of fast neutrons for shielding materials should be of great interest in the field of nuclear technology. The degradation in energy of fast neutrons mainly takes place by inelastic scattering processes. The uncertainties in inelastic scattering cross sections still remain a problem for an accurate calculation of neutron space energy distribution in thick shields. Inaccuracy of a few per cent in the average group cross section can lead to an unacceptable error in the neutron spectrum behind the shielding. When a biological shield is followed by a hydrogenous medium, a 10% change in the inelastic scattering cross section for an iron shield has a marked effect on the relaxation length of the neutron emerging into a subsequent water shield, amounting to 50% change after 40 cm<sup>(10)</sup>.

Although neutrons having energies of 14 MeV, are not directly important for shields and blankets of fission reactors, since they are above the extreme top end of the fission spectrum, generally regarded as having an upper limit of 10 MeV, the deep penetration in reactor shielding has some similarities to a monodirectional beam of such neutrons. Since, after crossing sufficient distances into the shield, only the forward peaking high energy end of the fission spectrum survives and in most shields they behave as monodirectional neutrons of about

8 MeV<sup>(11)</sup>, therefore a study of the attenuation and penetration of the latter can be given from those of the 14 MeV neutrons, which are in any case degraded in energy by the shield. Such studies can be easily carried out by using a monoenergetic beam of neutrons from accelerators produced from  ${}^3\text{T}(d,n){}^4\text{He}$  reaction.

In addition, a study of 14 MeV neutron attenuation is of prime importance to future fusion reactors, since a high proportion of the energy released escapes from the reactor through high energy neutrons.

The study of the neutron energy distribution and the variation of cross sections with energy for a hydrogenous medium, shows that the most penetrating neutrons are those which start with energies of about 8 MeV. Lower energy neutrons are attenuated more easily because of the higher cross sections, and higher energy neutrons are too few in number to be the major contributors to the dose outside a reactor shield. Thus, if an amount of hydrogen sufficient to ensure rapid moderation (about 20 collisions on average) to thermal energies following inelastic scattering is present in the shield, then the attenuation of neutrons by the other components of the shield can be described quite well by the neutron cross section in the vicinity of 8 MeV.

Neutron attenuation in non-hydrogenous media which relies mainly on inelastic scattering for high energy neutrons poses a much more difficult calculational problem because of the larger build up factors and the greater uncertainty in the cross sections. However, due to the large energy losses possible in single inelastic scatters, heavy materials are a valuable shielding component and for neutrons above 1 MeV, the mechanism is much more effective than elastic scattering by hydrogen.

The removal diffusion and multigroup diffusion methods are used to calculate the spatial energy distribution of fast neutrons. The multigroup calculations in various approximation also make it possible

to determine the spatial distribution of slowing down neutrons. To average the multigroup constants in the energy region of fast neutrons, the spatial energy distributions in the shielding materials and its distortion, when the shield thickness is increased or other materials are substituted, should be known. Such data has been obtained for several media, but only by a calculation method.

It is therefore of great interest to obtain experimental data on the spectra of fast neutrons after passage through different materials. In recent years a compilation of measurements have been carried out for some materials which are used in reactor technology<sup>(7.8)</sup>.

In the present work, new measurements are carried out for a similar investigation. 14 MeV neutrons from  ${}^3\text{T}(d,n){}^4\text{He}$  reaction have been used to study the behaviour of fast neutron energy spectrum passing through homogeneous and heterogeneous media of iron-graphite and iron polypropylene assemblies. The multigroup diffusion theory and removal diffusion theory are used for calculating the spatial energy distribution of fast neutrons after passing through different thicknesses of such assemblies. The cross section data used for these calculations are the 20-group cross section set due to Yiftah and Sieger<sup>(84)</sup>, and the Russian 25-group cross section set<sup>(85)</sup>.

CHAPTER 2NEUTRON INTERACTION WITH MATTER2.1 Introduction

In passing through matter, a neutron may interact with nuclei in a variety of ways, it may change direction, lose energy, or be absorbed by collisions with nuclei. As the neutron carries no electrical charge, there is no coulomb repulsion to prevent its interaction with nuclei, and it is thus able to cross the nuclear boundary even when moving at less than thermal velocity. If in a collision with a nucleus the total kinetic energy of the system is conserved, the process is called elastic scattering and may be written as  $X(n,n)X$  where  $X$  denotes the target nucleus. On the other hand if the nucleus after re-emission of a neutron is left in an excited state, the process is called inelastic scattering and is written as  $X(n,n')X^*$ . In referring to these processes it is common to say that the incident neutron has been elastically or inelastically scattered, since a neutron reappears after the interaction. However, this term is somewhat incorrect since the emerging neutron may not be the same neutron that originally struck the nucleus.

If instead of being scattered, the neutron is absorbed by the nucleus, it induces a nuclear reaction which leads to a different residual nucleus and a new end product. The most important of these reactions is the absorption of a neutron with the emission of a gamma photon  $(n,\gamma)$ . This process is known as radiative capture, and the reaction is written as  $X(n,\gamma)Y$ , where the symbol  $Y$  denotes the new nucleus. Neutron capture may also lead to the emission of charged particles in the  $(n,p)$  and  $(n,\alpha)$  reactions. For neutrons of higher energies two or more neutrons may be emitted following neutron capture. This is also a form of inelastic scattering.

A classification of the interaction of neutrons with nuclei is illustrated in figure 2.1. A detailed description of this process is given below.

## 2.2. Elastic Scattering X(n,n)X

The slowing down of fast neutrons is due below 0.5 MeV to elastic scattering collisions between the neutrons and the nuclei of the moderator<sup>(12)</sup>. Such collision can be treated by the methods of classical mechanics, assuming the neutrons and scattering nuclei to behave as perfect elastic spheres. By applying the principles of conservation of momentum and energy it is possible to derive a relationship between the scattering angle  $\theta$  and the energy of the neutron before and after collision with a nucleus of mass number A.

Assuming that  $E_1$  is the energy of the neutron before collision, hence the neutron energy after collision  $E_2$  is given by:

$$E_2 = E_1 \cdot \frac{A^2 + 2A \cos \theta + 1}{(A + 1)^2} \dots \dots 2.1$$

where  $\theta$  is the scattering angle in C system.

The mechanism of elastic scattering of neutrons can be conveniently regarded as being composed of two coherent contributions.

(a) Resonance Scattering, which is attributable to the formation of one of several decaying states of the compound nucleus (X + n) whose energies lie within about a level width from the energy of the initial n,X system, followed by decay of the compound nucleus and the emission of a neutron having the same energy as that of the original incident neutron.

(b) Potential Scattering, in which the neutron does not appreciably penetrate the nucleus to form a compound nucleus, but without sharing its energy with nucleons of the target is scattered much as it would be by a potential well. This part may also be considered as due to the large number of states of the compound nucleus which are far removed from the

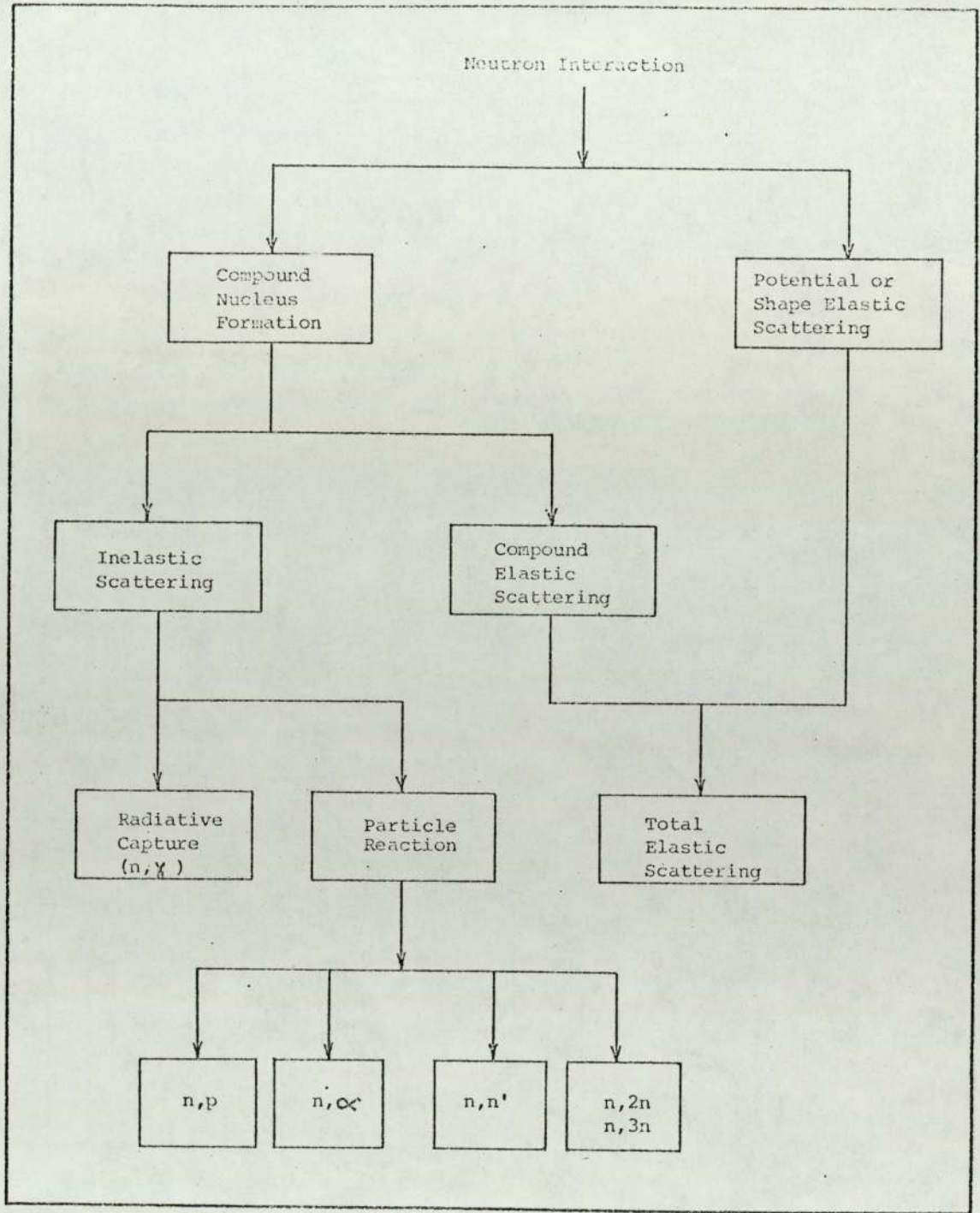


Figure 2.1. Classification of Neutron Induced Reactions.

incident energy.

For lower energy neutrons (less than about 1 MeV), the elastic scattering is nearly isotropic in the centre of mass system<sup>(1)</sup>. As the energy increases the anisotropy increases. For the resonance scattering the angular distribution is characteristic of the spins and parities of the levels of the compound nucleus involved and is more or less isotropic<sup>(2)</sup>. The potential scattering gives the distribution a forward peak (due to diffraction around the nucleus) which becomes more pronounced with increasing energy.

From the viewpoint of neutron attenuation, elastic scattering serves to alter the direction of the neutron and degrade its energy. Since the total kinetic energies of the incident neutrons and target nucleus are conserved in the elastic process. The relation between the energy transferred and the cosine of the scattering angle is given by a simple form in the centre of mass system.

$$\cos \psi = \frac{1 + A \cos \theta}{\sqrt{A^2 + 2A \cos \theta + 1}} \quad \dots \dots \dots 2.2$$

where  $\psi$  is the scattering angle observed in the Laboratory system, and A is the atomic mass of the target nucleus.

### 2.3 Inelastic Scattering $X(n, n') X^*$

When a fast neutron is captured by a target nucleus to form a compound nucleus, the latter may in some cases decay to an excited state with the emission of neutron of lower energy than that of the primary one. This process is not energetically possible until the incident neutron has enough energy to raise the target nucleus to its first excited state, plus the energy which is given to centre of mass motion by the collision. This threshold energy is generally high in both light and magic nuclei, where the level spacing are large. If  $E_{(ex)}$  represents the energy of an excited state of the target nucleus, then the minimum

or threshold energy  $E_{(th)}$  in the laboratory system required of the penetrating of neutron for production of inelastic scattering to this state is:

$$E_{th} = \frac{M + m}{M} \cdot E_{(ex)} \quad \dots \dots \dots 2.3$$

where  $M$  and  $m$  are the masses of the target nucleus and neutron respectively.

In general, if a monoenergetic beam of neutrons is incident on a target nucleus, a spectrum of neutron energies are emitted, since a number of levels of the target nuclei are accessible. The spectrum of these emitted neutrons consist of a series of groups corresponding to transitions to different levels. The relative intensities of these groups are determined by the partial widths for the different modes of decay of the compound nucleus. Some of the groups may appear as a continuous spectrum in the region where the levels of the target nuclei are very closely spaced.

The process of degrading the neutron energy by inelastic scattering is useful for the following reasons:

- (a) Owing to the fact that neutrons are uncharged particles, neutrons are therefore very often easier to use in the general studies of nuclear reactions and their interpretation in terms of various theoretical models.
- (b) It is a means of studying the nature of individual nuclear levels which may not easily be reached by other means.
- (c) Inelastic scattering is very important in problems of reactor design and shielding estimation. In the first case it is the main process by which fast neutrons are degraded in energy below the inelastic scattering threshold. Furthermore it produces gamma radiation, which has to be considered in all shielding problems.

## 2.4 Radiative Capture $X(n,\gamma)Y$

This process is energetically possible at all neutron energies, but is most probable at low energies (less than 1 KeV). However, at low energies some particle reaction with very light nuclei and fission with very heavy nuclei can take place.

When the neutron is captured by the nucleus  ${}^A_Z$ , the resultant compound nucleus  ${}^{A+1}_Z$  is formed in a highly excited state because the captured neutron brings into the system both its original kinetic energy and its binding energy, typically 7 - 8 MeV. Since the compound nucleus lies above its ground state, it can decay either by the re-emission of a neutron as in the scattering process or by emitting one or more gamma photons. However, the excitation energy of the compound nucleus is divided between its nucleons, and the emission of one of these nucleons is not possible until the nucleon obtains an energy in collisions with other nucleons greater than its binding energy in the nucleus. Therefore, one can expect that when the excitation energy is shared among a large number of nucleons, the average time that elapses before a nucleon can be emitted is much more than the average time required for gamma ray emission, and the compound nucleus may decay by emitting a gamma ray<sup>(1)</sup>. Since it is clear that a given excitation energy is shared among many more nucleons in a heavy nucleus than in a light nucleus, it follows that radiative capture is comparatively unimportant in lightest nuclei, with the exception of  ${}^1_1\text{H}$ , but becomes more probable in the heavier elements.

As mentioned above, the compound nucleus has an excitation energy approximately equal to the sum of the kinetic energy and the binding energy of the incident neutron. The system (compound nucleus) may release this excitation energy with the emission of a single gamma ray and go to its ground state. However, if the nucleus has some energy levels, intermediate between the excitation level and the ground state,

it may instead emit several gamma ray photons of lower energy on going to the stable state.

The existence of capture gamma rays greatly complicates the shielding problem, since it is no longer sufficient merely to slow down and capture the neutrons. Therefore, it becomes more significant to use a material as a neutron absorber which does not give gamma rays on capturing the neutron. Some isotopes such as  $^{10}\text{B}$  or  $^6\text{Li}$  on neutron capture emit charged particles which are easily stopped. In addition, both of these isotopes have very large capture cross sections at thermal energies.

### 2.5 Particle Reactions $X(n,p)Y$ , $X(n,\alpha)Z$ , $(n,2n)$ and $(n,3n)$

Neutrons may also disappear as a result of charged particle reactions, where the neutron is assimilated in the nucleus which may decay by the emission of other particles such as an  $\alpha$  particle, a proton, or two neutrons. The nucleus resulting from these interactions may be unstable and decay by further gamma ray or particle emission.

Particle reactions are most prevalent for neutron energies above about 1 MeV. Below that energy the reaction is generally inhibited either by the energetics of the process or by the coulomb barrier which must be penetrated by the reaction products. However, in the case of light elements they may occur at intermediate or thermal energies.

Some of these reactions are  $^{10}\text{B}(n,\alpha)^7\text{Li}$ ,  $^6\text{Li}(n,\alpha)^3\text{T}$  and  $^{14}\text{N}(n,p)^{14}\text{C}$ . These reactions are quite useful for depressing the thermal neutron flux without giving rise to energetic gamma rays.

For incident neutron of sufficiently high energy, i.e., greater than the binding energy of the last neutron in the nucleus, the emission of two or three neutrons becomes possible. This reaction could be regarded as a type of inelastic scattering in which the first neutron comes out with an energy less than the difference between the energy of the primary incident neutron and the threshold energy. In that case

the residual nucleus is in a virtual state having enough excitation energy to be able to emit a second neutron. In this energy region most of the neutrons emitted in the inelastic scattering process tend to have small energies, since the density of available states in the residual nucleus increases with the degree of excitation. This means that, if the incident neutron has an energy above the threshold of (n,2n) reaction it is likely that a second neutron will appear. Hence the (n,2n) reaction rapidly becomes more probable than the (n,n') reaction. Therefore, the bulk of the inelastic scattering is now included as part of the (n,2n) reaction.

The Q value of the (n,2n) reaction is equal to the binding energy of the most weakly bound neutron in the target nucleus. As in other reactions, the threshold energy in laboratory system is given by:

$$E_{th} = \frac{(A + 1)}{A} \cdot Q \quad \dots \dots \dots 2.4$$

where A is the mass number of the target nucleus.

This threshold energy is low for nuclei having weakly bound neutrons, i.e., the threshold energy is about 1.8 MeV for (n,2n) reaction of <sup>9</sup>Be. However, with most nuclei the threshold energy for the (n,2n) reaction is in the range from about 7 to 10 MeV.

In the case of (n,3n) reaction the relation between (n,3n) and (n,2n) reactions is similar to that between (n,2n) and (n,n') reaction. For the (n,3n) reaction the third neutron can be emitted if the target nucleus still has sufficient excitation energy after the emission of the second neutron in the (n,2n) reaction. Therefore the (n,3n) cross section rises from the (n,3n) threshold at the expense of the (n,2n) cross section, as indicated in figure 2.2. The threshold energy of the (n,3n) reaction is so high (ranges from 11 MeV to 30 MeV). Therefore, the (n,3n) reaction has no significance in fission reactor calculations,

since this threshold energy is above the extreme top end of the fission spectrum, which is regarded as having an upper limit of 10 MeV.

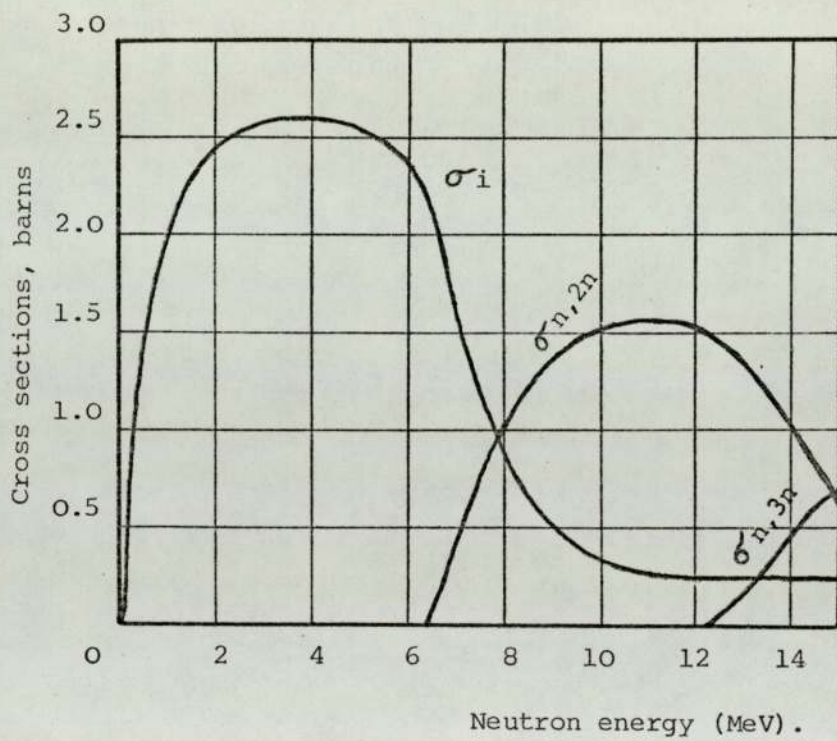


Figure 2.2. The Inelastic Scattering (n,2n) and (n,3n) cross sections of  $U^{238}$  Lamarsh, (1966).

CHAPTER 3FAST NEUTRON DETECTORS AND TECHNIQUES3.1 Introduction

Generally, the detection of a nuclear radiation is used not only to indicate the presence of nuclear particles, but also to give information about the amount (intensity) and energy and their related properties. A detection system usually consists of two parts, a detector for the presence and usually the energy of the incident particle and a measuring system to measure the output signals from the detector.

A great variety of techniques are available for measuring nuclear radiations. However, the detection of neutrons is in general more complicated than decay products of radioactive emitters because of their lack of charge and their very wide range of energies. Neutrons must therefore take part in a nuclear reaction which results in the emission of charged particles, which in turn interact with the detector and produce ionization and excitation of the molecules. In such cases the primary energy of the neutrons is dissipated through the emission of secondary charged particles and the detection takes place by the loss of energy of these secondary charged particles on their passage through matter. Therefore, it becomes clear that two media may be involved, one of which is a radiator, or often a scattering material, where the neutrons may interact to produce charged particles and another one which is a detection medium, in which the charged particles may dissipate their energies. These two components of a detector may be physically distinct, as in the case when protons are ejected from a hydrogenous foil by fast neutrons to spend their energy in ionizing gas in a space above the foil. In this case the energy dissipated in the scattering medium by the charged particles is wasted. On the other hand the two components may occupy

the same space as when the gas in the detector of the above example is itself homogeneous. In that case, the energy abstracted from the charged particle, from the moment of its production, is employed in the detection process. Therefore, there is considerable advantage to be gained in designing a system with combined reaction and detection media for the detection of neutrons.

A detailed discussion of the various neutron detectors is given in section 3.4.

### 3.2 The Main Parameters for Selecting a Neutron Detector

Usually, on choosing a neutron detector suitable for certain measurements, the following factors must be kept in consideration.

- a) The aim of the experiment and the experimental configuration.
- b) The energy range of neutrons to be measured.
- c) Flux magnitude and its variation.
- d) Detector sensitivity and energy resolution.
- e) Physical size of the detector and its perturbation of the neutron flux.
- f) Detector sensitivity to other nuclear radiation.

In the above list, the first two parameters are defined by experimental configuration, i.e., where the measurements will be carried out, inside or outside the medium under investigation and whatever the measurements, aim to give information about neutron energy or flux, and in what energy range will be performed. The flux magnitude and its variation is a critical parameter for choosing a suitable detector of known efficiency and cross section, i.e., measuring a low neutron flux requires a detector of high sensitivity or high cross section which is known as a function of neutron energy. Also a known sensitivity gives the absolute intensity of neutron spectrum.

In some measurements, the physical size of the detector is considered as a limiting factor, i.e., when the measurements have to

be carried out inside the medium (e.g. in some shielding investigations and reactor core parameter measurements) a large size will perturb the flux and if a re-entrant hole is made in the medium, it may distort the flux.

The last parameter which is concerned with detector efficiency to other nuclear particles is considered as a main important factor when choosing a neutron detector, since neutrons are usually measured in a background of other nuclear radiations (i.e. gamma rays). Therefore the detector should either be insensitive to gamma rays (threshold detectors) or give output pulses having different amplitudes or different shapes, so it becomes possible to eliminate the undesired pulses either by applying bias or pulse shape discrimination.

### 3.3 Reactions used in Neutron Detection

Owing to the fact that the neutron is an uncharged particle, the interaction of a neutron with the atomic structure of matter is effectively zero. However, a neutron may produce a charged particle either by collision or by initiation of a nuclear reaction. Therefore most of the neutron detectors are based upon one of the following processes.

#### 3.3.1 (n-p) Scattering

Most of the methods used to measure the fast neutron spectrum, involve a device which detects and measures proton recoil produced by the neutrons in some hydrogenous medium. The detection efficiency depends on the (n,p) scattering cross section of hydrogen. The dependence of cross section is a smooth function of energy and decreases from 13 barns to 1 barn in the neutron energy range (0.1 to 10 MeV)<sup>(16)</sup>. The (n,p) scattering is isotropic in the centre of mass system, so that the distribution in energy of the recoil protons produced by monoenergetic neutrons is constant from zero up to a maximum value, equal to the incident neutron energy. The energy of the recoil proton  $E_p$  is given by:

$$E_p = E_n \cos^2 \psi$$

where  $\psi$  is the angle which the recoil proton makes with the direction of the incident neutron of energy  $E_n$ .

If the incident neutrons are not monoenergetic and have an energy spectrum  $\phi_o(E_n)$ , recoil protons of energy  $E$  will be generated by neutrons of different energy, starting from  $E_n = E$ . In this case the number of recoil protons  $N(E)$  in a unit energy interval is given by:

$$N(E) = \int_E^{\infty} \frac{\phi_o(E_n) (1 - e^{-\Sigma d})}{E_n} dE_n \quad \dots \dots \dots 3.2$$

where  $\Sigma$  is the macroscopic scattering cross section of hydrogen and  $d$  is the detector thickness. Therefore it becomes possible to obtain the neutron energy spectrum  $\phi_o(E_n)$  by differentiating the recoil proton spectrum given by the above equation and is given by:

$$\phi_o(E_n) = \frac{E_n}{(1 - e^{-\Sigma d})} \cdot \frac{dN(E)}{dE} \quad \dots \dots \dots 3.3$$

Some of the proton recoil detectors to be discussed hereafter include proportional counters, counter telescopes, and organic crystal scintillators.

### 3.3.2. Neutron Induced Reactions

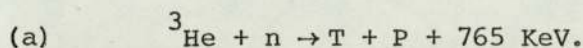
The very low interaction of neutrons with the field of charged particles makes it easy for neutrons to penetrate atomic nuclei. The new compound nucleus formed by the absorption of a neutron has an excess of energy due to the binding and kinetic energy of the neutron. This energy may be released by the ejection of energetic charged particles or by the emission of a gamma quantum. The new nucleus may be stable or unstable, and in the latter case it shows radioactive decay with a definite half-life. Such reactions may be initiated by slow neutrons

(exoergic reaction) or where extra kinetic energy is necessary by neutrons of energy above a given threshold value (endoergic reaction).

A detailed discussion of both reactions is given below.

### 3.3.2.1 Exoergic Reactions

Exoergic reaction is a process in which energy is released after the interaction of a nuclear particle with some specific nuclei. There are a few exoergic reactions which are of interest in neutron detection. These include:

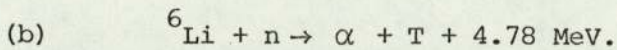


This reaction is more important for the detection of neutrons due to the following factors.

(a.1) The cross section is very high for slow neutrons (5,400 barns) and varies smoothly to 1.7 barns at 100 KeV down to 0.75 barns at 1 MeV and does not show strong resonances.

(a.2) The product nucleus has no excited states so that to each neutron energy there is a single reaction energy, i.e., a monoenergetic neutron source will be represented by a line spectrum, in the output from the spectrometer.

(a.3) The reaction is of moderately low energy. For thermal neutrons, the energy release is 0.765 MeV. Therefore the total energy from the capture of 1 MeV neutron is 1.76 MeV which is not so high that the outgoing particle (proton) becomes a serious problem, while at the same time the energy expended by electrons from gammas in a moderately sized  ${}^3\text{He}$  filled chamber is considerably less than 0.765 MeV so that their pulses will not distort the spectrum. However, there are some disadvantages of this reaction which are given for incident neutrons of energy above about 1 MeV, the recoiling  ${}^3\text{He}$  will have energy greater than 0.765 MeV. Therefore  ${}^3\text{He}$  recoils will appear above this peak due to the capture of thermal neutrons which are usually to some extent present. In addition,  ${}^3\text{He}$  is relatively rare and expensive.



This reaction has a cross section about 945 barns for neutrons of velocity  $2200 \text{ ms}^{-1}$  in case of a pure isotope. The cross section varies as  $\frac{1}{v}$  in the thermal region and has a peak of 2.75 barns at 265 KeV; drops down to 0.28 barns at 1.2 MeV and to 0.05 barns at 8 MeV<sup>(17,18)</sup>. The main advantage of this reaction is the high Q value so that pulses from electrons induced by high energy gammas will give energy in the counter much less than 4.78 MeV.

Lithium is used in scintillation counters as  ${}^6\text{LiI}$  crystals as well as in photographic plates for the thermal, slow and fast neutron spectrum measurements in health physics monitoring.

### (c) Thermal Fission

As this chapter deals with fast neutron detectors, only brief attention will be paid to thermal fission detectors which are used for measuring thermal neutron fluxes.

Thermally fissile materials such as  ${}^{233}\text{U}$ ,  ${}^{235}\text{U}$  and  ${}^{239}\text{Pu}$  are widely used for measuring thermal neutron fluxes for many purposes. They have considerable advantages over other neutron detectors where there is high gamma ray background, since the energy released per fission is relatively high giving fission fragments with about 80 MeV of energy each as compared with the energy from electrons due to gamma rays. The cross sections at thermal energies is about 500 to 750 barns which varies rapidly with resonances in the eV region. At neutron energy of about 100 KeV the cross section flattens off and becomes constant ( $\pm 10\%$ ) up to about 5 MeV.

#### 3.3.2.2 Threshold Detectors

For endoergic reactions, the kinetic energy of the reaction products is less than the kinetic energy of the initial particles by an amount equal to the reaction energy, i.e., energy is absorbed rather than liberated. However, this is obviously not true for fast neutron

fission e.g. for  $^{238}\text{U}$  fission takes place if the incoming neutron is a few MeV, while the total energy of the fission fragments is some 160 MeV. Nevertheless, fission in these cases is possible only with fast neutrons because there is a fission barrier, such that, if the compound nucleus has excitation energy less than this barrier it cannot undergo fission. This means that there is a threshold energy below which the reaction cross section is very small, or even zero.

Actually, a direct detection of an endoergic reaction is difficult, and one normally measures the activity of the radioactive products. Therefore, the radioactive product must have a suitable half-life so that the activity after irradiation can be followed for at least two half-lives. This is important, because other sources of activity may be present in the sample as a result of irradiation. In particular, it is essential that the effect of radiative capture (with slow neutrons) is minimized, either by a small radiative capture cross section or a widely differing half-life of the radiative products.

The main specific reactions which are of interest in neutron detection using threshold detectors are:

(a)  $(n,p)$  and  $(n,\alpha)$  Reactions

These reactions usually take place with light elements, since for heavy elements, the high coulomb barrier prevents particle emission. The cross section can be several hundred millibarns in the energy range of 1 to 4 MeV and varies rapidly over the range, because of resonance in the compound nucleus. The cross section becomes appreciable at a neutron energy which depends on the effect of resonances. The main threshold detectors of this reaction are  $^{31}\text{P}(n,p)^{31}\text{Si}$  and  $^{32}\text{S}(n,p)^{32}\text{P}$  with half-lives of 2.7 hours and 14 days respectively.

(b)  $(n,2n)$  Reactions

In this reaction a second neutron is ejected from the nucleus, so that the threshold energy is the binding energy multiplied by small

factors, allowing for centre of mass motion<sup>(21)</sup>. Above the threshold energy, the cross section generally rises to a fairly flat peak around 3 to 5 MeV above threshold, and then declines, due to competition. A typical detector is  $^{63}\text{Cu}$  (n,2n)  $^{62}\text{Cu}$  with half-life of 10 minutes.

(c) Fast Fission Reactions

For fissionable elements such as  $^{232}\text{Th}$ ,  $^{231}\text{Pa}$ ,  $^{234}\text{U}$ ,  $^{236}\text{U}$ ,  $^{238}\text{U}$ ,  $^{237}\text{Np}$  and  $^{240}\text{Pu}$ , the fission process takes place above a certain threshold energy. These nuclides are used usually for measuring fast neutron spectra, since the cross section above the threshold energies is relatively flat, and the threshold energies cover a range of considerable interest in fast reactor spectra<sup>(19)</sup>.

### 3.4 Different Detection Systems

Based on the above principles, several detectors become available for measuring neutron fluxes and energies for experiments having different environments. A brief discussion of the general characteristic for some systems used in fast neutron detection is given below.

#### 3.4.1. Counter Telescopes

The counter telescope is usually used for measuring the fast neutron spectrum at high energy range from about 1 MeV to 20 MeV<sup>(19)</sup>. The telescope consists essentially of a hydrogenous radiator (usually polyethylene  $\text{C}_n\text{H}_{2n}$ ), two or more proportional counters in line with scintillation detectors (NaI or CsI) whose outputs are sorted by a pulse height analyser.

The incident fast neutrons eject recoil protons from the radiator. The angle between the recoil protons and the detection of the incident neutrons is connected by a simple relation, (equation 3.1).

Only recoils which pass through an aperture of known dimension are counted by the scintillation counter which gives a differential spectrum instead of being a plateau. Since there are many sources of

pulses of low energy, spurious counts are suppressed by the aligned proportional counters. Coincidence between the three systems then effectively reject all particles except those which start from the radiator and end in the scintillator. The light output of the scintillator is thus a measure of the proton recoil energy which, along with a determination of  $\psi$ , allows the calculation of the neutron energy. By suitable selection of the counters and radiator thickness the energy loss in components of the system other than the scintillation phosphor can be kept small.

The important advantage of the counter telescope is the extremely low background counting rate, and its drawback is its low efficiency (about  $10^{-6}$  to  $10^{-4}$  count per neutron.cm<sup>-2</sup>).

#### 3.4.2. Proton Recoil Proportional Counters

Generally, a proportional counter is an ionization chamber with a fine wire anode to give a high electric field so that electrons can be multiplied by collision. The chamber incorporates a material from which charged particles will be released as a result of a nuclear reaction which the neutron causes<sup>(20,21)</sup>. For neutrons of high energy, elastic scattering (n,p) by hydrogen is often used for fast neutron detection, in which case hydrogen recoils are observed. The most frequently encountered counting gas incorporating hydrogen is methane (CH<sub>4</sub>) and ethylene (C<sub>2</sub>H<sub>4</sub>). The range of a recoiling proton of energy 0.1 MeV is about 2 mm in air at STP and 8 cm at 2 MeV, while at 10 MeV the range is about 100 cm, therefore at 10 MeV a gas field counter would require inordinately high pressures.

When the biasing on a proportional counter is such that only those pulses produced by protons having an energy greater than  $E_p$  are accepted, the measured count rate for neutrons of energy  $E_n$  is then proportional to:

$$C(E_n, E_p) = \phi(E_n) N_p \sigma(E_n) (E_n - E_p) / E_n$$

where  $N_p$  is the hydrogen atom content of the sensitive volume (atoms, cm<sup>-3</sup>) and  $\sigma(E_n)$  is the microscopic cross section. Practically  $E_p$  is about 0.1 to 0.2 MeV, since below this energy proton recoil pulses become difficult to distinguish from background electron pulses. However, for protons of energy above this limit the ability of the proportional counter to discriminate between particle types is very good, since it produces output pulses of different sizes depending on the particle types. This is particularly useful in neutron detection, where the neutrons often appear along with a high background of gamma radiation. Another important advantage of the proportional counter as a neutron detector is that the variation of the (n,p) scattering cross section is well known, making interpretation of experiments relatively easy. The sensitivity of a methane proportional counter falls typically in the range of 1 to 10 %.

### 3.4.3 Organic Scintillators

In recent years, the utilization of organic scintillators for measuring the energy spectrum of different radiation particles has enjoyed a wide application in various fields of science and technology<sup>(22)</sup>. They are available either as a pure crystal (stilbene) or in various combinations as liquid or solid solution e.g., NE-213 and NE-102. The main important advantages of organic scintillators are their high speed response ( $\sim 10^{-9}$  sec), high efficiency of detection of fast neutrons (10 - 30%), and besides providing exact information on the number, time of arrival and energy of nuclear particles, they can give information on the type of detected particles from differences in the decay of the scintillation. This becomes particularly important if measurements are to be carried out in mixed fields of radiation, i.e., when measuring the characteristic of a neutron field in the presence of the background of accompanying gamma radiation from a nuclear reaction or that emitted in nuclear reaction processes.

A detailed discussion of organic scintillators and their uses as fast neutron detectors is given in chapter 4.

### 3.5 Detectors Based on Exoergic Reactions

#### 3.5.1. ${}^6\text{LiI}(\text{Eu})$ Scintillators

The use of a scintillator of lithium 6 iodide activated with europium as a fast neutron spectrometer has been studied by various workers<sup>(23,27)</sup>. The  ${}^6\text{Li}(n,\alpha)\text{T}$  reaction provides a suitable mechanism for both slow and fast neutron detection. This reaction is exoergic with a  $Q$  value of 4.78 MeV. Analysis of the scintillation pulses permits a measurement of the energy distribution of the incoming neutrons, since the total energy released in the reaction products is the sum of  $Q + E_n$ . Irradiation of a  ${}^6\text{LiI}(\text{Eu})$  crystal with monoenergetic fast neutrons results in a pulse height spectrum containing a rather broad fast neutron peak whose width can be considerably reduced by cooling the crystal with liquid nitrogen.

The main advantages of a  ${}^6\text{LiI}(\text{Eu})$  scintillator as a neutron detector are:

- (a) Simple design and electronics,
- (b) good sensitivity, and
- (c) large  $Q$  value of reaction (4.78 MeV) permits discrimination against electron pulses produced by the ambient background. However, to measure fast neutrons, the detector must be cooled with liquid nitrogen to reduce the difference in the light output as a function of energy for  $\alpha$  and tritons. However, cooling does not completely overcome the non linear light output of the crystal which complicates the subtraction of the pulses produced by competing reaction  ${}^6\text{Li}(n,n'd)\alpha$  which has a light output versus energy different from the  ${}^6\text{Li}(n,\alpha)\text{T}$  reaction and its cross section is greater.

#### 3.5.2. The Long Counter

This device was originally designed by Hanson and McKibben<sup>(28)</sup>

to meet the requirements of measuring neutron flux for intermediate and high energy neutrons. It is a  $\text{BF}_3$  counter embedded in a cylinder of paraffin wax. High energy neutrons are moderated by the paraffin before entering the  $\text{BF}_3$  gas and being captured by the  $^{10}\text{B}(n,\alpha)^7\text{Li}$  reaction. Thermal neutrons are partially captured by the moderator and partially captured by  $^{10}\text{B}$ . By a suitable selection of the moderator configurations it becomes possible to achieve reaction rates which are substantially independent of neutron energy from 10 KeV to 10 MeV. Thus, the long counter furnishes a measure of neutron flux over a wide range of energy of interest in shielding.

The output response of a good quality long counter is a flat response in the energy range of 0.5 to 2 MeV, drops by about 10% at 225 KeV and by about 20% at thermal energy from its value at 0.5 MeV. In the high energy region the response is generally down by about 15% at 14 MeV. Above about 14 MeV the variation in response is affected by the resonance in the total cross section of carbon.

The detection efficiency of a  $\text{BF}_3$  long counter of 2" in diameter and 8" long filled with unenriched  $\text{BF}_3$  to a pressure of 2 atm is about 0.2 to 0.3%.

### 3.5.3. The Helium 3 Counter

The  $^3\text{He}$  spectrometer is still a useful detector for measuring the neutron spectrum in the energy range 0.1 to 1 MeV<sup>(29,30)</sup>. It is based on exothermic neutron induced reaction, where all the reaction products expend their energy in the counter system and therefore a monoenergetic neutron flux would produce a line spectrum. The reaction cross section is fairly large (5400 barns) for slow neutrons and varies slowly with energy. Another advantage of the  $^3\text{He}$  counter is that there are no resonances and no competing reactions, and the peak at 765 MeV due to thermal neutrons makes a convenient calibration check both for pulse height and resolution. The counter efficiency is typically

0.01 per cent depending on the  $^3\text{He}$  concentration.

A detailed description of the characteristic and performance of a proportional counter containing  $^3\text{He}$  plus krypton is given by Batchelor et al <sup>(29)</sup> 1955.

### 3.6 Detectors Based on Fission and Threshold Reactions

#### 3.6.1 Fission Counters

The main idea behind using fissile materials in fission counters is that the fission fragments are energetic charged particles and can produce ionization in gases. These fission fragments behave rather like  $\alpha$  particles in their interaction with matter. However, there are a few quantitative differences which ordinarily result in optimum values of such parameters as gas pressure and the plate spacing in a fission chamber which are somewhat different from those for an alpha chamber. The range of fission fragments is roughly half that of typical  $\alpha$  particles from radioactive decay. Alpha particles ionize most heavily near the end of their ranges while fission fragments ionize most heavily at the beginning. This can be turned to advantage, since all fissionable materials are alpha active, hence detection of the fission fragments takes place against a background of  $\alpha$  pulses which must be prevented from being recorded in some way. Therefore, if the detector is designed so that only the first half of the fission fragment range occurs in the active volume of the detector, most of the alpha particles will produce only a lightly ionized track in this volume compared to the very heavy track of the fission fragments. This permits an amplifier bias setting high enough to eliminate all single  $\alpha$  pulses and even pulses resulting from pile up of several alphas which may occur during the resolving time of the instrument.

In terms of technique, the fissionable materials can be incorporated into the sensitive volume of a gas ionization chamber or proportional counters. The fission rate is proportional to the neutron

flux. The fission fragments produce large ionization pulses which after amplification can be counted by the usual way.

### 3.6.2. Fissionable Foils

Fissionable materials such as  $^{232}\text{Th}$ ,  $^{231}\text{Pa}$ ,  $^{234}\text{U}$ ,  $^{236}\text{U}$ ,  $^{238}\text{U}$  and  $^{237}\text{Np}$  are used as fissionable foils for measuring the fast neutron spectrum. These foils, after neutron exposure, can be measured in a suitable counting arrangement for their induced fission activity.

### 3.6.3. Threshold Foils

In threshold detectors, the reaction does not proceed with neutrons of energy below a certain value. At neutron energies greater than 1 MeV the  $(n,p)$  and  $(n,\alpha)$  reactions are more prominent than the  $(n,\gamma)$  for many materials. The sulphur and phosphorus  $(n,p)$  reaction are probably the most widely used. They have effective threshold energies of about 3 MeV and 2.5 MeV respectively.

The  $(n,2n)$  and  $(n,n')$  reactions are also threshold radioactivant possibilities. Generally, the  $(n,2n)$  reactions occur at neutron energy much higher than needed in reactor studies ( $\sim 11$  MeV). The Cu  $(n,2n)$  reaction is widely employed as a threshold detector for measuring the spectrum of light energy neutrons from  $\text{T}(d,n)^4\text{He}$  reactions.

The main advantages of the threshold detectors are:

- (a) They are sensitive over a wide range of energy and flux by choosing materials with different cross sections.
- (b) The possibility of obtaining these radioactivants in different shapes and sizes makes it possible to introduce them in the medium in which the measurements are to be made without the introduction of voids.
- (c) It is also possible to select within limits, materials appropriate for various neutron energy ranges.

## 3.7 Semiconductor Detectors

Semiconductor detectors provide a suitable technique for neutron detection for a wide range of energy <sup>(31,32)</sup>. These detectors

are solid state ionisation chambers and detect charged particles. The neutrons to be measured have first to impart their energies to some type of charged particle. The basic mechanism then depends upon the production of electron positive hole pairs by the charged recoil particle in a p-n junction in the semiconductor. In the electric field existing at the junction such pairs are separated and can produce a large voltage pulse of the order of 1 mV for a 2 MeV energy absorption<sup>(32)</sup>. These pulses can be amplified and counted by appropriate electronics.

The energy transferred from the neutron to the charged particle may occur either in an external medium placed in front of the detector (i.e. coating the n-p junction with paraffin which serves as a source of recoil protons), or alternatively in a material of which the detector is constructed (i.e. such silicon), which emits either alpha particles or protons from the reaction  $^{28}\text{Si}(n,\alpha)^{25}\text{Mg}$  or  $^{28}\text{Si}(n,p)^{27}\text{Al}$ .

The first method gives a wide range of possibilities and has the disadvantages that in order to get a good energy resolution one is very limited in the choice of thickness and geometry of the medium, in addition to a poor neutron detection efficiency. In the second method the energy transfer takes place in the detector itself, therefore when the range of produced charged particles is short compared with the dimension of the active region, one expects to get as good resolution as that obtainable for the charged particle and a good detection efficiency. However, one is then limited to reactions which may take place in the material of the detector, namely (n,p) and (n, $\alpha$ ) reaction occurring in various isotopes of silicon.

The main advantages of semiconductor detectors, are their excellent energy resolution and good discrimination against gamma radiation, since the pulse heights are essentially proportional to the electron positive hole density in the n-p junction. However, the detector sensitivity is limited and restricts the use of these devices

to fluxes in excess of  $10^4$  neutrons.cm<sup>-2</sup>.sec<sup>-1</sup>. The typical counting efficiencies for existing devices range from  $10^{-4}$  to  $10^{-7}$  counts per neutron.cm<sup>-2</sup>. This, in addition to the fact that the semiconductors are subject to radiation damage, which limits their useful life.

### 3.8 Time of Flight Technique

In time of flight technique, the neutron energy is determined from a measurement of velocity, which can be obtained from the determination of a zero time related to the time at which the particle begins on its flight path, and measure of the time elapsed from zero time until the particle is detected at the end of its flight path.

The zero time can be determined by the detection of an event which occurs simultaneously with the emission of the particle (i.e. associated particle technique) or by the detection of a secondary event initiated by the particle in flight e.g. the scattering of neutrons through a known angle or by using a pulsed source of neutrons giving nanosecond pulses. However, such a method can be applied to a limited class of reaction.

The most recent and more general technique for measuring a zero time is that of the pulsed beam which can in particular be applied to all types of reactions and gives a zero time independent of the reaction mechanism<sup>(19)</sup>.

For all time of flight techniques, the neutron energy is given by:

$$E = 5.23 \times 10^3 \cdot \frac{D^2}{t^2} \text{ MeV}$$

where  $t$  is the flight time in nanoseconds and  $D$  is the flight path in metres. This relation can be used to evaluate the neutron energy in the range of 0.1 to 15 MeV where the flight path is of several metres.

In the light of the foregoing discussion it becomes clear that

the time of flight technique is the easiest method to interpret the neutron spectrum, but it requires a nanosecond pulsing of the neutron source. This is not possible with the available facilities attached with the SAMES accelerator. Thus this method is rejected in favour of the proton recoil scintillator using PSD to reject  $\gamma$  events. This latter method has the advantage of high detection efficiency compared with the other methods since organic scintillators have much greater mass of material than that of gas or thin film detectors.

CHAPTER 4NEUTRON SPECTROMETER4.1 Introduction

Neutron spectrometers with organic scintillators have been used for many years for measuring the number, time of arrival and energy of nuclear radiations<sup>(19,33,34,35,36)</sup>. Among these different types of scintillators are the stilbene crystals and liquid organic scintillators (e.g. type NE-213) which have found a widespread use in nuclear spectroscopy because they possess desirable physical characteristics. They exhibit good detection efficiency<sup>(35)</sup>, large size, high speed and particle discrimination capability<sup>(37,38,39,40,41)</sup>. Their disadvantages include non linear light output for heavy particles, the difficulty of relating the pulse spectrum to the neutron energy spectrum and smeared step like responses to monoenergetic neutrons. All of these difficulties have been largely overcome, and the use of these scintillators as an active element for measuring fast neutron spectra has become a widely applied technique.

4.2 Scintillator

A small 1" by 1.5" diameter cylinder of NE-213 scintillator was chosen for the present work because it offers a good compromise between efficiency and resolution. The scintillator is glass encapsulated and was purged with pure hydrogen to remove the undesirable oxygen which selectively quenches the slow component of light emission<sup>(13)</sup>. It is made with xylene, activators and POPOP as a wave length shifter. Naphthalene is added to enhance the slow component of light emission.\*

The NE-213 scintillator has the following desirable characteristics:

\* Manufactured by Nuclear Enterprises, Ltd., Edinburgh, Scotland.

- (a) It has an enhanced emission of delayed light which gives it good pulse shape discrimination between various pulses over a wide range of energy.
- (b) It has a slightly greater hydrogen content than stilbene<sup>(43,46)</sup>.
- (c) Since NE-213 is non crystalline, its response to neutrons is isotropic for suitable cell geometries.
- (d) Its response to alpha-particles and carbon recoils from 14 MeV neutrons is only about half the pulse height that is produced with stilbene scintillators<sup>(45)</sup>.

#### 4.3 Discrimination against gamma rays

The discrimination between recoil electron and recoil proton pulses during this measurement was performed using the method of zero crossing technique which was first proposed by Alexander and Goulding<sup>(47)</sup> and used by many other workers<sup>(48,49,50,52,53)</sup>. Like all other various methods of pulse shape discrimination the zero crossing technique makes use of information contained in the time dependence of the current pulse of the photomultiplier. The current pulse is formed of two components, one of short decay time and the other with a longer decay time. The energy contained in the longer term decay component is quite different for the electron and proton, assuming equal recoil energies. When the pulses are integrated and differentiated by two differentiating networks (double delay line clipping), the cross over point is different for the neutron and gamma rays as shown in figure 4.1. The timing of the cross over with respect to the start of the pulse is sensitive to decay components in the scintillation but insensitive to pulse amplitudes. By measuring the zero crossing time the pulse shapes and hence the particle types can be determined.

The main advantages of the method of zero crossing technique are that it is suitable for use over a large dynamic range of pulse amplitude, it is capable of operating at a high counting rate and it can use only dynode signals, thus allowing independent use of anode

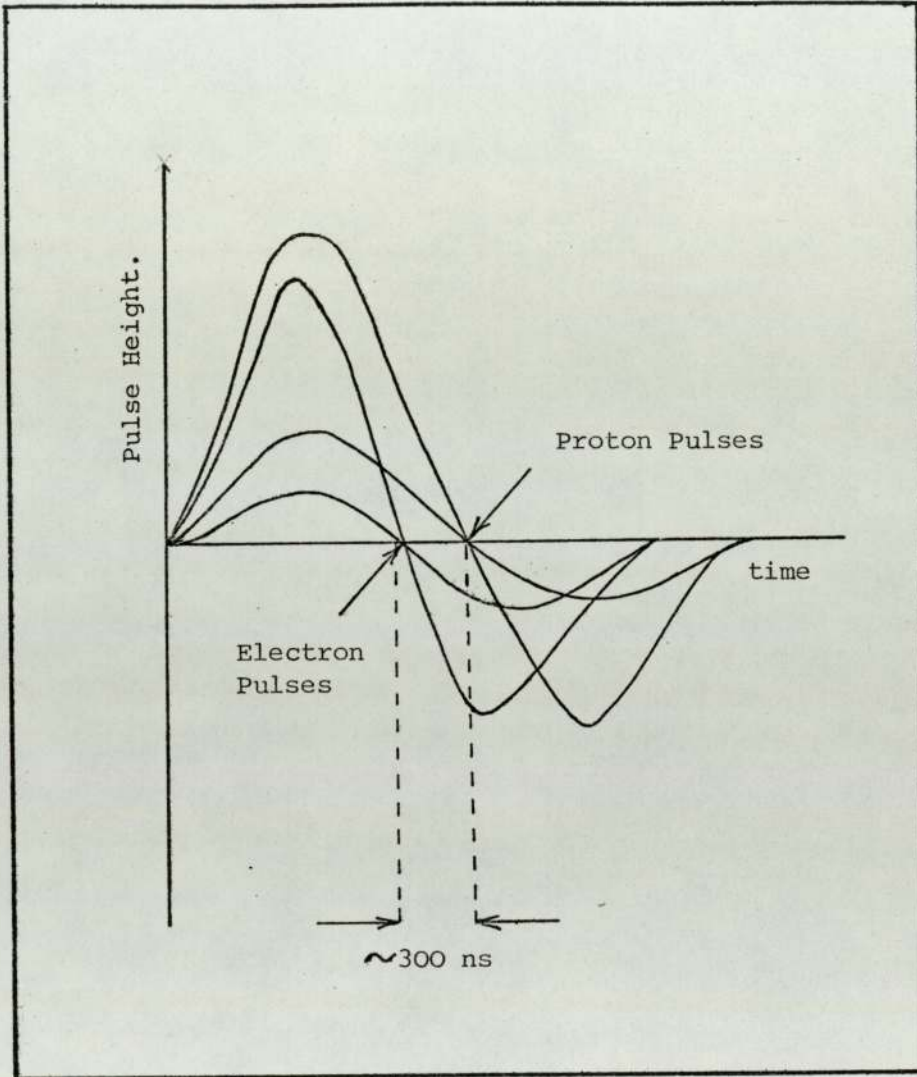


Figure 4.1. Idealised shape of the Doubly Differentiated Dynode Pulses.

signals for fast timing. This, in addition to the fact that it only requires relatively simple electronic circuitry.

The method adopted by McBeth et al<sup>(49)</sup> is used for differentiating between the electron and proton pulses which seems to be a very convenient and simple technique. This method is based on measuring the time difference between the fast anode current pulse and the zero crossing of a doubly differentiated voltage pulse obtained from a suitable dynode.

A detailed description of the zero crossing system based on the above mentioned method is given hereafter in a description of the spectrometer.

#### 4.4 Measuring and P.S.D. Systems

The NE-213 scintillator was coupled to a 14 stage photomultiplier tube type 56 AVP (see figure 4.2). This type of photomultiplier was chosen because it has a high degree of time definition and a high time resolution which are required for fast measurements (coincidence). The dynode chain appropriate to P.S.D. is shown in figure 4.3. with a block diagram of the spectrometer. The cathode is operated at approximately -1900 V and the anode near earth potential. A high voltage supply capable of supplying  $\sim 2\text{mA}$  to the dynode chain is necessary.

With this high gain photomultiplier the amplitude of the current pulse at the anode is not proportional to the amplitude of the scintillation pulse. Due to the lack of information contained in this pulse, it is only used as a time reference signal and as such it can be used simultaneously to generate a signal for use in coincidence circuitry and as a time marker signal for use in P.S.D.

Linear signals are taken from dynode number 10. The current pulses are directly integrated with the decoupling capacitor and resistor network at this dynode. This gives a current pulse with a voltage step of rise time determined by the scintillation decay times and the time

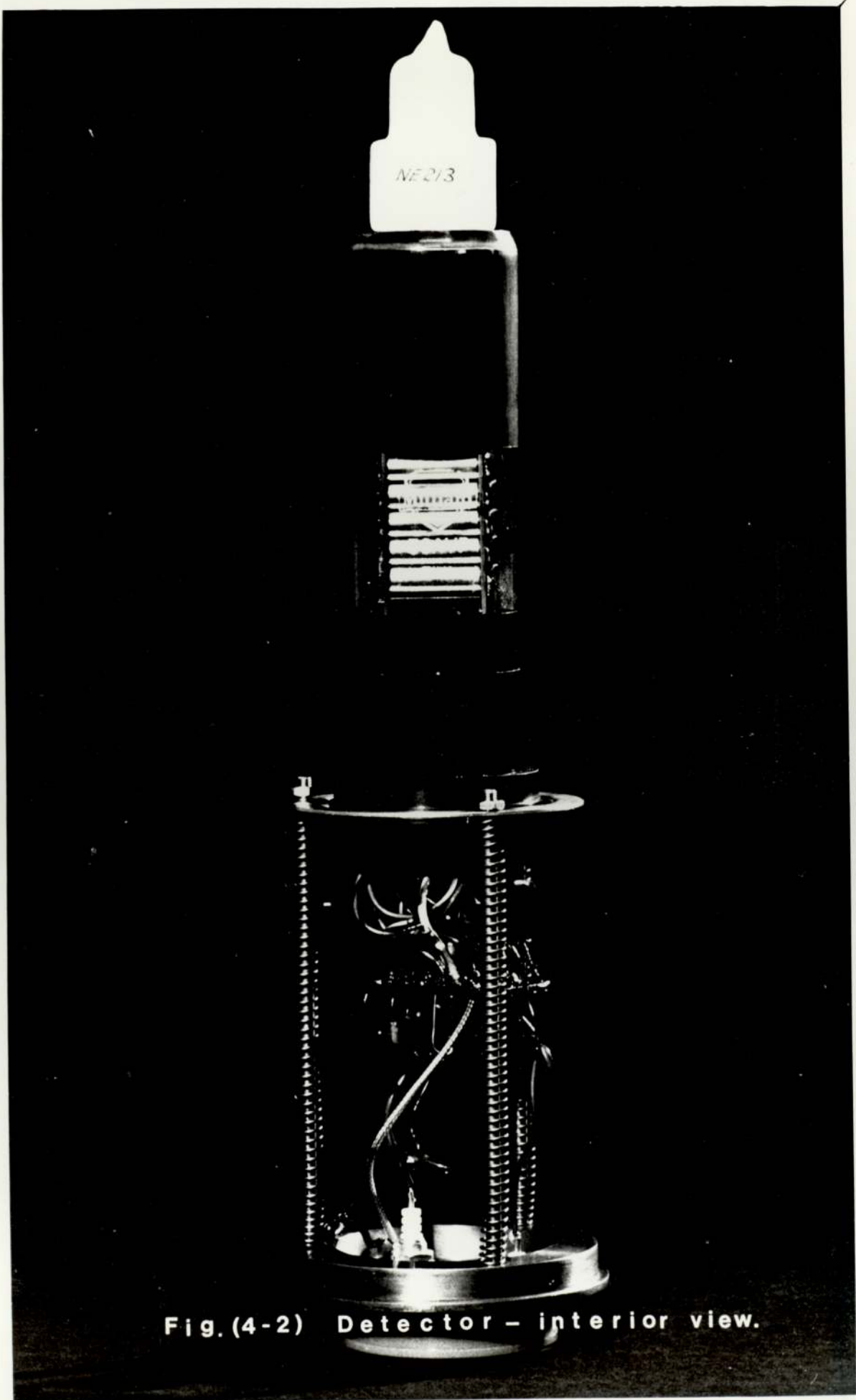


Fig.(4-2) Detector - interior view.

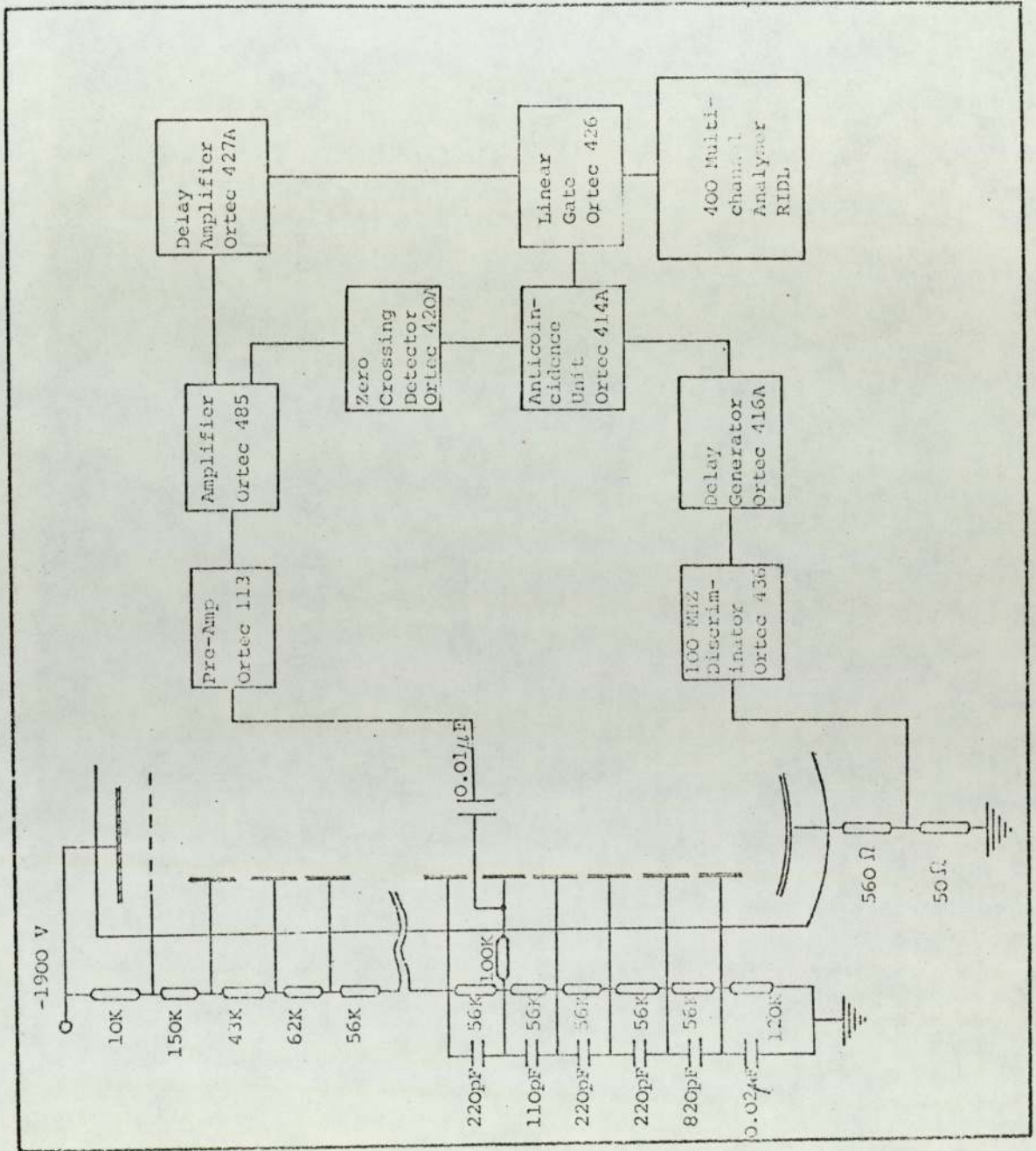


Figure 4.3. Dynode Chain and Block Diagram of the P.S.D. System.

constant of the resistor and capacitor network at the dynode.

In this system of P.S.D. the preamplifier is non shaping and the amplification and double differentiation are accomplished in the main amplifier by means of resistor capacitor networks. This amplifier gives an output of bipolar voltage pulses which pass through the base line at different times<sup>which</sup> depend on the shape of the input pulses (particle type) but independently of their amplitude (particle energy). Measurement of the width of these pulses is difficult to perform in practice owing to the necessity of triggering the measuring instrument. However this problem can be overcome by using the anode current pulse as a zero time reference and to measure the time difference between this signal and the zero crossing of the dynode voltage pulses. The zero crossing discriminator is used to measure the zero crossing times of these doubly differentiated pulses. This discriminator is capable of measuring this time difference to an accuracy of  $\pm 1$  ns.

Small time differences ( $\leq 1 \mu s$ ) are commonly measured by time to pulse amplitude converters which produce output signals of amplitude proportional to the time difference between the input signals. In this system the time to amplitude converter is substituted by a coincidence system. In that case the P.S.D. is set up by measuring the count rate at the output of the anticoincidence as a function of the delay in the delay and gate generator. The delay and gate generator is adjusted to produce an anticoincidence pulse with a falling edge occurring before the leading edge of the electron zero crossing signal. Therefore, any zero crossing signals that are overlapped by the delayed anode pulse are then blocked by the anticoincidence unit.

Figure 4.4 illustrates the time relation between the various pulse forms for simultaneous excitation of the NE-213 liquid scintillator by neutrons and gamma rays from an Am- $\alpha$ -Be source.

The main advantages of this anticoincidence method are its

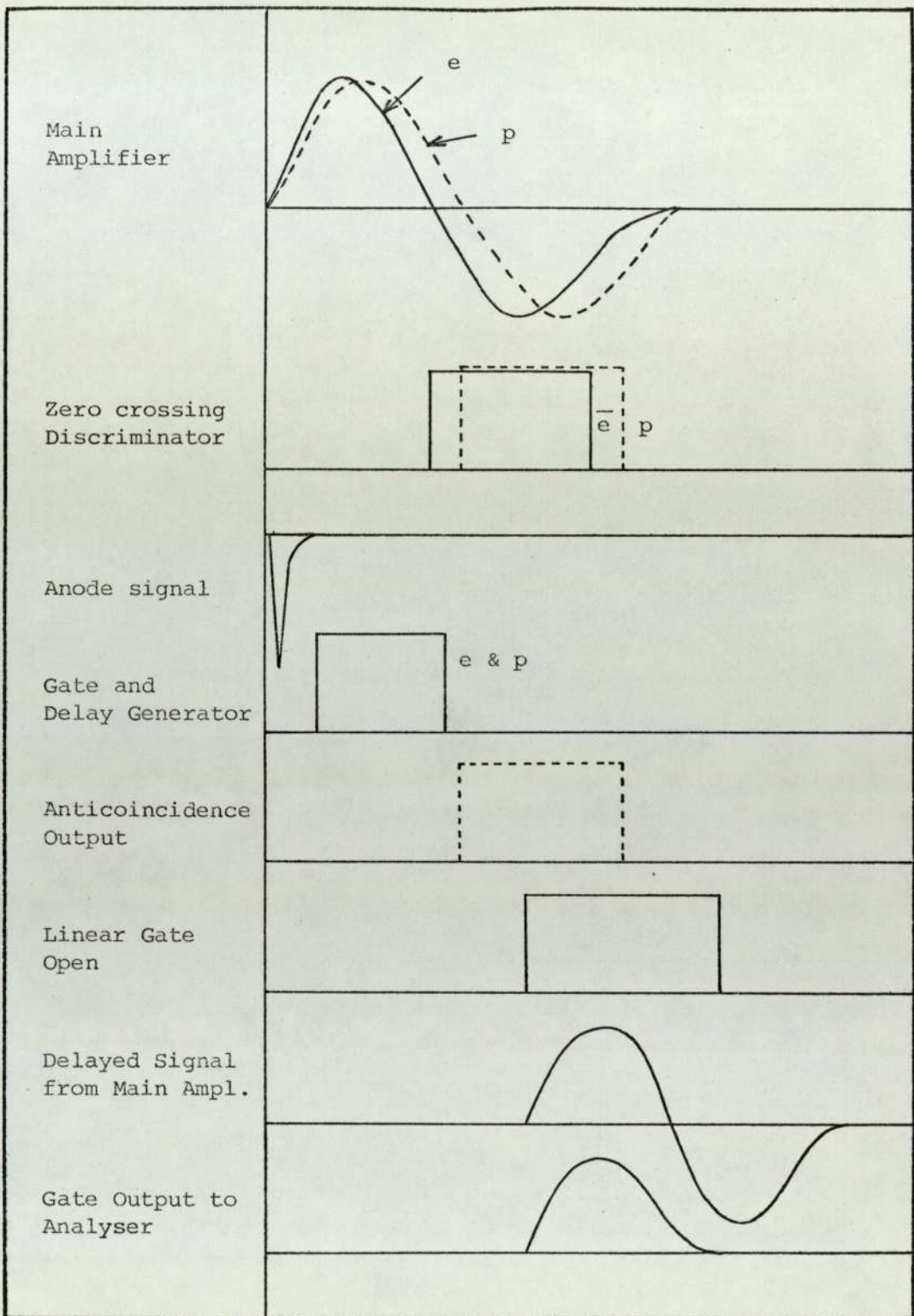


Figure 4.4. Time Relation amongst the Output Pulses at Various Points in the System.

simplicity, (less cost) and the delay of the P.S.D. signal relative to the output pulse at the linear amplifier is reduced by approximately 4  $\mu$ sec. This can be extremely useful in subsequent gating operation. Moreover, this system is equally efficient in rejecting either particle type.

After filtering the recoil proton pulses from the recoil electron pulses in the anticoincidence unit, the output pulses are applied to the linear gate which controls the passage of the linear delayed pulses coming from the main amplifier through the delay amplifier. The sorted proton pulses from the linear gate are then supplied to the input of a 400 channel (RIDL) pulse amplitude analyser.

Figure 4.5 presents a photograph of the measuring system with the control panel of the SAMES Accelerator.

#### 4.5 Calibration of the Spectrometer

The value of pulse height of light yield  $P(E)$  and the efficiency are known as a characteristic of the scintillator but not of the spectrometer as a whole. However a spectrometric measurement is concerned with the analysis of pulse amplitude distributions  $V(E)$ . The amplitude of these pulses is proportional to the number of photons in a light pulse arriving at the photocathode of the photomultiplier and is in turn related to the amount of energy absorbed in a scintillator. In this case:

$$V(E) = \text{constant} \cdot P(E) \quad \dots \dots \dots 4.1$$

where the constant is the energy relation between pulse height and light output

However, the above relation for certain models of spectrometer is sometimes distorted due to the characteristic of electronic devices used in such a spectrometer. Such distortion can be expressed through a complementary factor  $D(E)$  which depends on energy, i.e.,

$$V(E) = \text{constant} \cdot P(E) \cdot D(E) \quad \dots \dots \dots 4.2$$

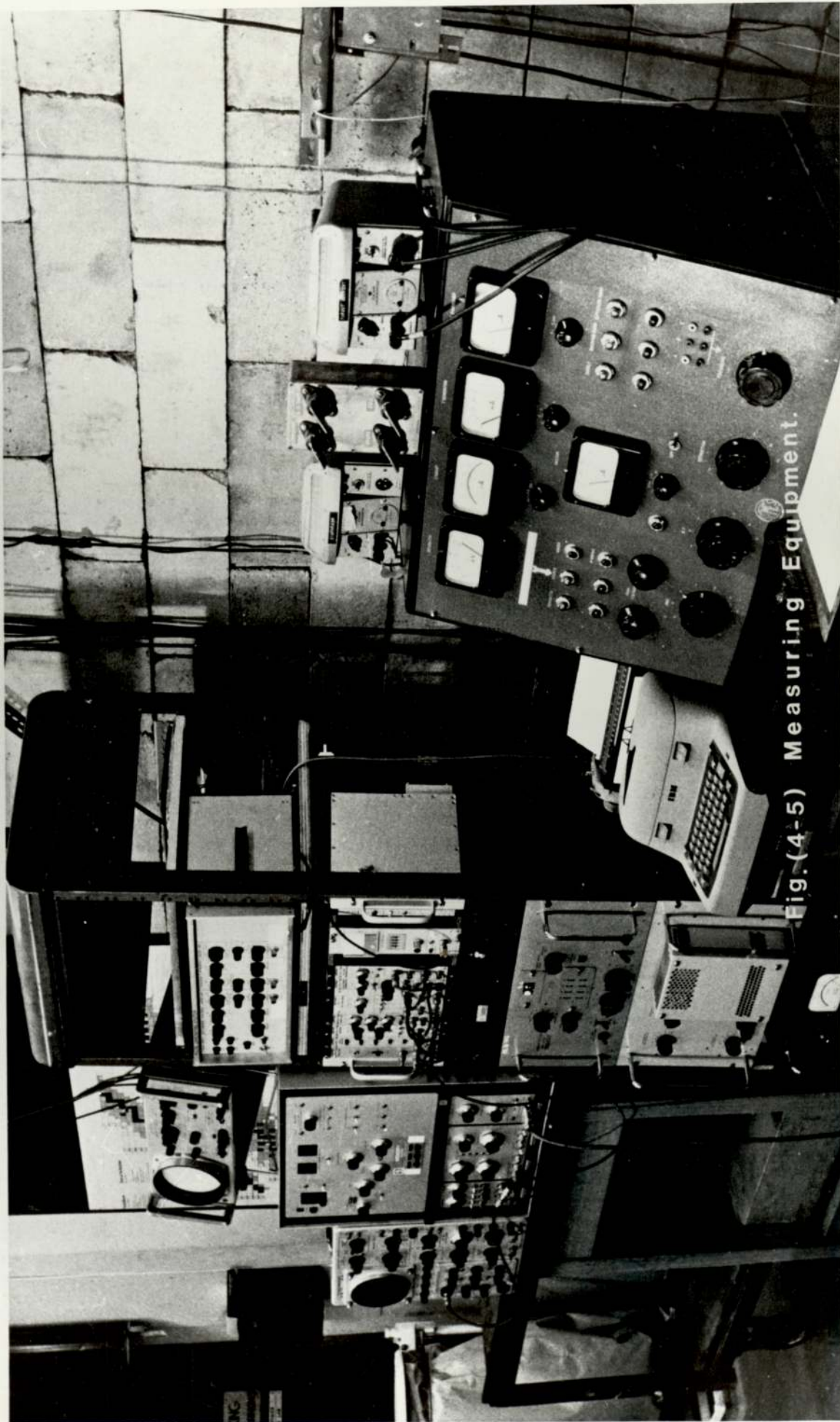


Fig. (4-5) Measuring Equipment.

Therefore, for each practical case, especially when adjusting a new spectrometer a certain run of measurements should be performed to test the spectrometer (spectrometer calibration), if the calibration results in  $D(E) = 1$ , this means the absence of non linear distortions, otherwise the necessary corrections have to be introduced, most conveniently these corrections are introduced into the value of  $P(E)$  and consequently  $dP/dE$ .

Thus, to adjust, calibrate and measure the constants for a new spectrometer, a set of measurements and tests have to be performed. Such measurements which were carried out for the spectrometer are described as follows.

#### 4.5.1. Spectrometer Linearity

The spectrometer linearity was tested by means of gamma ray sources  $^{137}\text{Cs}$ ,  $^{22}\text{Na}$ ,  $^{60}\text{Co}$  and also with gamma rays of 4.43 MeV accompanying the formation of neutrons in  $^{241}\text{Am}-\alpha\text{-Be}$  source. The pulse amplitude (channel number) is plotted against the maximum energy of the Compton electron ( $E_{\text{max}}$ ) generated as a result of the Compton scattering process with the scintillator. For gamma quanta of energy  $E_0\gamma$ , the value of  $E_{\text{max}}$  can be calculated as:

$$E_{\text{max}} = E_0\gamma - \frac{E_0\gamma}{1 + \frac{2E_0\gamma}{0.51}} \quad \dots \dots \dots 4.3$$

where  $E_{\text{max}}$  and  $E_0\gamma$  are measured in MeV.

The value of the maximum energy ( $E_{\text{max}}$ ) is taken according to the prescription of Flynn et al <sup>(27)</sup> is approximately 13% above the Compton edge half-height for our system.

Figure 4.6 shows the relation between the pulse amplitude and  $E_{\text{max}}$  over a wide range of amplification of the main amplifier. It is clear that the spectrometer remained linear over this wide range of energy and magnification.

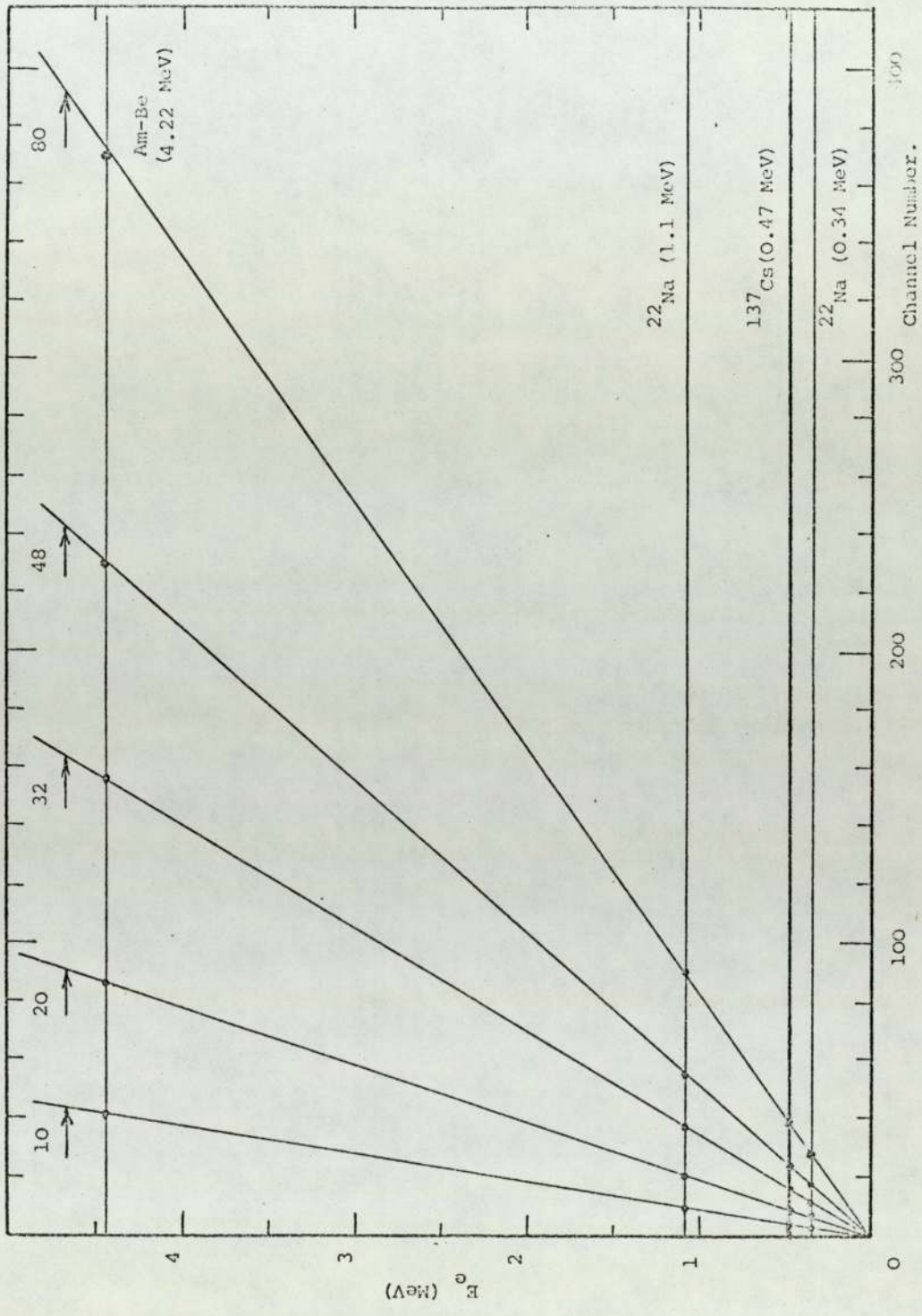


Figure 4.6. Relations between Pulse Amplitude and Electron Energy  $E_{\text{max}}$  for different amplifications.

#### 4.5.2. Relation between Recoil Proton and Electron Pulses

This was determined at two specific neutron energies by using a monoenergetic beam of neutrons of energies 14.13 MeV from  $T(d,n)^4\text{He}$  and 2.48 MeV from  $D(d,n)^3\text{He}$  reactions and with gamma ray sources to determine the relationship between electron and proton energies which give the same pulse height. The measured values of pulse height for these two specific neutron energies are compared with those given by other workers (45,58,61,68), after normalising their data to the present experimental value at 14 MeV. The relations between pulse height and particle energy are presented in figure 4.7. A good agreement between the measured values and that of the others can be seen from this figure. Thus the relation between the pulse height and energy of the proton recoil can be calculated from these two formulae derived from those given by Maier et al (68) 1968. These are given as:

$$E_p = 3.48 E_e^{2/3} \text{ for } E_e < 1.85 \text{ MeV} \quad \dots \dots 4.4$$

$$E_p = 1.78 (E_e + 1.1) \text{ for } E_e > 1.85 \text{ MeV} \quad \dots \dots 4.5$$

Based on these two equations the pulse height spectrum in the analyser can be converted to an energy distribution of recoil protons.

#### 4.5.3. Gain Standardization and Energy Scale

Gain standardization is one of the most troublesome problems in reproducing the experiment measurements. This was ensured during these measurements by measuring the  $^{22}\text{Na}$  pulse height spectrum before and after each neutron measurement.

The energy scale or channel width of the analyser was also found by measuring the pulse height of the Compton electrons. A check was also made on the assumed calibration by measuring the spectrum of neutrons from a standard source. This was carried out in our case by

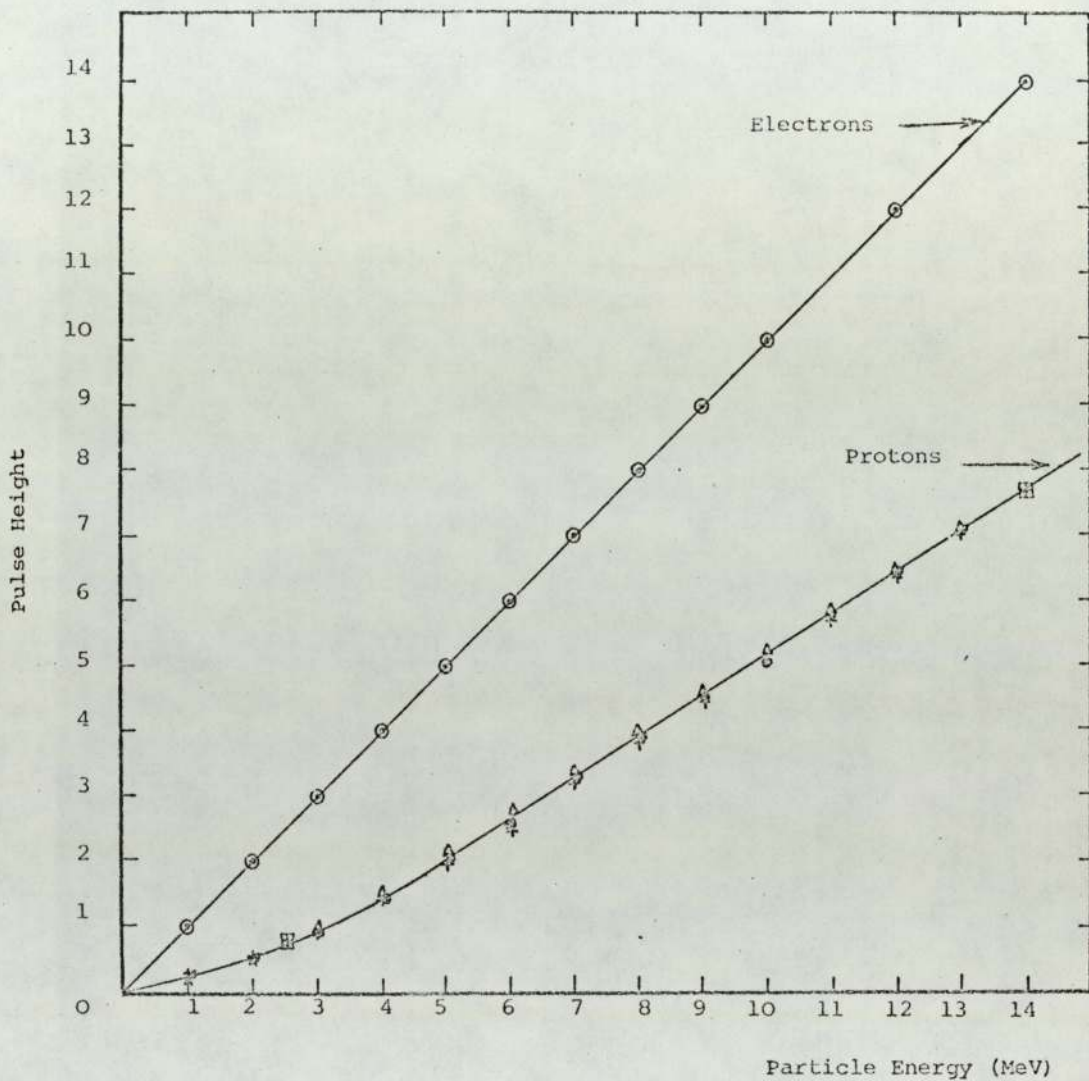


Figure 4.7. Relationships between pulse height and energy for electrons and protons

- ⊙ Verbinski et al (1968)
- + Batchelor et al (1961)
- △ Smith et al (1968)
- Maier et al (1968)
- Present Work

(All normalized to our results at 14 MeV)

using a  $^{241}\text{Am}$ - $\alpha$ -Be source and is discussed hereafter.

#### 4.5.4. Discrimination Capability

The spectrometer sensitivity to rejection of gamma background was tested by using gamma rays from  $^{60}\text{Co}$  and neutron and gamma rays from Am-Be source. The  $^{60}\text{Co}$  source has a strength of about  $1\ \mu\text{Ci}$  and a dose rate of about  $0.6\ \text{m rad h}^{-1}$  at a distance of 5 cm which is the distance between the source and detector. The neutron source has a neutron yield of about  $2.5 \times 10^6\ \text{ns}^{-1}$  and a gamma dose at the distance from the detector (50 cm) of about  $10\ \text{m rad h}^{-1}$ .

Measurements were carried out for Am-Be and  $^{60}\text{Co}$  and another for Am-Be only, in both cases the measurements were performed with and without PSD. When the PSD was used to discriminate against gamma rays the pulse height distribution due to gamma rays from  $^{60}\text{Co}$  was entirely eliminated from the measured spectrum as shown in figure 4.8. The remaining pulse height spectrum is identical with that from the Am-Be source when PSD was used to eliminate the 4.43 gamma rays from the de-excitation of  $^{12}\text{C}$ .

#### 4.6 Corrections for losses in electronics

Another important calibration consisted of measuring the correction factors for losses due to the electronics used to separate proton pulses from gamma pulses. This was performed for the present spectrometer by measuring the pulse height distributions from the  $\text{T}(d,n)^4\text{He}$  reaction both with and without the use of the neutron gamma ray discriminator. The two differ only by the losses due to the pulse shape discriminator since essentially no gamma ray pulses occurred in this reaction. The ratio between the two was used to eliminate the distortion due to pulse shape discrimination. Figure 4.9 presents the two pulse height distributions of the 14 MeV neutron measured with and without PSD.

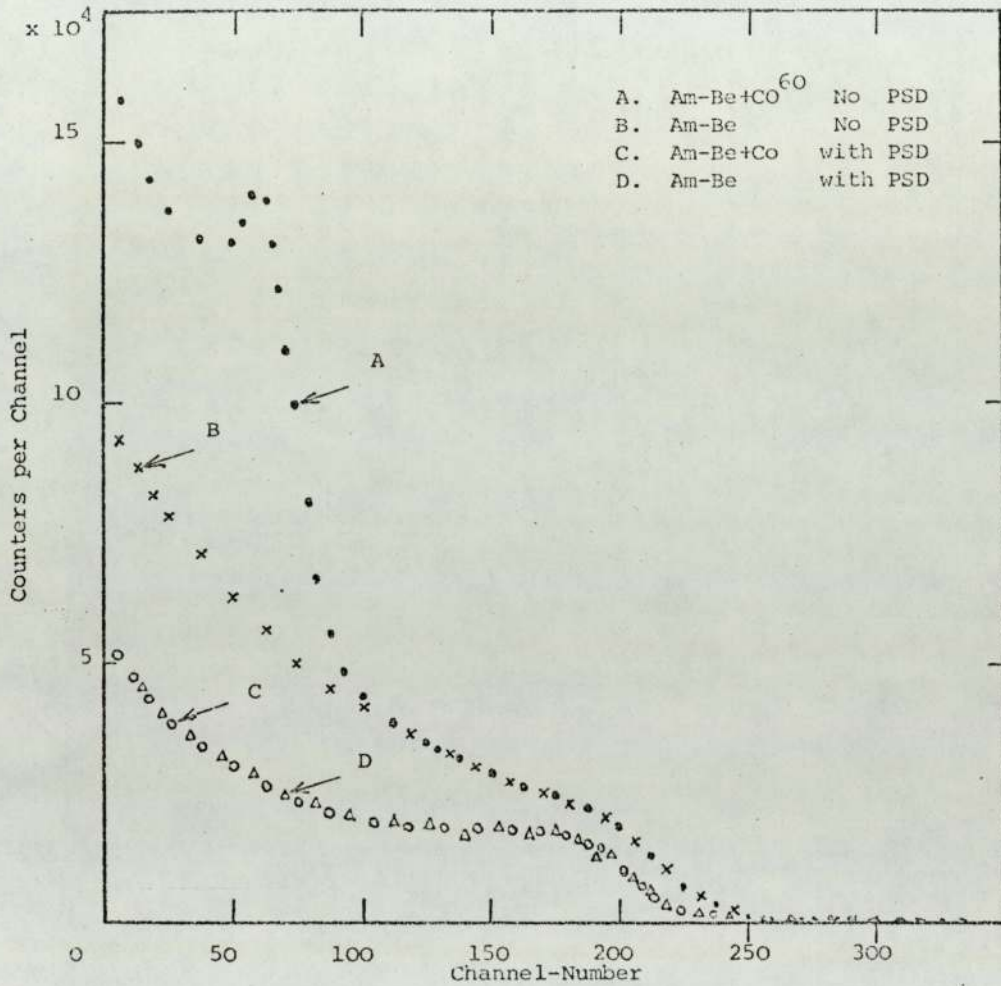


Figure 4.8. Pulse Height Distribution in NE-213 Bombarded Simultaneously with Neutrons and Gamma Rays. The anticoincidence zero crossing method has been used to eliminate gamma induced events.

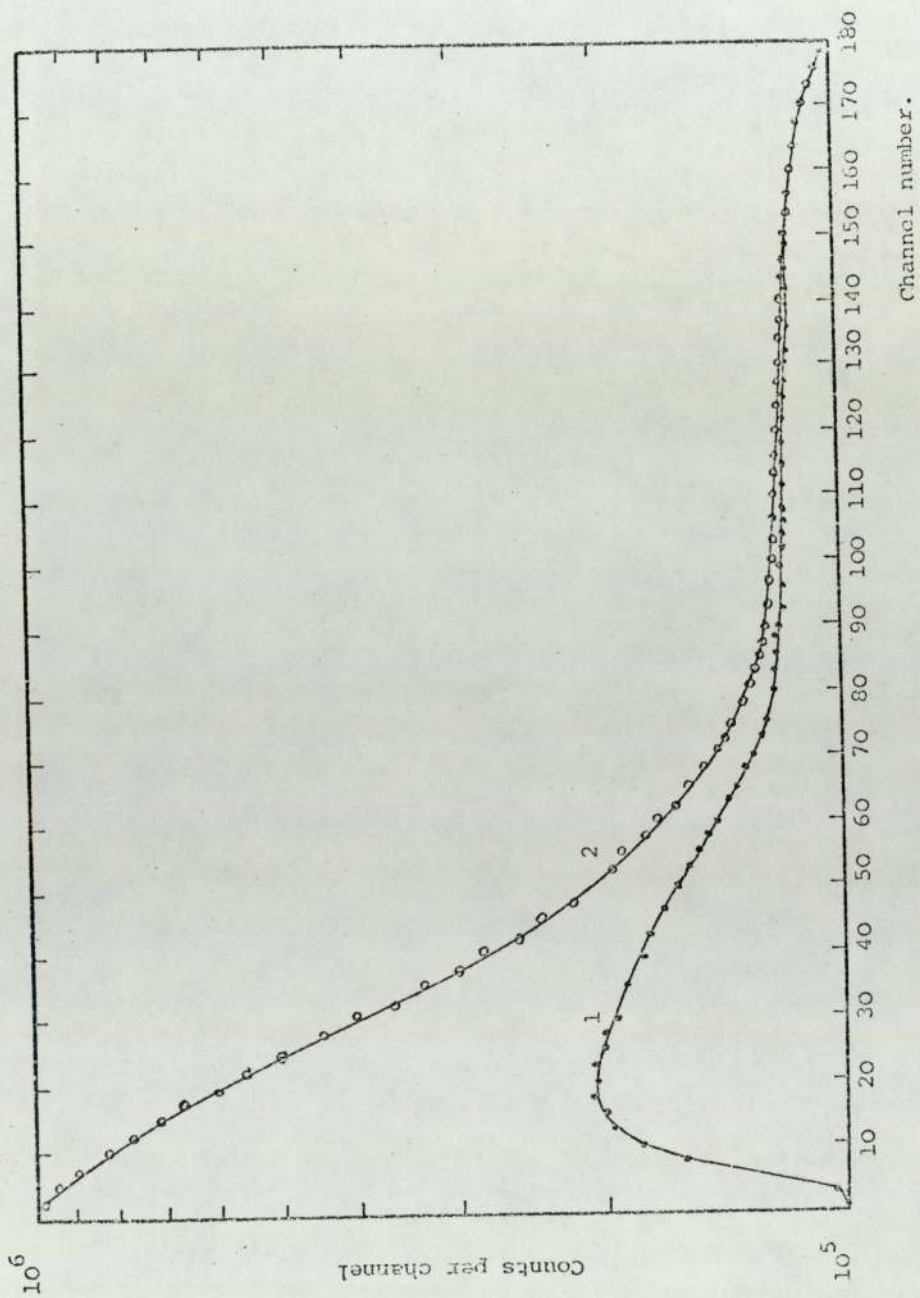


Figure 4.9. Pulse Height Distributions of 14 MeV Neutrons Measured with (1) and without (2) Pulse Shape Discrimination.

4.7 Detector Efficiency

In organic scintillators neutrons are detected by the charge deposited by protons recoiling from collisions with neutrons. The efficiency for this process, in accordance with Swartz and Owen<sup>(19)</sup> is:

$$\epsilon_n = n_H \sigma_{n,H} (1 - e^{-aL}) / a \quad \dots \dots \dots 4.6$$

where L = the detector length in cm and

$$a = n_H \cdot \sigma_{n,H} + n_C \cdot \sigma_{n,c}$$

The NE-213 scintillator used in this work has the parameters:

$$\text{Chemical formula} = (\text{CH}_{1.21})_n$$

$$\text{Density} = 0.867 \text{ gm. cm}^{-3}$$

number of hydrogen nuclei,

$$N_H = 0.04826 \times 10^{24} \text{ atoms.cm}^{-3}$$

and a number of carbon nuclei

$$N_C = 0.039862 \times 10^{24} \text{ atoms.cm}^{-3}$$

The values of  $\epsilon_n$  were calculated using the above formula for neutron energies between 0.1 - 15 MeV. The data of scattering cross section for hydrogen were obtained from the relation of Wasson<sup>(81)</sup> 1968 as:

$$\begin{aligned} \sigma_{n,H} = & 5.603 (1 + 7.417E + 0.1105 E^2) \\ & + 0.8652 / (1 + 0.2427E + 0.0028E^2) \text{ barns/atom} \end{aligned}$$

and the total neutron cross sections for carbon  $\sigma_{n,c}$  were taken as in reference<sup>(60)</sup>. The calculated values of  $\epsilon_n$  against neutron energy  $E_n$  are plotted in figure 4.10.

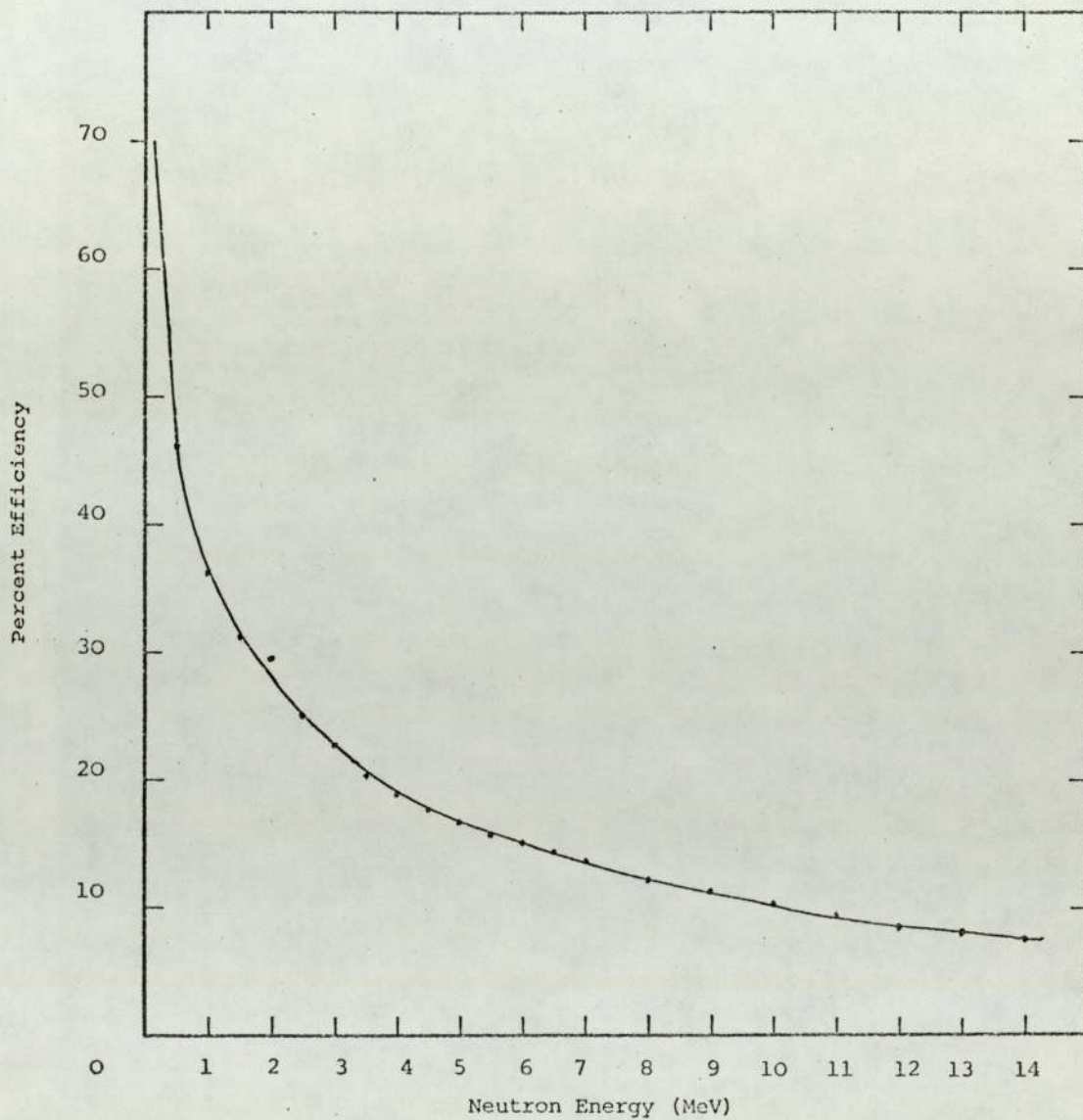


Figure 4.10. Neutron Efficiencies for NE-213 of 1" length

#### 4.8 Corrections for Scintillator Size

Most of the analytical methods used to transform the pulse amplitude distribution into neutron energy distribution contain a correction factor B which depends on the scintillator size and is a function of neutron energy. This factor contains the effect of second scattering from hydrogen and wall effects (protons which lose only part of their energy in the scintillator). These two effects are treated together since they both depend upon scintillator size. As scintillator size increases second scattering becomes more important while wall effects become less important. In accordance with Brock and Anderson<sup>(82)</sup> this factor is:

$$B = 1 - 0.78 \frac{R_m}{L'} + 0.09 n_H \sigma_{n,H} L + 0.077 n_H \cdot \frac{\sigma_{n,H}^4 r^4}{\eta_H} \quad 4.7$$

where  $R_m$  = the range of a proton in  $\text{mg.cm}^{-2}$ ,

This is calculated using the relation given by Schutter<sup>(43)</sup>, 1966

$$R_m = 1.7382 (E + 0.15045)^{1.8194} \text{ mg.cm}^2 \quad \dots \dots \dots 4.8$$

$r$  = the scintillator radius in cm.

$L'$  = the scintillator thickness in  $\text{mg.cm}^{-2}$ .

$L$  = the scintillator thickness in cm.

$n_H$  = the number of hydrogen atoms  $\text{cm}^{-3}$  and

$\sigma'_{n,H}$  = the value of the microscopic cross section of hydrogen ( $\sigma_{n,H}$ ) at 0.068E.

In the above equation the second term is the correction for wall effect and the last two terms are the corrections for second scattering.

This correction factor was calculated over a range of proton energies (0 - 15 MeV) for the NE-213 scintillator which was used in this spectrometer and was applied to the unfolded neutron spectrum to eliminate

the distortion effects due to the scintillator size. The variation of this correction factor with neutron energy for the NE-213 scintillator used in this work is given in figure 4.11.

#### 4.9 Unfolding Methods

Usually, the experimental data given by any spectrometric measurements do not produce directly the desired information on the energy distribution of the recorded particles. Most often, to obtain such information, the raw data must be interpreted and unscrambled before an evaluation of the quantities which the experiment was designed to measure, can be obtained. This is the situation in the measurement of the energy spectrum of neutrons whenever the detection system is based on the proton recoil technique. The experimental pulse amplitude distribution collected in this type of neutron energy spectrometry are directly related to the energy spectrum of the recoil protons. An appropriate analysis or unfolding method must therefore be performed on the measured pulse amplitude distribution to evaluate the neutron energy spectrum. In this work the method of differentiation is used. This is considered as the simplest and most accurate method<sup>(59)</sup>.

Assume that a scintillator of thickness  $d$ , receives in unit time a number of neutrons  $\phi_o$  of energy  $E_{no}$ . The number of recoil protons in unit time due to a single scattering event is given by:

$$N = \phi_o \left[ 1 - \exp(-\Sigma \cdot d) \right] \dots \dots \dots 4.9$$

where  $\Sigma$  is the macroscopic total scattering cross section of neutrons by hydrogen nuclei in a scintillator.

With the assumption that neutron scattering in the centre of mass system is spherically symmetrical as is the real case up to  $E_{no} \sim 15$  MeV<sup>(19)</sup>, the number of recoil protons with energy  $E$  in the unit energy interval is:

$$N(E) = \phi_o \cdot (1 - e^{-\Sigma d}) / E_{\max} \dots \dots \dots 4.10$$

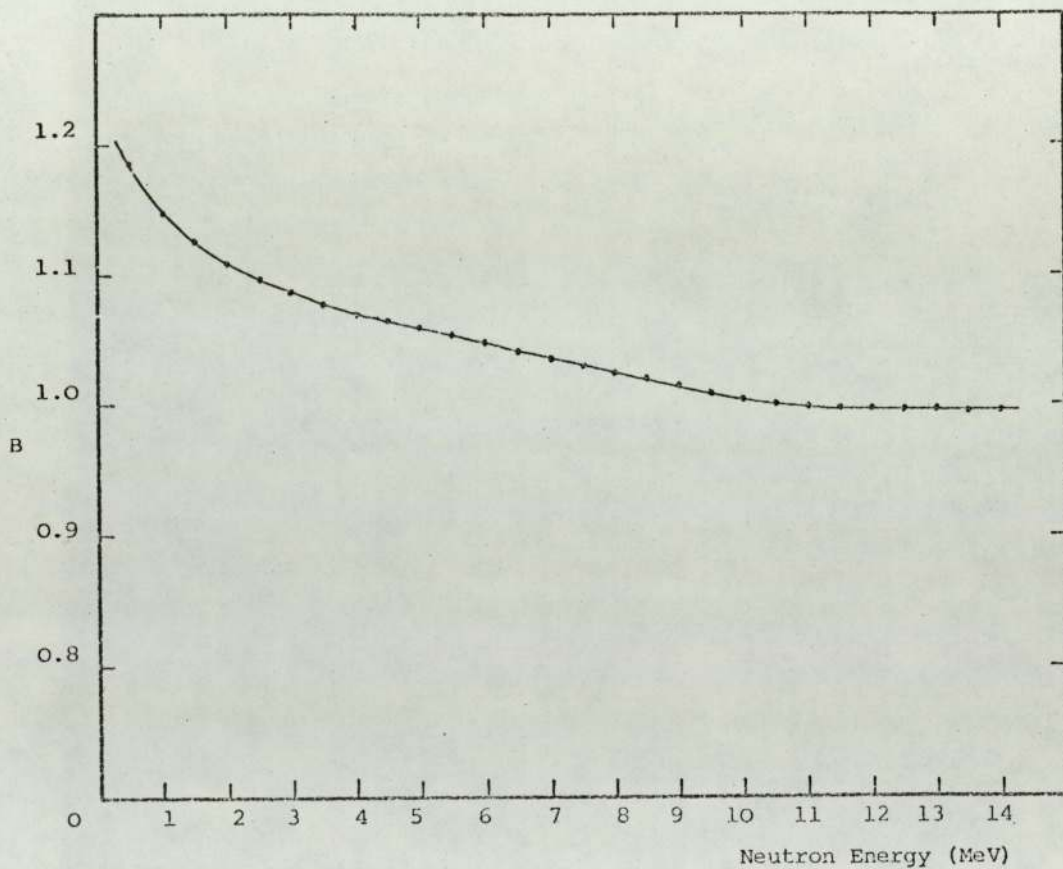


Figure 4.11. Shape Correction Factors for the N-213 Scintillator used for the Measurements,  $3/2$ " diameter by 1" long ( $28.956 \text{ cm}^3$ ).

Since the maximum value of energy which the recoil proton can gain from the scattering of neutrons by hydrogen nuclei is equal to the neutron energy  $E_{no}$ , therefore:

$$N(E) = \phi_o (1 - e^{-\Sigma d}) / E_{no} \quad \dots \dots 4.11$$

If the scintillator receives neutrons of a complicated energy spectrum  $\phi_o(E_n)$ , recoil protons of energy E will be generated by neutrons of different energy starting from  $E_n = E$ . In this case the number of recoil protons in a unit energy interval is:

$$N(E) = \int_E^\infty \frac{\phi_o(E_n) \cdot (1 - e^{-\Sigma d})}{E_n} dE_n \quad \dots \dots 4.12$$

Differentiating this equation:

$$\frac{dN(E)}{dE} = \frac{\phi_o(E_n) \cdot (1 - e^{-\Sigma d})}{E_n}$$

or

$$\phi_o(E_n) = \frac{dN(E)}{dE} \cdot \frac{E_n}{(1 - e^{-\Sigma d})} \quad \dots \dots 4.13$$

This means that the neutron spectrum can be obtained from the energy distribution of the recoil protons by differentiation.

Experimentally, the measured data are the pulse amplitude distribution  $N(V)$  but not the recoil proton energy distribution  $N(E)$ . However, these values are unambiguously inter-related. Assume that protons of energy E produce pulses of amplitude V. Therefore the number of such protons in the interval dE should be equal to the number of pulses with amplitude V within the interval dV, i.e.

$$N(E) \cdot dE = N(V) \cdot dV$$

or

$$N(E) = N(V) \frac{dV}{dE} \quad \dots \dots \dots 4.14$$

The derivative over E from this equation is:

$$\begin{aligned} \frac{dN(E)}{dE} &= \frac{d}{dE} \left[ N(V) \frac{dV}{dE} \right] \\ &= \frac{d}{dV} \left[ N(V) \frac{dV}{dE} \right] \frac{dV}{dE} \quad \dots \dots \dots 4.15 \end{aligned}$$

substituting this value into equation 4.13 therefore:

$$\phi_o(E_n) = \frac{d}{dV} \left[ N(V) \frac{dV}{dE} \right] \cdot \frac{dV}{dE} \cdot \frac{E_n}{(1 - e^{-\Sigma d})} \quad \dots \dots \dots 4.16$$

By differentiating equation 4.1 with respect to energy and substituting the value of  $\frac{dV}{dE}$  into equation 4.16, then this equation becomes

$$\phi_o(E_n) = \frac{E_n}{A(1 - \exp(-\Sigma d))} \cdot K^2 \cdot \frac{d}{dV} \left[ N(V) \frac{dP}{dE} \right] \frac{dP}{dE} \cdot \frac{1}{B} \dots 4.17$$

where K = the constant in equation (4.1) and is the relation between pulse height and light output.

A = the scintillator area in  $\text{cm}^2$  and

B = the correction factor for scintillator size

In fact, such transformation is made for an idealized form of recoil proton energy distributions. However, many experiments have shown this approach to be reasonably accurate for measuring real neutron spectra<sup>(59,67)</sup>.

Naturally, the real pulse amplitude distribution even for monoenergetic neutrons is impossible to describe analytically. For this reason, numerical methods have to be used for the determination of the derivative. This circumstance is a source of pronounced errors,

especially with a small step of differentiation and insufficient statistics. To minimize such errors, Kazanisky et al<sup>(59)</sup> suggested the least squares method for the determination of the derivative. In this method the spectrum is expressed over five adjacent points with a pitch  $\Delta V$  in the form of a second order parabola, then

$$\frac{d}{dV} \left[ N(V) \frac{dV}{dE} \right] = \frac{d}{dV} f(V_i)$$

$$= \frac{2f(V_{i-2}) + f(V_{i-1}) - f(V_{i+1}) - 2f(V_{i+2})}{10 \cdot \Delta V} \dots 4.18$$

Thus the analysis of the result was reduced to a multiplication of the measured pulse height  $N(V)$  by  $\frac{dP}{dE}$  for each channel, then differentiating with respect to pulse height followed by multiplication by the correction factor for the efficiency.

The dependence of the photomultiplier pulse height upon the energy of proton recoils was calculated using these two relations given before in (4.5.2).

This method has been used in the present work for a computer program NEUTRSPECT given in Appendix 3, to restore the neutron energy spectra from the measured pulse amplitude distributions.

#### 4.10 Smoothing of Data

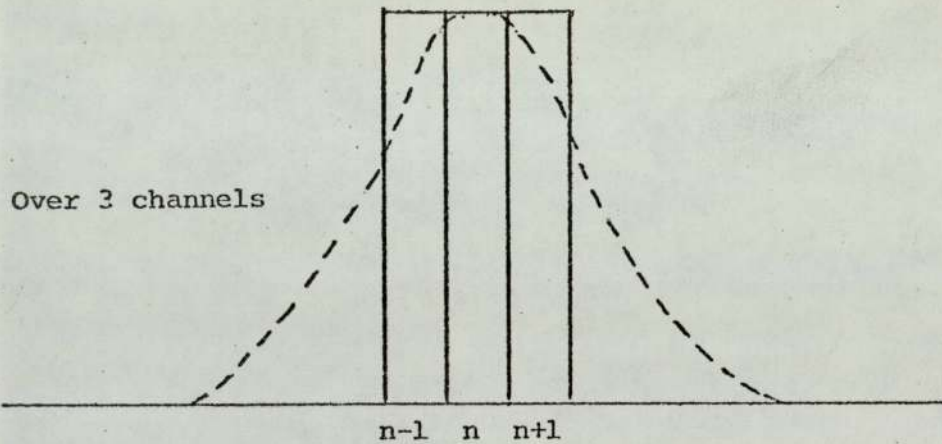
The measured pulse amplitude data contain fluctuations which are produced in the detection system and associated experimental equipment. These fluctuations, if ignored, may give fluctuations in the spectrum which have a larger amplitude than the structure of the actual neutron spectrum. Therefore, the measured apparatus spectrum has to be smoothed before using the unfolding method. This was performed in the present work by the following method, assuming a Gaussian distribution over 3, 5 or 7 channels and taking a weighted average, as overleaf.

This method reduces the effect of statistical uncertainties in any one point at the expense of broadening the energy resolution. Since pulse height is not linearly related to proton energy the effect on energy resolution varies throughout the energy range. The standard deviation of the averaging functions used is:

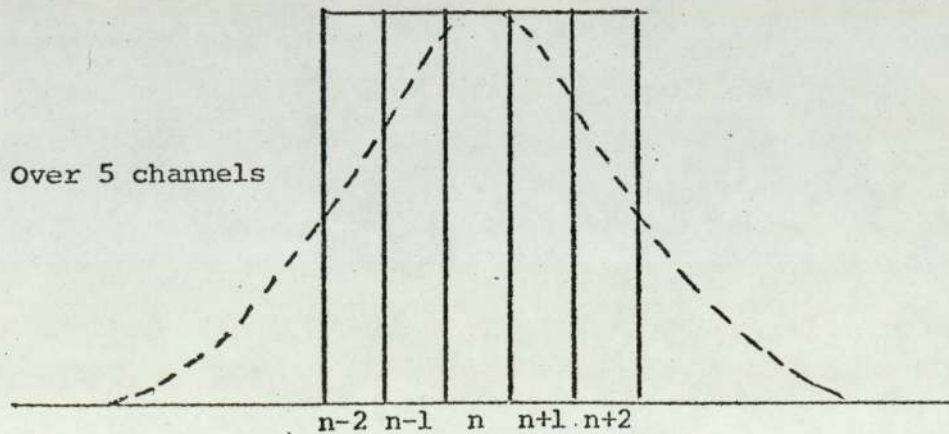
3 points  $\pm$  1 channel width

5 points  $\pm$  1.5 channel width

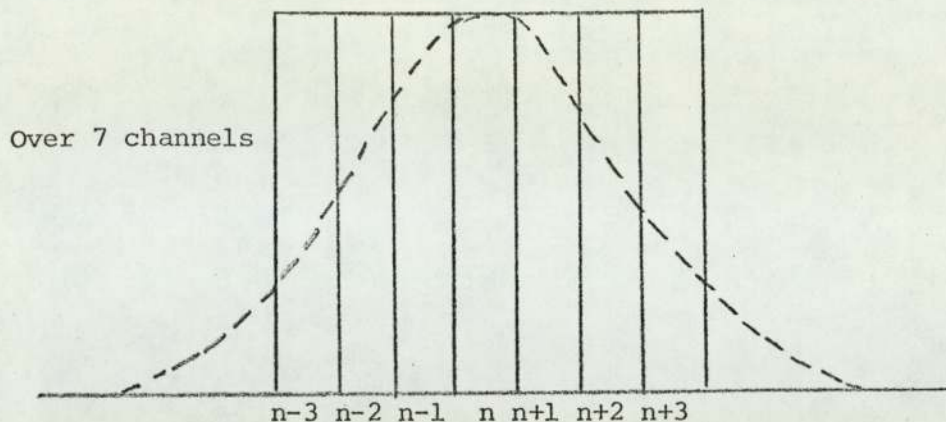
7 points  $\pm$  2 channel width



$$\bar{C}_n = 0.5 \times C_n + 0.25 (C_{n-1} + C_{n+1})$$



$$\bar{C}_n = 0.312 \times C_n + 0.229 (C_{n-1} + C_{n+1}) + 0.111 (C_{n-2} + C_{n+2})$$



$$\bar{C}_n = 0.236 \times C_n + 0.198 (C_{n-1} + C_{n+1}) + 0.117 (C_{n-2} + C_{n+2}) + 0.067 (C_{n-3} + C_{n+3})$$

#### 4.11 Effect of Statistical Uncertainties in Counts

The uncertainty in the measured pulse height distribution due to the statistical processes in the interaction of neutrons with the scintillator has been checked using the standard deviation method. This was performed by re-analysing the pulse amplitude distribution for one measurement after alternating the number of counts ( $n$ ) per channel to  $n \pm \sqrt{n}$ . The given data show that for high counts there is no significant difference between the analysed neutron spectra. The maximum variation observed was  $< 4\%$  between extreme results (typically  $< 1\%$ ) at about 1000 counts per channel - typical of the high energy end of the pulse height distribution. The smoothing of the raw data was carried out over each 5 channels and the given analysed spectrum was averaged over 3 adjacent channels.

#### 4.12 Test with $^{241}\text{Am}$ - $\alpha$ -Be Source

A useful check of the validity of the measuring and unfolding techniques is to measure the continuous spectrum of neutrons from a standard neutron source. By analysing the position of maxima and minima in the neutron energy distribution and comparing these with known peaks in the distribution a check on the calibration can be made.

To calibrate the spectrometer which was used in the present work, a neutron spectrum of 1 Ci  $^{241}\text{Am}$ - $\alpha$ -Be source has been measured with

threshold energy range  $\sim 0.5$  MeV. The source is supplied by Radio-Chemical Centre, Amersham, U.K., and has a yield of  $2.5 \times 10^6$  n/sec. The source was covered by a 3 mm lead sheet to cut off the 60 KeV gamma rays from  $^{241}\text{Am}$ . Since it was not possible to perform the measurement with the scattering objects at distances more than 1 m away from the detector and the source, the method of shadow bar was used to eliminate the undesired scattered neutrons from the source spectrum. In that method the neutron spectrum is measured once with the source at 50 cm distance from the detector, then followed with another measurement with a bar of paraffin and boric acid placed along the axis between the source and the detector. This paraffin bar has a length of 25 cm and a diameter which is slightly greater than the source diameter. In both cases the measurements were carried out under the same conditions. The data given with the latter measurement is then subtracted from the previous one and, thereby eliminated the back scattered neutrons from the original source spectrum.

Figure 4.12 presents the present Am-Be spectrum after analysing the measured recoil proton spectrum with another measured one using a stilbene scintillator<sup>(63)</sup> and another calculated one using the most recent data of neutron angular distributions<sup>(64)</sup>. From this figure it can be seen that our measured spectrum agrees well with the others. The slight differences in the intensities at the observed peaks can be attributed to the different compositions of the sources in the given cases. As seen also from this figure the coincidence in the position of maxima and minima shows the absence of non linear distortions in the electronics of the present spectrometer for the neutron energy range of interest.

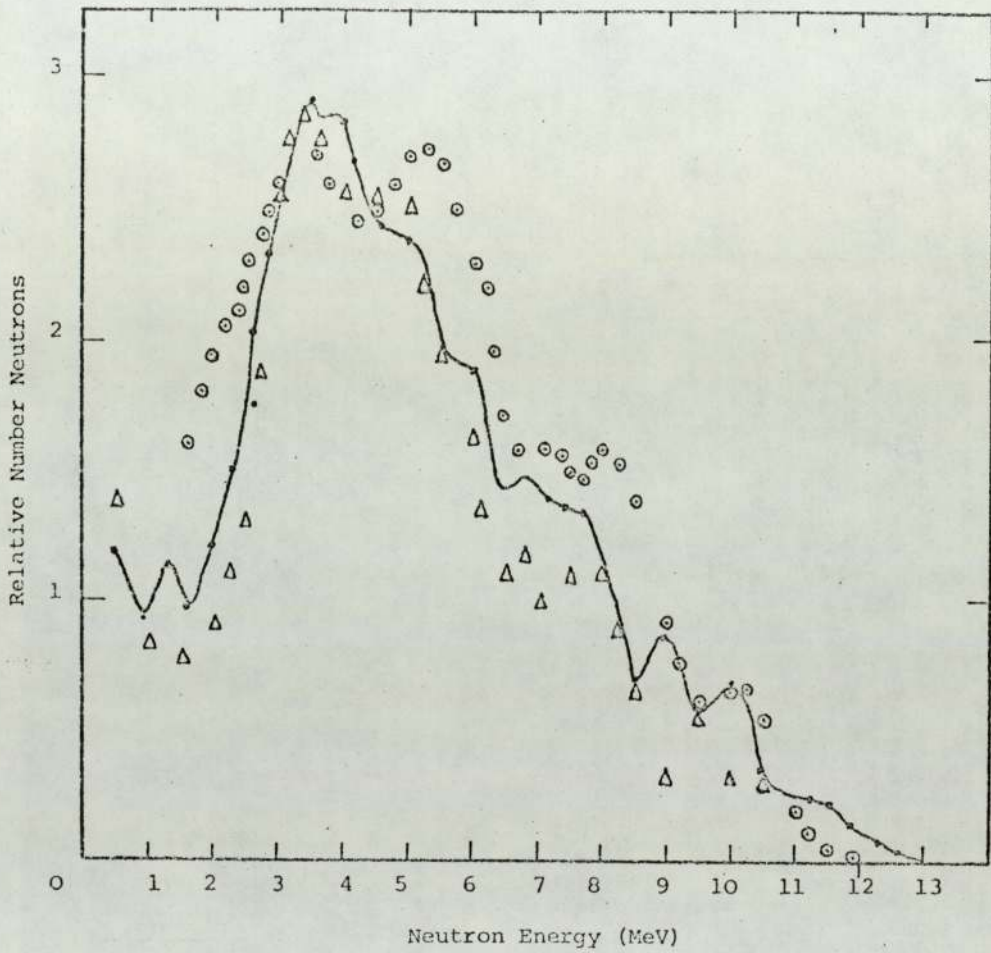


Figure 4.12. Comparison of Neutron Spectrum of Am-Be Source Determined by various methods.

- ~ Present Work
- ⊙ Thompson et al (1965)
- Δ Vijaya et al (1973)

CHAPTER 5SHIELDING ASSEMBLIES AND NEUTRON SOURCE5.1 Introduction

The spectra of fast neutrons which have passed through layers of iron and homogeneous and heterogeneous mixtures of iron-graphite and iron-polypropylene media have been measured for roughly cylindrical assemblies containing a point source of 14 MeV neutrons from the  $T(d,n)^4\text{He}$  reaction. Measurements were performed at the surface of the cylinder along a radius from the source. All measurements have been made with the NE-213 scintillation spectrometer described before in Chapter 4. Measurements have been performed for different thicknesses of these materials in the range 5 up to 40 cm. The intensity of the neutron source was measured by detecting the alpha particle associated with the neutron in the reaction using a plastic scintillator placed at 73 cm in the alpha flight tube.

5.2 Shielding Assemblies

The shielding assemblies were supported horizontally at the edges of a concrete chamber. This chamber is built of concrete bricks. The inner dimensions of the cell were such that the assemblies were securely supported and the walls sufficiently far away to reduce the back scattered neutrons. The wall thickness is quite sufficient to shield against fast neutrons. Figure 5.1 shows the SAMES Accelerator and the experiment assembly.

5.2.1. Iron Assembly

For iron shielding assembly, a mild steel plate of 122 cm x 40 cm and 1.27 cm thick was used to build up the required thickness. The upper and lower parts of the cylinder were mostly made of the larger plates while the sides were made of 5 cm, 10 cm and 15 cm

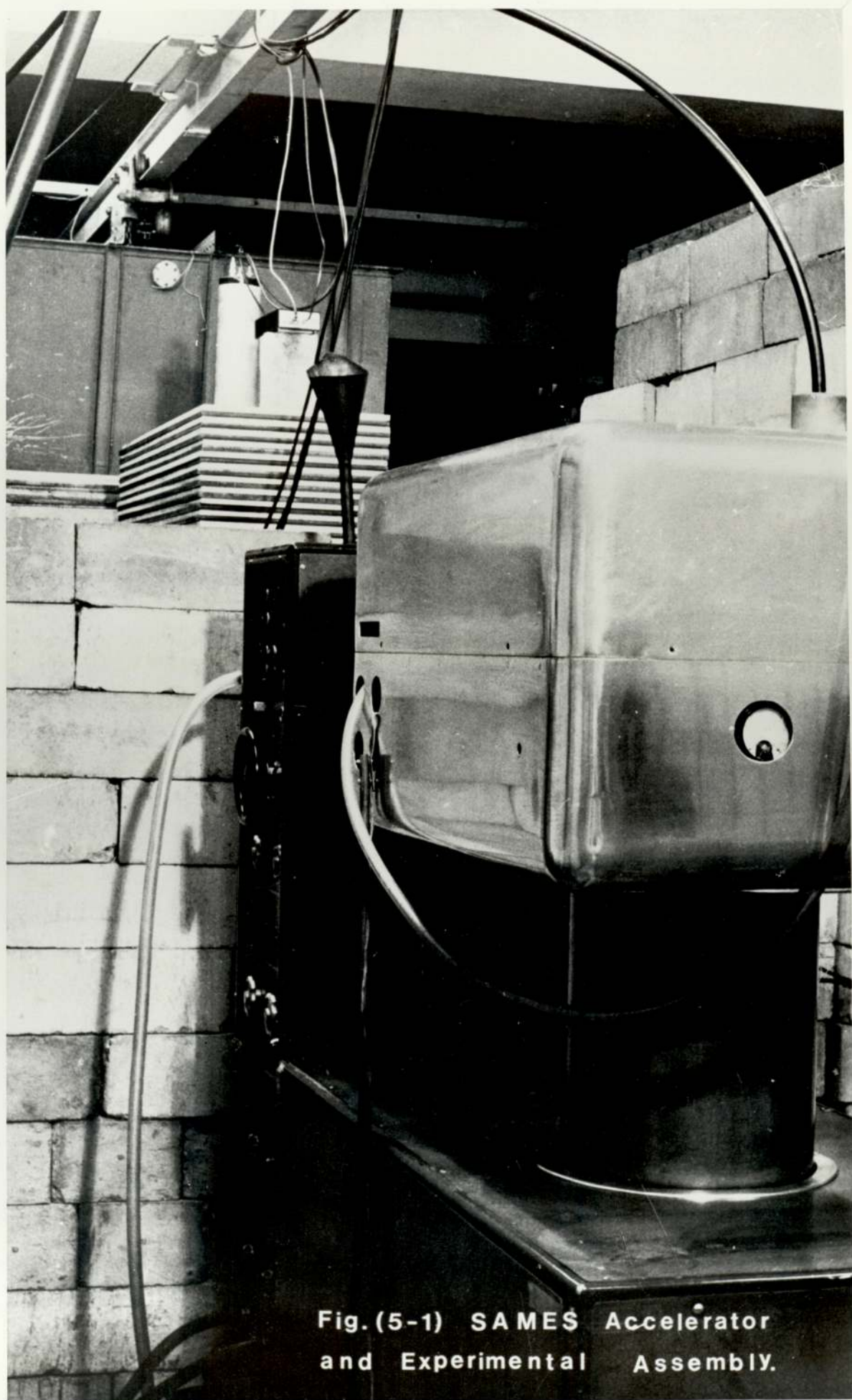


Fig. (5-1) SAMES Accelerator  
and Experimental Assembly.

pieces arranged to give a roughly circular profile of  $\sim 28$  cm diameter. A hole was made on the left side of the cylinder for the alpha flight tube, figures 5.2 and 5.3. The target was placed centrally at  $\sim 14$  cm below the bottom plate. Measurements were carried out for thicknesses 5, 10, 15 ....30 cms with the detector placed adjacent to the surface of the top plate.

#### 5.2.2. "Homogeneous" Media Assemblies

The layout and construction of "homogeneous" media of iron graphite and iron polypropylene shield was similar to those of iron assemblies. In the case of polypropylene assemblies the required thickness was built up by putting an iron plate followed by a polypropylene plate which has the same dimension. This was repeated.

In the case of "homogeneous" media of iron graphite assemblies, the pattern is slightly different from the counterpart of iron polypropylene assemblies. This is due to the fact that graphite was available in the form of 2.54 cm thick plates of 76.2 cm x 5.08 cm wide. In that case the required thickness was obtained by putting two plates of iron followed by one layer of graphite plates.

#### 5.2.3. Heterogeneous Shields Assemblies

The neutron spectra behind a heterogeneous shield can be studied by means of the two layer configurations. Theoretical calculations were performed on heterogeneous media having the two layer and effectively homogeneous configurations of non-graphite and iron polypropylene materials. The calculated data show that for the two layer form, if the first layer is the heavy material, it is more effective on neutron attenuation than the multilayer form of having the same thickness and materials. Thus, in the present work, the measurements were carried out on the two layer configurations as well as effectively homogeneous systems.

In both iron graphite and iron polypropylene shields, the

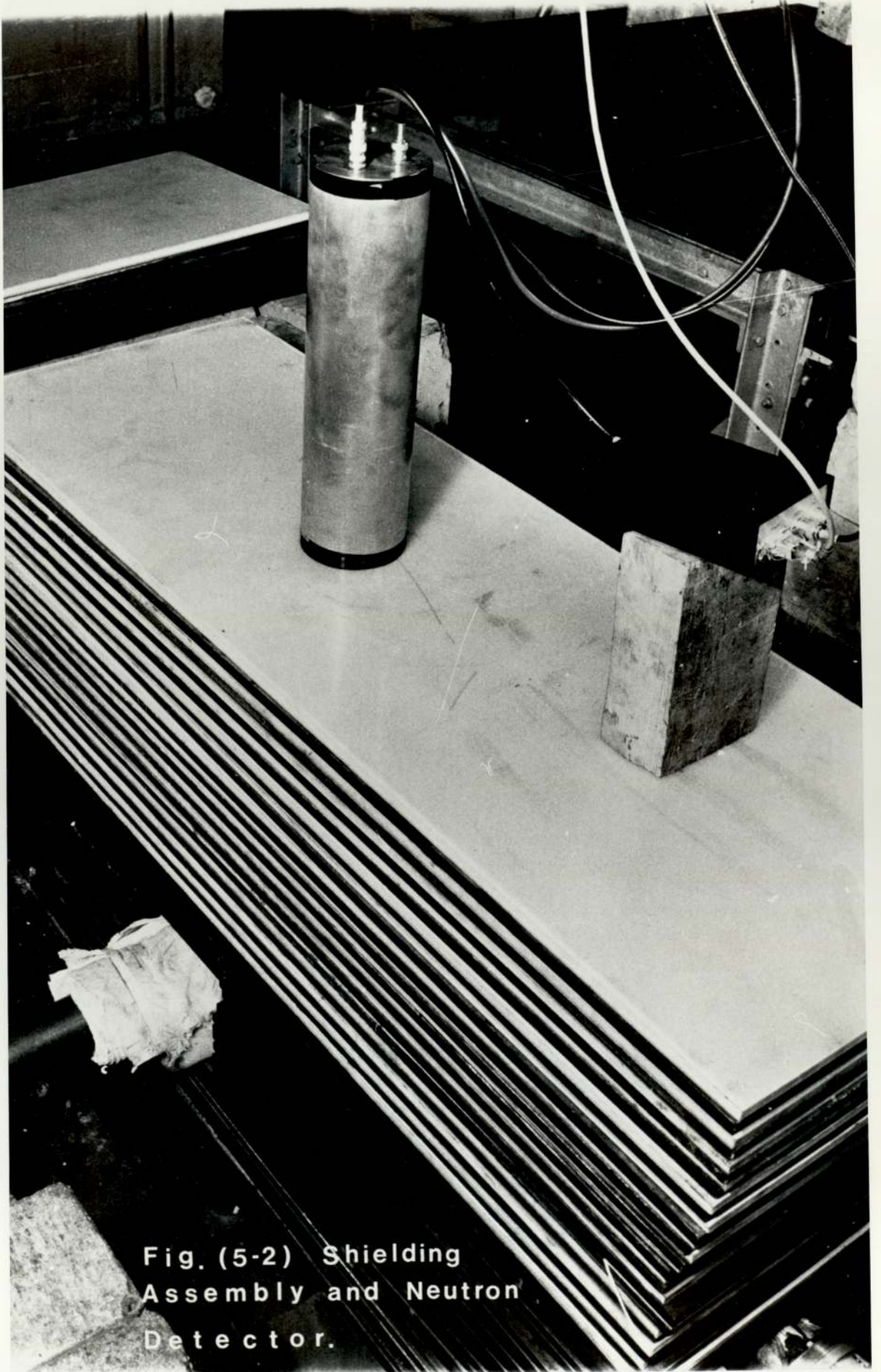


Fig. (5-2) Shielding  
Assembly and Neutron  
Detector.

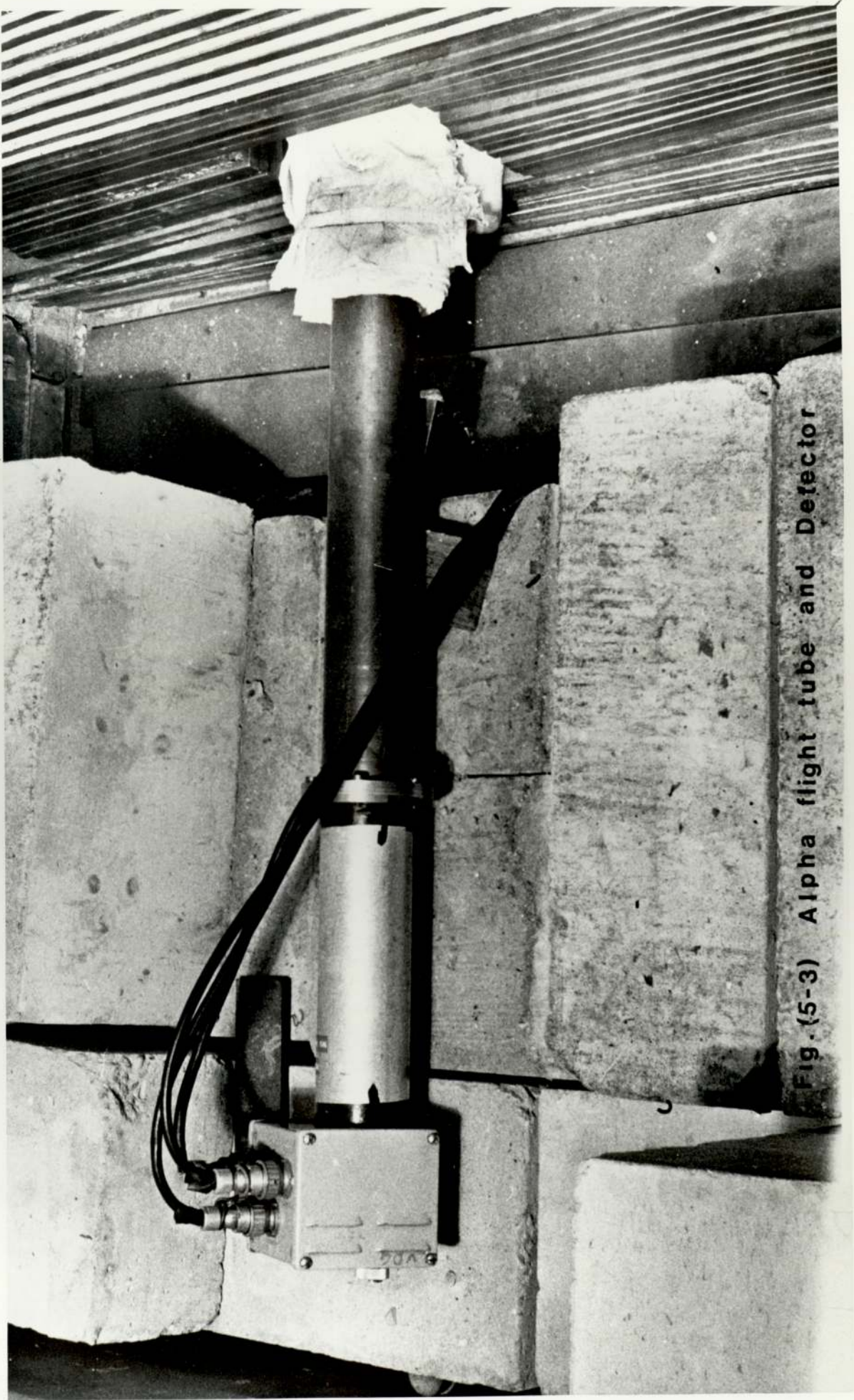


Fig. (5-3) Alpha flight tube and Detector

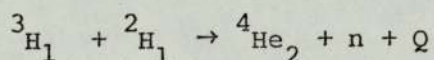
required thickness was obtained by constructing an iron layer followed by a layer of polypropylene or graphite which has the same thickness. For different configurations the thickness of both layers was measured by the same ratio. This allows a two-layer configuration having a 1:1 ratio by volume of both elements.

### 5.3 Neutron Production

Neutrons at an energy of 14.13 MeV, were obtained from the T(d,n)He reaction by the bombardment of a tritium-titanium target with a deuteron beam of energy  $\approx 120$  KeV using a SAMES type-J accelerator<sup>(72)</sup>. Neutrons produced at  $90^\circ$  to the direction of the deuteron beam have energy of about 14 MeV and an energy spread less than 100 KeV.

#### 5.3.1. Neutrons from T(d,n)He Reaction

Neutrons of high energy can be supplied by the T(d,n)He reaction:



This is an exoergic reaction with a Q value of +17.578 MeV. Because of the high Q value, the variation of neutron energy with deuteron energy is very small. At a deuteron energy of about 120 KeV the neutron energy varies around 14.0 MeV at  $90^\circ$  by only about  $\pm 0.5\%$ . The alpha particle produced in the reaction associated with the 14 MeV neutron has an energy of about 3.5 MeV. The kinematics of this type of reaction, tables of energies of the reaction products as well as the conversion factor from the laboratory system to the centre of mass system are available in several works<sup>(73,74,75,76)</sup>.

The variation of neutron energy with the emission angle at different deuteron energies is given by Saker et al<sup>(76)</sup> 1958. A similar calculation was performed to compute the relation between the energy of the emitted neutrons and alpha particles and the angle which

they make with the direction of the incident deuteron for different deuteron energies. Table 5.1 presents the variation of angular energy of neutrons and alpha particles for deuteron energy of 120 KeV. The variation of angular energy of the emitted neutron at different deuteron energies is presented in figure 5.4. The study of this figure indicates that the emitted neutrons are monoenergetic around  $90^{\circ}$  to  $100^{\circ}$  to the direction of the incident deuteron and the energy spread increases in either direction away from this region being maximum in the forward direction ( $0^{\circ}$ ). Also the spread increases with increasing deuteron energy.

### 5.3.2. Target

The targets used are of the type TRT-51, supplied by the Amersham Radio Chemical Centre of the UKAEA. The target has a copper backing disc of 2.82 cm diameter and 0.25 mm thickness. A very thin layer of titanium of 2.5 cm diameter and 6.7 mg/square inch is deposited by vacuum evaporation and tritium is absorbed on this. Titanium absorbs tritium by exothermic occlusion involving the formation of a solid solution and interstitial compounds. The composition of the compound varies from tritium:titanium as from 1:1 to 2:1 in these layers. They can withstand up to  $200^{\circ}\text{C}$  in vacuo<sup>(77)</sup>, beyond which tritium begins to come out. The typical target total activity is about 5 Ci.

There is some uncertainty about the tritium distribution in these targets, but in fact this depends upon the manufacturing technique and conditions. However, the possible distribution of tritium and the average energy and yield are available from the published literature<sup>(78,79,80)</sup> and is relatively unimportant at low bombarding energies from its effect on the emitted neutron spectrum.

### 5.4 Measurement of Neutron Yield by Associated Particle

In measuring the neutron yield by the detection of the associated particles, the knowledge of the angular distribution of the

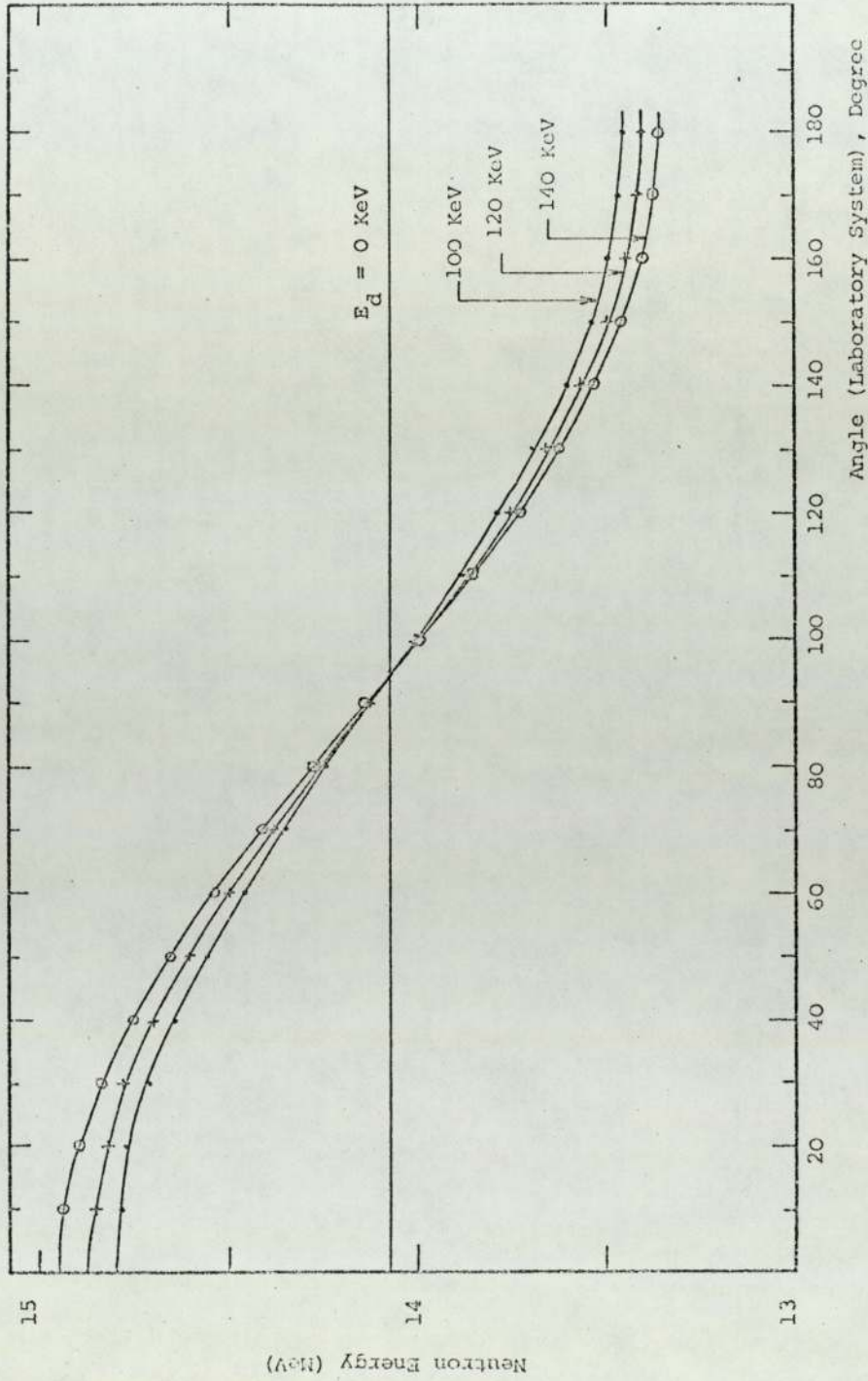


Figure 5.4. Angular Energy Variation of the Neutrons at Different Deuteron Energies from the D-T Reaction.

alpha particles is necessary in order to transform the number of counts to the total yield. For deuteron beams of energy below 200 KeV, the angular distribution of both neutron and alpha particles are isotropic in the centre of mass system, so that the angular distribution in the laboratory system and the degree of anisotropy can be accurately computed, (Table 5.1.). The alpha anisotropy considerations can be by-passed if they are detected at an angle of  $90^\circ$  to the incident deuteron beam, since at  $90^\circ$  the angular distribution in the laboratory system is almost the same as in the centre of mass system. Therefore, at the bombarding energies used in the present work, the alpha detector is placed at  $90^\circ$  to the direction of the deuteron beam. A similar effect is found for neutrons emitted at  $90^\circ$ .

The associated alpha particle emitted in the  $T(d,n)^4\text{He}$  reaction has an average energy of about 3.5 MeV which is high enough for accurate counting by a suitable detector placed facing the target.

In the present work an early attempt was made to count the alpha particles with a silicon surface barrier detector placed inside the beam tube at a distance of 68 cm from the target in the backward direction near the deuteron beam at an angle of  $178^\circ$  to it. Unfortunately it seemed that the detector was affected by either the presence of fast neutrons or more likely secondary electrons produced in the beam tube. It proved impossible to use the SSB for yield measurement during this work due to inconsistent behaviour, particularly loss of gain with time.

After a complete study of the available alpha detectors which are suitable for this geometry it was found that a thin disc of plastic scintillator can be used for such work. The main advantages of the plastic scintillator are its insensitivity to radiation damage, and the possibility of using a very thin piece makes it possible to discriminate against any scattered neutron or electrons. Its disadvantages are that it needs a bulky photomultiplier tube and electronic components in contact with the scintillator. However, this was overcome by using a

Table 5.1

Variations of Angular Energy for Neutrons and Alpha Particles,

Deuteron Energy = 120 KeV

Anisotropy Factor ( $\alpha$ )	Alpha Energy MeV	Angle <sup>o</sup>	Neutron Energy MeV	Anisotropy Factor (n)
1.2193	4.3096	0.000	14.8870	1.0528
1.2157	4.2960	10.000	14.8722	1.0520
1.2049	4.2557	20.000	14.8373	1.0495
1.1873	4.1908	30.000	14.7804	1.0456
1.1638	4.1042	40.000	14.7036	1.0402
1.1353	3.9998	50.000	14.6095	1.0336
1.1029	3.8821	60.000	14.5011	1.0260
1.0678	3.7558	70.000	14.3822	1.0176
1.0312	3.6256	80.000	14.2565	1.0087
0.9946	3.4960	90.000	14.1280	0.9997
0.9588	3.3711	100.000	14.0007	0.9906
0.9252	3.2542	110.000	13.8783	0.9820
0.8944	3.1783	120.000	13.7675	0.9739
0.8673	3.0556	130.000	13.6624	0.9666
0.8444	2.9779	140.000	13.5749	0.9603
0.8263	2.9164	150.000	13.5044	0.9553
0.8131	2.8719	160.000	13.4526	0.9516
0.8051	2.8450	170.000	13.4210	0.9493
0.8024	2.8360	180.000	13.4104	0.9483

flight tube at  $90^\circ$  to accommodate the scintillation counter. The target was inclined at  $45^\circ$  to the direction of both the incident deuteron beam and the axis of the flight tube. This can be seen in figure 5.5.

#### 5.4.1. Scintillator and Measuring System

An 8mm dia x 0.5 mm thick disc of NE-102A plastic scintillator coupled to a 6097B photomultiplier tube was placed inside the flight tube at a distance of  $73.2 \pm 0.1$  cm from the target. A very thin film of aluminium coated polycarbonate was used to exclude light and prevent the passage of the scattered deuterons to the scintillator. A small brass aperture of accurately measured diameter was placed in front of the detector to define the solid angle of the alpha particles with the detector. The output pulses from the photomultiplier anode are applied to a cathode follower which is connected directly to the housing of the photomultiplier. The output signals from the cathode follower were supplied through  $\sim 15$  m cable to the input of an amplifier, type 1430 A. After amplification, the alpha pulses were counted by a scaler, type 1009 E, which was biased to discriminate against any undesired noise pulses. A block diagram of the electronics used for detecting and counting the alpha particles is shown in figure 5.6.

#### 5.4.2. Geometry Factor

In order to determine the real number of alpha particles and in turn the absolute number of neutrons during certain measurement, the number of alpha counts by the detector have to be reduced by a factor which is called the geometry factor. This factor depends on the solid angle which the detector made with the source, i.e., the detector area and the distance of the detector from the source.

Assuming that  $S_0$  is the source strength of an isotropic  $\alpha$ -source in the laboratory system,  $C_\alpha$  is the alpha particle counts by the detector at R cm away from the source and having a circular aperture of diameter D held normally to the line joining it with the source.

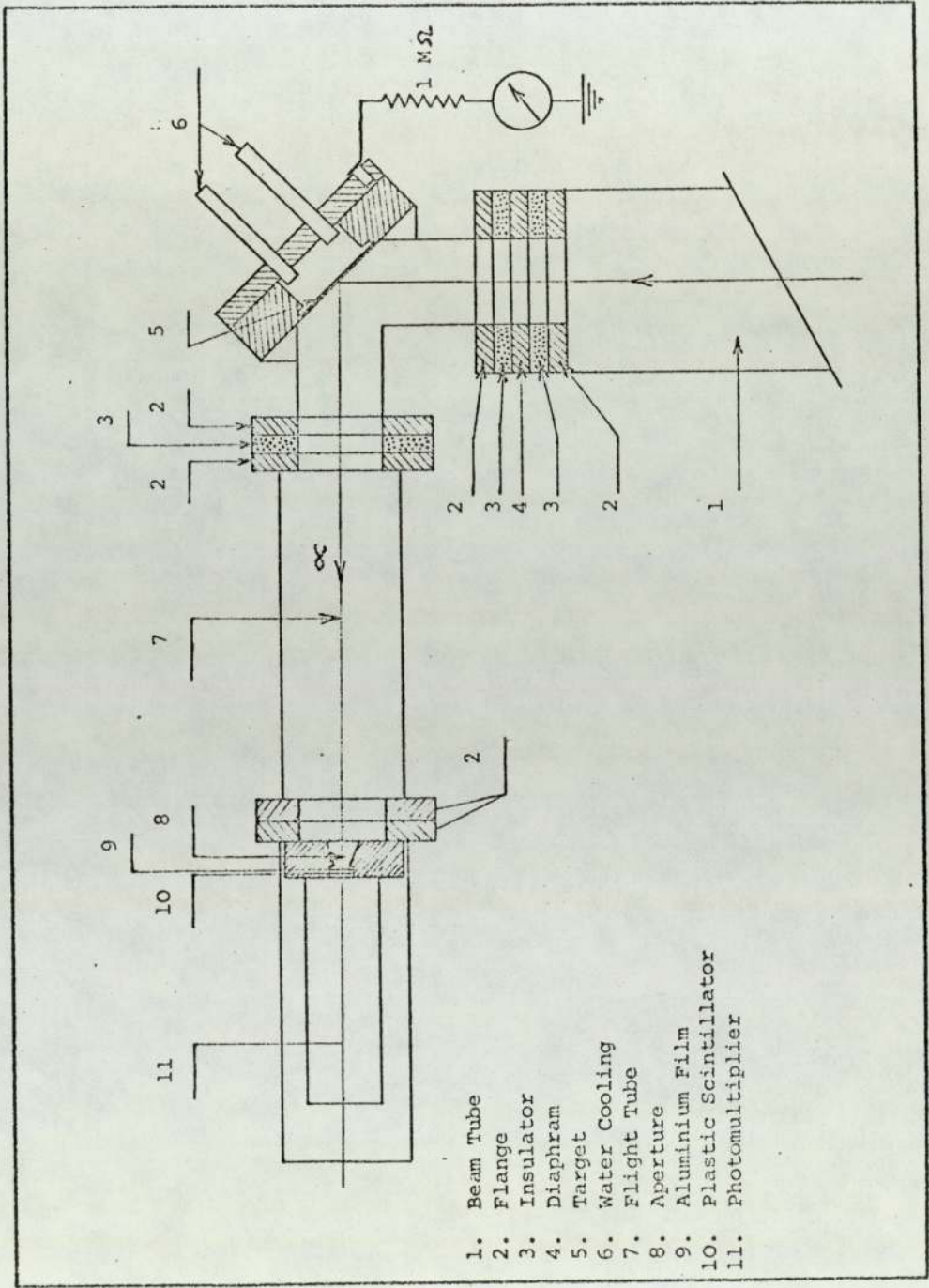


Figure 5.5. Target Assembly and  $\alpha$ -flight Tube.

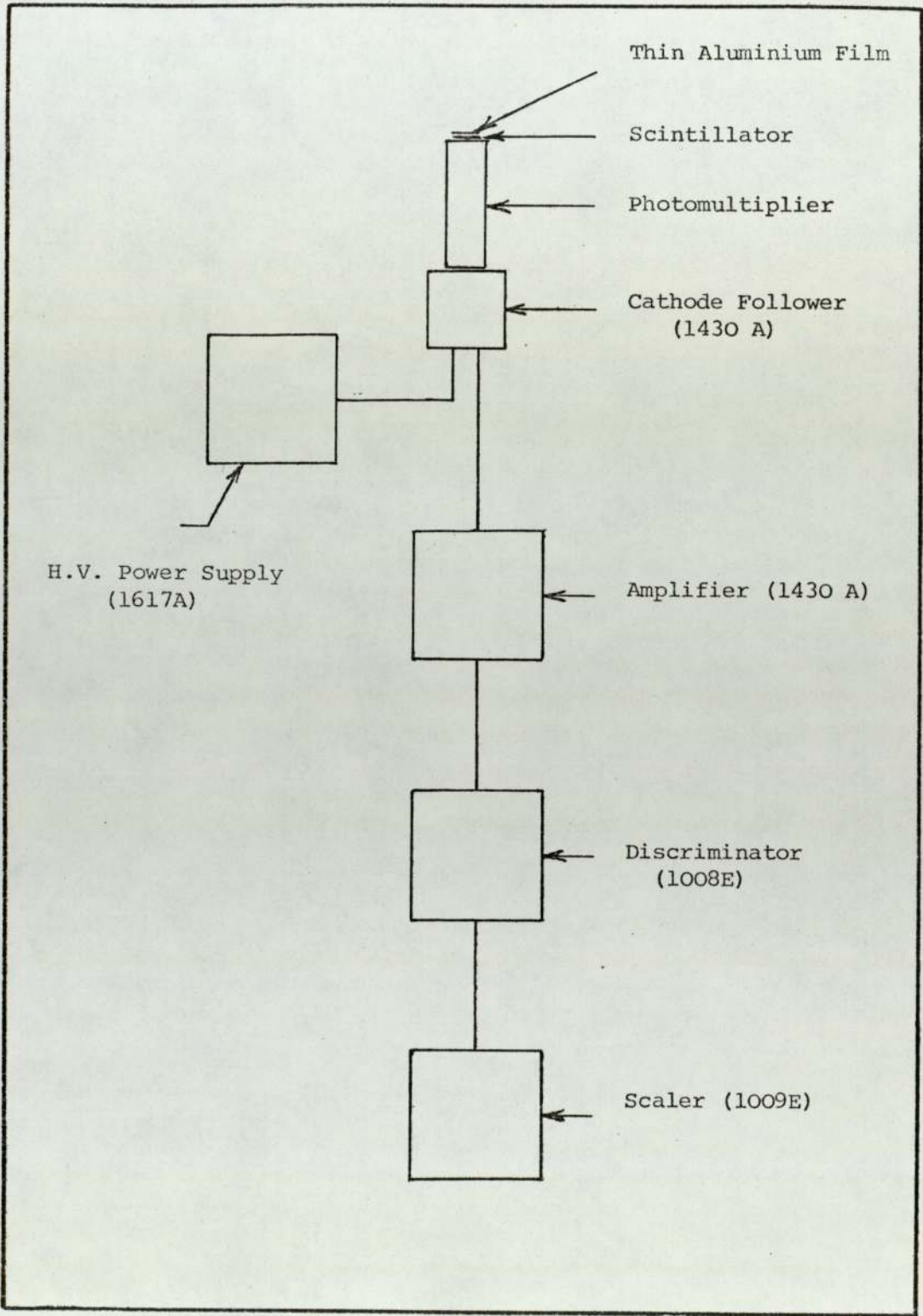


Figure 5.6. Block Diagram of the Electronics for Detecting and Counting the Alpha Particles

Therefore, the source strength can be given by:

$$C_{\alpha} = S_o \cdot \Delta\Omega \quad \dots \dots \dots 5.1$$

where  $\Delta\Omega$  is the solid angle which is given by:

$$\Delta\Omega = \frac{\pi D^2/4}{4\pi R^2} = \frac{D^2}{(4R)^2} \quad \dots \dots \dots 5.2$$

Assuming that R is large and the target area is small enough so that it is effectively a point source as viewed by the detector therefore:

$$S_o = C_{\alpha} \frac{16R^2}{D^2} = C_{\alpha} G \quad \dots \dots \dots 5.3$$

where G is termed the geometry factor which is the inverse of the solid angle as defined by equation 5.3.

As seen from the above equations that the squared values of R and D are used, thus R and D have to be accurately obtained. The value of D is measured with accuracy of  $\pm 0.001$  cm using a Universal measuring machine "Genevoise". Several measurements were taken and the mean gave an average diameter of  $4.9314 \pm 0.013$  mm. The distance from the target was measured as  $73.2 \pm 0.2$  cm. This gave the geometry factor a value of  $3.508 \times 10^5$  ( $\pm 2\%$ ).

The value of G was used in the computer program written for the analysis of data to normalize all the measurements to the same source strength, thus allowing an absolute measurement of the neutron spectra in all experiments.

CHAPTER 6METHODS AND COMPUTATIONAL TECHNIQUES USED  
FOR CALCULATIONS OF NEUTRON PENETRATION6.1 Introduction

The passage of neutrons through matter is similar in some aspects to gaseous diffusion or the diffusion of heat. Because of the extremely small density of neutrons in nuclear reactors, collisions between neutrons are rare<sup>(12)</sup>. Neutron migration involves a large number of random collisions which are mainly between neutrons and the nuclei of the medium. The rigorous treatment of these collisions was described by the transport method formulated by Maxwell and Boltzmann in the last century. This method can be used to predict the neutron flux distribution throughout the medium.

Some of the problems arising in the design of nuclear reactors and in shielding calculations can be attributed to the complicated nature of the necessary mathematics or to the lack of information and the uncertainties in cross section data. Although slowing down by inelastic scattering is of great importance, especially in the design of fast reactors, in the standard textbooks<sup>(119,120)</sup> inelastic processes are completely neglected.

The transport method which has been widely used for several years, for the study of neutron attenuation is monoenergetic, therefore the study of a wide energy range must be represented by a group structure. Inaccuracy of a few percent in the average group cross section can lead to an unacceptable error in the estimation of the neutron flux behind the shielding. Even if the effective group cross sections are known with a good accuracy, the value of the effective group cross sections of an interaction can be changed with the shield thickness if the groups

are too wide in energy, due to changing neutron spectrum.

In the past the application of the Boltzmann transport theory to practical design calculations was rarely made and the majority of shield arrangements have been determined by empirical methods such as the kernel approach<sup>(88)</sup> or removal diffusion theory. These methods were mainly based on the results of experimental studies of neutron attenuation in certain materials. The application of the neutron transport equation to the study of neutron slowing down problems started in 1937 with Ornstein-Ohlenbek<sup>(89)</sup> and Fermi<sup>(90)</sup>.

Since 1950, the technical development of high speed computers with large storage capacities has led to a wider application of numerical methods for solving the transport equation. This resulted in several hundred different reactor codes which were written for over 20 types of digital computer<sup>(91)</sup>. Unfortunately, the computational techniques of these codes are rarely discussed in the published papers, usually the name of the code is mentioned. Therefore, the choice of a method which is suitable for a certain application is uncertain.

In the following section, the approach of the Boltzmann transport theory and the different methods which are commonly used in shielding calculations are described in outline.

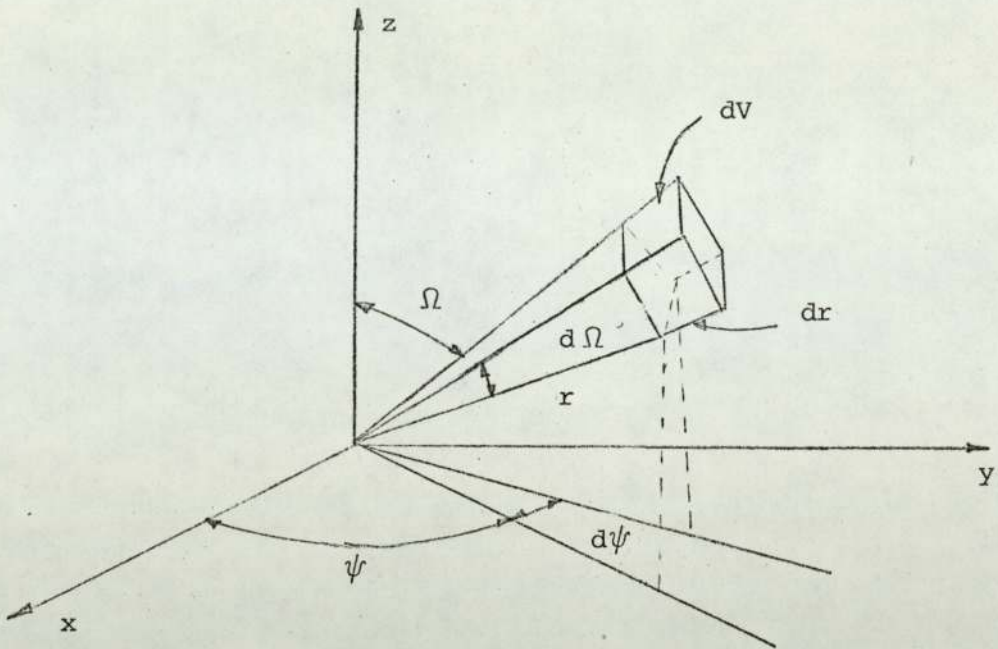
## 6.2 The Boltzmann Transport Equation

The approach is to consider a small volume element  $dV$  located at a certain point in the system and to derive an expression for the various ways in which neutrons having a given energy, and moving in a specified direction, enter and leave this volume element.

The neutron density  $N$  in the volume element  $dV$  at a point  $r$  can change, due to one of these three effects.

- (1) Neutron leakage from the system without collision.
- (2) Neutron collisions which can lead to change in neutron energy and direction.

(3) The presence of neutron sources in the system.



If  $\Omega$  is a unit vector in the direction of the velocity of a neutron with lethargy  $U$  ( $U = \ln E_0/E$ , where  $E_0$  is the initial neutron energy), then  $N(r, \Omega, U, t) dr d\Omega dU$  is the number of neutrons whose velocities lie in the solid angle  $d\Omega$  about  $\Omega$  and whose lethargies are between  $U$  and  $U + dU$  all measured at time  $t$ .

In the case of neutron balance, that is neutron losses are equal to neutron gains or  $d\phi/dt = 0$ , then  $N(r, \Omega, U, t)$  can be derived simply from the different effects.

The change of the distribution function of neutron leakage from the system in the direction of  $\Omega$  is

$$\mathbf{v} \cdot \nabla N(r, \Omega, U) \dots \dots \dots 6.1$$

where  $\nabla$  is the gradient operator.

Since any collision changes the direction and/or the lethargy of the neutron, the removal rate is:

$$\Sigma_t(r, U) \cdot \mathbf{v} N(r, \Omega, U) \dots \dots \dots 6.2$$

where  $\Sigma_t$  is the macroscopic total cross section and is given by:

$$\Sigma_t(r,U) = \Sigma_e(r,U) + \Sigma_i(r,U) + \Sigma_a(r,U)$$

in which  $\Sigma_e$ ,  $\Sigma_i$  and  $\Sigma_a$  are the macroscopic elastic, inelastic and absorption cross sections respectively.

The rate of elastic collisions at the point  $r$  experienced by neutrons of  $V'$  and lethargy  $U'$  is given by:

$$\Sigma_e(r,U') \cdot V' N(\Omega, U') \quad . . . . . 6.3$$

if  $g_e(\Omega', U'; \Omega, U)$  is the relative probability of a neutron being left with velocity parameter  $(\Omega, U)$  as a result of an elastic collision before which its velocity parameter were  $(\Omega', U')$ , then the number of neutrons scattered into the beam per second is:

$$\int_{U-\epsilon_e}^U du \int d\Omega' V' \Sigma_e(r,U') N(r, \Omega', U') \cdot g_e(\Omega', U'; \Omega, U) \quad . . . . . 6.4$$

where  $U - \epsilon_e$  represents the lowest lethargy from which neutrons may be elastically scattered into  $U$ ; it is assumed that the function  $g_e(\Omega', U'; \Omega, U)$  is normalized to unity; i.e.,

$$\int d\Omega \int dU g_e(\Omega', U'; \Omega, U) = 1$$

Similarly the number of neutrons scattered into the beam at point  $r$  experienced by neutrons of velocity  $V'$  is:

$$\int_{U-\epsilon_i}^U dU' \int d\Omega' V' \Sigma_i(r,U') N(r, \Omega', U') \cdot g_i(\Omega', U'; \Omega, U) \quad . . . . . 6.5$$

The production of neutrons at point  $r$  with velocity parameters  $(\Omega, U)$  is

$$S_0(r, \Omega, U) + g_f(U) \int_0^\infty dU' \int d\Omega' v' \nu(U') \Sigma_f(r, U') N(r, \Omega', U') \dots 6.6$$

where  $S_0$  is an external source and includes sources of delayed neutrons,  $\nu$  is the number of prompt neutrons produced per fission,

$\Sigma_f$  = the macroscopic fission cross section.

$g_f(U)$  is the relative probability that the fission neutron is born with lethargy  $U$ . The probability  $g_f$  is also normalized to unity, i.e.,

$$\int d\Omega \int dU g_f(U) = 4\pi \int dU g_f(U) = 1$$

Setting

$$\phi(r, \Omega, U) = N(r, \Omega, U)$$

from the forgoing relations, the equation of continuity can be derived as:

$$\begin{aligned} & \Omega \cdot \nabla \phi(r, U, \Omega) + \Sigma_t(r, U) \cdot \phi(r, \Omega, U) \\ &= \int_{U-\epsilon_e}^U dU' \int d\Omega' \Sigma_e(r, U) \phi(r, \Omega', U') \cdot g_e(\Omega', U'; \Omega, U) \\ &+ \int_{U-\epsilon_i}^U dU' \int d\Omega' \Sigma_i(r, U') \phi(r, \Omega', U') \cdot g_i(\Omega', U'; \Omega, U) \\ &+ g_f(U) \int_0^\infty dU' \int d\Omega' \nu(U') \Sigma_f(r, U') \cdot \phi(r, \Omega', U') \\ &+ S_0(r, U, \Omega) \dots 6.7 \end{aligned}$$

and is called the Boltzmann transport equation, which is the fundamental

relation of neutron kinetics.

The quantity  $\phi(r, U, \Omega)$  is defined as the angular flux, since it is a function of the direction  $\Omega$

### 6.3 Methods used for Solution of the Transport Equation

Solutions of the Boltzmann transport equation are inherently complex due to the integro-differential form of the equation. An exact solution of the equation is limited to a few highly specialised problems, and the most practical techniques are approximate methods. The most general ones are the spherical harmonics expansion, the discrete ordinate technique and the moment method. A family of methods stemming from the spherical harmonics expansion; spherical harmonics method, the Legendre expansion, the  $P_1$  approximation or diffusion theory with and without energy dependence, the  $P_n$  approximation etc. There are also some other methods which are composit in nature, such as the removal diffusion method and Monte Carlo method which is dependent on the statistical simulation of the physical processes.

#### 6.3.1. The Spherical Harmonics Method

The spherical harmonics method is an approximation to the Boltzmann transport equation consisting of a series of differential equations which are independent of the angular direction  $\Omega$ . This is done by expanding the functions  $\phi$ ,  $g_e$ ,  $g_i$  and  $g_f$  in the transport equation in terms of spherical harmonics. First it is assumed that these functions can be written as an infinite power series in the variable  $\mu$  with coefficients that depend on  $z$ .

$$\mu = \cos \theta \quad \dots \dots \dots 6.8$$

where  $\theta$  is the angle between the  $z$  axis and  $\Omega$ , and  $d\Omega = d\mu d\psi$  where  $\psi$  is the azimuthal angle.

Assume that the medium is isotropic and homogeneous so that

the cross sections are independent of  $z$  and the scattering processes are azimuthally symmetric about the initial direction of motion of the neutron. Then:

$$\begin{aligned} g_e(\mu', U'; \mu, U) &= g_e(U', U, \mu_0) \\ &= \sum_{\ell=0}^{\infty} \frac{2\ell+1}{4\pi} \cdot g_{e,\ell}(U':U) P_{\ell}(\mu_0) \dots 6.9 \end{aligned}$$

Similarly,

$$\begin{aligned} g_i(\mu', U'; \mu, U) &= g_i(U', U, \mu_0) \\ &= \sum_{\ell=0}^{\infty} \frac{2\ell+1}{4\pi} \cdot g_{i,\ell}(U', U) P_{\ell}(\mu_0) \dots 6.10 \end{aligned}$$

where  $P_{\ell}$  is the Legendre polynomial of degree  $\ell$  and

$$\mu_0 = \Omega \cdot \Omega' = \cos \theta_0$$

The angular neutron flux is expressed as:

$$\phi(z, \mu, U) = \sum_{\ell=0}^{\infty} \frac{2\ell+1}{4\pi} \cdot \phi_{\ell}(z, U) \cdot P_{\ell}(\mu) \dots 6.11$$

and

$$S_0(z, \mu, U) = \sum_{\ell=0}^{\infty} \frac{2\ell+1}{4\pi} \cdot S_{0,\ell}(z, U) P_{\ell}(\mu) \dots 6.12$$

Substituting the above relation into the transport equation and using the recurrence relation for Legendre polynomials,

$$\int_{-1}^1 P_{\ell}(\mu) P_n(\mu) d\mu = \begin{cases} \frac{2}{2\ell+1} & \text{if } n = \ell \\ 0 & \text{if } n \neq \ell \end{cases} \dots 6.13$$

the spherical harmonic form of the Boltzmann transport equation can be obtained.

The application of the spherical harmonics technique to the transport equation is inherently difficult and becomes formidable for multigroup energy cases. However, the method has been described for slab, spherical and cylindrical geometries<sup>(95,96)</sup> and a somewhat simplified approach has been reported for more complex geometries<sup>(97)</sup>. The method has been extended also to cover anisotropic scattering and the approaches have been applied in the  $P_3$  and  $P_5$  approximation<sup>(98,99)</sup>.

### 6.3.2. The Discrete Ordinates Method

The method was originally proposed by Wick<sup>(103)</sup> and is developed by the astrophysicist Chandrasekhar<sup>(104)</sup>. In 1953 Carlson<sup>(100)</sup> improved the method and used it to solve the transport equation. It was originally developed for the case of isotropic scattering and has been extended to take account of anisotropic scattering by using the transport cross section as given by:

$$\sigma_{tr} = \sigma_s \left[ 1 - \int_{-1}^{+1} \mu f_e(\mu) d\mu \right] \dots\dots\dots 6.14$$

where  $f_e(\mu)$  is the angular distribution of scattered neutrons.

In this method the integral in the transport equation is approximated by a discrete ordinate quadrature. The solid angle is divided into  $N$  segments and discrete directions and weights. For a plane and spherical geometry the range of  $\mu$  from  $-1$  to  $+1$  is divided into equal intervals and  $\phi(\mu)$  is taken to vary linearly with  $\mu$  in each interval. The range of integration over  $\mu$  is then divided into equal sub-intervals,  $N$ . Let the points which define these sub-intervals be:

$$\mu_n \quad (n = 0, 1, \dots\dots\dots N), \text{ so that}$$

$$\mu_0 = -1 \text{ and } \mu_N = 1$$

The number of intervals  $N$  defines the order of approximation. The angular flux for a certain energy group ( $i$ ) can be given by:

$$\begin{aligned} \phi_i(r, \mu) &= \frac{\mu - \mu_{n-1}}{\mu_n - \mu_{n-1}} \cdot \phi_i(r, \mu_n) \\ &+ \frac{\mu_n - \mu}{\mu_n - \mu_{n-1}} \cdot \phi_i(r, \mu_{n-1}) \quad \dots \dots 6.15 \end{aligned}$$

This approximation is then used to reduce the one velocity transport equation to a set of  $N$  equations in  $N+1$  variables,  $\phi(r, \mu_n)$ . An additional equation is obtained by setting  $\mu = -1$  directly in the one velocity Boltzmann transport equation. The resulting set is then solved numerically for the fluxes.

The method is now one of the most important analytical tools in reactor criticality and shielding calculations. It has the advantage of being more suited to large digital computers since it is basically a difference technique. An account of the method and the machine programmes which are available to solve the resulting set of equations has been given by Ackroyd and Pendlebury<sup>(105)</sup>.

### 6.3.3. The Moments Method

The moments or polynomial method is a semi-numerical technique which has been used with good effect to generate quite accurate solutions to the Boltzmann transport equation. The method was proposed by Spencer and Fano (1951)<sup>(106)</sup> and was used by Goldstein and Wilkins (1954)<sup>(107)</sup> for extensive computer calculations to obtain build up factors and differential energy spectra for infinite homogeneous media as a function of penetration.

The initial steps involved are similar to those in the well known spherical-harmonic method in neutron slowing down theory, in which the angular flux is expanded in a series of Legendre polynomials. By this means it reduces the original equation of three variables ( $\Omega, r, U$ )

to a sequence of coupled integro-differential equations of two variables  $(r, U)$ . As a further simplification these equations are multiplied by  $P_\ell(\omega)$  and integrated over all solid angles; in this way one obtains a double sequence of linear integral equations for the spatial moments of the Legendre coefficients.

The method is considered as an accurate way for solving the Boltzmann transport equation for both gamma rays and neutrons in an infinite homogeneous media with simple sources. However, the matter is more complicated for neutrons than in the gamma case, because of the rapid changes in neutron cross sections with energy and because neutrons undergo many collisions before absorption.

The main achievement of the moment method has been the determination of fast neutron space energy distribution by a method which correctly takes account of the anisotropy of elastic scattering. However, the method is not directly applicable to reactor design calculations since infinite and heterogeneous media are involved.

#### 6.3.4. The Diffusion Theory

The diffusion theory is a simplified method for solving the Boltzmann transport equation by assuming that all neutrons have the same lethargy ( $U$ ) and under the conditions that, the scattering processes with nuclei do not involve any change in the neutron energy. The basic assumption of the elementary diffusion theory is the validity of Fick's Law<sup>(13)</sup>, which states that the net current of neutrons in the direction away from the region of greater neutron density is proportional to the negative gradient of the neutron flux  $\phi(r')$

$$J(r) = -D \cdot \text{grad } \phi(r) \quad \dots \dots \dots 6.16$$

where  $D$  is the diffusion coefficient, having the dimension of length.

The above relation is valid only for the diffusion of neutrons

in regions which are not closer to boundaries than two or three mean free paths, the absorption cross section is very small and the neutrons are scattered without loss in energy.

For a system in the steady state  $\left[ \frac{dn}{dt} = 0 \right]$  the neutron flux satisfies the simple second order differential equation

$$D \nabla^2 \phi - \Sigma_a \phi + S = 0 \quad \dots \dots \dots 6.17$$

where  $\nabla^2$  is the Laplacian operator and  $\Sigma_a$  is the absorption cross section.  $\Sigma_a$  can be determined from the scattering and absorption properties of the medium, i.e., the macroscopic scattering and capture cross sections and the average cosine of the scattering angle  $\bar{\mu}_0$ . For neutrons of energy less than a few hundred KeV diffusing in a medium consists of a single element of atomic weight  $A$ ,  $\bar{\mu}_0$  is given by

$$\bar{\mu}_0 = \frac{2}{3A}$$

In the case of a medium which is a mixture of elements in which the  $i$  th element has an atomic scattering cross section equal to  $\sigma_{is}$

$$\bar{\mu}_0 = \frac{\sum_i \left[ N_i \sigma_{is} \left( \frac{2}{3A_i} \right) \right]}{\sum_i [ N_i \sigma_{is} ]} \quad \dots \dots \dots 6.18$$

where  $N_i$  is the number density of the  $i$  th type of atoms in the mixture.

At a plane boundary between a diffusion medium and a vacuum, the neutron flux varies in such a way that linear extrapolation would require the flux to vanish at a definite (extrapolated) distance 'd' beyond the boundary:

$$d = 0.67 \lambda_t \quad \dots \dots \dots 6.19$$

where  $\lambda_t$  is the transport mean free path of the medium and is given by:

$$\lambda_t = \frac{1}{\sum_s (1 - \mu_{0s})} \quad \dots \dots \dots 6.20$$

For treatment of a continuous energy spectrum, the energy range is divided into discrete groups and each group is treated separately with its appropriate parameters.

### 6.3.5 Fermi Age Theory

Among the methods which are used to solve the Boltzmann transport equation is the Fermi-Age or slowing down theory. Comprehensive descriptions of this method are readily available in the published literature (108, 109, 110). The theory treats the succession of discrete energy losses in individual collisions by which neutrons are actually slowed down as equivalent to a continuous slowing down process which results in the same average rate of energy loss. It provides an approximate value of the flux of neutrons as a function of space and energy due to a given source of fast neutrons in an elastically scattering and non absorbing medium. The flow in and out of a certain element may be expressed in terms of the slowing down density  $q(r, U)$  which is defined as the number of neutrons crossing a lethargy level  $U$  per cubic centimeter per second. The number entering  $dU$  is  $q(r, U)$  and the number leaving  $dU$  is  $q(U+du, r)$ . Thus,

$$S(U)dU = q(r, U) - q(r, U + dU) \quad \dots \dots \dots 6.21$$

or

$$S(U)dU = - \frac{dq(r, U)}{dU} dU \quad \dots \dots \dots 6.22$$

Combining equations 6.21, 6.22 and cancelling a common  $dU$ :

$$D(U) \nabla^2 \phi(r, U) = \frac{dq(r, U)}{dU} \quad \dots \dots \dots 6.23$$

omitting the designation of functional dependence

$$D \nabla^2 \phi = \frac{dq}{dU} \quad \dots \dots \dots 6.24$$

The relation between flux and slowing down density is given by:

$$\phi = \frac{q}{\xi \Sigma_s} \quad \dots \dots \dots 6.25$$

therefore

$$D \nabla^2 q = \xi \Sigma_s \frac{dq}{dU} \quad \dots \dots \dots 6.26$$

A new variable  $\tau(U)$  is now introduced, defined by:

$$\tau(U) = \int_0^U \frac{D}{\xi \Sigma_s} dU \quad \dots \dots \dots 6.27$$

therefore equation 6.26 becomes

$$\nabla^2 q = \frac{dq}{d\tau} \quad \dots \dots \dots 6.28$$

equation 6.28 is known as the Fermi-age equation, the quantity  $\tau(U)$  is called the Fermi age of the neutrons.

From the foregoing discussion, the Age theory applies to a medium in which there is no absorption of neutrons but it can be shown that with a slight modification, the age equation can be used for a weakly absorbing medium. It is found that if  $q(U)$  is the solution of the equation for the case of no absorption, then the corresponding slowing down density  $q^*(U)$  for the case of weak absorption is given to a sufficient approximation by:

$$q^*(U) = P(U) \cdot q(U)$$

where  $p(U)$  is the resonance escape probability for neutrons of energy  $(U)$ . Therefore, at any energy, the slowing down density with absorption that satisfies the Fermi Age equation may be taken as equal to the slowing down density solution of the Fermi equation without absorption at the same energy, multiplied by the resonance escape probability for that energy.

The method's usefulness for shielding calculations is limited by the fact that its accuracy decreases with distance from the source and that it breaks down completely at distances which are much smaller than those usually encountered in reactor shields.

#### 6.4 Monte Carlo Method

The Monte Carlo method is a stochastic process which is applicable to problems involving a series of random events such as the behaviour of neutrons with matter. In these problems, the histories of a large number of neutrons or photons are followed from collision to collision. In going from one collision to another, the problem is to determine the distance travelled before the next collision takes place, the type of collision which takes place and the energy and direction of the neutron after the collision. The distance which the particle travels from one collision to the next depends on its mean free path  $\lambda$ , which is a function of the neutron energy and the material in which it is moving.

The main advantage of the Monte Carlo method comes from its applicability to general geometric configurations and relative freedom from idealizing assumptions without unduly adding to the machine time. Its obvious disadvantage is the large computing time that can be required in design problems. However, with the availability of large high speed computers the method has become a powerful tool for detailed study of shielding and reactor design. A survey for the application of the method for shielding and reactor calculations is given by

Goertzel and Kalos (1958)<sup>(110)</sup>. Its application to transport and reactor problems has also been surveyed briefly by Kalos and Wile (1957)<sup>(111)</sup>.

#### 6.5 The Removal Diffusion Method

The removal diffusion method is a process in which the slowing down of fast neutrons on deep penetration in a shield may be regarded as a two step process. The high energy of the neutron is degraded significantly by the 'removal' collision, then followed by a diffusion process which is unlikely to result in very much net travel. The penetration of the forward directed neutrons is therefore described by a removal process which consists of an exponential and a geometrical attenuation factor and diffusion theory then predicts their migration following such collision.

The uncollided neutron flux can be obtained from the knowledge of the removal cross section  $\Sigma_{rem}$  which is available from the experimental data, and in cases where this is not available it is equated to the transport cross section  $\Sigma_t$ . When the transport cross section is used, the calculation is called the Spinney Method<sup>(112)</sup>. In this method the energy range of the neutrons is divided into a number of energy intervals and assuming that the monoenergetic diffusion theory is applicable to the neutrons within each interval.

The Spinney Method was applied with the age theory to predict the subsequent slowing down after a 'removal' collision, but later Avery et al (1960)<sup>(113)</sup> have used the removal calculation in conjunction with multigroup diffusion theory to describe the penetration of the forward directed neutrons and the diffusion theory to predict their migration following such collision when their angular distribution is nearly isotropic.

A detailed description of the method is given in conjunction with the multigroup diffusion calculation.

## 6.6 Comparison of the Computational Methods

When comparing the different methods which are used for reactor shielding calculations one is led to consider the Monte Carlo method, the  $S_n - P_\ell$  expansion method and the direct numerical integration of the Boltzmann transport equation which, if applied with sufficient diligence and finesse of calculational details are the most accurate methods. These represent an exact solution to the Boltzmann equation which describes all the processes of interaction and transport of neutrons through matters.

From the standpoint of available and working machine codes, the Monte Carlo method is considered as the most developed for practical design calculations. The method can incorporate in principle any arbitrary geometry, source anisotropy and scattering properties and still gives the more accurate solution. However, the Monte Carlo method has some limitations due to the time needed to build up accuracy and the large amount of computer store needed which makes the method less attractive for common use; but in complex and possibly three dimensional geometries, the method is more suited, since the random sampling technique is least restricted to particular source geometries.

The Monte Carlo code (O5R) which has been developed at the Oak Ridge National Laboratory unfortunately proved unsuitable for running on computers available to the author, due to its large amount of storage space and length of calculation as well as incompatibility of certain sub-routines with the available computers. Of the different methods for calculation, the  $S_n - P_\ell$  method which produces good neutron penetrating results in simple geometries with less computer time than the other accurate methods since a  $P_3$  expansion of the cross section is then generally adequate. The method is more widely used for fast reactor analysis. The geometry of the problem to be solved was not sufficiently simple, neither was a suitable computer available for existing codes, so this method too had to be rejected.

The use of the spherical harmonics method, i.e.,  $P_n$  approximations and the polynomial expansion method are most widely used for multilayered shields. Due to their increasing complexities, the higher order approximations for multigroup calculations are limited to slab geometry only and they become impracticable for application to other geometries. General application of the  $P_n$  approximation seems to offer no particular advantages over the  $S_n$  method. A consistent  $P_n$  i.e.  $P_n - P_\ell$  would in theory produce results as good as the  $S_n - P_\ell$  calculations. However, the  $S_n$  method, though less elegant than the  $P_n$  approximation, possesses the advantage of being more suited to modern high speed computers, since it is basically a difference technique.

The removal diffusion calculation has proved itself as a good tool for calculating the penetration of the 14 MeV neutrons through shielding materials (115, 116, 117). The primary 14 MeV neutron flux could be represented by an exponential and geometrical fall off, while the down-scattered secondary neutrons are treated by the diffusion calculation since the scattered neutrons can be expected to be adequately isotropic.

According to the discussion in published work<sup>(10,120,121)</sup>, one can find that the removal diffusion calculation is probably a good tool for reactor shielding design. The different machine codes were studied and was found that in the RASH code<sup>(115)</sup> the transfer of neutrons is allowed only to the adjacent groups, which does not represent the inelastic scattering of neutrons that can traverse almost any number of groups in one collision. However, the different aspects of the RASH code were found useful and have been taken into consideration during writing the programme for the present calculations. The programme was made to suit the limitations of the available computer and is suitable for testing the value of multigroup cross section sets designed for fast reactor and shielding calculations. In order to do this it is an advantage to be able to neglect angular dependence of cross sections

since this is a further uncertainty in evaluating the worth of data. Such a method is less suitable for very thin layers since angular dependence of flux is then more influenced by the differential cross sections.

CHAPTER 7SPECTRA CALCULATIONS BY MULTIGROUP DIFFUSIONAND REMOVAL DIFFUSION METHODS7.1 Introduction

The spectra of fast neutrons which have passed through homogeneous and heterogeneous media of iron, graphite and polypropylene media of different thicknesses have been calculated by using the combination of multigroup diffusion and removal diffusion equations. The diffusion coefficient calculated with higher order corrections for anisotropic scattering was used instead of the commonly used transport mean free path divided by three.

The source of data, i.e., cross sections and inelastic scattering probabilities for the multigroup calculation was the 20 group cross section set due to Yiftah and Sieger<sup>(84)</sup>. The set covers a range of neutron energy from 500 eV up to 14 MeV with ten groups above 0.3 MeV and has a wide application to fast reactor experiments.

Calculations have also been carried out using the Russian ABBN set<sup>(85)</sup>, with a highest energy limit of 10.5 MeV. Two other groups with energy boundaries at 12 and 14 MeV have been supplemented from the Yiftah-Sieger set. The inelastically scattered neutrons from the 14 - 12 MeV and 12 - 10.5 MeV groups can move to any of the lower groups of ABBN; the down scattering probabilities for these two groups given in the Yiftah-Sieger set have been modified to match the group boundaries of the ABBN set.

7.2 Multigroup Methods of Calculation

In multigroup methods of calculation, the energy range is divided into a number of intervals. The number of groups depends upon the accuracy desired and the machine capabilities available, (the larger

the number of groups, the higher the accuracy, provided that the data are accurately known. Within the  $g$  th group, which extends from lethargy  $U_{g-1}$  to  $U_g$ , neutrons are assumed to diffuse according to the one velocity diffusion equation as they leak out of the system or move to other lower energy groups by elastic or inelastic collisions.

The flux  $\phi_g(r)$  of neutrons in the  $g$  th group can be defined then by the integral,

$$\phi_g(r) = \int_{U_{g-1}}^{U_g} \phi(r, U) \cdot dU \quad \dots \dots \dots 7.1$$

where  $U_g$  and  $U_{g-1}$  are the upper and lower lethargies of the group respectively and  $\phi(r, U)$  is the lethargy dependent flux at the point  $r$ .

### 7.3 Group Constants

The diffusion coefficient and interaction cross sections are described in terms of suitably averaged diffusion coefficients and cross sections and are known as group constants.

In order to obtain averaged values of these constants for a process in a particular group, it is necessary to know the neutron spectrum within the group. The spectrum may be known in certain problems, e.g., in the thermal system, it is given as  $\frac{1}{E}$ , and  $\phi(U)$  can be taken as constant and the thermal group is given by a Maxwellian. In fast systems there is no such well defined spectrum and several groups are needed for correct representation.

A sufficient number of groups must be taken so that cross sections vary smoothly across a group. Reasonably accurate average cross sections can then be calculated by assuming a constant flux across a group. The accuracy of these averages could possibly then be improved by recalculating them using an average flux gradient per group as given by the initial calculations. This is, however, not feasible with the available cross section sets due to lack of detailed fundamental data.

### 7.3.1. Diffusion Coefficient

The diffusion of neutrons within the  $g$  th group can be described by an average diffusion coefficient given as:

$$D_g = \frac{\int_{U_{g-1}}^{U_g} D(U) \nabla^2 \phi(r, U) dU}{\int_{U_{g-1}}^{U_g} \nabla^2 \phi(r, U) dU} \dots\dots\dots 7.2$$

where  $\nabla^2$  is the Laplace operator.

The value of  $D_g$  is usually a function of  $r$  unless  $\phi(r, U)$  can be written as a separable function of  $r$  and  $U$ <sup>(13)</sup>:

$$\phi(r, U) = f(r) \cdot \phi(U)$$

where  $\phi(U)$  is the lethargy dependent part of  $\phi(r, U)$ . This is never strictly true, but it must be assumed in order to carry out the group calculation. Therefore equation 7.2 becomes:

$$D_g = \frac{1}{\phi_g} \int_{U_{g-1}}^{U_g} D(U) \cdot \phi(U) \cdot dU \dots\dots\dots 7.3$$

In the case of isotropic scattering in the laboratory system, which is true only at low energies, the value of  $D_g$  can be calculated from the methods of transport theory ( $D = \frac{\lambda_{tr}}{3}$ ). But for anisotropic scattering and for greater accuracy  $D_g$  should be determined from the transcendental equation<sup>(13)</sup>.

$$\frac{\Sigma_s}{2} \left( \frac{D}{\Sigma_a} \right)^{\frac{1}{2}} \cdot \ln \left[ \frac{\Sigma_t + \left( \frac{\Sigma_a}{D} \right)^{\frac{1}{2}}}{\Sigma_t - \left( \frac{\Sigma_a}{D} \right)^{\frac{1}{2}}} \right] = \frac{1 + 3D \Sigma_s \bar{\mu}}{1 + 3D \Sigma_t \bar{\mu}} \dots\dots\dots 7.4$$

where  $\Sigma_t$ ,  $\Sigma_s$  and  $\Sigma_a$  are the macroscopic total, scattering and

absorption cross sections respectively, and  $\bar{\mu}$  is the average value of the cosine of the scattering angle in the laboratory co-ordinate system.

### 7.3.2. Group Cross Sections

Neutrons may disappear from the  $g$  th group either in an absorption interaction or as a result of an elastic or inelastic scatter. If the value of the cross sections of the various events are known for the energy region of interest then they will be averaged within groups with respect to flux, therefore:

$$\Sigma_{x,g} = \frac{\int_{U_{g-1}}^{U_g} \Sigma_x(U) \cdot \phi(r,U) \cdot dU}{\int_{U_{g-1}}^{U_g} \phi(r,U) \cdot dU} \dots\dots\dots 7.5$$

where  $\Sigma_{x,g}$  may be  $\Sigma_a$ ,  $\Sigma_s$  or  $\Sigma_f$ .

If it is assumed again that the flux can be represented by a separable function, equation 7.5 becomes:

$$\Sigma_{x,g} = \frac{1}{\phi_g} \int_{U_{g-1}}^{U_g} \Sigma_x(U) \cdot \phi(U) \cdot dU \dots\dots\dots 7.6$$

This equation has to be numerically integrated since the flux does not have a simple numerical form.

The transfer of neutrons from the  $g$  th group to the  $(g + i)$  th group (where  $i = 1, 2, 3, \dots, N$ ) can be described by the group transfer cross sections  $\Sigma_{(g \rightarrow g+i)}$ . These are defined so that  $\Sigma_{(g \rightarrow g+i)} \cdot \phi_g(r)$  is equal to the number of neutrons which are transferred from the  $g$  th to the  $(g + i)$  group per  $\text{cm}^3/\text{sec}$  at the point  $r$ .

The transfer cross section  $\Sigma_{(g \rightarrow g+i)}$  is given by:

$$\Sigma_{(g \rightarrow g+i)} = \Sigma_s(g \rightarrow g+i) + \Sigma_{in}(g \rightarrow g+i) \dots\dots\dots 7.7$$

where  $\Sigma_s$  and  $\Sigma_{in}$  are the transfer elastic and inelastic cross section for the given system.

Consider first the evaluation of the elastic transfer cross section  $\Sigma_s(g \rightarrow g + i)$ . The value of this constant depends on both the nuclear properties of the material in the system and the number of energy groups used in calculation. In particular, if the maximum increase in lethargy of neutrons undergoing elastic collision is less than the energy width of energy group, neutrons from one group can be elastically scattered only into the adjacent group; i.e. they cannot skip groups. In that case  $i = 1$ ,  $\Sigma_s(g \rightarrow g + 1)$ , and the groups are said to be directly coupled at least as far as elastic scattering is concerned. The minimum neutron energy after an elastic collision is  $1/\alpha$  times its initial energy:

where  $\alpha = \left( \frac{A - 1}{A + 1} \right)^2$  and is a property of scattering medium.

Therefore the condition for direct coupling by elastic scattering is given by:

$$\ln(1/\alpha) \leq \Delta U_g \quad \dots \dots 7.8$$

for all groups.

where  $\Delta U_g = U_g - U_{g-1}$

The constants  $\Sigma_s(g \rightarrow g + 1)$  can be computed for the directly coupled situation in the following way.

From equation 7.6 assuming  $\Sigma_{x,g} = \Sigma_{s,g}$ , the total number of scattering collisions per  $\text{cm}^3 \cdot \text{sec}^{-1}$  in the  $g$ th group is  $\Sigma_{s,g} \cdot \phi(g)$ . If  $\bar{\xi}_g$  is the average lethargy increase in an elastic collision in the  $g$ th group, it follows that neutrons require  $\Delta U_g / \bar{\xi}_g$  collisions on average in order to traverse that group. If there are  $\Sigma_{sg} \cdot \phi_g$

collisions per c.c. per second in the  $g$  th group, therefore, the number of neutrons scattered out of the  $g$  th group per c.c. per second must be  $\bar{\xi} \Sigma_{sg} \phi_g \Delta U_g$ .

Since these neutrons necessarily must enter the  $(g + 1)$  th group in the directly coupled case, the cross section is thus:

$$\Sigma_s (g \rightarrow g + 1) = \frac{\bar{\xi} \cdot \Sigma_{sg}}{\Delta U_g} \dots \dots \dots 7.9a$$

In the case of anisotropic scattering in the centre of mass system, the transport correction may be introduced, thus equation 7.9 becomes:

$$\Sigma_s (g \rightarrow g + 1) = \frac{\bar{\xi} \cdot \Sigma_{sg} (1 - \mu)}{\Delta U_g} \dots \dots \dots 7.9b$$

In the case of hydrogenous media, the situation is more complicated, since with a hydrogen nucleus the neutron may lose all its energy in a single collision, so that neutrons can be scattered from any group to all other groups of lower energy. If it is assumed that neutrons can be scattered into the lethargy interval in the  $(g + 1)$  th group as a result of collision in the lethargy of the  $g$  th group, the number arriving per  $\text{cm}^3 \cdot \text{sec}^{-1}$  in  $dU'$  from the group is given by:

$$\text{number scattered into } dU' = \int_{U_{g-1}}^{U_g} \Sigma_s(U) \cdot \phi(U) \cdot P(U \rightarrow U') dU \dots 7.10$$

where  $P(U \rightarrow U')$  is the probability distribution function for elastically scattered neutrons.

The total number of neutrons transferred from the  $g$  th group to the  $(g + 1)$  th group is therefore:

$$\text{number transferred} = \int_{U_g}^{U_{g+1}} \int_{U_{g-1}}^{U_g} \Sigma_s(U) \phi(U) \cdot P(U \rightarrow U') dU dU' \dots \dots \dots 7.11$$

If it is assumed that the flux  $\phi(U)$  and  $\Sigma_s(U)$  are reasonably constant in the lethargy interval defined by the  $g$  th group then equation 7.11 can be written as:

$$\Sigma_s(g \rightarrow g+1) = \frac{\Sigma_s}{U_g} \int_{U'=U_g}^{U_{g+1}} \int_{U=U_{g-1}}^{U_g} P(U \rightarrow U') dU \cdot dU' \quad \dots \dots 7.12$$

The group transfer cross sections for inelastic scattering can be computed in much the same manner as for the elastic scattering, if the inelastic scattering probability distribution function  $P(U \rightarrow U') dU'$  is known. For low energy incident neutrons where the energy levels can be resolved the excitation functions for the individual levels are used; the values are experimental results supplemented by the optical model calculations. Above the energy where the levels overlap (above 5 MeV for iron), the evaporation model of Weisskopf is used. The expression in this model is characterised by nuclear temperature which is slowly varied from group to group as it varies with incident neutron energy<sup>(13)</sup>.

### 7.3.3. Fission

In the case of presence of fissile materials in the system, it becomes necessary to define the average fission cross section for each group. For the  $g$  th group  $\Sigma_{fg}$  is given by:

$$\Sigma_{fg} = \frac{1}{U_g} \int_{U_{g-1}}^{U_g} \Sigma_f(U) dU \quad \dots \dots 7.13$$

In addition, the fraction of fission neutrons emitted into the  $g$  th group  $X_g$ , and the mean number of neutrons emitted when fission caused by a neutron of the  $g$  th group  $\nu_g$  have to be defined as well.

Specifically, these are given by:

$$X_g = \int_{U_{g-1}}^{U_g} X(U) dU \quad \dots \dots 7.14$$

where  $\int_0^{\infty} X(U) dU = 1$

and

$$\nu_g = \frac{1}{U_g} \int_{U_{g-1}}^{U_g} \nu(U) \cdot dU \quad \dots \dots \dots 7.15$$

#### 7.4 Multigroup Equations

Assume that there are N groups, namely;  $g = 1, 2, 3, \dots, N$ , where  $g = 1$  is the group of highest energy and N represents lowest energy. Therefore, using the various constants mentioned before, it becomes possible to write diffusion equations describing the behaviour of the neutrons within each group.

The equation for the first group with a fission source is given as:

$$D_1 \cdot \nabla^2 \phi_1(r) - \Sigma_{a,1} \phi_1(r) - \left[ \sum_{i=2}^N \Sigma_s(1 \rightarrow i) \right] \phi_1(r) + X_1 \sum_{i=1}^N \nu_i \Sigma_{fi} \phi_i(r) = 0 \quad \dots \dots \dots 7.16$$

where  $\phi$  is merely a function of  $\bar{r}$  within the group.

The first term gives the loss of neutrons due to leakage from the system, the second is the loss due to absorption, the third is the loss due to scattering collisions (elastic and inelastic) from the first group to all other groups, and the last term is equal to the total number of fission neutrons appearing in the first group as a result of fission occurring in all other groups.

The equation for any other group indicated by i (provided  $i \neq 1$ , e.g., the group of highest energy is excluded) is then given by:

$$D_g \cdot \nabla^2 \phi_g(r) - \Sigma_{a,g} \phi_g(r) - \left[ \sum_{i>g}^N \Sigma(g \rightarrow i) \right] \phi_g(r) + \sum_{i=1}^{g-1} \Sigma(i \rightarrow g) \phi_i(r) + X_g \sum_{i=1}^N \nu_i \Sigma_{fi} \phi_i(r) = 0 \quad \dots \dots \dots 7.17$$

Here again, the second term represents the true absorption in the  $g$  th group. The third term gives the number of neutrons scattered from the  $g$  th group to all lower energy groups, the fourth term is equal to the number of neutrons scattered into the  $g$  th group from all higher energy groups and the last term gives the number of fission neutrons produced in the  $g$  th group from fission in all other groups. In the case of no fissile materials, this last term does not appear.

### 7.5 Solution of the Equations

Since the assembly used for measurement of the neutron spectra during this work is a cylinder with a point source at the centre, the group equations are solved for spherical symmetry which is a reasonably close representation along a radius of the cylinder starting from the source. The one dimensional Laplacian operator is given by:

$$\nabla^2 = \frac{\partial^2}{\partial r^2} + \frac{2}{r} \frac{\partial}{\partial r} \quad \dots \dots 7.18$$

was written in finite difference form. It is assumed that the region under consideration is composed of concentric spherical shells, in each of which,

- (a) The diffusion coefficient and the macroscopic absorption cross section are constants,
- (b) The flux depends only on  $r$ , the distance from the centre of symmetry to point  $r$ .
- (c) The neutron current will have a radial component only, the net current is zero at the inner boundary i.e., at the inner radius of the innermost spherical shell except for energy groups having a source located at the centre of the sphere.
- (d) The flux is zero at the extrapolated distance, i.e., at a further distance of  $0.71 \lambda_{tr}$  from the outer radius.

The programme FASTNFLUX used by a previous investigator<sup>(122)</sup>

has been modified to suit the flux calculation for a multilayer configuration and is presented with a numerical scheme for solving the group equation in appendix 1.

### 7.6 Removal Diffusion Calculations

In 1950, Albert and Welton<sup>(123)</sup> introduced the concept of removal cross section to describe the attenuation of neutron in hydrogenous media. Their removal theory accounted only for the first part of the two step process described before in chapter 6. The theory was particularly useful when small changes of thickness or materials were made. The main use for it was to perturb measured or rigorously calculated values, while its main difficulty encountered was in the application of the theory in cases in which there was insufficient hydrogen in the medium to apply the theory. Without sufficient hydrogen a neutron might not be removed by a collision with a heavy nucleus even through degraded in energy. However, at high neutron energy inelastic collisions with heavy nuclei are necessary to make this valid.

The removal cross sections for the various elements must be determined by experiment, although it has been shown that they have roughly  $2/3$  of the total cross section evaluated at 8 MeV<sup>(124)</sup>. This was attributed to the fact that the flux defined by the kernel includes those neutrons which have made glancing collisions. It suggests that the removal cross section is effectively the same as the transport cross section  $\Sigma_t$ , i.e.

$$\Sigma_r = \Sigma_{tr} = \Sigma_t - \bar{\mu} \Sigma_s \quad \dots \dots 7.19$$

where  $\bar{\mu}$  is the mean cosine of the scattering angle in the laboratory system.

Avery<sup>(113)</sup> 1960 derived values of  $\Sigma_r$  for the eighteen energy groups, each of width 1 MeV, covering fission spectrum from 0 to 18 MeV neutrons, using the result of Feshbach and Weisskopf who had predicted

the ratio of transport to total cross section as a function of atomic weight and energy on the basis of the theoretical model of the nucleus.

It was found from the experimental results that the spatial distribution of monoenergetic neutrons above certain threshold for most reactor materials, may conveniently be described by the following expression (125).

$$\phi(r, E_0) = \frac{Q}{4\pi r^2} \cdot e^{-\Sigma_r \cdot d} \quad \dots \dots \dots 7.20$$

where  $Q$  = the strength of the source

$d$  = the shield thickness

$r$  = the distance between the source and detector

$\Sigma_r$  = the macroscopic removal cross section at the initial energy.

For penetration through several materials, the exponent in the above equation is replaced by the sum of the products of the removal cross section and the thickness of each material along the line of sight path from the source to the point in the shield; it can be obtained by the simple volume average

$$\Sigma_r = \frac{\sum_i \Sigma_i(r) V_i}{\sum_i V_i} \quad \dots \dots \dots 7.21$$

where  $V_i$  is the volume ratio occupied by the  $i$  th element.

In calculating the flux distribution by the removal diffusion equations during this work the first group flux was described by removal equation 7.20 instead of equation 7.16. The removal cross section data for the material under investigation were taken the same as those derived by Avery et al, for neutrons at 13.5 MeV energy.

CHAPTER 8EXPERIMENTAL AND CALCULATED LEAKAGE SPECTRA AND THEIR ANALYSIS8.1 Introduction

The measured and calculated spectra of fast neutrons which have passed through layers of iron, homogeneous and heterogeneous media of iron-graphite and iron-polypropylene are presented in this chapter. All measurements have been made with a scintillation spectrometer with NE-213 scintillator in which gamma background is discriminated by a zero crossing technique. The multigroup method was used to calculate the energy distribution of fast neutrons behind such media. The multigroup cross section sets used for iron and carbon were that due to Yiftah and Sieger (1964)<sup>(84)</sup> with uppermost boundary at 14 MeV and the Russian ABBN data (Abagyan) (1962)<sup>(85)</sup> with uppermost boundary at 10.5 MeV - the top two groups up to 14 MeV have been supplemented from the Yiftah-Sieger set. The group cross data for hydrogen were taken from the cross section data of Hughes (1957)<sup>(16)</sup>. In order to correctly predict the down scattering by hydrogen to any energy group below, the data were introduced into the calculations as pseudo-inelastic cross sections and probabilities. The values of the microscopic removal cross sections which have been used with the multigroup calculations were taken from the tabulated values of microscopic cross sections calculated by Avery et al<sup>(113)</sup>.

All the measured and calculated results are normalized to a source strength of  $1.5 \times 10^9$  neutrons per second.

Removal cross sections for 14 MeV neutrons for iron, carbon and hydrogen have been experimentally determined from the measured neutron fluxes behind iron and homogeneous and heterogeneous shields of iron-graphite and iron-polypropylene. These values agree well with

the theoretical predictions by Avery et al<sup>(113)</sup>.

## 8.2 Deformation of Fast Neutron Spectra behind Iron Shields

The measured spectra for neutrons of energies between 0.5 and 14 MeV passing through iron layers of thicknesses 10, 20 and 30 cm which correspond to 2, 4 and 6 mfp for 14 MeV neutrons are presented in figures 8.1, 8.2 and 8.3. The spectra are plotted as neutrons per sec per cm<sup>2</sup> per MeV versus neutron energy in MeV.

The figures show that for neutrons of energy  $E_n \geq 3$  MeV the form of the spectrum and its slope do not change as the layer thickness increases, but remain approximately the same. However, at the same time, in the low energy region below  $E_n = 3$  MeV a considerable increase in the number of neutrons of lower energies with increasing iron layer thickness is observed, i.e., there is a relative accumulation of number of neutrons with lower energies. This can be attributed to the fact that in heavy materials such as iron, the inelastic scattering causes neutron slowing down and in each interaction the neutron energy is considerably decreased. The inelastic scattering cross section is not strongly dependent on the energy in the range above about 3 MeV, while at  $E_n < 3$  MeV it decreases sharply with decreasing energy<sup>(16)</sup>.

These figures also present the calculated spectra by multigroup diffusion and removal diffusion calculations. It is quite evident from the figures that the measured spectra behind all thicknesses agree within the limits of experimental error with that calculated by the removal diffusion method in the energy range 0.5 - 12 MeV, while for thicknesses 20 and 30 cms the spectra calculated by the diffusion method are lower than the others.

For neutrons of the first energy group (12 - 14 MeV) a remarkable difference between the measured and calculated spectra are observed. This discrepancy may partly be explained by the difference in experimental and theoretical geometries, the uncertainties in group constants used

in calculation and the depression in pulse height due to the leakage of some recoil protons at this high energy from the scintillator before releasing their energies.

### 8.3 Deformation of Fast Neutron Spectra behind a Homogeneous and Heterogeneous Shields of Iron-Graphite

The spectra of fast neutrons behind a homogeneous and heterogeneous media of iron graphite materials (1:1 by volume) have been measured and are presented in figures 8.4 to 8.11. The homogeneous shield was built up from successive layers, 2.5 cm thick, of iron and graphite. In the case of the heterogeneous shield, the graphite layer has been placed behind the iron and nearest to the spectrometer detecting element.

From these figures it can be seen that for homogeneous shields the leakage spectra have nearly the same shape for all thicknesses for neutrons of energies between 3 to 14 MeV. However, for neutrons of  $E_n < 3$  MeV the slope of the spectrum increases with the increase of shield thickness. For heterogeneous media the slope and shape of the spectra do not change as layer thicknesses increase and remain approximately the same for all thicknesses throughout the whole neutron energy range (0.5 - 14 MeV).

These figures also present the calculated leakage spectra for those media given by the diffusion and removal diffusion calculations. It is seen that a good agreement between the measured and calculated spectra given by the removal diffusion calculation can be observed which improves with the decreasing of neutron energy and thickness of material. However, it can be seen that there is a slight difference between the spectra given by the diffusion calculation and the other ones. This difference increases with increasing neutron energy and material thickness. It can also be seen that this difference is more evident for a heterogeneous shield especially at higher energy groups and changes rapidly with the increasing of layer thickness. For neutrons in the

first energy group (12 - 14 MeV), there is a remarkable difference between the average neutron fluxes given by calculation and that measured. This can also be attributed to the same reasons mentioned before for iron shield.

From these figures it can also be seen that in the measured spectra maxima and minima are found in the neutron energy range  $\sim 3$  to 10 MeV which can be explained by the irregularities in the energy dependence of the total cross section for interaction of neutrons with carbon nuclei. As the graphite layer thickness increases, the irregularities in the spectra become more evident.

#### 8.4 Deformation of Fast Neutron Spectra behind Homogeneous and Heterogeneous Shields of Iron-Polypropylene

The measured and calculated spectra of fast neutrons passing through homogeneous and heterogeneous media of iron-polypropylene shields (1:1 by volume) are given in figures 8.12 to 8.19. The homogeneous shields were built up from successive plates of iron and polypropylene each of thickness 1.25 cm. The heterogeneous media were formed from two layers with the polypropylene layer placed behind the iron layer and near to the detector.

From these figures it can be seen that for homogeneous media the spectra shapes and their slopes do not change and remain approximately the same for the energy range 0.5 to 12 MeV and do not change with the increase of material thickness. However, for a heterogeneous shield, the spectrum shape becomes more flat and its slope decreases as the material thickness increases.

The figures also show that for homogeneous shields the measured spectra satisfactorily agree with those calculated using the removal diffusion and diffusion methods for media of thicknesses 10 and 20 cm and at lower neutron energies. However, for heterogeneous shields, the measured spectra show higher values than those calculated by both

methods. This difference increases with the increase in material thickness and neutron energies. For both the homogeneous and heterogeneous media, the spectra calculated by the group diffusion calculation are lower than that given by the removal-diffusion calculation. For homogeneous media this difference increases smoothly with the increase in material thickness and neutron energy, while it increases rapidly with the increasing of material thicknesses and neutron energies for a heterogeneous shield.

For neutrons in the first energy group (12 - 14 MeV), the average measured fluxes are lower than the calculated ones. This also can be attributed to the same reasons mentioned before for iron and iron-graphite shields.

#### 8.5 Comparisons between the Leakage Spectra through Different Media of the Same Thickness

The measured neutron fluxes behind various thicknesses of iron and homogeneous and heterogeneous shields of iron graphite and iron-polypropylene are shown in figures 8.20 to 8.27, for eight energy groups separately from 14 MeV to 0.8 MeV. To obtain these curves the measured fluxes were integrated over the group boundaries used for the extended Abagyan data set. The relations are plotted as neutron fluxes per  $\text{cm}^2$  per sec versus shield thickness  $D$ .

The figures show that iron is the most effective shield for fast neutron attenuation of the first, second and third group, i.e. neutrons in the energy range from 14 MeV to 6.5 MeV. They also show within this energy range shields of homogeneous iron polypropylene are more effective than the other measured mixtures of heterogeneous iron-polypropylene or of homogeneous and heterogeneous iron-graphite. It is evident that the heterogeneous iron-graphite shields are the poorest attenuators for neutrons of energies from 14 MeV to 2.5 MeV.

In the fourth group (6.5 - 4 MeV) iron and homogeneous iron-

polypropylene shields compete for the best neutron attenuator. For neutrons of the fifth up to the eighth group, homogeneous iron-polypropylene followed by the heterogeneous shields of these elements are the best for neutron attenuation, while iron and homogeneous shields of iron-graphite show the least neutron attenuation. This can be attributed to the fact that within these energy ranges, where the elastic scattering with hydrogen is predominant and the cross section increases with the decreasing of neutron energy, shields of the two layer form with iron layer preceding the polypropylene one are more effective for low energy neutron attenuation. However, for iron shields, the flux attenuation is least at lower neutron energies since the values of the inelastic scattering cross section which is the main removal mechanism in iron decreases with decreasing neutron energy.

#### 8.6 Determination of the Removal Cross Sections

In the removal diffusion calculations, the removal cross sections are used to determine the number of neutrons which are removed from the first energy group by removal collisions and which are treated as sources for a multigroup diffusion calculation. It is obvious from equation 7.20 that the value of the removal cross section can be determined if the flux values at two different radial positions are known.  $\Sigma_{rem}$  can be given by:

$$\Sigma_{rem} = - \frac{(\log_e \phi_{R_1} \cdot R_1^2 - \log_e \phi_{R_2} \cdot R_2^2)}{R_2 - R_1} \quad \dots \dots \dots 8.1$$

where  $\phi_{R_1}$  and  $\phi_{R_2}$  are the neutron leakage fluxes from outer boundaries at radial positions  $R_1$  and  $R_2$  respectively.

From equation 8.1, it is clear that the determination of  $\Sigma_{rem}$  does not need the knowledge of the absolute source strength, also the uncertainty in the absolute efficiency of the detector and that in source strength determination by the neutron monitor do not enter during the

evaluation of  $\Sigma_{\text{rem}}$ . However, the most likely uncertainty can be due to the measuring of  $R_n$ , since  $R_n$  is squared and multiplied by the neutron flux  $\phi_{R_n}$ .

In this work the average value of  $R_n$  was determined from the knowledge of  $R_o$  which is the distance from the neutron source and inner boundary of the shield. The average value of  $R_o$  was determined from several measurements and is given as  $R_o = 14 \pm 0.25$  cm. This was added to the material thickness which is determined from the knowledge of plate thicknesses.

The values of the measured neutron fluxes behind iron and homogeneous and heterogeneous shields of iron-graphite and iron-polypropylene are multiplied by  $R^2$  and plotted against  $R$  for the first energy group (14 - 12 MeV), and are presented in figures 8.28 to 8.32. The figures also show the calculated group one fluxes by the removal and diffusion calculation methods after multiplication by  $R^2$ .

#### 8.6.1 $\sigma_{\text{rem}}$ for iron

The graphs shown in figure 8.28 are the measured and calculated values of the leakage neutron fluxes for the iron assembly. From the measured relation the average value of the macroscopic removal cross section  $\Sigma_{\text{rem}}$  has been determined by the least squares fit to be

$$\Sigma_{\text{rem}} = 0.1278 \pm 0.0047 \text{ cm}^{-1}$$

Compared with  $0.1255 \text{ cm}^{-1}$  used in the calculations.

This value of the macroscopic removal cross section gives a microscopic removal cross section for 14 MeV neutrons of

$$\sigma_{\text{rem}} = 1.506 \pm 0.055 \text{ barns}$$

using these values for the iron

$$\text{density } \rho = 7.83 \text{ g/cm}^3 \quad \text{and}$$

$$\text{number density } N_D(\text{Fe}) = 0.0845 \text{ atoms/cm}^3$$

This measured value of  $\sigma_{\text{rem}}$  for iron agrees quite well with the value calculated by Avery et al<sup>(113)</sup>. The latter is based on the results of Feshbach and Weisskopf who had predicted the ratio of transport to total cross section as a function of atomic weight and energy on the basis of the theoretical model of the nucleus. From these tabulated values, the value of  $\sigma_{\text{rem}}$  at 13.5 MeV is 1.48 barns and at 14.5 MeV is 1.39 barns.

It should be noted that the energy of the source neutrons is 14.1 MeV but that the removal cross section was determined from the investigated leakage flux between 12 and 14 MeV. Due to degradation mainly by elastic collisions, the average energy of neutrons in this group will be less than 14.1 MeV for any finite thickness of shield.

#### 8.6.2. $\sigma_{\text{rem}}$ for carbon

The value of the microscopic removal cross section  $\sigma_{\text{rem}}$  for carbon has been derived from the given values of  $\Sigma_{\text{rem}}$  determined from the relations of  $\phi_R \cdot R^2$  against R for a homogeneous and heterogeneous shields of iron graphite which are presented in figures 8.29 and 8.30 for the first energy group (14 - 12 MeV). These relations give the following values of macroscopic cross section

$$0.099 \pm 0.001 \text{ cm}^{-1} \text{ for the homogeneous shield and}$$

$$0.100 \pm 0.088 \text{ cm}^{-1} \text{ for the heterogeneous shield.}$$

Compared with  $0.0993 \text{ cm}^{-1}$  used in the calculations.

Using the measured value of  $\Sigma_{rem}$  for iron and the following characteristic parameters for carbon

$$\text{Density } \rho = 1.718 \text{ gm.cm}^{-3} \quad \text{and}$$

$$\text{Number density } N_D(\text{C}) = 0.08613 \text{ atoms.cm}^{-3}$$

The average value of the microscopic removal cross section  $\sigma_{rem}$  is given as

$$\sigma_{rem} = 0.83 \pm 0.11 \text{ barns.}$$

This value of  $\sigma_{rem}$  for carbon agrees within experimental error with Avery's value at 13.5 MeV which is 0.85 barns.

#### 8.6.3 $\sigma_{rem}$ for hydrogen

Figures 8.31 and 8.32 show the relations between  $\phi_{Rn} \cdot R_n^2$  versus  $R_n$  for 14 - 12 MeV neutron for both homogeneous and heterogeneous shields of iron-polypropylene. From these relations the values of macroscopic removal cross section are found to be

$$0.11 \pm 0.035 \text{ cm}^{-1} \text{ for the homogeneous shield} \quad \text{and}$$

$$0.107 \pm 0.059 \text{ cm}^{-1} \text{ for the heterogeneous shield.}$$

Compared with  $0.109 \text{ cm}^{-1}$  used in the calculations.

The investigated polypropylene has the following characteristic parameters

Chemical formula  $C_n H_{2n}$

$$\text{Density } \rho = 0.95 \text{ gm.cm}^{-3}$$

$$\text{Number density of carbon } N_D(\text{C}) = 0.0409 \text{ atoms.cm}^{-3} \quad \text{and}$$

$$\text{Number density of hydrogen } N_D(\text{H}) = 0.0818 \text{ atoms.cm}^{-3}$$

Using these parameters and the previous measured values of the  $\Sigma_{\text{rem}}$  for iron and carbon, the value of the microscopic removal cross section  $\sigma_{\text{rem}}$  for hydrogen can be derived from these two measured values of  $\Sigma_{\text{rem}}$  for iron-polypropylene shields, these are:

$$0.75 \pm 0.12 \text{ barns from the homogeneous shield}$$

and

$$0.64 \pm 0.17 \text{ barns from the heterogeneous shield.}$$

These two values give this average value of the microscopic cross section for hydrogen

$$\sigma_{\text{rem}} = 0.69 \pm 0.10 \text{ barns}$$

It is evident that the value of  $\sigma_{\text{rem}}$  derived from the homogeneous shields agrees quite well with Avery's value at 13.5 MeV which is 0.75 barns. However, for the heterogeneous shields a lower value for  $\sigma_{\text{rem}}$  is obtained but there is still agreement within the experimental error with Avery's value. This points out the need for very high accuracy in the measurements when determining the removal cross section of one component of a mixture by subtraction.

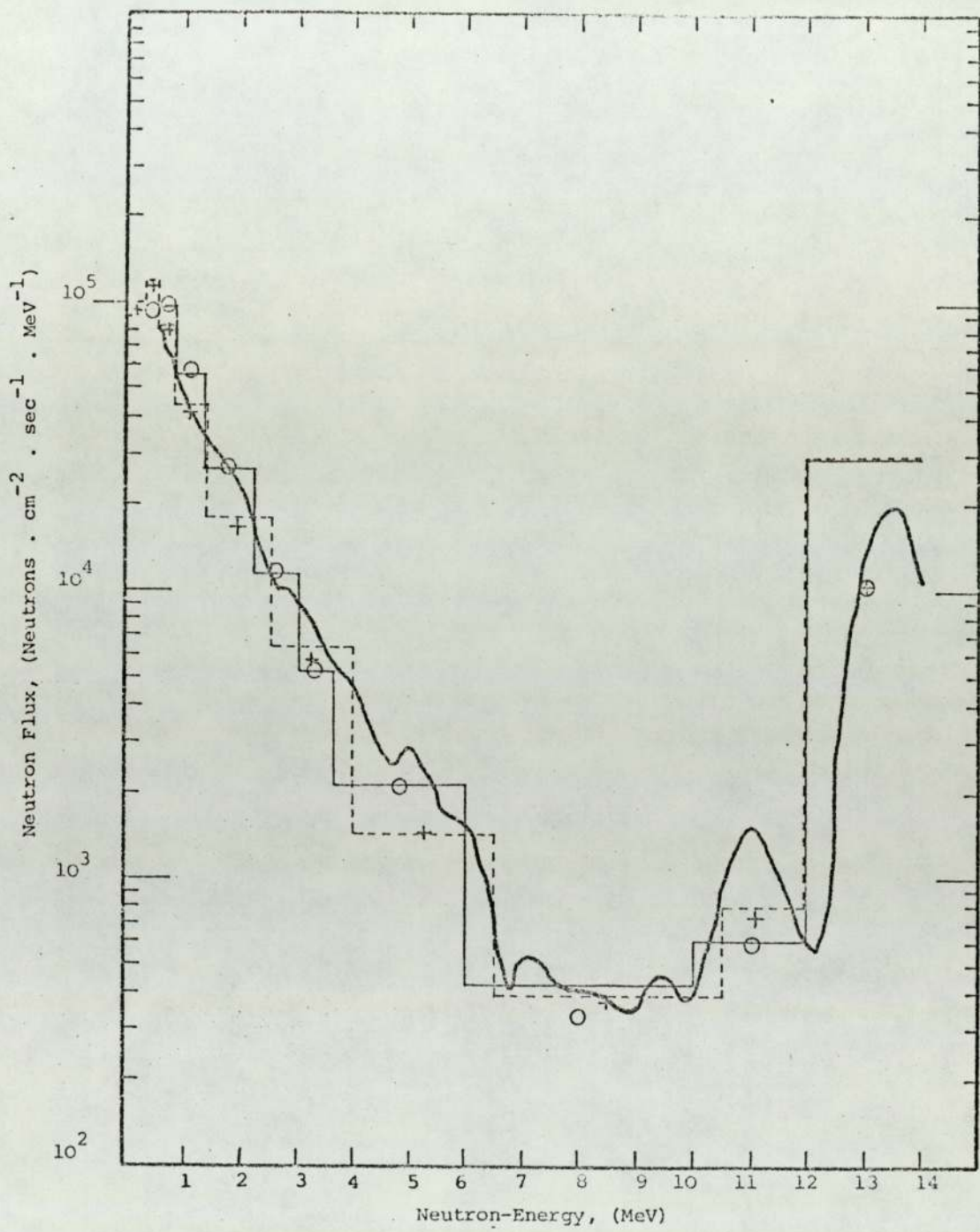


Figure 8.1. Spectra of Fast Neutrons behind an Iron Shield of Thickness 10 cm

- YOM-20, Removal Calculations
  - ABBN, Removal Calculations
- YOM-20, Diffusion Calculations
  - + ABBN, Diffusion Calculations
  - Measured

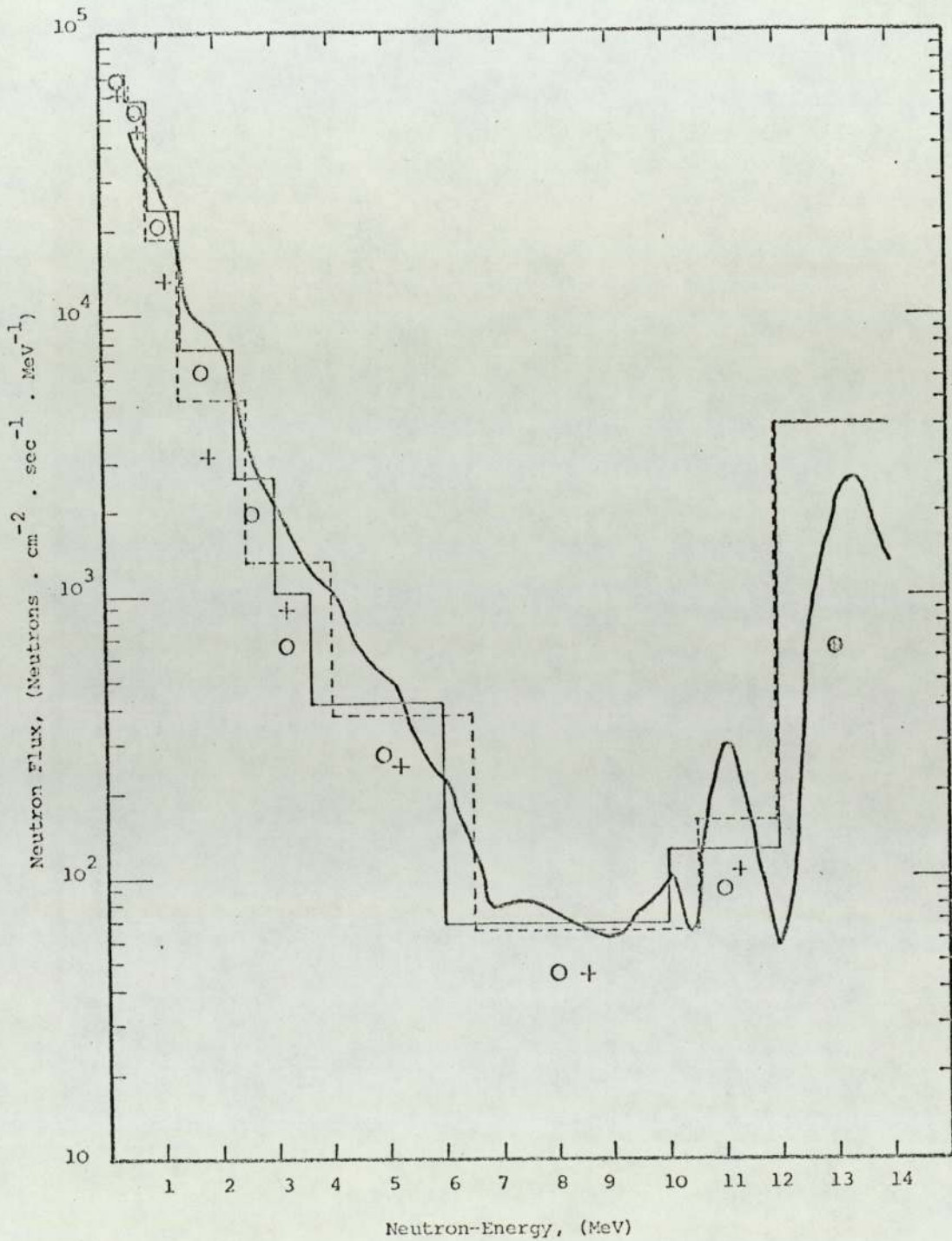


Figure 8.2. Spectra of Fast Neutrons behind an Iron Shield of Thickness 20 cm

- |  |  |
|--|--|
|  YOM-20, Removal Calculations |  YOM-20, Diffusion Calculations |
|  ABBN, Removal Calculations   |  ABBN, Diffusion Calculations   |
|  |  Measured                       |

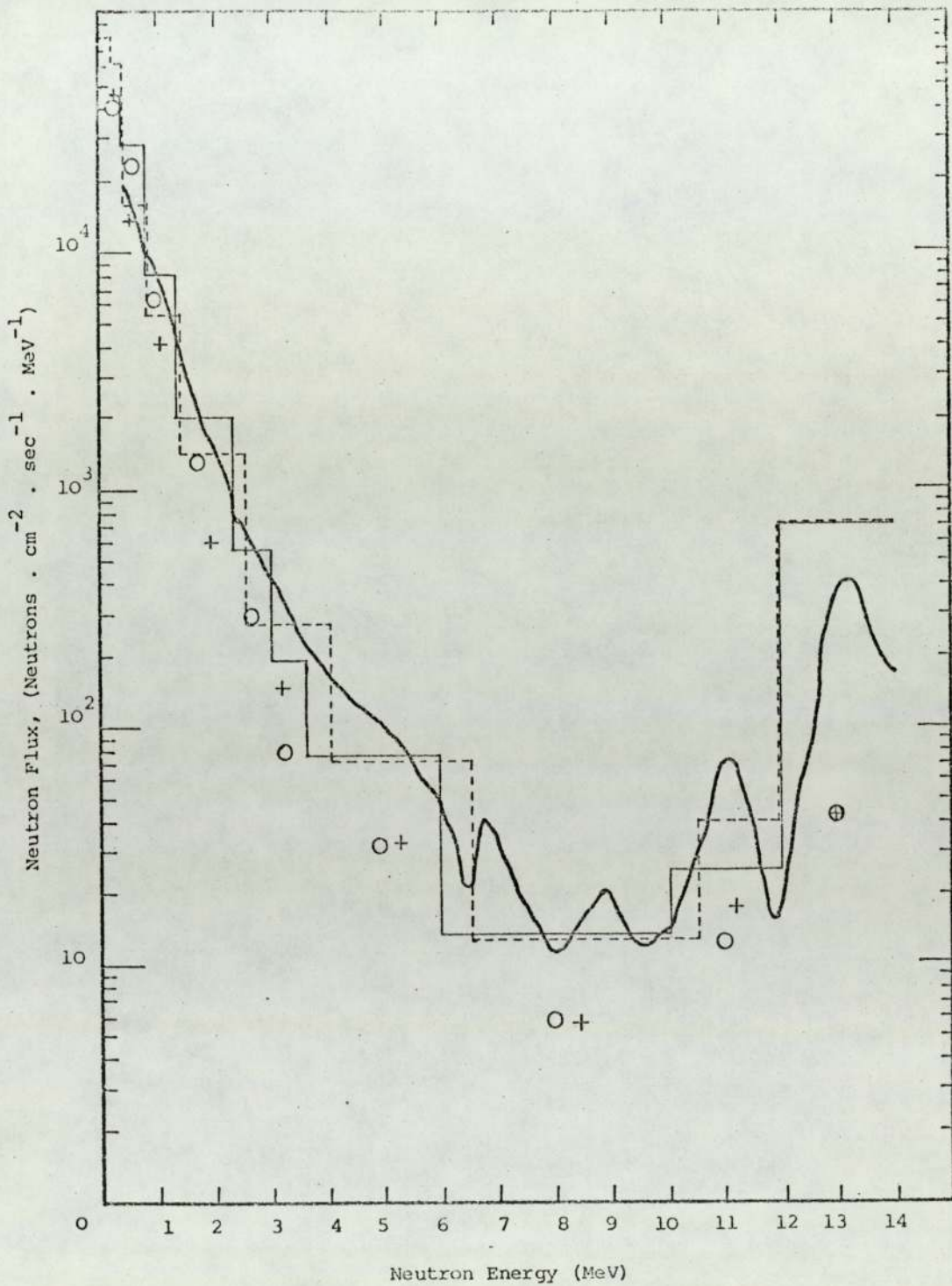


Figure 8.3. Spectra of Fast Neutrons behind an Iron Shield of Thickness 30 cm

 YOM-20, Removal Calculations	 YOM-20, Diffusion Calculations
 ABBN, Removal Calculations	 ABBN, Diffusion Calculations
	 Measured

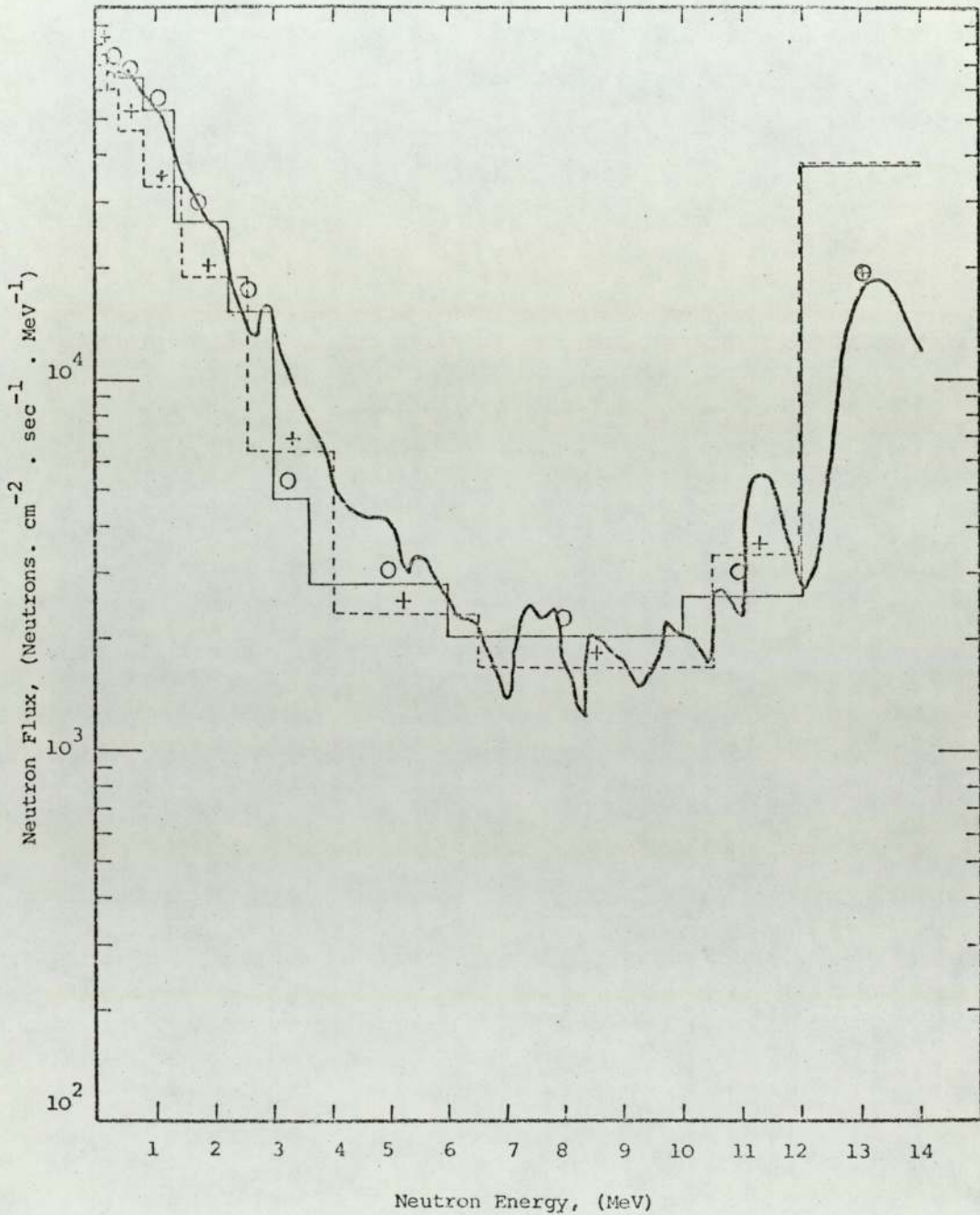


Figure 8.4. Fast Neutron Spectra behind a Homogenous Shield of Iron-Graphite of thickness 10 cm

 YOM-20, Removal Calculations	 YOM-20, Diffusion Calculations
 ABBN, Removal Calculations	 ABBN, Diffusion Calculations
	 Measured

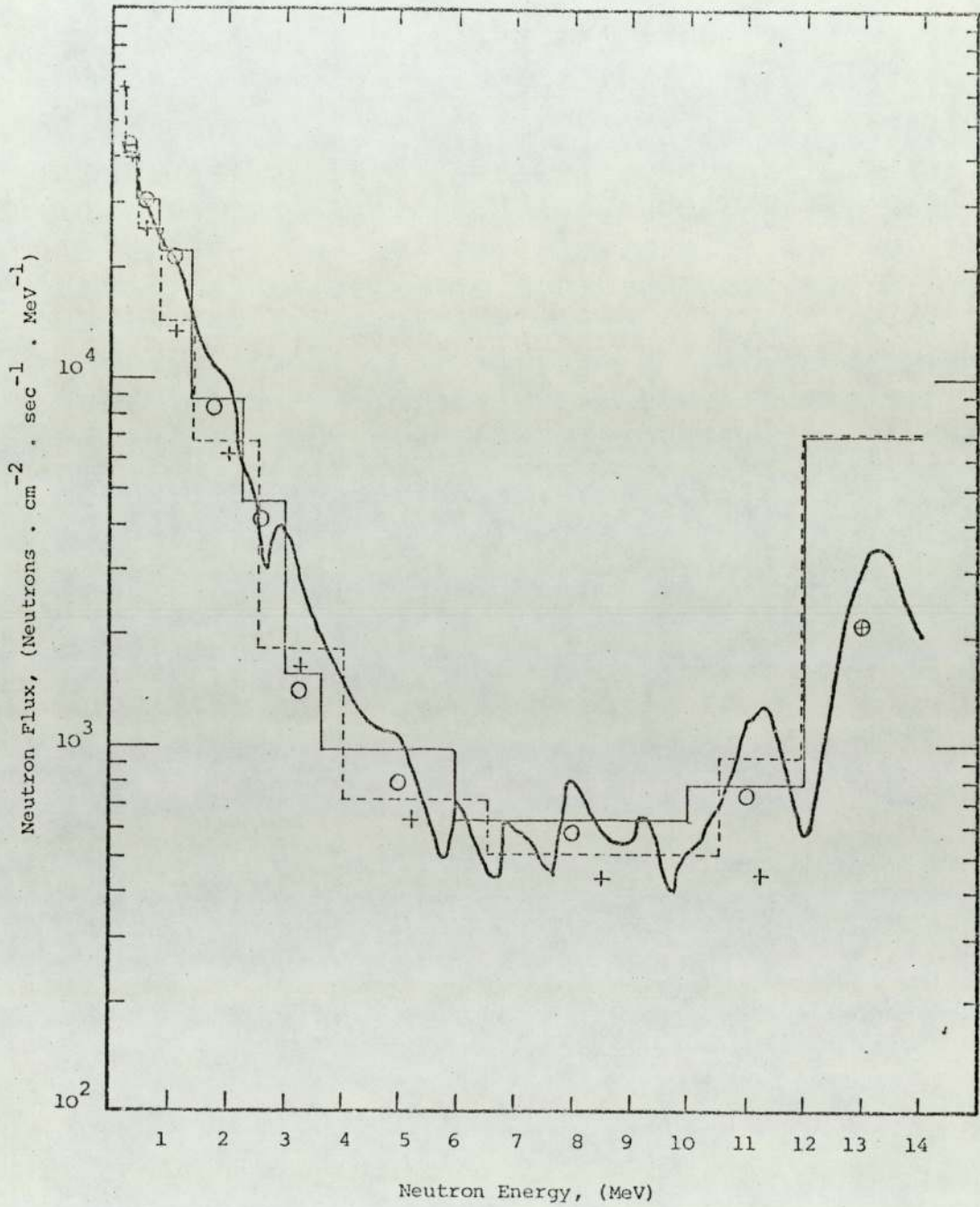


Figure 8.5. Fast Neutron Spectra behind a Homogenous Shield of Iron-Graphite of thickness 20 cm

- |       |                              |   |                                |
|-------|------------------------------|---|--------------------------------|
| —     | YOM-20, Removal Calculations | ○ | YOM-20, Diffusion Calculations |
| - · - | ABBN, Removal Calculations   | + | ABBN, Diffusion Calculations   |
| —     |                              | ~ | Measured                       |

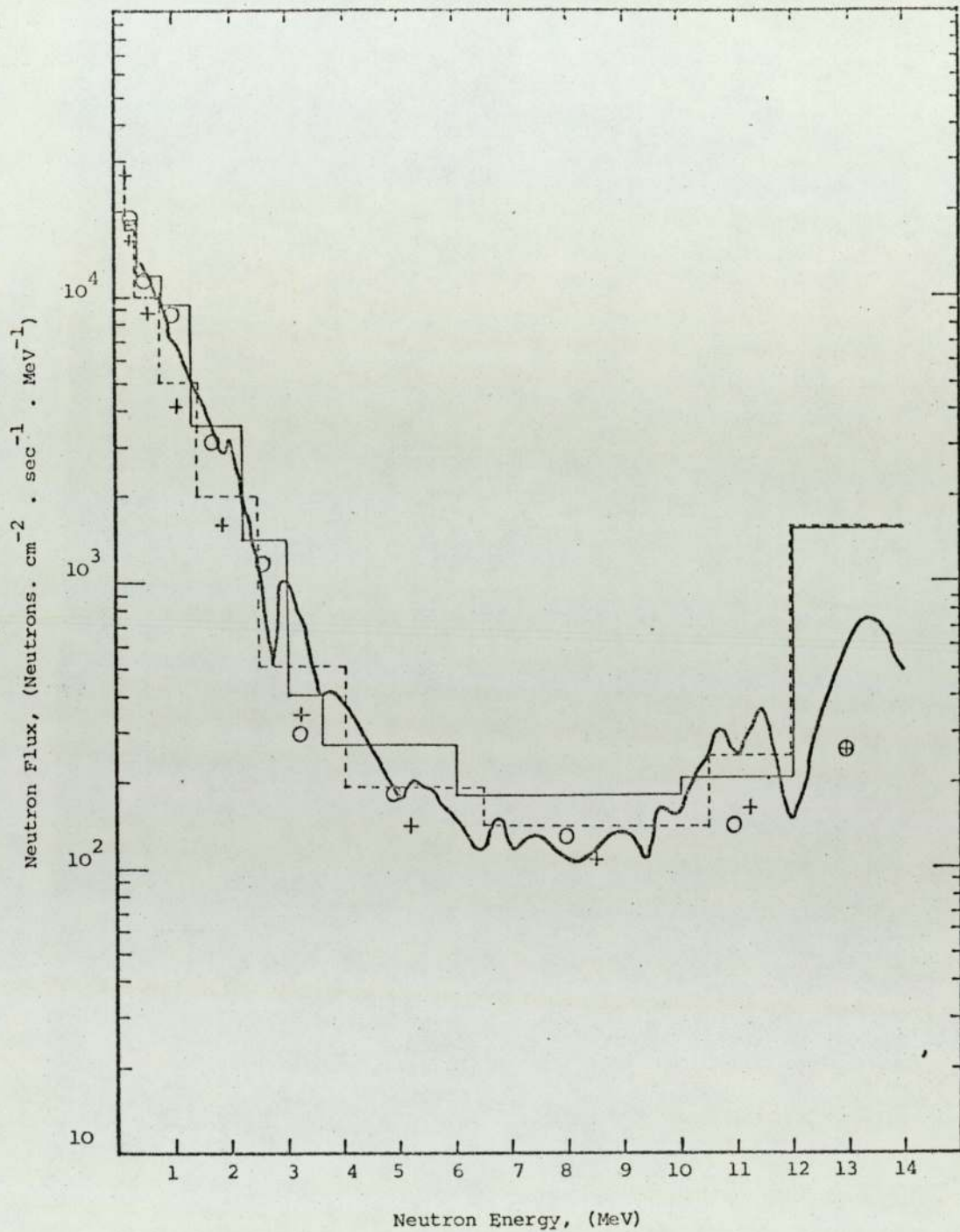


Figure 8.6. Spectra of Fast Neutrons behind a Homogenous Shield of Iron-Graphite of thickness 30 cm

 YOM-20, Removal Calculations	 YOM-20, Diffusion Calculations
 ABEN, Removal Calculations	 ABEN, Diffusion Calculations
	 Measured

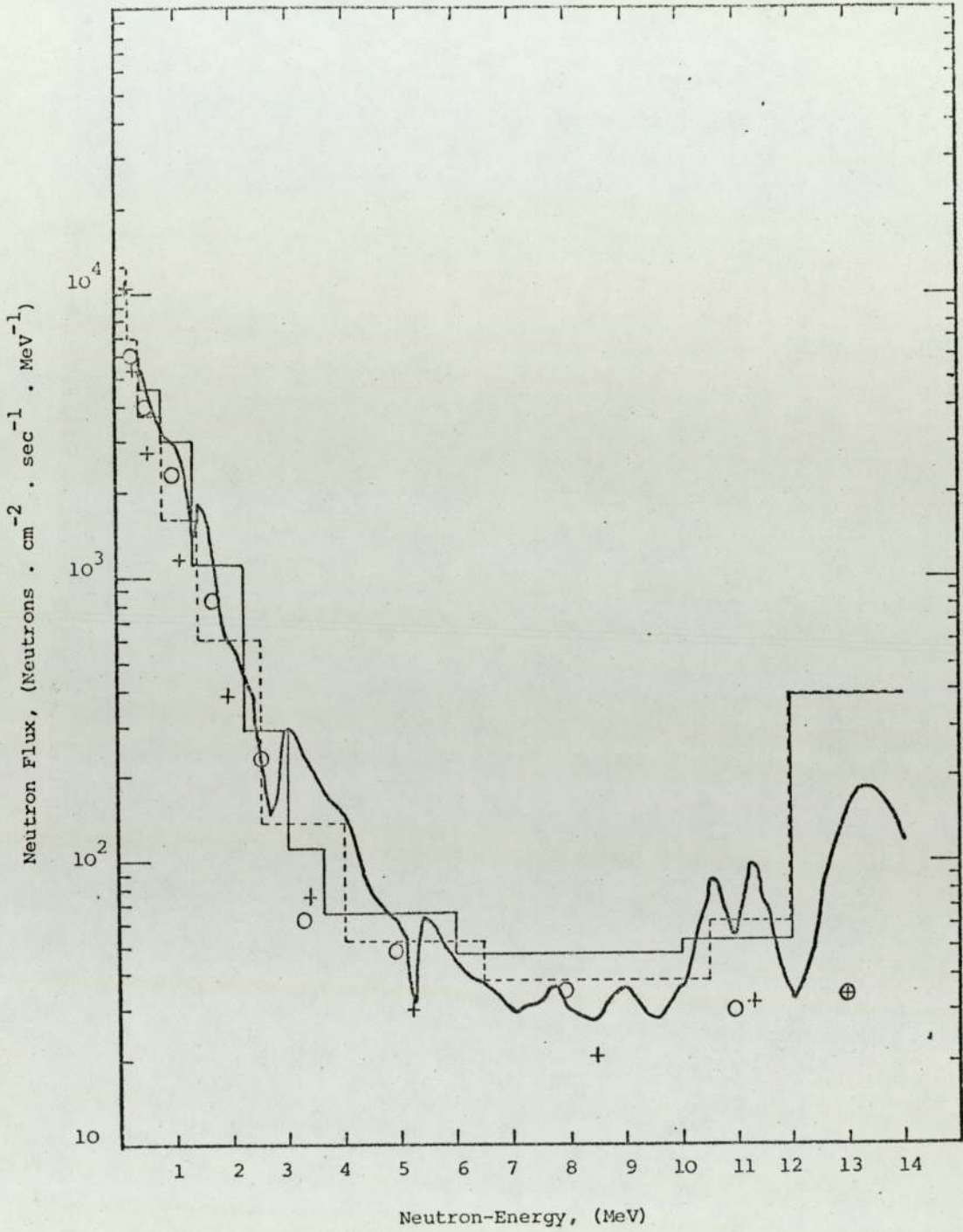


Figure 8.7. Spectra of Fast Neutrons behind a Homogenous Shield of Iron-Graphite of thickness 40 cm

—	YOM-20, Removal Calculations	○	YOM-20, Diffusion Calculations
- - -	ABBN, Removal Calculations	+	ABBN, Diffusion Calculations
~		~	Measured

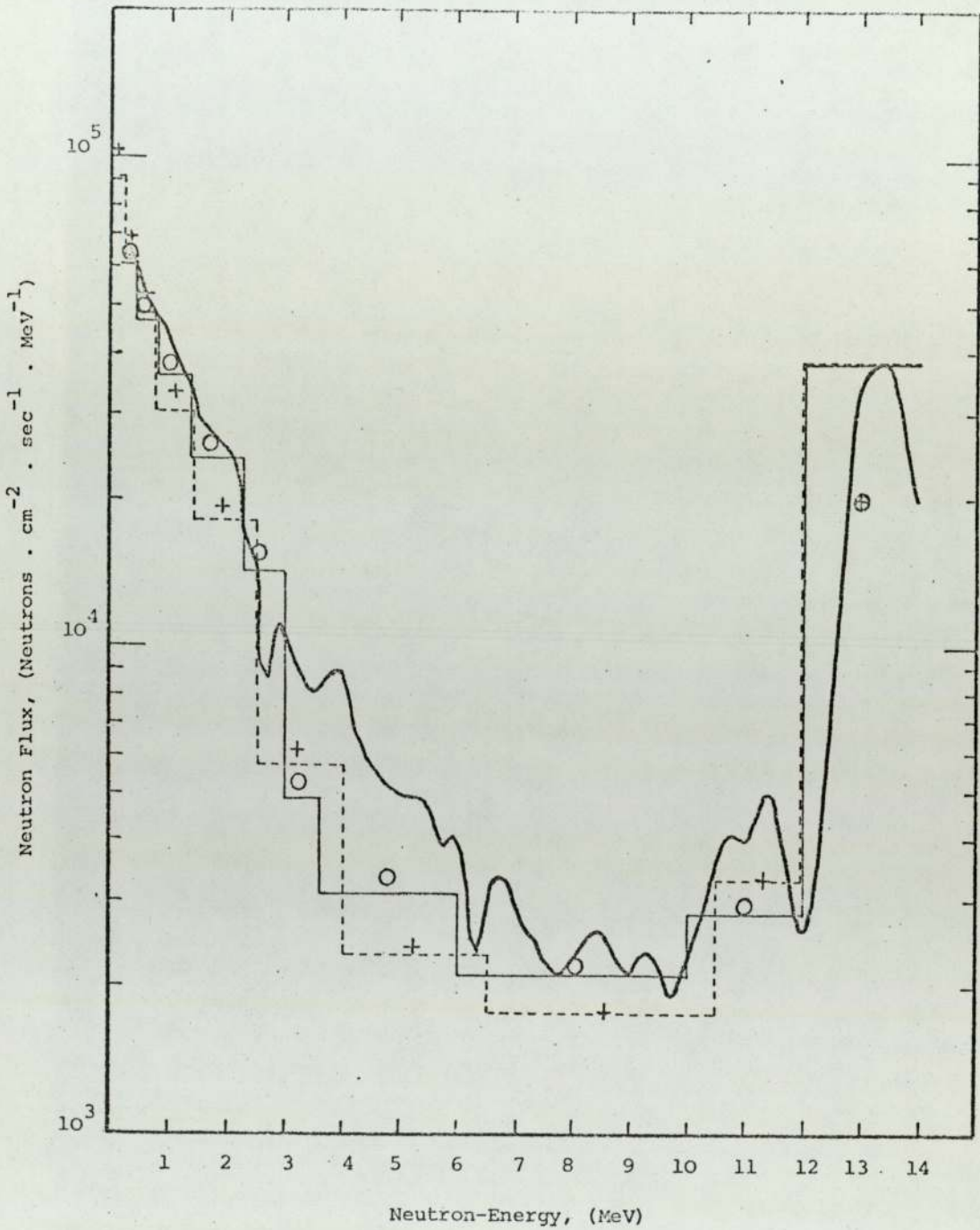


Figure 8.8. Spectra of Fast Neutrons behind a Heterogeneous Shield of Iron-Graphite of thickness 10 cm

- |                             |                               |
|-----------------------------|-------------------------------|
| YOM-20 Removal Calculations | YOM-20 Diffusion Calculations |
| ABBN, Removal Calculations  | ABBN, Diffusion Calculations  |
| Measured                    |                               |

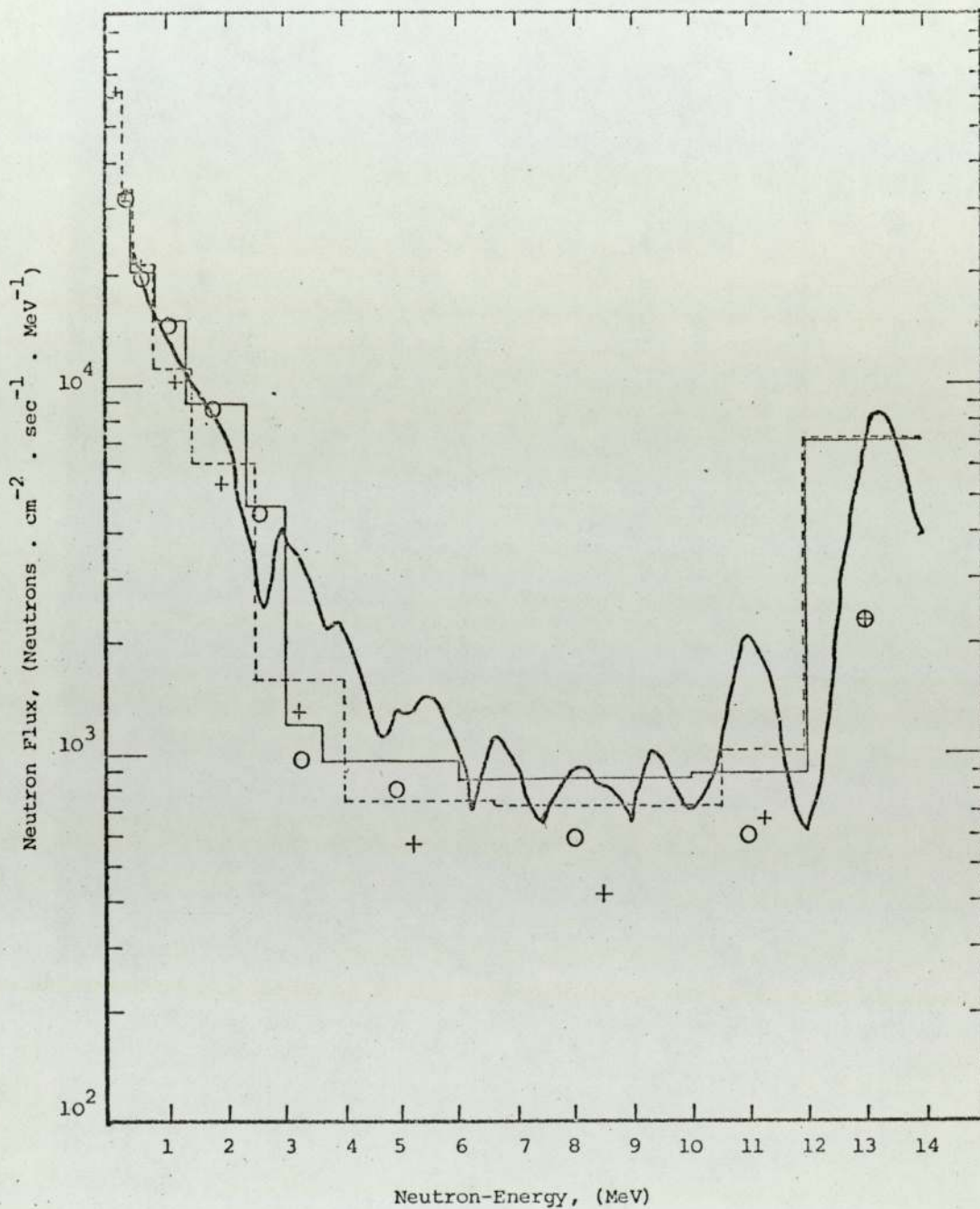


Figure 8.9. Spectra of Fast Neutrons behind a Heterogeneous Shield of Iron-Graphite of Thickness 20 cm

 YOM-20, Removal Calculations	 YOM-20, Diffusion Calculations
 ABBN, Removal Calculations	 ABBN, Diffusion Calculations
	 Measured

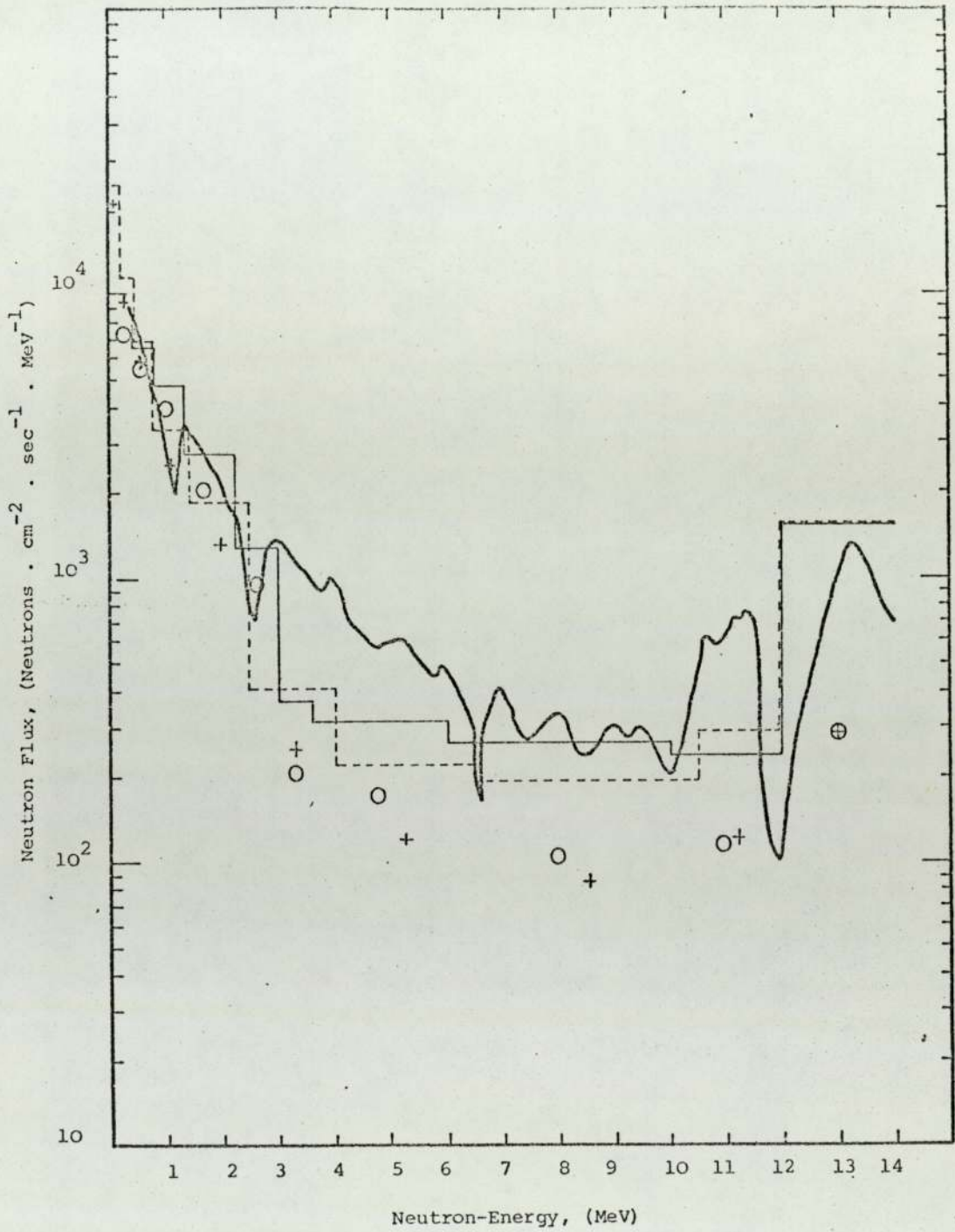


Figure 8.10. Spectra of Fast Neutrons behind a Heterogeneous Shield of Iron-Graphite of Thickness 30 cm

YOM-20, Removal Calculations	YOM-20, Diffusion Calculations
ABBN, Removal Calculations	ABBN, Diffusion Calculations
	Measured

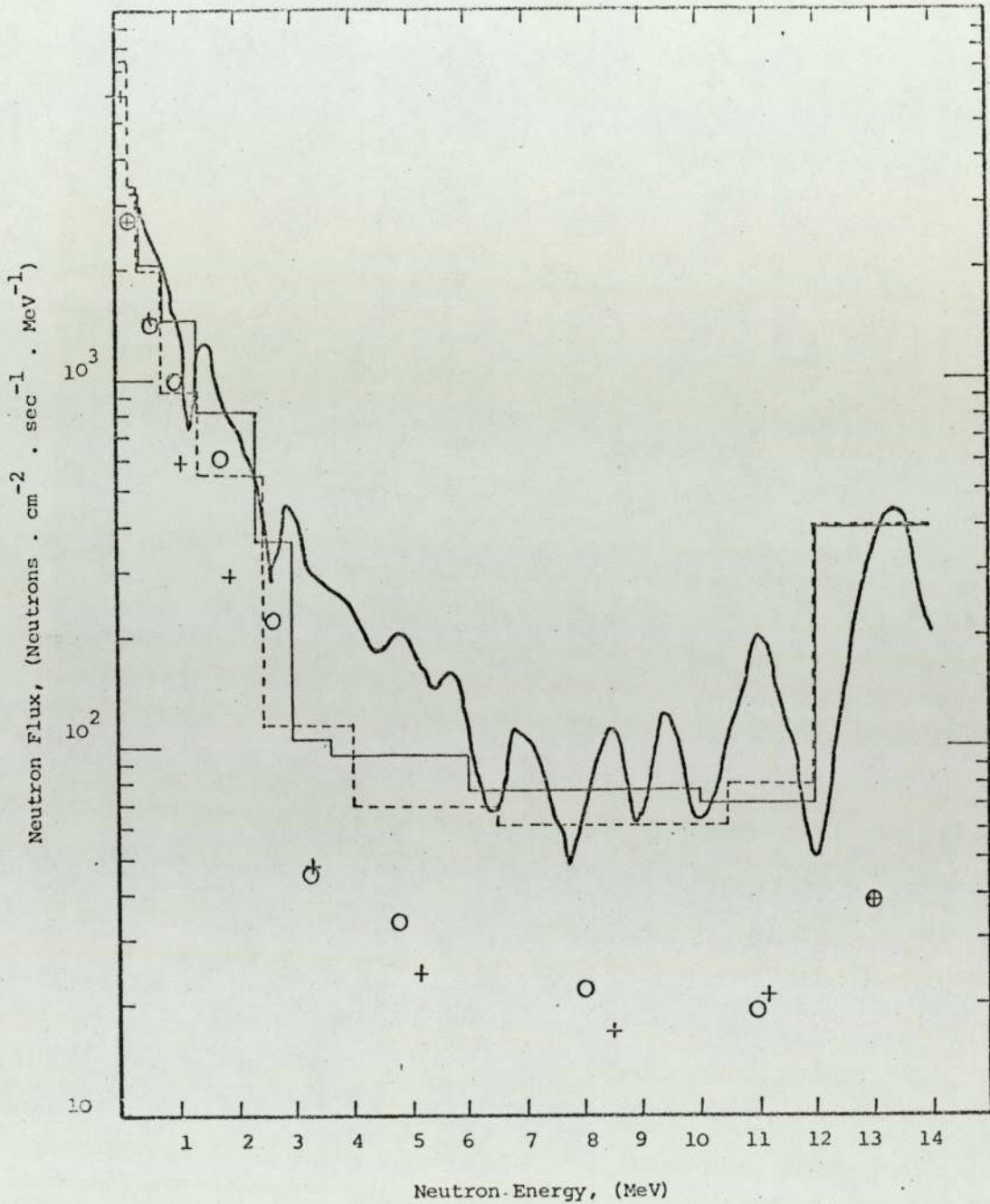


Figure 8.11. Spectra of Fast Neutron behind a Heterogeneous Shield of Iron-Graphite of thickness 40 cm

	YOM-20, Removal Calculations		YOM-20 Diffusion Calculations
	AEBN, Removal Calculations		AEBN, Diffusion Calculations
			Measured

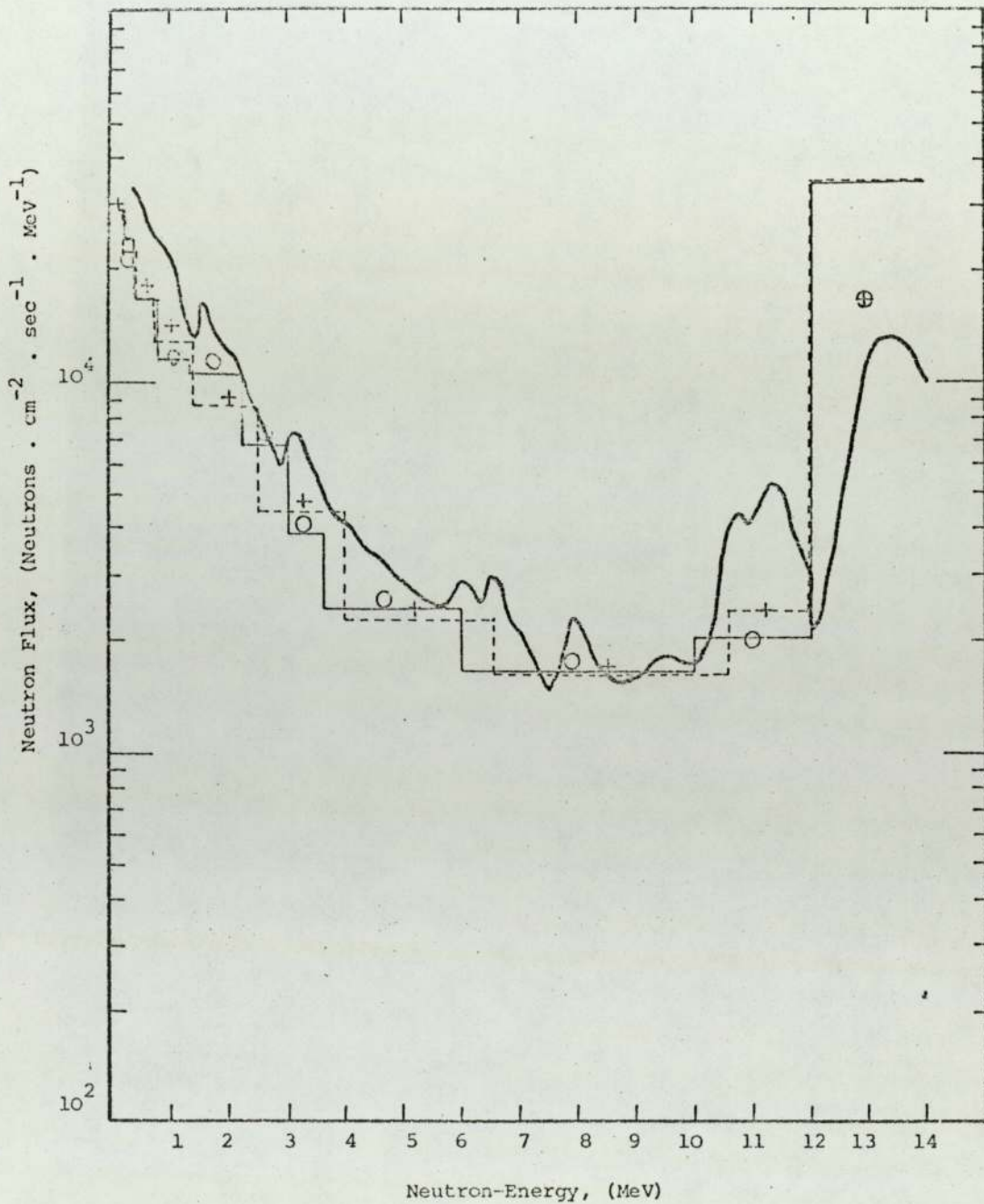


Figure 8.12. Spectra of Fast Neutrons behind a Homogeneous Shield of Iron-Polypropylene of thickness 10 cm.

—	YOM-20, Removal Calculations	○	YOM-20, Diffusion Calculations
- - -	ABBN, Removal Calculations	+	ABBN, Diffusion Calculations
—		~	Measured

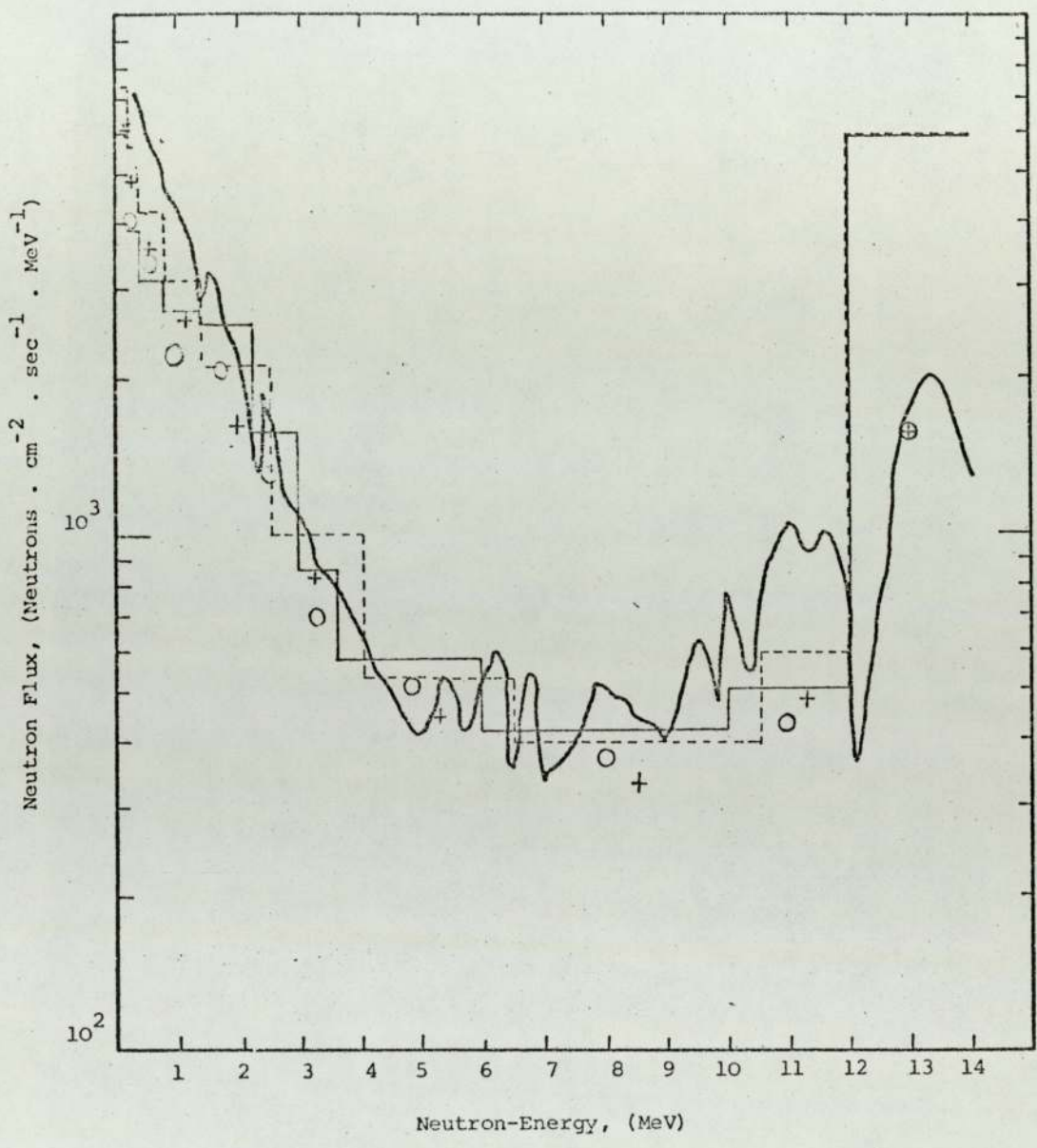


Figure 8.13. Spectra of Fast Neutrons behind a Homogeneous Shield of Iron-polypropylene of thickness 20 cm.

- YOM-20, Removal Calculations
 

 YOM-20, Diffusion Calculations
- ABBN, Removal Calculations
 

 ABBN, Diffusion Calculations
- Measured

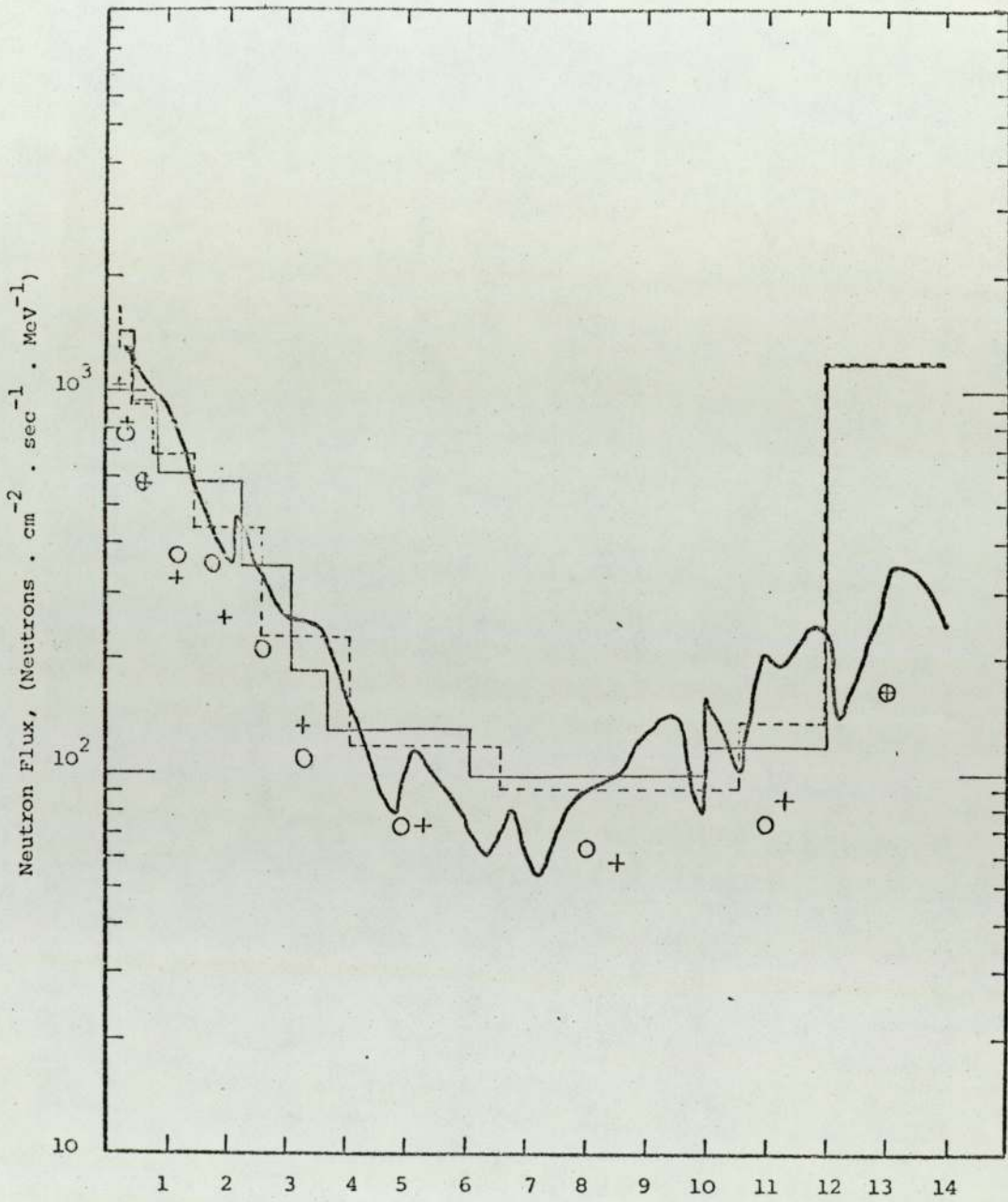


Figure 8.14. Spectra of Fast Neutrons behind a Homogeneous Shield of Iron-polypropylene of thickness 30 cm.

- |           |                              |   |                                |
|-----------|------------------------------|---|--------------------------------|
| —         | YOM-20, Removal Calculations | ○ | YOM-20, Diffusion Calculations |
| - · - · - | ABBN, Removal Calculations   | + | ABBN, Diffusion Calculations   |
| —         |                              | ~ | Measured                       |

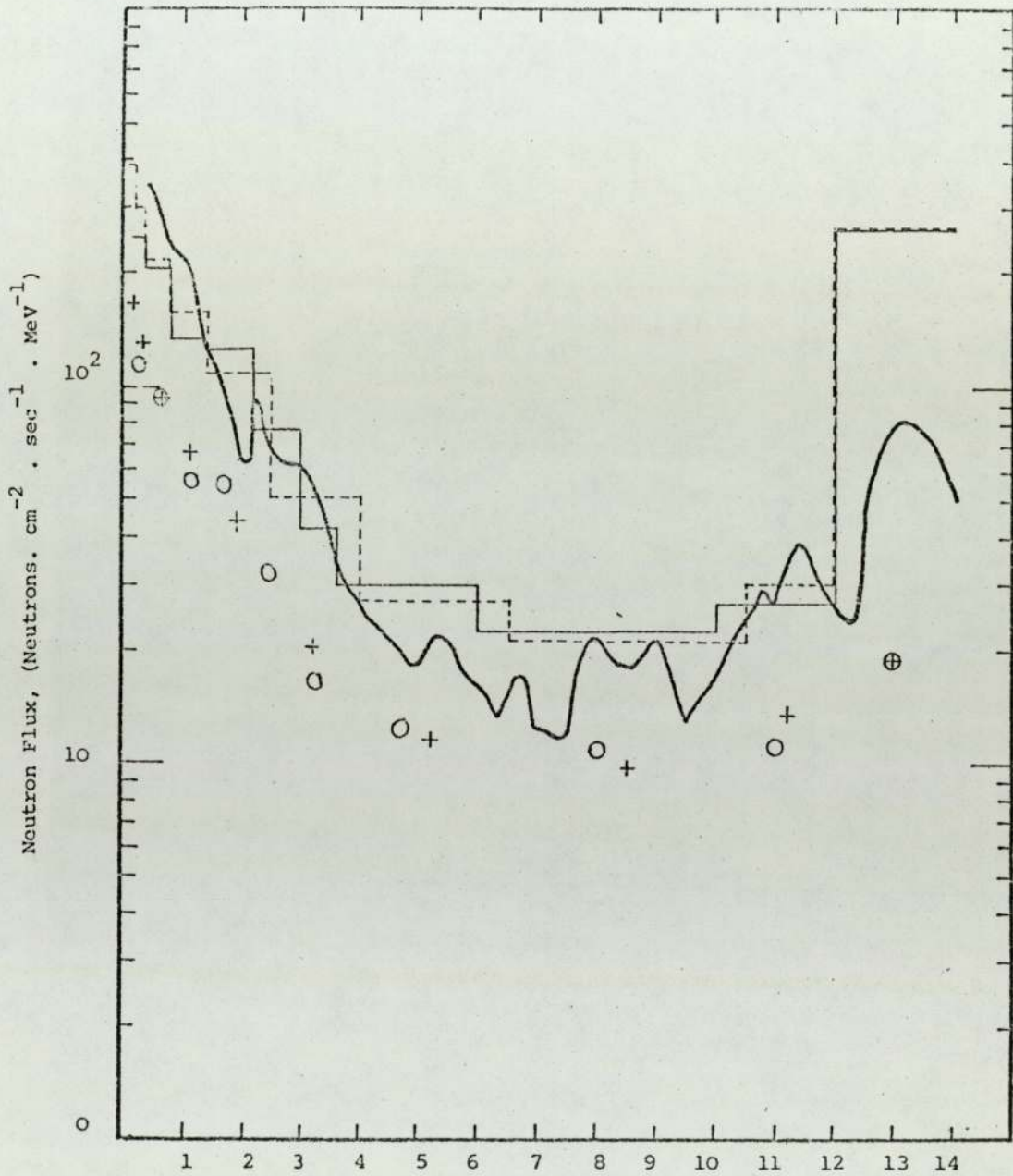


Figure 8.15. Spectra of Fast Neutrons behind a Homogeneous Shield of Iron-polypropylene of thickness 40 cm.

 YOM-20, Removal Calculations	 YOM-20, Diffusion Calculations
 ABBN, Removal Calculations	 ABBN, Diffusion Calculations
	 Measured

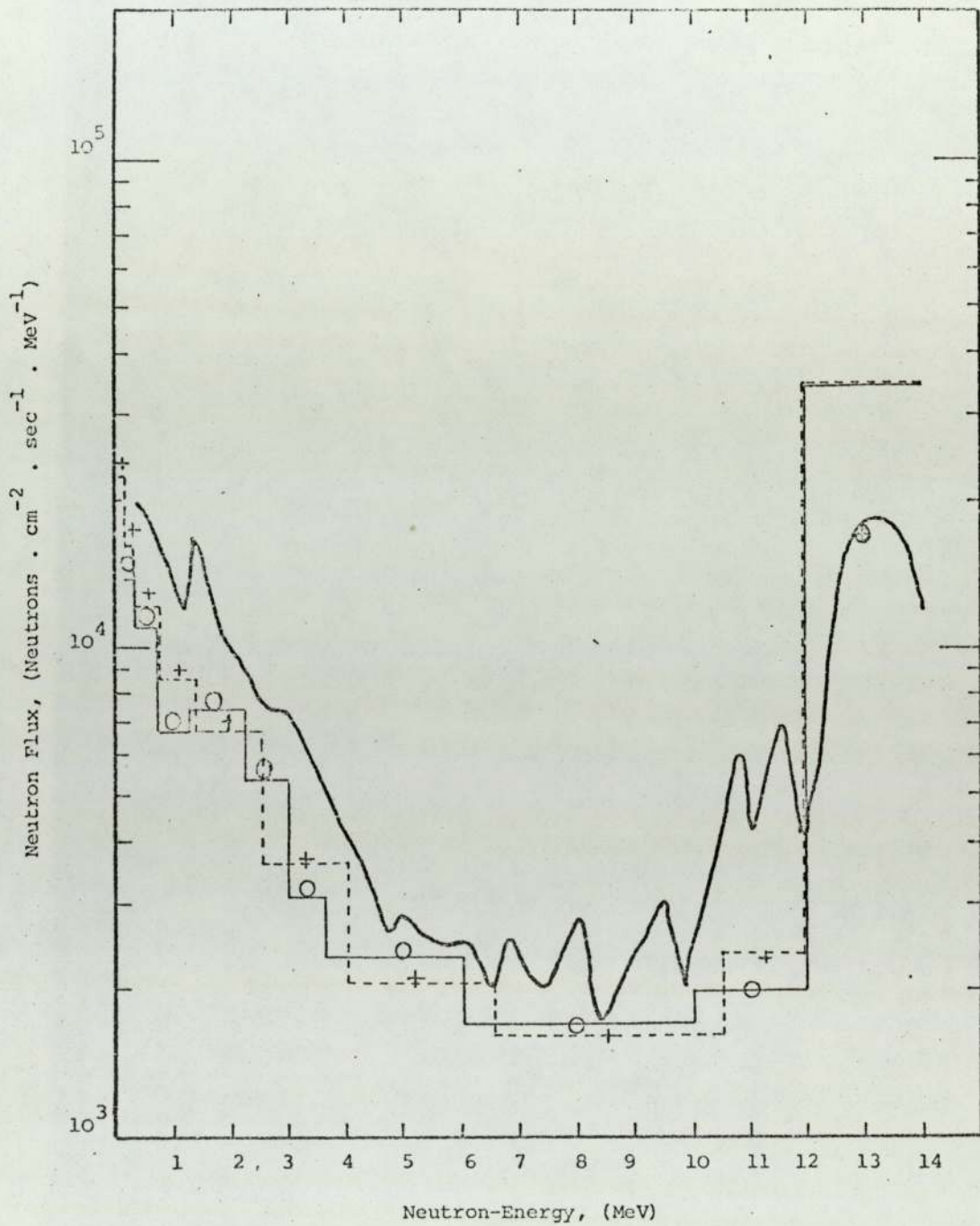


Figure 8.16. Spectra of Fast Neutrons behind a Heterogeneous Shield of Iron-polypropylene of thickness 10 cm.

— YOM-20, Removal Calculations      o YOM-20, Diffusion Calculations  
 - - - ABBN, Removal Calculations      + ABBN, Diffusion Calculations  
 ~~~~~ Measured

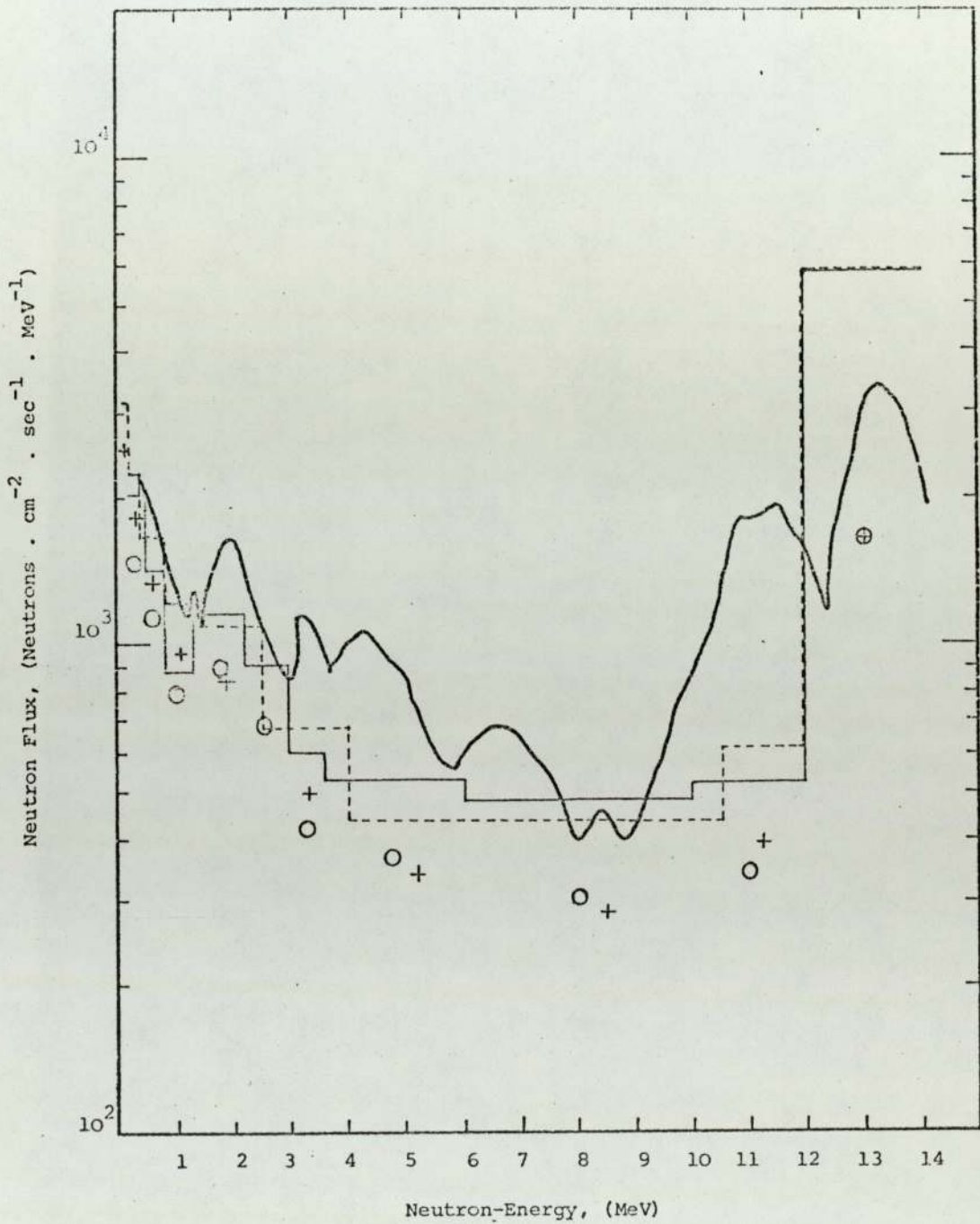


Figure 8.17. Spectra of Fast Neutrons behind a Heterogeneous Shield of Iron-Polypropylene of thickness 20 cm.

|           |                              |   |                               |
|-----------|------------------------------|---|-------------------------------|
| —         | YOM-20, Removal Calculations | o | YOM-20 Diffusion Calculations |
| - · - · - | ABBN, Removal Calculations   | + | ABBN, Diffusion Calculations  |
| —         |                              | ~ | Measured                      |

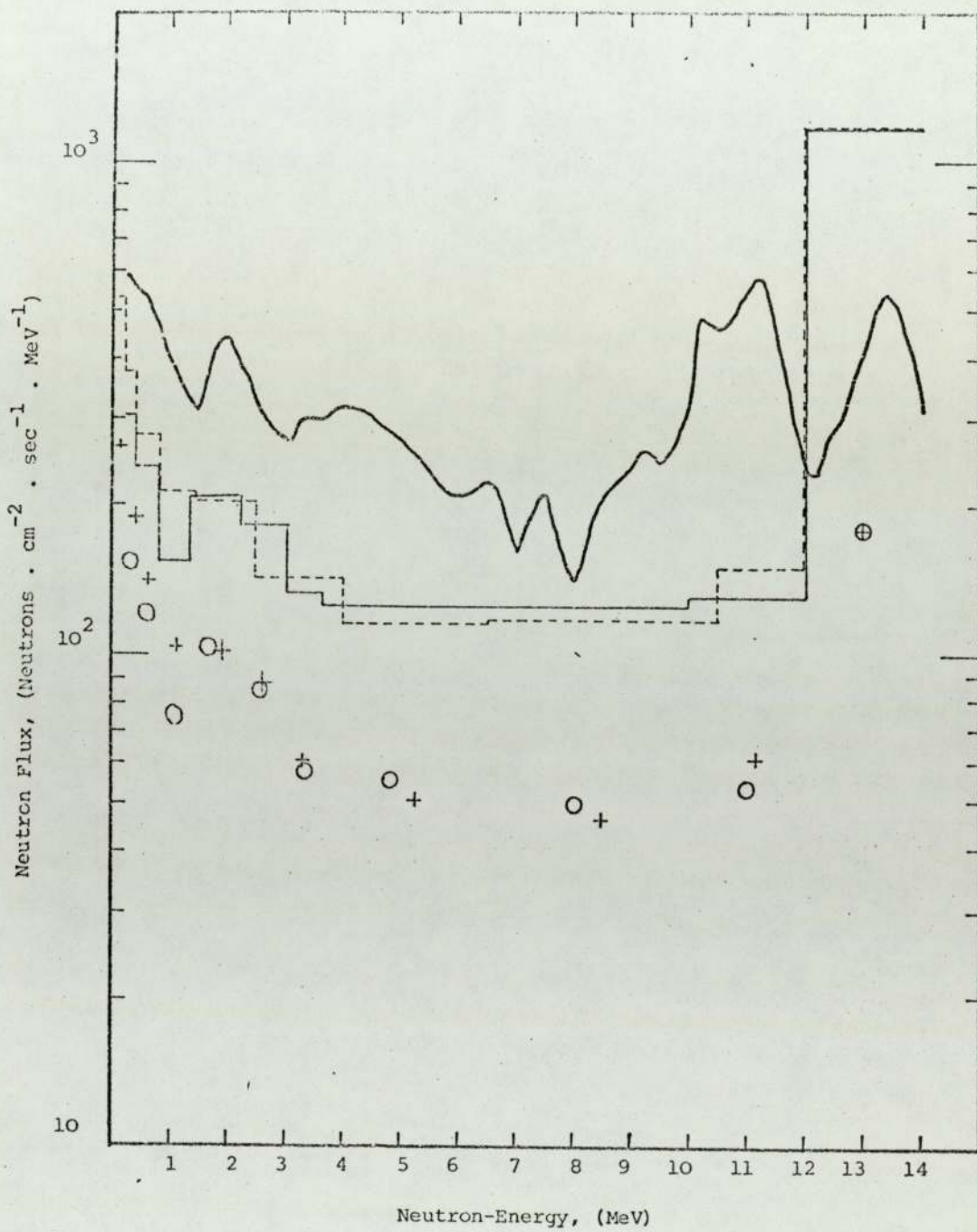


Figure 8.18. Spectra of Fast Neutrons behind a Heterogeneous Shield of Iron-polypropylene of thickness 30 cm.

|           |                              |   |                                |
|-----------|------------------------------|---|--------------------------------|
| —         | YOM-20, Removal Calculations | o | YOM-20, Diffusion Calculations |
| - · - · - | ABBN, Removal Calculations   | + | ABBN, Diffusion Calculations   |
| —         |                              | ~ | Measured                       |

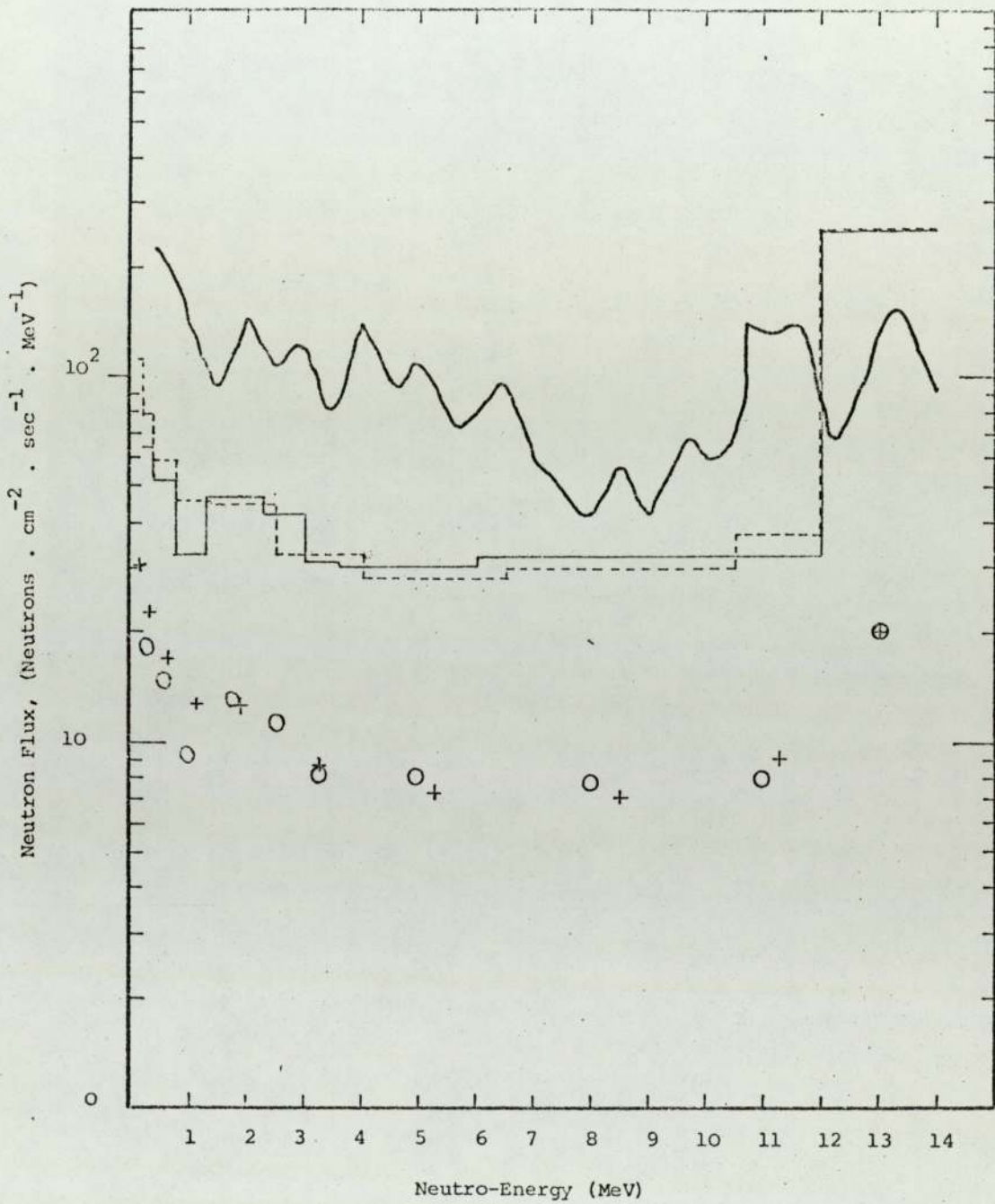


Figure 8.19. Spectra of Fast Neutrons behind a Heterogeneous Shield of Iron-polypropylene of thickness 40 cm

|                                                                                     |                              |                                                                                     |                                |
|-------------------------------------------------------------------------------------|------------------------------|-------------------------------------------------------------------------------------|--------------------------------|
|  | YOM-20, Removal Calculations |  | YOM-20, Diffusion Calculations |
|  | ABBN, Removal Calculations   |  | ABBN, Diffusion Calculations   |
|  |                              |                                                                                     | Measured                       |

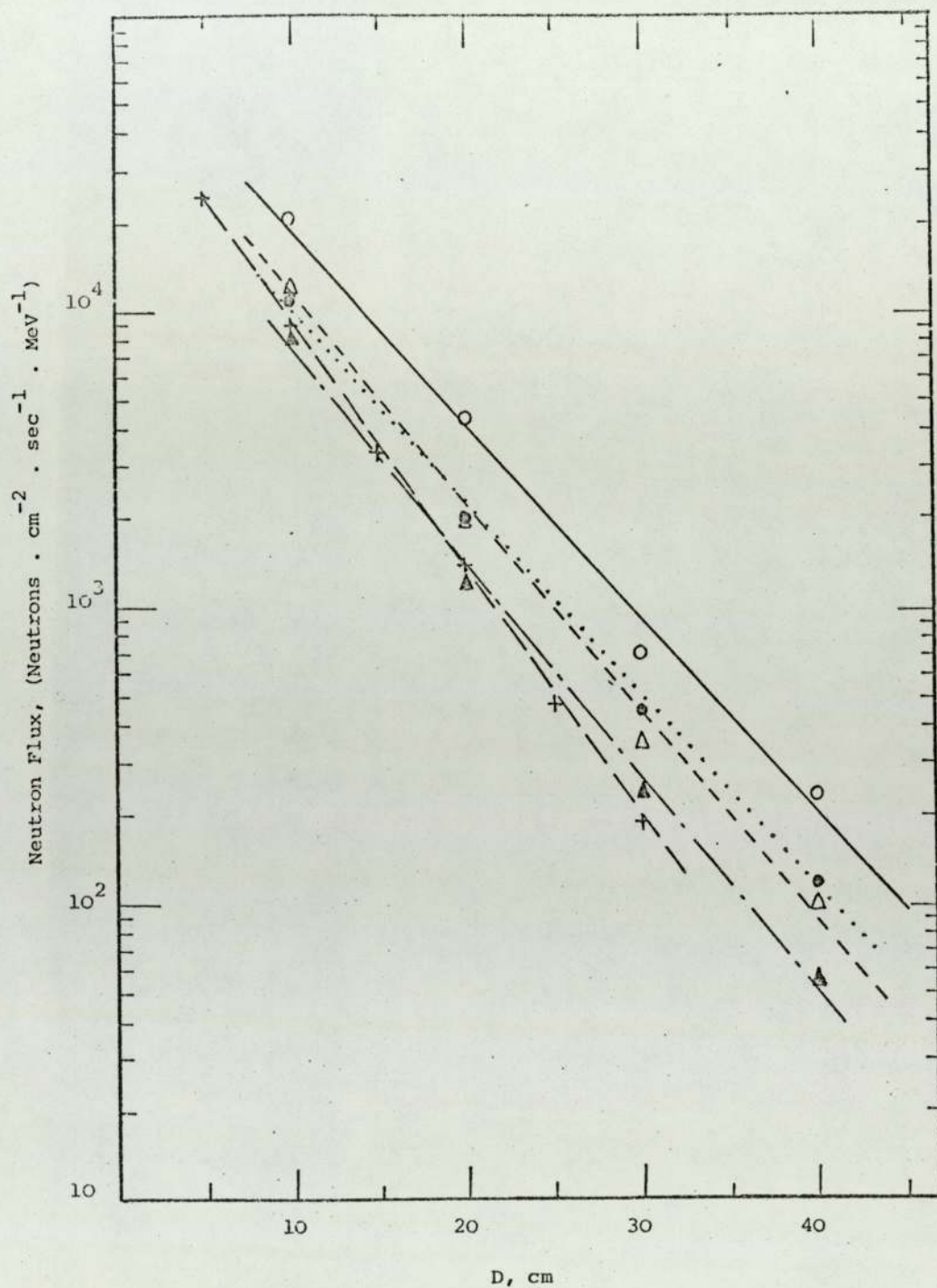


Figure 8.20. Measured Intensity of Neutrons behind Homogenous and Heterogeneous Shields for 1st Group (12 - 14 MeV)

- |   |                          |   |                            |
|---|--------------------------|---|----------------------------|
| + | Iron                     | ○ | Hetero. Fe/C               |
| ● | Homo. Fe/C               | △ | Hetero. Fe/CH <sub>2</sub> |
| ▲ | Homo. Fe/CH <sub>2</sub> |   |                            |

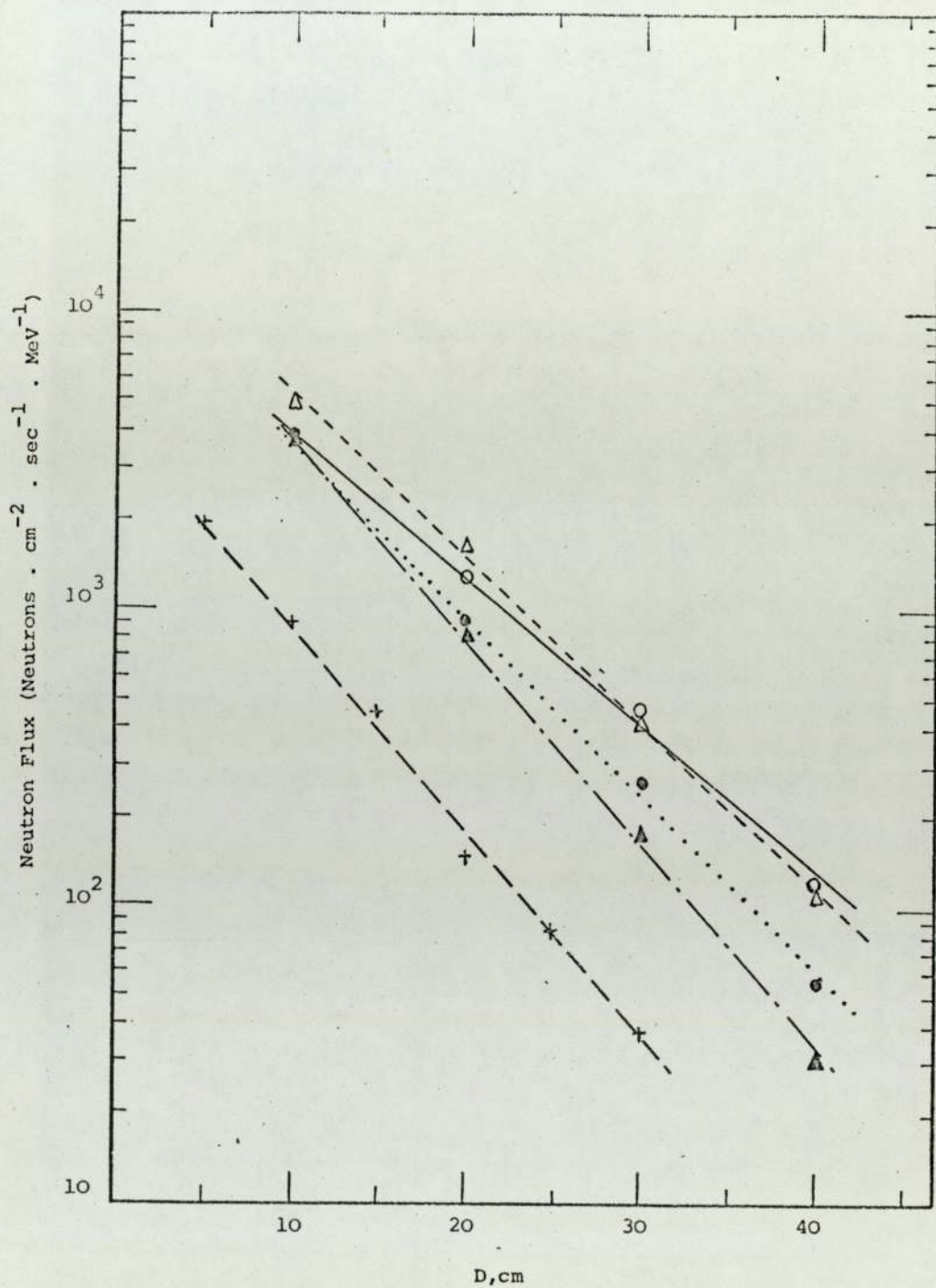


Figure 8.21. Measured Intensity of Neutrons behind Homogeneous and Heterogeneous Shields for 2nd Group (12 - 10.5 MeV)

- |   |              |   |                           |
|---|--------------|---|---------------------------|
| + | Fe           | ▲ | Homo Fe/CH <sub>2</sub>   |
| ● | Homo. Fe/C   | △ | Hetero Fe/CH <sub>2</sub> |
| ○ | Hetero. Fe/C |   |                           |

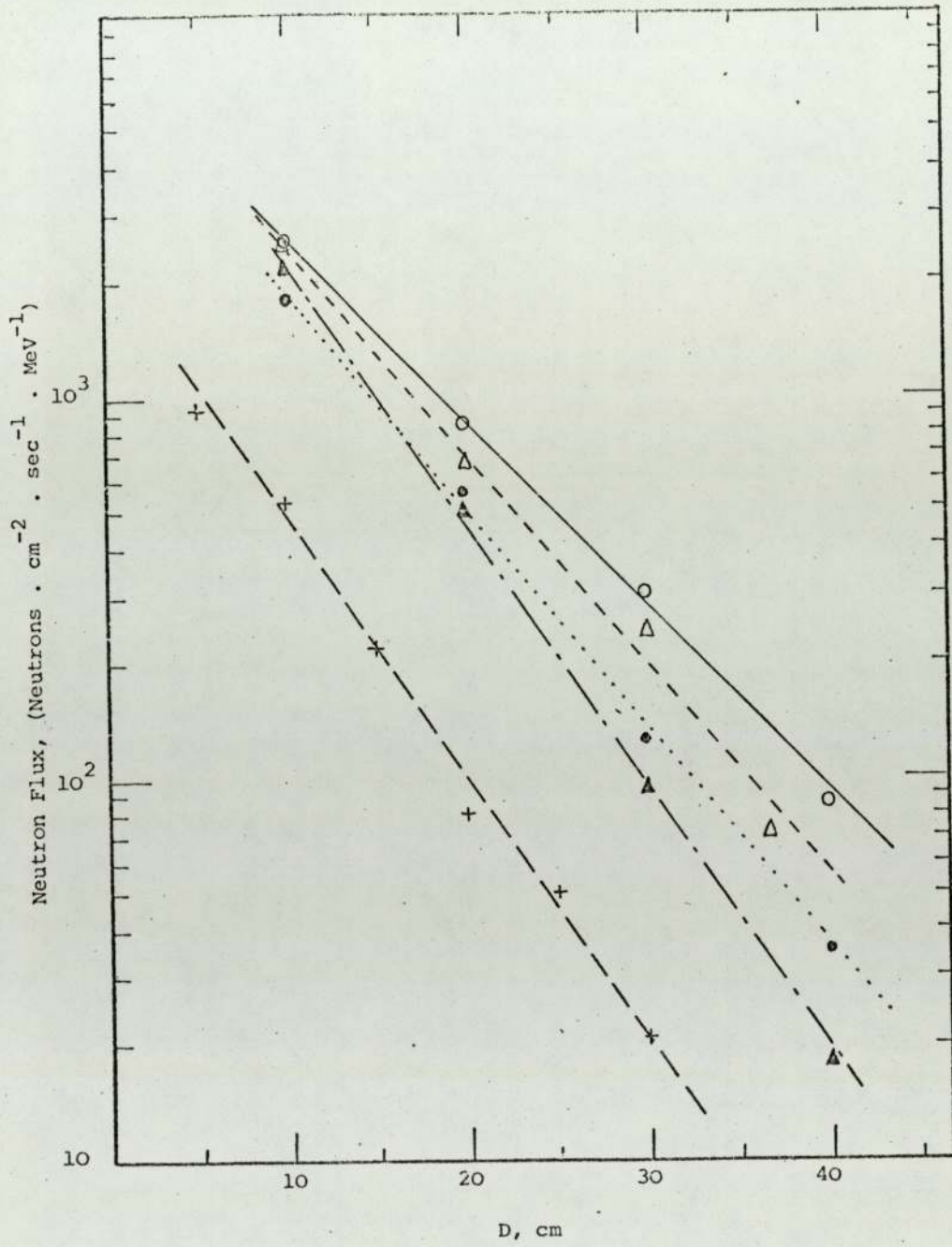


Figure 8.22. Measured Intensity of Neutrons behind Homogenous and Heterogeneous Shields for 3rd Group (6.5 - 10.5 MeV)

- |   |                           |   |                           |
|---|---------------------------|---|---------------------------|
| + | Fe                        | ▲ | Homo. Fe/CH <sub>2</sub>  |
| ● | Homo. Fe/C                | △ | Hetero Fe/CH <sub>2</sub> |
| ○ | Hetero Fe/CH <sub>2</sub> |   |                           |

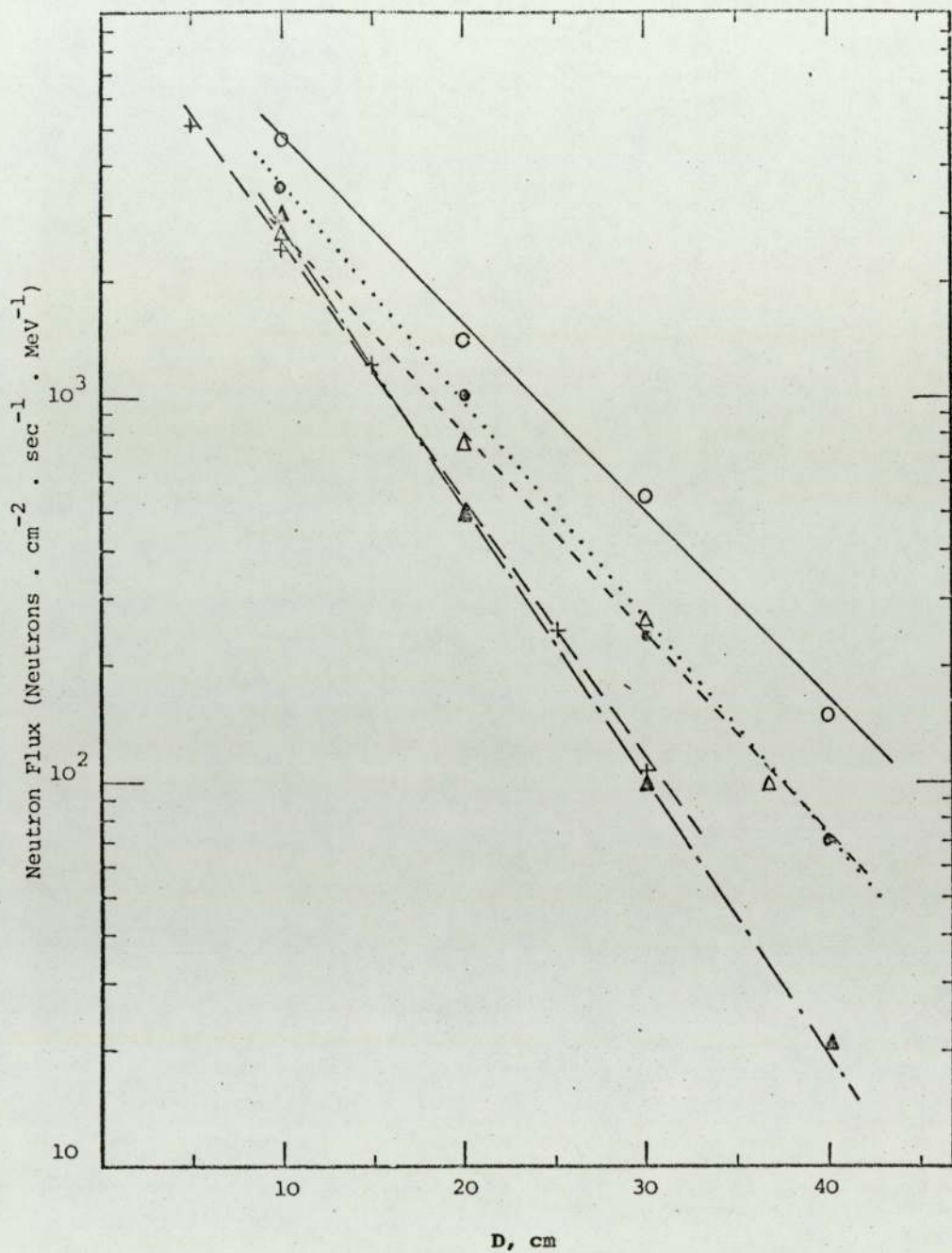


Figure 8.23. Measured Intensity of Neutrons behind Homogenous and Heterogeneous Shields for 4th Group (4 - 6.5 MeV)

- |   |              |   |                            |
|---|--------------|---|----------------------------|
| + | Fe           | Δ | Homo. Fe/CH <sub>2</sub>   |
| o | Homo. Fe/C   | Δ | Hetero. Fe/CH <sub>2</sub> |
| O | Hetero. Fe/C |   |                            |

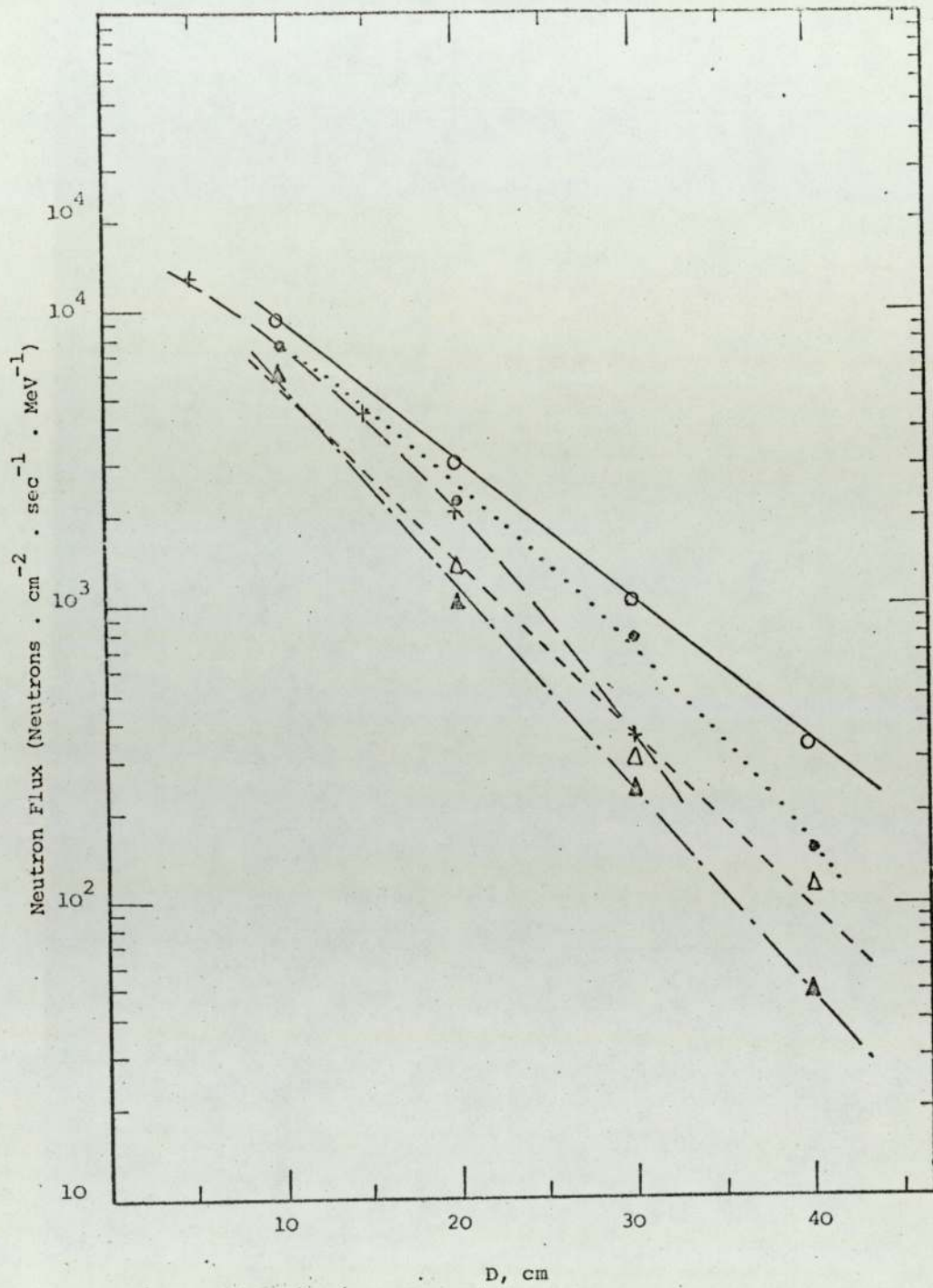


Figure 8.24. Measured Intensity of Neutrons behind Homogenous and Heterogeneous Shields for 5th Group (2.5 - 4 MeV)

- + Fe
- Homo. Fe/C
- Hetero. Fe/C
- ▲ Homo Fe/CH<sub>2</sub>
- △ Hetero Fe/CH<sub>2</sub>

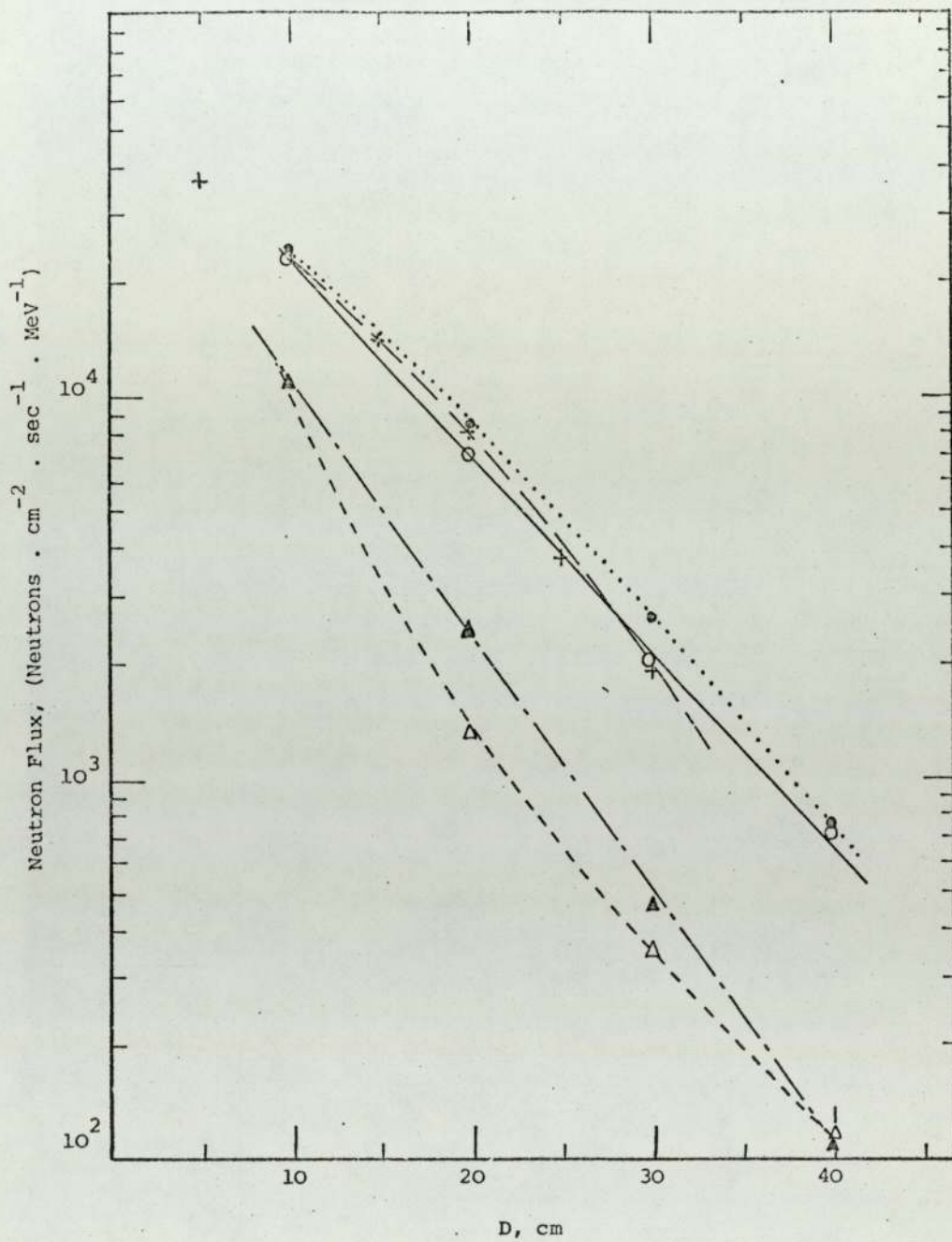


Figure 8.25. Measured Intensity of Neutrons behind Homogenous and Heterogeneous Shields for 6th Group (1.4 - 2.5 MeV)

- |   |              |   |                           |
|---|--------------|---|---------------------------|
| + | Fe           | ▲ | Homo Fe/CH <sub>2</sub>   |
| ● | Homo. Fe/C   | △ | Hetero Fe/CH <sub>2</sub> |
| ○ | Hetero. Fe/C |   |                           |

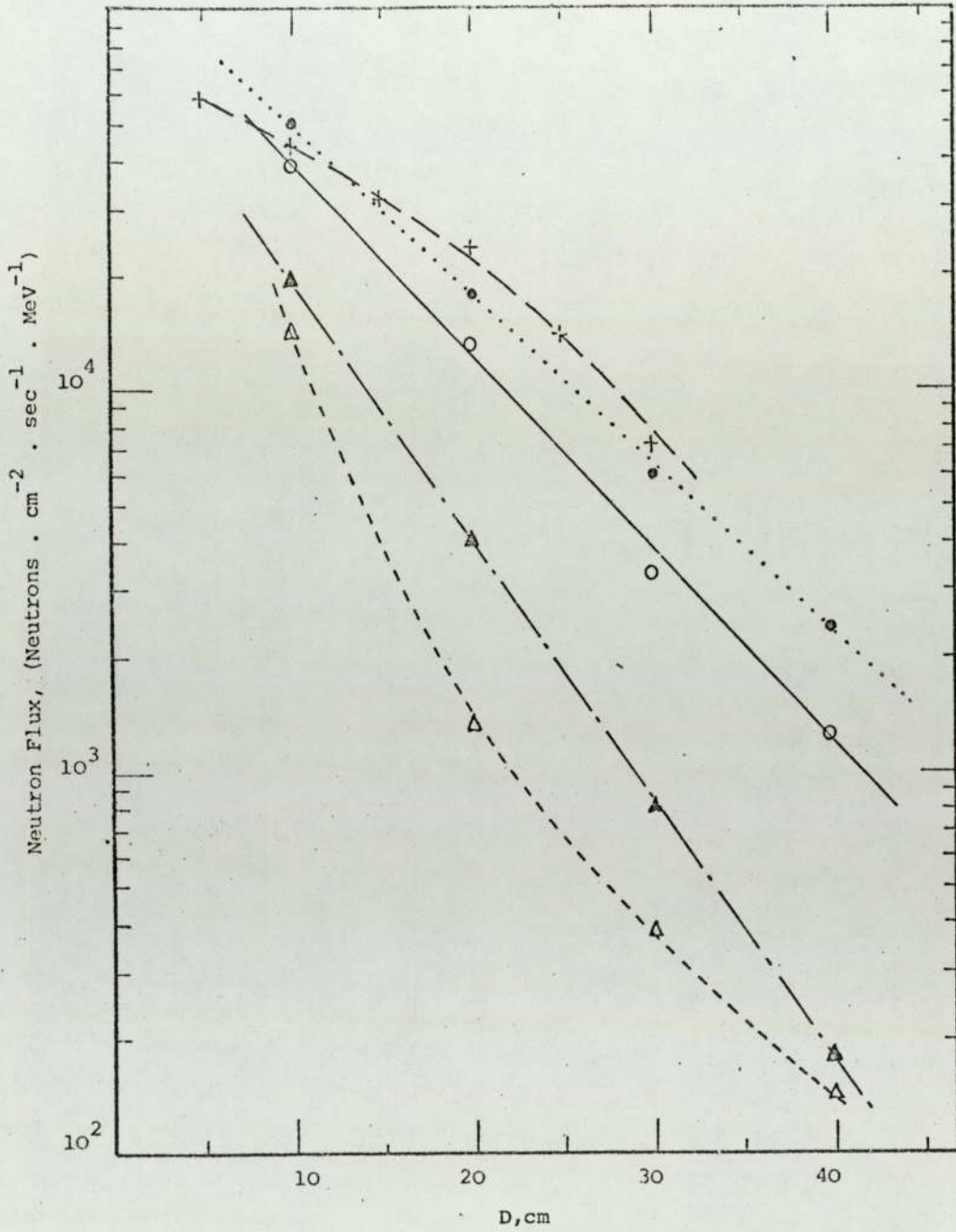


Figure 8.26. Measured Intensity of Neutrons behind Homogenous and Heterogeneous Shields for 7th Group (0.8 - 1.4 MeV)

- |   |             |   |                           |
|---|-------------|---|---------------------------|
| + | Fe          | ▲ | Homo Fe/CH <sub>2</sub>   |
| • | Homo. Fe/C  | △ | Hetero Fe/CH <sub>2</sub> |
| O | Hetero Fe/C |   |                           |

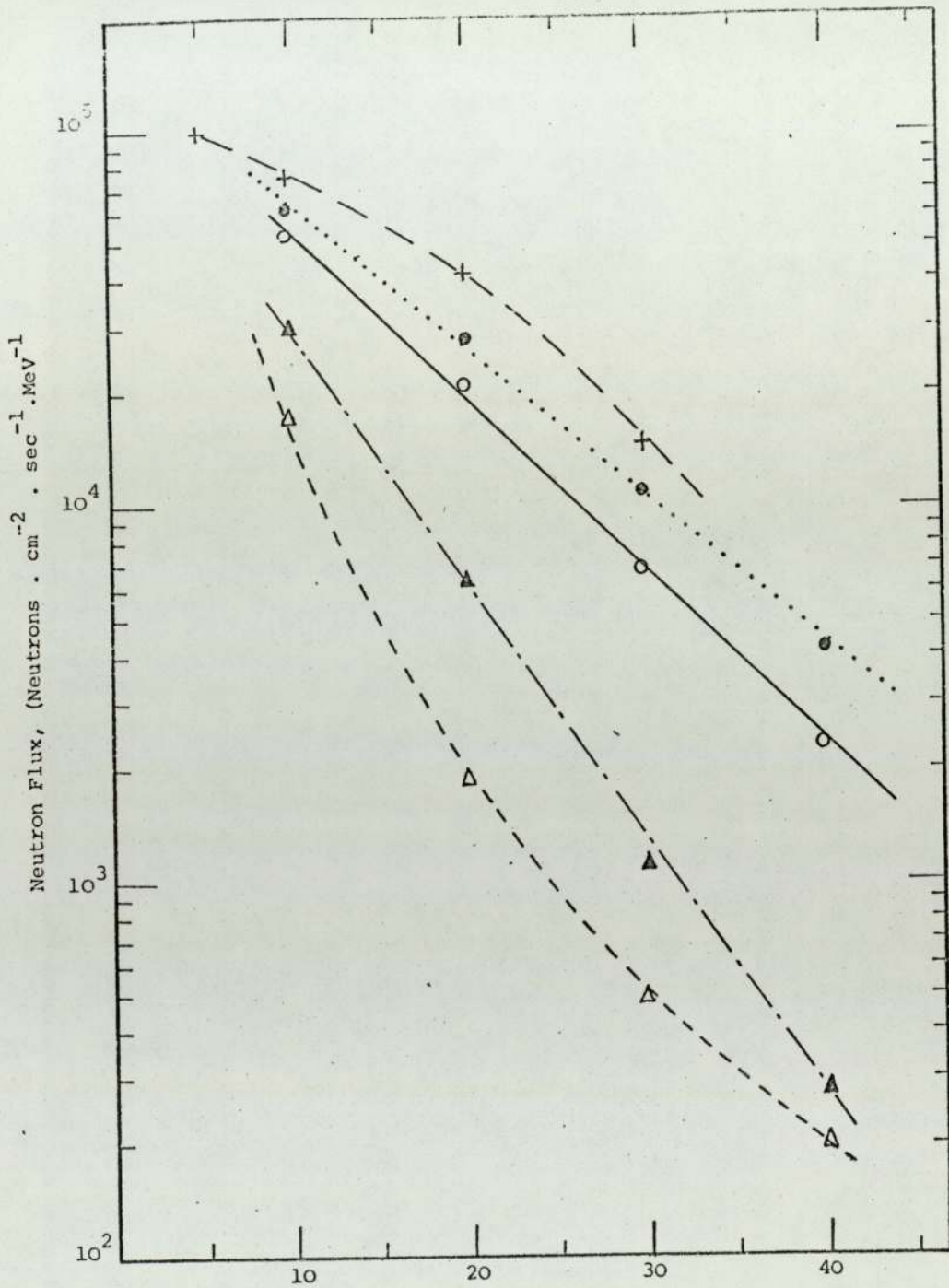


Figure 8.27. Measured Intensity of Neutrons behind Homogenous and Heterogeneous Shields for 8th Group (0.4 - 0.8 MeV)

- |                |                              |
|----------------|------------------------------|
| + Fe           | ▲ Homo. Fe/CH <sub>2</sub>   |
| • Homo. Fe/C   | △ Hetero. Fe/CH <sub>2</sub> |
| ○ Hetero. Fe/C |                              |

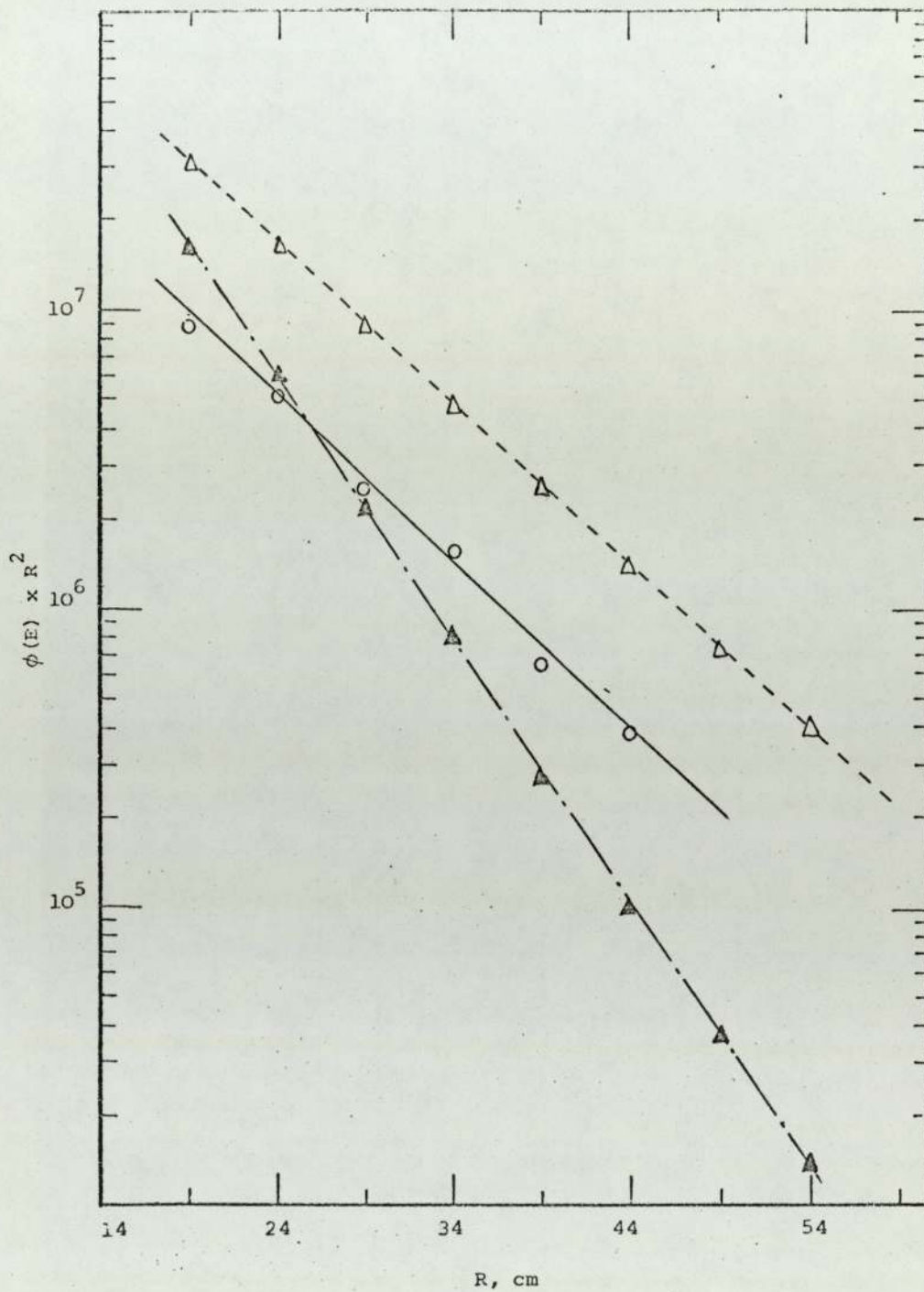


Figure 8.28. (14 - 12 MeV Neutron Flux)  $\times R^2$  behind Homogenous Iron Shields

- Measured
- △ Removal Calculations
- ▲ Diffusion Calculations

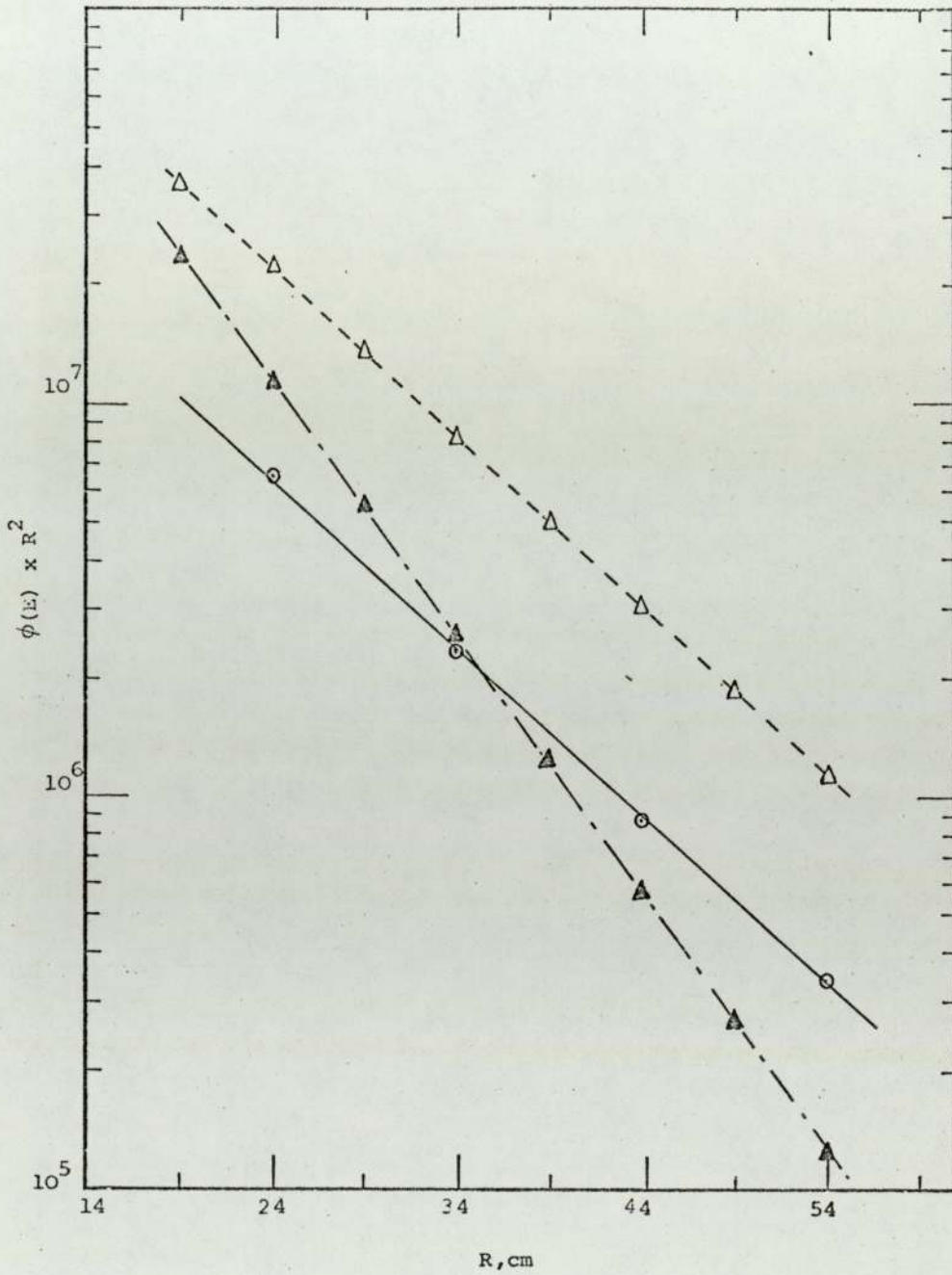


Figure 8.29. (14 - 12 MeV Neutron Flux)  $\times R^2$  behind Homogenous Iron-Graphite Shields

- ⊙ Measured
- △ Removal Calculations
- ▲ Diffusion Calculations

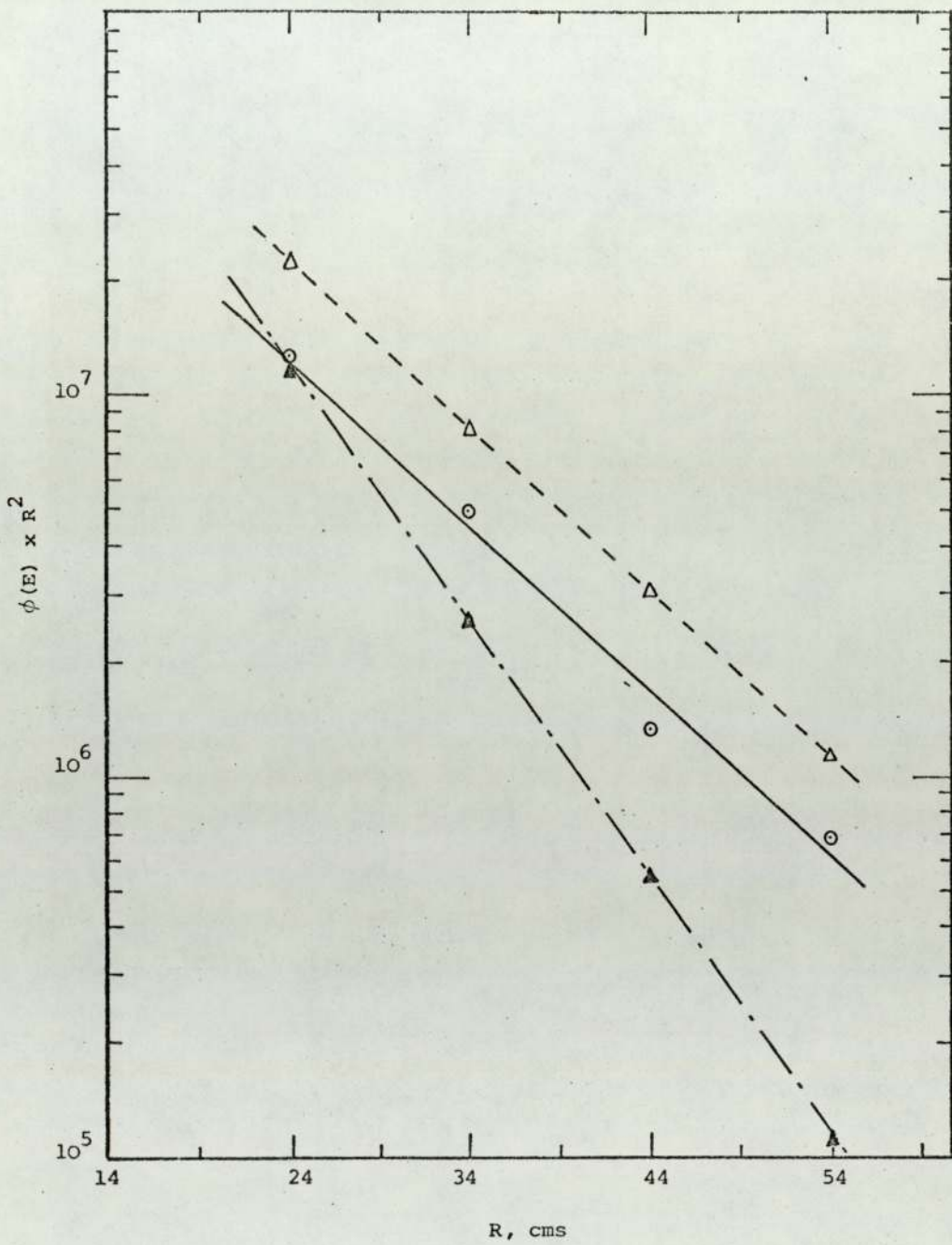


Figure 8.30. (14 - 12 MeV Neutron Flux)  $\times R^2$  behind Heterogeneous Iron-Graphite Shields

- Measured
- △ Removal Calculations
- ▲ Diffusion Calculations

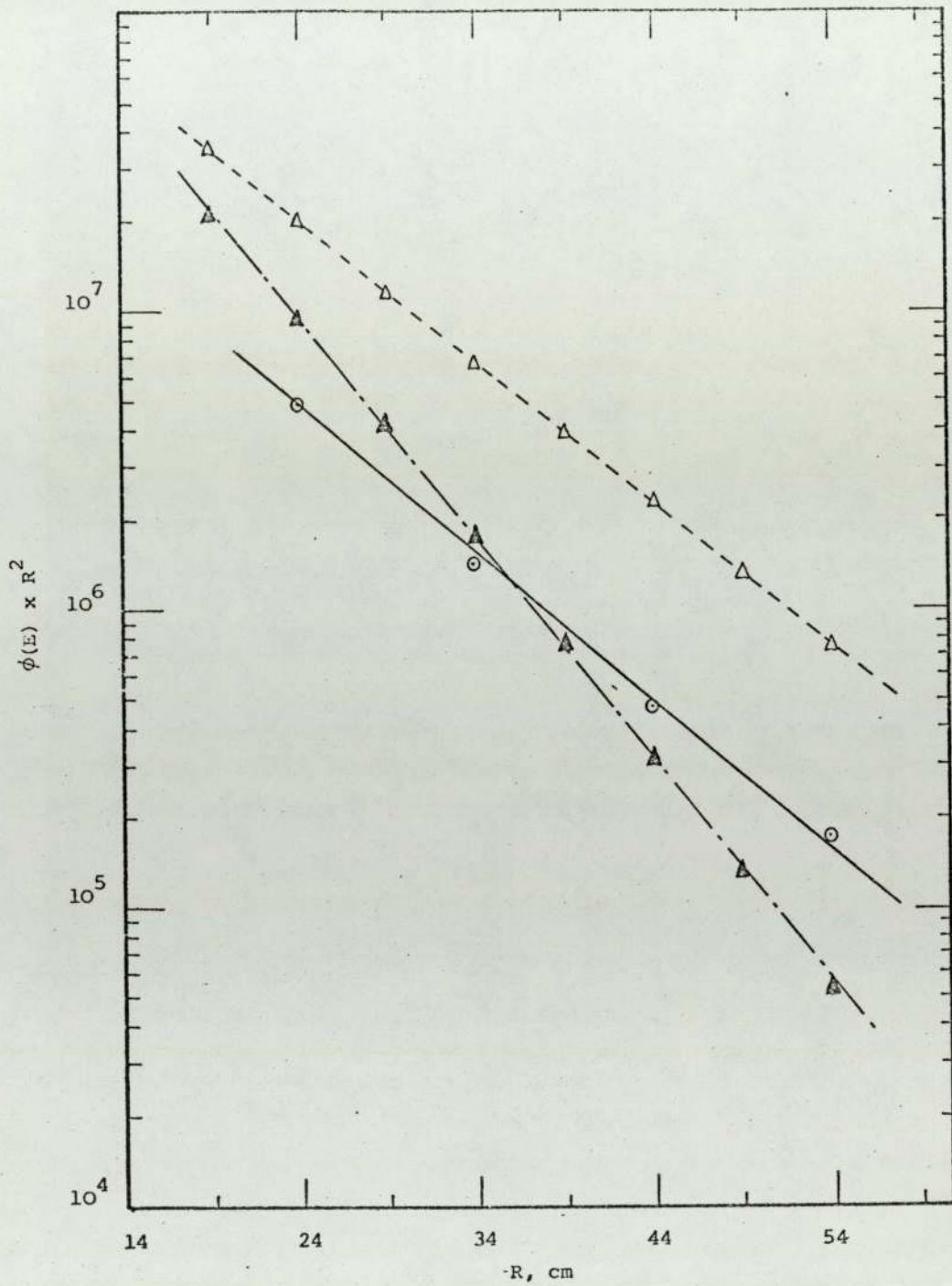


Figure 8.31. (14 - 12 MeV Neutron Flux)  $\times R^2$  behind Homogenous Iron-Polypropylene Shields

- Measured
- △ Removal Calculations
- ▲ Diffusion Calculations

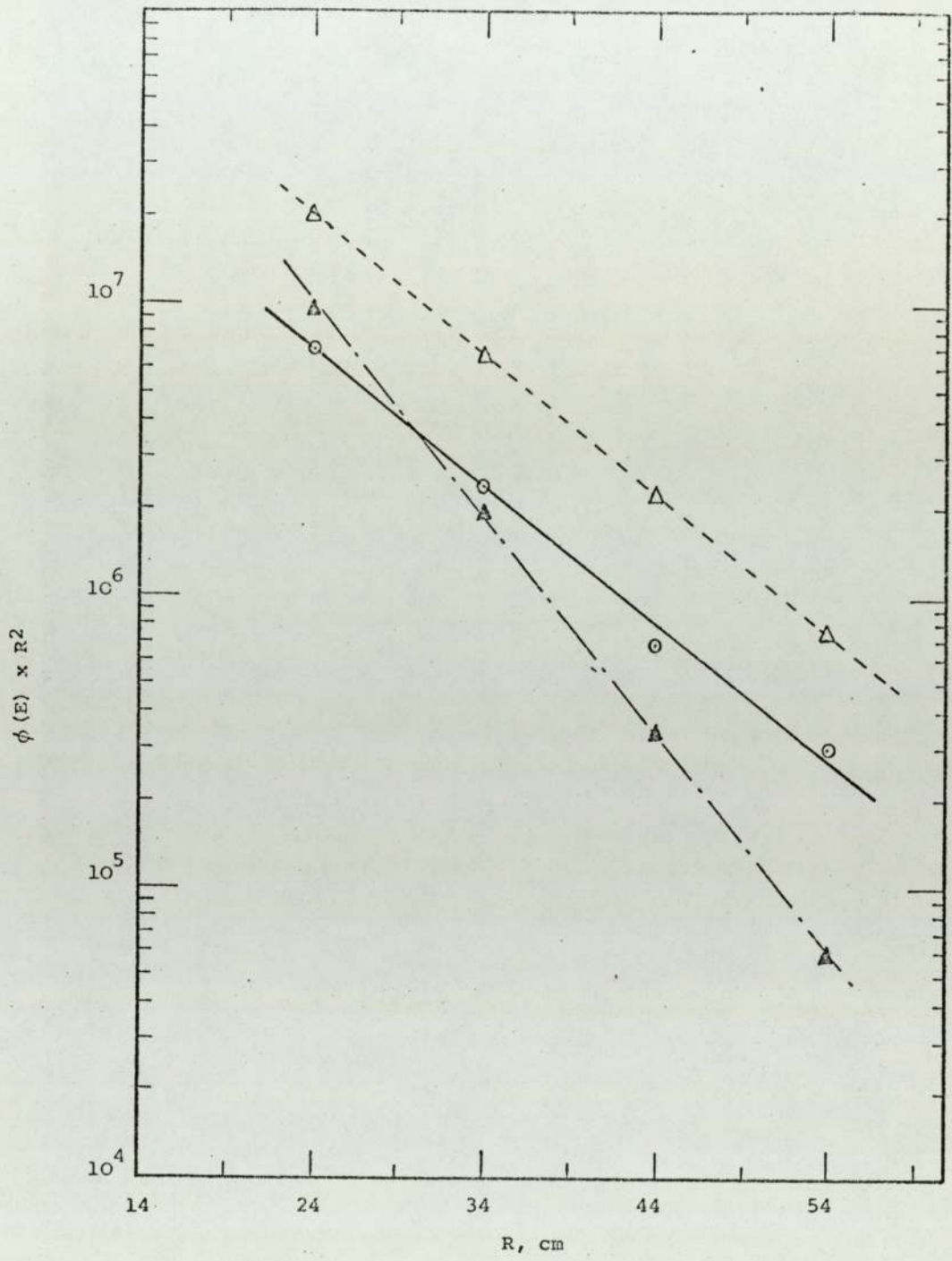


Figure 8.32. (14 - 12 MeV Neutron Flux)  $\times R^2$  behind Heterogeneous Iron-Polypropylene Shields

- Measured
- △ Removal Calculations
- ▲ Diffusion Calculations

CHAPTER 9General Conclusions

The observed and calculated neutron energy spectra resulting from transmission of 14 MeV neutrons through shields of iron (steel) and homogeneous and heterogeneous shields of iron graphite and iron polypropylene of different thicknesses have been discussed in chapter 8. The following conclusions may be drawn from these results.

(i) Shields of iron and mixtures of iron polypropylene seem to be the best for attenuation of the 14 MeV neutrons over the range of thicknesses measured, whilst shields of a mixture of iron-graphite are the least good for the attenuation of neutrons of this group. For iron shields, the proportion of 14 MeV and degraded neutrons in the spectrum, remain remarkably constant over the range of thicknesses measured.

(ii) The overall spectral shapes show, for the materials investigated, that the lowest intensity occurs in the range 10 - 6 MeV with increasing intensities below this energy range. For the thickest arrangement of iron followed by polypropylene however, the neutron intensity in the degraded region only varies by about a factor of two, much less than in all the other shields studied.

(iii) Neutrons degraded to the third energy group (10 - 6 MeV) have least intensity in iron shields for all the measured thicknesses and have the highest values for heterogeneous media of iron-graphite.

(iv) Neutrons degraded to 4 - 0.5 MeV have the highest intensity behind shields of iron and iron-graphite of different configurations. This could be due to the fact that neutrons in this energy region are produced by inelastic scattering, but at this energy range further degradation by inelastic scattering in iron is not very likely.

Therefore iron is not good below this energy. Also, graphite as being

a relatively heavy moderator, is not very effective in degrading neutron energies by large amounts over a short distance. However, for two layers (heterogeneous) shields of iron polypropylene the degraded neutrons in this energy range have the least intensity over all the measured thicknesses. This could be due to the large energy losses possible in single elastic neutron scatters from hydrogen, and also to the increasing hydrogen elastic cross section with decreasing neutron energy.

(v) From the above comments, it appears that no single shield is ideal. Iron is very effective for energy ranges where inelastic scattering process is predominant, while one can find that shields containing hydrogen are best for a low energy range. Therefore, shields composed of thick layers of a heavy element followed by another one containing hydrogen nuclei ( $\text{Fe} + \text{CH}_2$  or  $\text{H}_2\text{O}$  and  $\text{Fe} + \text{FeCH}_2$  or  $\text{FeH}_2\text{O}$  and possibly  $\text{Fe} + \text{metallic hydrates}$ ) could be the best compromise for fast neutron attenuation. However, these may not be ideal for shielding against gamma rays which are generated inside the shield by inelastic collisions and neutron capture. Therefore, shields composed of a layer of a heavy element, followed by a hydrogenous layer followed by another layer of heavy element (for example,  $\text{Fe} + \text{FeCH}_2 + \text{Fe}$ ), may be the best for nuclear radiation attenuation. Carbon does not seem to be much use for fast neutron attenuation over short distances.

(vi) The removal cross sections at 14 MeV have been determined for iron, graphite and hydrogen. There is agreement between these measured and the values calculated by Avery et al <sup>(113)</sup> within experimental error. Avery et al computed the removal cross sections for most of the reactor materials from 0.5 to 17.5 MeV, but these values cannot be considered certain until they are experimentally verified. Since the same basis of calculation has been used over the whole energy range it gives hope that the other values of these authors are also reliable.

(vii) At 14 MeV, the absolute value of the measured flux is low

compared with the calculated value. This could be due to fall off of detector efficiency in this range which might be due to uncertainties in hydrogen and carbon total cross sections used for the scintillator shape correction factor discussed in chapter 4. It is also possible that the model used for this correction factor is not adequate at 14 MeV.

(viii) The data also show that the cross section sets of the ABBN and YOM-20 both give reasonable agreement between calculation and experimental spectra provided that an exponential removal model is used for the uncollided primary neutron flux. The YOM-20 carbon data appears however to give slightly better fit than ABBN in the region 4 to 1.4 MeV.

From the tabulated cross sections it is possible to deduce an average elastic scattering cross section by multiplying the elastic removal cross section by the lethargy width of the group divided by the logarithmic energy decrement. This gives for carbon in YOM-20 groups 5, 6 and 7 scattering cross sections of 1.8, 1.2 and 1.5 barns respectively whereas for the ABBN groups 5 (corresponding to YOM-20 groups 5 and 6) and 6, the values are 2.0 and 1.8 barns respectively. Little difference is found in the other values. It is therefore suggested that the YOM-20 data are to be preferred for carbon.

(ix) For the homogeneous Fe/CH<sub>2</sub> shields the agreement between theory and experimental values of neutron flux is reasonable but for the heterogeneous assemblies (CH<sub>2</sub> following Fe) the calculated flux is lower than the measured flux over the whole energy range, the effect increases with thickness. The general shape of the spectrum is, however, well predicted. This effect could be explained by the very anisotropic scattering of neutrons by hydrogen (predominant in CH<sub>2</sub>) which would tend to increase the number of forward scattered neutrons above that predicted by diffusion theory which implicitly assumes isotropic scattering. In the homogeneous case however the hydrogen is diluted by the iron which

would tend to produce randomly directed neutrons at all points in the shield.

The removal diffusion model would therefore appear to be adequate for the homogeneous mixtures but produces a severe under estimate of the degraded flux for the heterogeneous shield containing hydrogen.

For the non-hydrogenous shields the removal diffusion model also appears to be perfectly adequate.

(x) The degraded neutrons born inside the medium can be calculated with reasonable agreement with the measured values, provided that the diffusion coefficient  $D$  is evaluated by the Lamarsh equation<sup>(13)</sup>. However, the concept of diffusion coefficient has little meaning for the highly directional source neutrons and so the exponential removal model gives a better fit for these energies.

(xi) The agreement between the measured and calculated data show that the utilization of scintillation method with NE-213 scintillator is an effective technique for measuring neutron spectra over a wide range of energies in the presence of gamma ray background. They also show that the differential method used for converting the measured pulse amplitude distribution into a neutron spectrum is justified despite its simplicity compared with the potentially more exact method of matrix inversion.

(xii) Finally, these methods could be applied to further studies on different geometries especially those widely used in reactor technology (such as spherical shells) of different configuration and widely used reactor shielding materials such as barytes concrete (density =  $3.5 \text{ g/cm}^3$ ), iron concrete (density =  $4.5 \text{ g/cm}^3$ ) and ordinary concrete (density =  $2.3 \text{ g/cm}^3$ ).

Further investigations could be made for multilayer shields, for example, for spherical shells and for plane assemblies having large dimensions normal to the thickness. Different calculation models for example transport theory, should also be tried.

It may also be useful to study materials which can be used in

future for shielding of mobile reactors such as metal hydrates. A further check on the usefulness of these shields would be to compare the emitted gamma rays produced by inelastic scattering and neutron capture.

APPENDIX 1

NUMERICAL SCHEME USED FOR MULTIGROUP FLUX CALCULATIONS

For any group the general diffusion equations can be abbreviated as:

$$D \nabla^2 \phi - A \phi + b = 0 \quad \dots \dots \text{Al.1}$$

where  $A$  = the sum of the neutron sinks.

$$= \Sigma_a + \Sigma_{er} + \Sigma_{in}$$

$b$  = the sum of the neutron sources

$$= s + \Sigma_{er} \phi + \Sigma (\Sigma_{in} \phi)$$

$$\nabla^2 = \frac{d^2}{dr^2} + \frac{c}{r} \cdot \frac{d}{dr} \quad \dots \dots \text{Al.2}$$

$$c = 0 \text{ for slab } )$$

)

$$= 1 \text{ for cylinder } )$$

)

$$= 2 \text{ for sphere } )$$

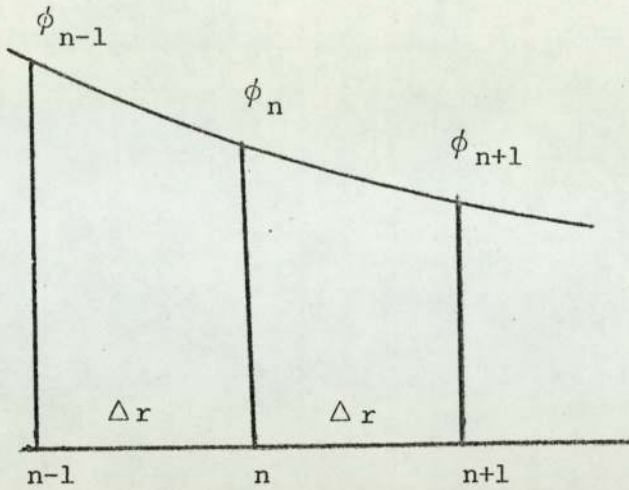
$\dots \dots \text{Al.3}$

The diffusion equation is then given by:

$$D \left( \frac{d^2 \phi}{dr^2} + \frac{c}{r} \cdot \frac{d \phi}{dr} \right) - A \phi + b = 0 \quad \dots \dots \text{Al.4}$$

equation Al.4 can best be solved by expressing the diffusion equations by a finite difference equation.

The method is first illustrated by assuming a homogeneous medium which is divided into a mesh structure of equidistant mesh spacing  $\Delta r$ . The distance of the  $n$ -th mesh point  $r_n$  from the centre of the source is  $r_n = n \cdot \Delta r$ . If  $\phi_n$  is the flux at this point, therefore for one dimensional cases, the following approximation can be made.



$$\frac{d\phi}{dr} = \frac{\phi_{n+1} - \phi_{n-1}}{2\Delta r} \quad \dots \dots \text{Al.5}$$

and

$$\frac{d^2\phi}{dr^2} = \frac{\phi_{n+1} - 2\phi_n + \phi_{n-1}}{(\Delta r)^2} \quad \dots \dots \text{Al.6}$$

In both these equations the error in the approximation is of the order of  $\Delta r^2$  and can be quite small provided  $\Delta r$  is small. Substitute equations Al.5 and Al.6 into equation Al.1.

$$D \left\{ \frac{\phi_{n+1} - 2\phi_n + \phi_{n-1}}{(\Delta r)^2} + \frac{c}{r} \cdot \frac{\phi_{n+1} - \phi_{n-1}}{2\Delta r} \right\} - A\phi_n + b = 0$$

$\dots \dots \text{Al.7}$

This can be re-arranged to give:

$$\phi_{n+1} = M_n \phi_n - N_n \phi_{n-1} - R_n \quad \dots \dots \text{Al.8}$$

$$\text{where } M_n = \frac{2 + A(\Delta r)^2/D}{1 + C\Delta r/2r} \quad \dots \dots \dots \text{ Al.9a}$$

$$N_n = \frac{2r - C\Delta r}{2r + C\Delta r} \quad \dots \dots \dots \text{ Al.9b}$$

$$R_n = \frac{b}{D} \frac{(\Delta r)^2}{1 + C\Delta r/2r} \quad \dots \dots \dots \text{ Al.9c}$$

From a computational point of view it is more convenient to write equation Al.8 in the form

$$\phi_n = \alpha_n \phi_{n+1} + \beta_n \quad \dots \dots \dots \text{ Al.10}$$

where  $\alpha_n$  and  $\beta_n$  are constants given as

$$\alpha_n = (M_n - N_n \alpha_{n-1})^{-1} \quad \dots \dots \dots \text{ Al.11}$$

$$\beta_n = (N_n \beta_{n-1} + R_n) \quad \dots \dots \dots \text{ Al.12}$$

#### Al.1 Boundary Conditions

Sufficient numbers of boundary conditions must be used to provide a unique solution of neutron distribution problems by means of the diffusion equations, these are given by:

(a) The neutron flux must be finite and non-negative in the region where the diffusion equation applies.

(b) At the boundary between a diffusion medium and free space, the neutron flux varies in such a manner that linear extrapolation would require the flux to vanish a definite (extrapolation) distance beyond

the boundary.

(c) The flux and the net neutron current densities at a plane interface between two diffusion media must be equal and continuous.

A1.1.1 Inner Boundary (at  $n = M$ )

The inner boundary condition is obtained from known neutron current which can be derived from the source specification.

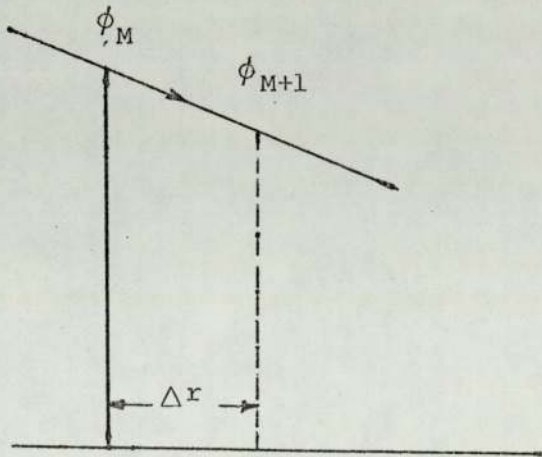
(i) Current density  $J$  incident on inner surface

$$\text{slab } J = Q \quad \dots \dots \text{A1.13a}$$

$$\text{cylinder } J = \frac{Q}{2\pi r} = \frac{Q}{2\pi M \cdot \Delta r} \quad \dots \dots \text{A1.13b}$$

$$\text{sphere } J = \frac{Q}{4\pi r^2} = \frac{Q}{4\pi (M \cdot \Delta r)^2} \quad \dots \dots \text{A1.13c}$$

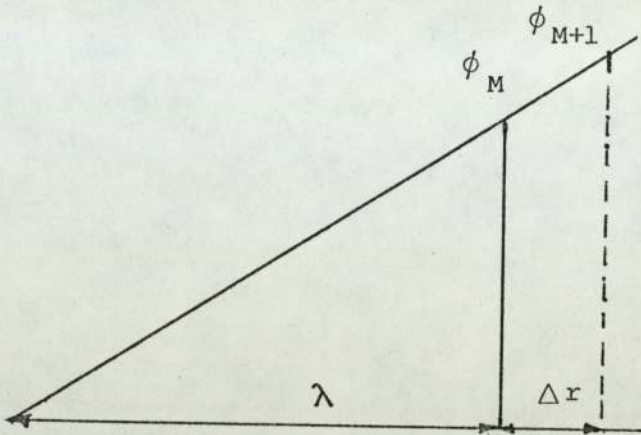
where  $Q$  is the source strength ( $\text{neutrons} \cdot \text{sec}^{-1}$ )



$$J = D_M \frac{(\phi_M - \phi_{M+1})}{\Delta r}$$

$$\therefore \phi_M - \phi_{M+1} = \frac{J \cdot \Delta r}{D_M} \quad \dots \dots \text{A1.14}$$

(ii) Flux extrapolates to zero at a distance  $\lambda$  inside the inner boundary.



$$\phi_M / \lambda = \phi_{M+1} / (\lambda + \Delta r) \quad \dots \dots \text{A1.15}$$

$$\therefore \phi_M - \phi_{M+1} \frac{\lambda}{\lambda + \Delta r} = 0$$

(iii) Flat flux at inner boundary

$$\lambda = \infty$$

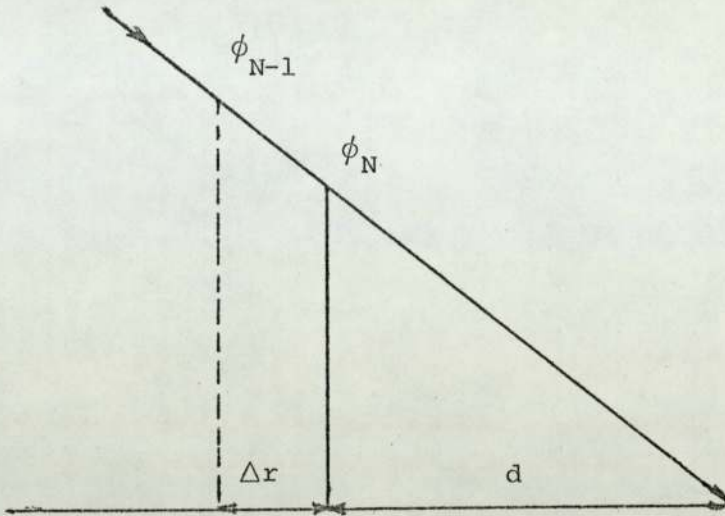
$$\therefore \phi_M - \phi_{M+1} = 0 \quad \dots \dots \text{A1.16}$$

#### A1.1.2 Outer Boundary (n = N)

Flux becomes zero at a distance  $d$  called the linear extrapolation distance given by:

$$d = 0.71 \lambda_{tr} \quad \dots \dots \text{A1.17}$$

where  $\lambda_{tr}$  = mean transport free path.



$$\phi_N/d = \frac{\phi_{N-1}}{(d + \Delta r)}$$

$$\therefore \phi_N - \phi_{N-1} \left( \frac{d}{d + \Delta r} \right) = 0 \quad \dots \dots \text{A1.18}$$

comparing equations A1.13 and A1.20 we get:

$$\phi_N = \frac{\beta_N}{1 + \frac{\Delta r}{d} \alpha_N - \alpha_N} \quad \dots \dots \text{A1.19}$$

### A1.1.3. Boundary at the surface between two adjacent materials

For calculating the neutron flux distribution in a heterogeneous shield consisting of two layers of materials with different nuclear properties, the interface or boundary conditions are customarily specified by taking the flux  $\phi$  and the normal current  $D \nabla \phi$  as continuous at the

interface.

Therefore:

$$\phi_{(r)} = \phi'_{(r)} \quad \dots \dots \text{Al.20}$$

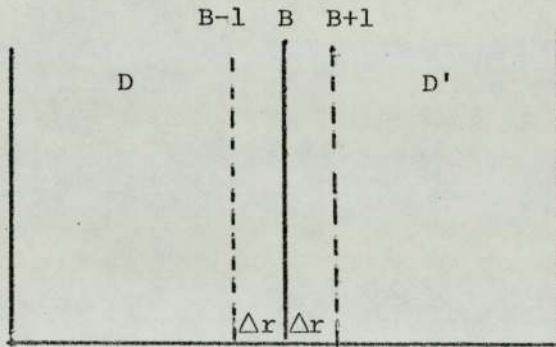
and

$$D \frac{d\phi}{dr} = D' \frac{d\phi'}{dr} \quad \dots \dots \text{Al.21}$$

in which the primed and unprimed values indicate the sides of the interface at r

If the boundary is denoted by a subscript B we have that

$$\phi_B = \phi'_B \quad \dots \dots \text{Al.22}$$



$$D \frac{\phi_{B+1} - \phi_{B-1}}{2\Delta r} = D' \frac{\phi'_{B+1} - \phi'_{B-1}}{2\Delta r'} \quad \dots \dots \text{Al.23}$$

and from Al.8

$$\phi_{B+1} = M_B \phi_B - N_B \phi_{B-1} - R_B \quad \dots \dots \text{Al.24}$$

$$\phi'_{B+1} = M'_B \phi'_B - N'_B \phi'_{B-1} - R'_B \quad \dots \dots \text{Al.25}$$

By using Al.24 and Al.25 in Al.23  $\phi'_{B-1}$  and  $\phi_{B+1}$  can now be eliminated.

From Al.23

$$\ell \left\{ M_B \phi_B - N_B \phi_{B-1} - R_B - \phi_{B-1} \right\}$$

$$\left\{ \phi'_{B+1} + (\phi'_{B+1} - M'_B \phi'_B + R'_B) \frac{1}{N'_B} \right\} \dots \dots \dots \text{Al.26}$$

where

$$\ell = \frac{D\Delta r'}{D'\Delta r} \dots \dots \dots \text{Al.27}$$

From equation Al.26

$$\ell \left\{ M_B + \frac{M'_B}{N'_B} \right\} \phi'_B = \ell (N_B + 1) \phi_{B-1} + \left( \frac{N'_B + 1}{N'_B} \right) \phi'_{B+1}$$

$$+ \frac{\ell R_B N'_B + R'_B}{N'_B}$$

where we have used the fact that  $\phi_B = \phi'_B$ .

But  $\phi_{B-1} = \alpha_{B-1} \phi_B + \beta_{B-1}$  from equation Al.26

$$\therefore \phi_{B-1} = \alpha_{B-1} \phi'_B + \beta_{B-1} \dots \dots \dots \text{Al.28}$$

Therefore

$$\left\{ \frac{\ell M_B N'_B + M'_B}{N'_B} \right\} \phi'_B = \ell (N_B + 1) \alpha_{B-1} \phi'_B$$

$$+ \ell (N_{B+1}) \beta_{B-1} + \left( \frac{N'_B + 1}{N'_B} \right) \phi'_{B+1} + \frac{\ell R_B N'_B + R'_B}{N'_B}$$

$$\begin{aligned}
 \text{i.e.} \quad & \left\{ \frac{\ell^{M_B N'_B + M'_B}}{N'_B} - \ell^{(N_B + 1)} \alpha_{B-1} \right\} \phi'_B \\
 & = \frac{N'_B + 1}{N'_B} \phi'_{B+1} + \frac{N'_B + 1}{N'_B} \left\{ \frac{\ell^{R_B N'_B + R'_B}}{N'_B + 1} \right. \\
 & \quad \left. + \beta_{B-1} \ell^{N'_B} \left( \frac{N_B + 1}{N'_B + 1} \right) \right\}
 \end{aligned}$$

$$\text{i.e.} \quad \phi'_B = \left\{ \frac{\ell^{M_B N'_B + M'_B}}{N'_B + 1} - \alpha_{B-1} \ell^{N'_B} \left( \frac{N_B + 1}{N'_B + 1} \right) \right\}^{-1}$$

$$\begin{aligned}
 & \phi'_{B+1} + \left\{ \frac{\ell^{M_B N'_B + M'_B}}{N'_B + 1} - \alpha_{B-1} \ell^{N'_B} \right. \\
 & \quad \left. \left( \frac{N_B + 1}{N'_B + 1} \right) \right\}^{-1}
 \end{aligned}$$

$$\times \left\{ \frac{\ell^{R_B N'_B + R'_B}}{N'_B + 1} + \beta_{B-1} \ell^{N'_B} \left( \frac{N_B + 1}{N'_B + 1} \right) \right\}$$

$$\text{i.e.} \quad \phi'_B = (x - \alpha_{B-1} \cdot y)^{-1} \phi'_{B-1}$$

$$+ (z + \beta_{B-1} \cdot y) (x - \alpha_{B-1} \cdot y)^{-1} \dots \dots \dots \text{Al.29}$$

where

$$x = \frac{\ell^{M_B N'_B + M'_B}}{N'_B + 1} \dots \dots \dots \text{Al.30a}$$

$$y = \ell^{N'_B} \left( \frac{N_B + 1}{N'_B + 1} \right) \dots \dots \dots \text{Al.30b}$$

$$z = \frac{\ell^{R_B N'_B + R'_B}}{N'_B + 1} \dots \dots \dots \text{Al.30c}$$

If equation Al.29 is compared with equation Al.10 it is seen that boundary crossing conditions for  $\alpha$  and  $\beta$  must be

$$\alpha_B = (x - \alpha_{B-1} \cdot y)^{-1} \dots \dots \text{Al.31}$$

$$\beta_B = \alpha_B (z / \beta_{B-1} \cdot y) \dots \dots \text{Al.32}$$

Al.2 Calculation Scheme

- (a) Arrays of  $D_n, \Sigma_n$  and  $b_n$  are needed at every point
- (b) Calculate  $\alpha_M$  and  $\beta_M$  depending on inner boundary conditions:

|                                         | $\alpha_M$                                             | $\beta_M$                      |
|-----------------------------------------|--------------------------------------------------------|--------------------------------|
| Point source                            | -1                                                     | $\frac{J \cdot \Delta r}{D_M}$ |
| $\phi = 0$ at $r = M\Delta r - \lambda$ | $-\left(\frac{1}{1 + \frac{\Delta r}{\lambda}}\right)$ | 0                              |
| $\phi = \text{flat}$                    | -1                                                     | 0                              |

- (c) For n ranging from M+1 to N-1 calculate  $\alpha_n$  and  $\beta_n$  from equations Al.11, Al.12, Al.31 and Al.32
- (d) Calculate  $\phi_N$  from equation Al.19
- (e) For n ranging from N-1 to M calculate the fluxes using equation Al.10

For multigroup calculations start with the highest energy group where for shielding calculations:

The neutron current J will be finite and in general  $S_n$  will be zero unless there is inelastic scattering from group  $l \rightarrow$  group  $l$ .

Work down the energy groups in turn using:

$$\phi_n = \sum_{i=1}^{g-1} \sum_{i \rightarrow g} \phi_i + \sum_{i=1}^{g-1} \sum_{i \rightarrow g} \phi_i$$

Unless hydrogen is present the second part of the expression is just

$\sum_{g-1 \rightarrow g} e \phi_{g-1}$  provided that the lethargy width of any group is greater than the logarithmic energy decrement.

APPENDIX 2

PROGRAM FASTNFLUX: MULTIGROUP FLUX CALCULATIONS

BY DIFFUSION AND REMOVAL DIFFUSION METHODS.

```

'BEGIN' 'COMMENT' PYSTF017,ZFASTNEFLUX,MULTIGROUP FINITE DIFFERENCE
        CALCULATIONS FOR FAST NEUTRON FLUXES, NON ITERATIVE;
'INTEGER' C,G,I,J,K,M,N,NN,NMAT, FN,NSTOP, SCN, ITN, N1, N2, L;
'REAL' ND, DR, O, AA, CC, RR, Z, Y, W;
SELECT OUTPUT (0);
G:=READ; 'COMMENT' NUMBER OF ENERGY GROUPS;
DR:=READ; 'COMMENT' MESH INTERVAL;

'BEGIN'
'REAL' 'ARRAY' SFIS, SCAP, STR, SEL, SINT, NU, XI(1:G), MU, FIS, NUF, CAP, TR, EL,
        REM, SC, MSC, DI(1:G, 1:2), PI(1:G, 1:G), FBC(1:G+1),
        IN(1:G-1, 2:G, 1:2);
        FN:=READ; 'COMMENT' 1=FISSION, 0=NO FISSIION;
        NSTOP:=READ; 'COMMENT' NO OF ITERATIONS, IF FN=0, NSTOP=1;
'FOR' I:=1 'STEP' 1 'UNTIL' G+1 'DO'
        FBC(I):=READ;
'FOR' I:=1 'STEP' 1 'UNTIL' G 'DO'
        XI(I):=READ;
'FOR' L:=1, 2 'DO'

'BEGIN'
'FOR' I:=1 'STEP' 1 'UNTIL' G 'DO'
'BEGIN'
        SC(I, L):=0;
        MS(I, L):=0;
        FI(I, L):=0;
        NU(I, L):=0;
        CAP(I, L):=0;
        TR(I, L):=0;
        EL(I, L):=0;
        REM(I, L):=0;
'END';

'FOR' I:=1 'STEP' 1 'UNTIL' G-1 'DO'
'FOR' J:=I+1 'STEP' 1 'UNTIL' G 'DO'
        IN(I, J, L):=0;
NMAT:=READ; 'COMMENT' NUMBER OF MATERIALS;
'FOR' K:=1 'STEP' 1 'UNTIL' NMAT 'DO'
'BEGIN'
        ND:=READ; 'COMMENT' NUMBER DENSITY;
        'FOR' I:=1 'STEP' 1 'UNTIL' G 'DO'

'BEGIN'
        MU(I, L):=READ; 'COMMENT' MEAN SCATTERING COSINE;
        NU(I):=READ; 'COMMENT' NEUTRONS PER FISSIION;
        SF(I):=READ; 'COMMENT' MICROSCOPIC FISSIION;
        STR(I):=READ; 'COMMENT' MICROSCOPIC TRANSPORT;
        SEL(I):=READ; 'COMMENT' MICROSCOPIC ELASTIC;
        SCAP(I):=READ; 'COMMENT' MICROSCOPIC CAPTURE;
        SINT(I):=READ; 'COMMENT' MICROSCOPIC INFLASTIC TOTAL;

```

```

      'FOR' J:=1 'STEP' 1 'UNTIL' G 'DO'
      PCI,JJ:=RFAD; 'COMMENT' INELASTIC PROBABILITIES;
    'END';

```

```

'FOR' I:=1 'STEP' 1 'UNTIL' G 'DO'
  'BEGIN'

```

```

CAP(I,LJ):=CAP(I,LJ)+SCAP(IJ)*ND;
AA:=(STR(IJ)-SINT(IJ)-SCAP(IJ)-SFIS(IJ))*ND;
      BB:=AA/(1-MUC(I,LJ));
TR(I,LJ):=TR(I,LJ)+AA;
SC(I,LJ):=SC(I,LJ)+BB;
MSC(I,LJ):=MSC(I,LJ)+BB*MUC(I,LJ);
      AA:=SFIS(IJ)*ND;
FIS(I,LJ):=FIS(I,LJ)+AA;
NUF(I,LJ):=NUF(I,LJ)+AA*NUC(IJ);
FL(I,LJ):=FL(I,LJ)+SFL(IJ)*ND;
REM(I,LJ):=REM(I,LJ)+SINT(IJ)*ND*(1-PCI,IJ);
  'END';

```

```

      'FOR' I:=1 'STEP' 1 'UNTIL' G-1 'DO'
      'FOR' J:=I+1 'STEP' 1 'UNTIL' G 'DO'
      INCI,J,LJ:=INCI,J,LJ+SINT(IJ)*ND*PCI,JJ;
    'END';

```

```

'FOR' I:=1 'STEP' 1 'UNTIL' G 'DO'
  'BEGIN'
  REM(I,LJ):=REM(I,LJ)+FL(I,LJ)+CAP(I,LJ)+FIS(I,LJ);
      MUC(I,LJ):=MSC(I,LJ)/SC(I,LJ);
  Y:=REM(I,LJ)/SC(I,LJ);
  W:=0.21;
  AA:=0.9;

```

```

'FOR' W:=W+0.05 'WHILE' AA 'LE' 1 'DO'
  'BEGIN'
  Z:=SQRT(Y/W);
  AA:=EXP(2*Z*(1+3*W*MUC(I,LJ)/(1+3*W*MUC(I,LJ)*(1+Y)))*(1+Y-Z)/(1+Y+Z));
  BB:=W-0.06;
  'END';

```

```

W:=BB;
AA:=0.9;

```

```

'FOR' W:=W+0.01 'WHILE' AA 'LE' 1 'DO'
  'BEGIN'
  Z:=SQRT(Y/W);
  AA:=EXP(2*Z*(1+3*W*MUC(I,LJ)/(1+3*W*MUC(I,LJ)*(1+Y)))*(1+Y-Z)/(1+Y+Z));
  BB:=W-0.011;
  'END';

```

```

W:=BB;
AA:=0.9;

```

```
'FOR' V:=V+0.001 'WHILE' AA 'LE' 1 'DO'
'BEGIN'
Z:=SQRT(Y/V);
AA:=EXP(2*Z*(1+3*U*MU(I,LJ))/(1+3*U*MU(I,LJ)*(1+Y)))*(1+Y-Z)/(1+Y+Z);
RD:=V-0.001;
'END';
```

```
DI(LJ):=RB/SC(I,LJ);
'END';
```

```
'FOR' I:=1 'STEP' 1 'UNTIL' G 'DO'
'BEGIN'
NEWLINE(1);
PRINT(I,2,0);
PRINT(MU(I,LJ),1,6);
PRINT(FIS(I,LJ),1,6);
PRINT(TSI(I,LJ),1,6);
PRINT(EL(I,LJ),1,6);
PRINT(REM(I,LJ),1,6);
PRINT(SC(I,LJ),1,6);
PRINT(MU(I,LJ),2,3);
PRINT(DI(I,LJ),1,6);
PRINT((2.13*DI(I,LJ)),1,6);
'END';
```

```
NEWLINE(1);
'FOR' I:=1 'STEP' 1 'UNTIL' G-1 'DO'

'FOR' J:=I+1 'STEP' 1 'UNTIL' G 'DO'
'BEGIN'
PRINT(IN(I,J,LJ),1,6);
NEWLINE(1);
'END';
'END';
```

```
C:=READ; 'COMMENT' SLAB 0, CYLINDER 1, SPHERE 2;
NEWLINE(2);
SPACE(30);
WRITETEXT(('C='));
PRINT(C,2,0);
SCN:=READ; 'COMMENT' GR1 FLUX 0=CALC 1=READ 2=EXP REM CALC;
NEWLINE(1);
SPACE(30);
WRITETEXT(('SOURCE='));
PRINT(SCN,2,0);
'IF' SCN=0 'THEN'
  C:=READ;
'IF' SCN=2 'THEN'
'BEGIN'
C:=READ;
AA:=READ; 'COMMENT' GR1 EXPONENTIAL REMOVAL CROSS SECTION;
CC:=READ; 'COMMENT' GR1 EXPONENTIAL REMOVAL CROSS SECTION;
'END';
```

```

NEXT:
M:=READ; 'COMMENT' INNER BOUNDARY AT MDR;
'IF' M<0 'THEN' 'GOTO' LAST;
N1:=READ; 'COMMENT' OUTER BOUNDARY AT N1DR;
'IF' N1 < 0 'THEN' 'GOTO' FIN;
N2:=READ; 'COMMENT' OUTER BOUNDARY AT N2DR;

'BEGIN'
'REAL' 'ARRAY' F[1:G,M:N2],A,B[M-1:N2],SCE1[M:N1],SCE2[N1:N2];
NEWLINE(4);
SPACE(40);
WRITE TEXT('('THICKNESS%=')');
PRINT((N2-M)*DR,3,0);
WRITE TEXT('('CM)');
NN:=((N2-M+1)'/10)*10+E-1;
SELECT OUTPUT (0);
NEWLINE(3);
  I:=1;
'IF' SCN=1 'THEN'
'BEGIN'
  'FOR' J:=M 'STEP' 1 'UNTIL' N2 'DO' F[1,J]:=READ;
  I:=2;
'END';

'IF' SCN=2 'THEN'
'BEGIN'
'FOR' J:=M 'STEP' 1 'UNTIL' N1-1 'DO'
'BEGIN'
'IF' C=0 'THEN' F[1,J]:=0*EXP(-AA*DR*(J-M));
'IF' C=1 'THEN' F[1,J]:=0*EXP(-AA*DR*(J-M))/(6.284*DR*J);
'IF' C=2 'THEN' F[1,J]:=0*EXP(-AA*DR*(J-M))/(12.568*DR*DR*J*J);
'END';

'FOR' J:=N1 'STEP' 1 'UNTIL' N2 'DO'
'BEGIN'
'IF' C=0 'THEN' F[1,J]:=0*EXP(-CC*DR*(J-M));
'IF' C=1 'THEN' F[1,J]:=C*EXP(-CC*DR*(J-M))/(6.284*DR*J);
'IF' C=2 'THEN' F[1,J]:=C*EXP(-AA*DR*(N1-M)-CC*DR*(J-N1))/
(12.568*DR*DR*J*J);
'END';
I:=2;
'END';

ITN:=1;
ITERATE:

'IF' I=1 'THEN'
'BEGIN'

```

```

ACM-1J:=1;
  'IF' C=0 'THEN' BCM-1J:=0*DR/D(I,1J);
  'IF' C=1 'THEN' BCM-1J:=0/(6.284*M*D(I,1J));
  'IF' C=2 'THEN' BCM-1J:=0/(12.568*DR*M*M*D(I,1J));
  'FOR' J:=M 'STEP' 1 'UNTIL' N1 'DO'
SCE1(J):=0;
'FOR' J:=N1 'STEP' 1 'UNTIL' N2 'DO'
SCE2(J):=0;
'END';

AGAIN:

'IF' I>1 'THEN'
'BEGIN'
ACM-1J:=1;
  BCM-1J:=0;
  'FOR' J:=M 'STEP' 1 'UNTIL' N1 'DO'
  'BEGIN'
SCE1(J):=EL(I-1,1J)*F(I-1,JJ);
  'FOR' K:=1 'STEP' 1 'UNTIL' I-1 'DO'
SCE1(J):=SCE1(J)+IN(K,I,1J)*F(K,JJ);
  'IF' FN=1 'AND' ITN >1 'THEN'
  'FOR' K:=1 'STEP' 1 'UNTIL' G 'DO'
SCE1(J):=SCE1(J)+X(I)*NUF(K,1J)*F(K,JJ);
  'END';

'FOR' J:=N1 'STEP' 1 'UNTIL' N2 'DO'
'BEGIN'
SCE2(J):=EL(I-1,2J)*F(I-1,JJ);
  'FOR' K:=1 'STEP' 1 'UNTIL' I-1 'DO'
SCE2(J):=SCE2(J)+IN(K,I,2J)*F(K,JJ);
  'IF' FN=1 'AND' ITN >1 'THEN'
SCE2(J):=SCE2(J)+X(I)*NUF(K,2J)*F(K,JJ);
'END';
'END';

  'FOR' J:=M 'STEP' 1 'UNTIL' N1-1 'DO'
  'BEGIN'
A(J):=(2*J+C)/(2*J*(2+REM(I,1J)*DR*DR/D(I,1J))-(2*J-C)*A(J-1));
B(J):=A(J)*((2*J-C)*B(J-1)+2*J*SCE1(J)*DR*DR/D(I,1J))/(2*J+C);
'END';

A(N1):=(2*N1+C)/(D(I,1J)/(2*D(I,2J))*(2+REM(I,1J)*DR*DR/D(I,1J))*(2*N1-C)+
1/2*(2+REM(I,2J)*DR*DR/D(I,2J))*(2*N1+C)-(2*N1-C)*D(I,1J)/D(I,2J)*A(N1-1));
B(N1):=A(N1)*(SCE1(N1)/(2*D(I,2J))*DR*DR*(2*N1-C)+SCE2(N1)/(2*D(I,2J))*
(2*N1+C)*DR*DR+B(N1-1)*D(I,1J)/D(I,2J)*(2*N1-C))/(2*N1+C);
'FOR' J:=N1+1 'STEP' 1 'UNTIL' N2 'DO'
'BEGIN'
A(J):=(2*J+C)/(2*J*(2+REM(I,2J)*DR*DR/D(I,2J))-(2*J-C)*A(J-1));
B(J):=A(J)*((2*J-C)*B(J-1)+2*J*SCE2(J)*DR*DR/D(I,2J))/(2*J+C);
'END';

```

```

F[I,N2]:=B[N2]/(1+A[N2]*(DR/(2.13*B[I,2])-1));
'FOR' K:=N2-1 'STEP'-1 'UNTIL' M 'DO'
  F[I,K]:=A[K]*F[I,K+1]+B[K];
I:=I+1;
'IF' I 'LE' G 'THEN' 'GOTO' AGAIN;
ITN:=ITN+1;

'IF' ITN 'LE' NSTOP 'THEN'
'BEGIN'
  'IF' SCN=0 'THEN' I:=1;
  'IF' SCN>0 'THEN' I:=2;
  'GOTO' ITERATE;
'END';

'FOR' I:=1 'STEP' 1 'UNTIL' G 'DO'
'BEGIN'
NEWLINE(2);
WRITETEXT('('GROUP=')');
PRINT(I,2,0);
NEWLINE(1);
NM:=((N2-M+1)'/10)*10+M-1;

'FOR' J:=M 'STEP' 10 'UNTIL' NN 'DO'
'BEGIN'
  'FOR' K:=J 'STEP' 1 'UNTIL' J+9 'DO'
    PRINT(F[I,K],0,3);
    NEWLINE(1);
'END';

J:=NN;
'FOR' J:=J+1 'WHILE' J 'LE' N2 'DO'
PRINT(F[I,J],0,3);
NEWLINE(1);
WRITETEXT('('CURRENT%AT%OUTER%BOUNDARY=')');
'IF' SCN=2 'AND' I=1 'THEN'
PRINT((F[I,N2])/(F[B1]-E[B2]),0,3) 'ELSE'
PRINT((F[I,N2])/(2.13*(E[B1]-F[B1+1])),0,3);
'END';
'END';
'GOTO' NEXT;
FIN:
LAST:
'END';
'END';
****

```

10.47.05←

TIMED OUT 10.47.05

APPENDIX 3

PROGRAM FASTNSPEC: TRANSFORMATION OF PULSE AMPLITUDE DISTRIBUTION INTO  
NEUTRON ENERGY DISTRIBUTION BY DIFFERENTIAL METHOD

```

'BEGIN'
  'COMMENT' : SPP0709, NEUTSPEC, MEGAHID R., TRANSFORMATION OF PULSE
  AMPLITUDE DISTRIBUTION INTO NEUTRON ENERGY DISTRIBUTION,
  DIFFERENTIAL METHOD;
  'INTEGER' I, J, K, L, M, JJ, LL;
  'INTEGER' MIN, MAX;
  'REAL' G, SS, O, F, CM, AR;
  'INTEGER' LOG;
  'INTEGER' J1, J2;
  'INTEGER' IROW;
  'REAL' 'ARRAY' NEU[1:4];
  'REAL' 'ARRAY' NI[1:1];
  'REAL' FLOT;
  'REAL' EMAX, DV, DL, DLL;
  'REAL' 'ARRAY' EPS[0:150], SCF[0:30];
  'PROCEDURE' OPENPLOT;
  'EXTERNAL';

  'PROCEDURE' CLOSEPLOT;
  'EXTERNAL';

  'PROCEDURE' HGLOT(X, Y, A, B);
  'REAL' X, Y;
  'INTEGER' A, B;
  'EXTERNAL';

  'PROCEDURE' HGPSCALE(X, N, S, XMIN, DX, K);
  'VALUE' N, S, XMIN, DX, K;
  'ARRAY' X;
  'REAL' S, XMIN, DX;
  'INTEGER' N, K;
  'EXTERNAL';

  'PROCEDURE' HGPAXISV(X, Y, BCD, N, S, THETA, XMIN, DX, GAP, NH);
  'VALUE' X, Y, N, S, THETA, XMIN, DX, GAP, NH;
  'INTEGER' N, NH;
  'ARRAY' BCD;
  'REAL' X, Y, S, THETA, XMIN, DX, GAP;
  'EXTERNAL';

  'PROCEDURE' STRARR(A, N, S);
  'ARRAY' A;
  'INTEGER' N;
  'STRING' S;
  'EXTERNAL';

  'PROCEDURE' HGPLOGAXIS(X, Y, BCD, NC, S, THETA, MIN, MAX);
  'REAL' X, Y, S, THETA;
  'INTEGER' NC, MIN, MAX;
  'ARRAY' BCD;
  'EXTERNAL';

```

```

'PROCEDURE' HGPSYMBL(X,Y,HT,BCD,TH,N);
'VALUE' X,Y,HT,TH,N;
'ARRAY' BCD;
'REAL' X,Y,HT,TH;
'INTEGER' N;
'EXTERNAL';

'PROCEDURE' HGPNUMBER(X,Y,HT,FLOT,THETA,I,J,K);
'VALUE' X,Y,HT,FLOT,THETA,I,J,K;
'REAL' X,Y,HT,FLOT,THETA;
'INTEGER' I,J,K;
'EXTERNAL';

'PROCEDURE' PLOTSCROSS(X,Y,SIZE);
'REAL' X,Y,SIZE;
'BEGIN'
  'REAL' S;
  S:=SIZE/2.0;

  HGPLOT(X,Y,3,0);

  HGPLOT(X+S,Y,2,0);

  HGPLOT(X-S,Y,1,0);

  HGPLOT(X,Y,1,0);

  HGPLOT(X,Y+S,1,0);

  HGPLOT(X,Y-S,1,0);

  HGPLOT(X,Y,1,0);

'END';

IROW:=0;
J1:=20;
J2:=4;
LOG:=LN(10);
OPENPLOT;
HGPLOT(-5.0,10.0,0,4);
STRARR (NEU,J1,('NEUTRON%ENERGY%(MEV)'));
  STRARR(N,J2,('N(E)'));

EMAX:=READ; 'COMMENT' MAXIMUM ELECTRON ENERGY FOR CALIBRATION;
I:=READ; 'COMMENT' INITIAL CHANNEL NUMBER OF INTEREST;
J:=READ; 'COMMENT' FINAL CHANNEL NUMBER OF INTEREST;
G:=READ; 'COMMENT' GEOMETRY FACTOR;
Q:=READ; 'COMMENT' SOURCE STRENGTH;
AR:=READ; 'COMMENT' AREA OF THE DETECTOR;
  'FOR' L:=0 'STEP' 1 'UNTIL' 150 'DO'
  EPS[L]:=READ; 'COMMENT' NEUTRON DETECTION EFFICIENCY;
  'FOR' LL:=0 'STEP' 1 'UNTIL' 30 'DO'
  SCFILL]:=READ; 'COMMENT' SHAPE CORRECTION FACTOR;

```

NEXT:

```

FLOT :=READ; 'COMMENT' NUMBER OF EXPERIMENT;
'IF' FLOT <0 'THEN' 'GOTO' FINAL;
K:=READ; 'COMMENT' CHANNEL NUMBER AT HALF PEAK OF EMAX;
CM:=READ; 'COMMENT' ALPHA PARTICLE COUNTS BY THE MONITER;

'BEGIN'
'REAL' 'ARRAY' COUNT, C, EE, EP, DPDE, A, EFF, DDVA, NF, NFC, NFA, CA, NFA2,
CB, EFFN, B, CMULT[I:J];
DV:=EMAX/K;
SS:=G*CM;
F:=Q/SS;

'FOR' M:=I 'STEP' 1 'UNTIL' J 'DO'
'BEGIN'
EE[M]:=M*DV;

'IF' EE[M] 'LE' 1.85 'THEN'
EP[M]:=3.48*(EE[M]^0.667)
'ELSE'
EP[M]:=1.78*(EE[M]+1.1);

'IF' EP[M] 'LE' 5.25 'THEN'
DPDE[M]:=0.245*EP[M]^0.5;
'IF' EP[M] 'GE' 5.25 'THEN'
DPDE[M]:=0.564;
'END';

'FOR' M:=I 'STEP' 1 'UNTIL' J 'DO'
'BEGIN'
L:=ENTIER(EP[M]*10);
'IF' L 'GT' 149 'THEN'
L:=149;
DL:=EP[M]*10-L;
EFF[M]:=EPS[L]*(1-DL)+EPS[L+1]*DL;
'END';

'FOR' M:=I 'STEP' 1 'UNTIL' J 'DO'
'BEGIN'
LL:=ENTIER(EP[M]*2);
'IF' LL 'GT' 29 'THEN'
LL:=29;
DLL:=EP[M]*2-LL;
B[M]:=SCF[LL]*(1-DLL)+SCF[LL+1]*DLL;
'END';

'BEGIN'
'FOR' M:=I 'DO'
EFFN[M]:=EFF[M];

```

```

      'FOR' M:=I+1 'DO'
EFFN[M]:=0.5*EFF[M]+0.25*(EFF[M-1]+EFF[M+1]);
      'FOR' M:=I+2 'STEP' 1 'UNTIL' J-2 'DO'
EFFN[M]:=0.312*EFF[M]+0.229*(EFF[M-1]+EFF[M+1])
      +0.115*(EFF[M-2]+EFF[M+2]);
      'FOR' M:=J-1 'DO'
EFFN[M]:=0.5*EFF[M]+0.25*(EFF[M-1]+EFF[M+1]);
'FOR' M:=J 'DO'
EFFN[M]:=EFF[M];
'END';

```

```

      'FOR' M:=I 'STEP' 1 'UNTIL' J 'DO'
'BEGIN'
CMULT[M]:=READ; 'COMMENT' NUMBER OF COUNTS AT CERTAIN
                CHANNEL NUMBER;
'END';

```

```

'BEGIN'
'FOR' M:=I 'STEP' 1 'UNTIL' 320 'DO'
COUNT[M]:=CMULT[M]*31.8*M*(-0.5915);
'FOR' M:=320 'STEP' 1 'UNTIL' J 'DO'
COUNT[M]:=CMULT[M];
'END';

```

```

'BEGIN'
      'FOR' M:=I 'DO'
      C[M]:=COUNT[M];
'FOR' M:=I+1 'STEP' 1 'UNTIL' J-1 'DO'
      C[M]:=0.5*COUNT[M]+0.25*(COUNT[M-1]+COUNT[M+1]);
'FOR' M:=J 'DO'
      C[M]:=COUNT[M];
'END';

```

```

'BEGIN'
'FOR' M:=I 'DO'
CA[M]:=C[M];
'FOR' M:=I+1 'DO'
CA[M] :=0.5*C[M]+0.25*(C[M-1]+C[M+1]);
'FOR' M:=I+2 'STEP' 1 'UNTIL' J-2 'DO'
CA[M]:=0.312*C[M]+0.229*(C[M-1]+C[M+1])
      +0.115*(C[M-2]+C[M+2]);
'FOR' M:=J-1 'DO'
CA[M] :=0.5*C[M]+0.25*(C[M-1]+C[M+1]);
'FOR' M:=J 'DO'
CA[M]:=C[M];
'END';

```

```

'BEGIN'
'FOR' M:=I 'DO'
CB[M]:=CA[M];

```

```

'FOR' M:=I+1,I+2 'DO'
CB[M]:=0.5*CA[M]+0.25*(CA[M-1]+CA[M+1]);
'FOR' M:=I+3 'STEP' 1 'UNTIL' J-3 'DO'
CB[M]:=0.236*CA[M]+0.198*(CA[M-1]+CA[M+1])
      +0.117*(CA[M-2]+CA[M+2])+0.067*(CA[M-3]+CA[M+3]);
'FOR' M:=J-2,J-1 'DO'
CB[M]:=0.5*CA[M]+0.25*(CA[M-1]+CA[M+1]);
      'FOR' M:=J 'DO'
CB[M]:=CA[M];
'END';

```

```

      'FOR' M:=I 'STEP' 1 'UNTIL' J 'DO'
'BEGIN'
A[M] :=CB[M]*DPDE[M];
'END';

```

```

      'FOR' M:=I,I+1 'DO'
DDVA[M]:=(-11*A[M]+3*A[M+1]+7*A[M+2]+A[M+3])/(20*DV);

```

```

      'FOR' M:=I+2 'STEP' 1 'UNTIL' J-2 'DO'
DDVA[M]:=(2*A[M-2]+A[M-1]-A[M+1]-2*A[M+2])/(10*DV);

```

```

      'FOR' M:=J-1,J 'DO'
DDVA[M]:=(-21*A[M]+13*A[M-1]+17*A[M-2]-9*A[M-3])/(20*DV);

```

```

      'FOR' M:=I 'STEP' 1 'UNTIL' J 'DO'
'BEGIN'
NF[M]:=((EP[M]/EFFN[M])*DDVA[M]*DPDE[M]);
      NFC[M]:=NF[M]*F*(1/AR)*(1/B[M]);
'END';

```

```

NEWLINE(4);
SPACE (20);
WRITETEXT ((' EXPERIMENT%NUMBER%='));
PRINT(FLOT,3,0);
NEWLINE (2);
SPACE (20);
WRITETEXT (('K%='));
PRINT (K,3,0);
NEWLINE (2);
SPACE (20);
WRITETEXT (('EMAX%='));
PRINT(EMAX,2,3);
WRITETEXT (('MEV'));
NEWLINE (2);
SPACE (20);
WRITETEXT (('CHANNEL%WIDTH%='));
PRINT(DV,1,3);
WRITETEXT (('MEV%P%CHANNEL'));
NEWLINE (2);
SPACE (20);
WRITETEXT (('Q%='));
PRINT (Q,0,3);

```

```

NEWLINE (2);
SPACE (20);
WRITETEXT ('('GEOMETRY%%FACTOR%=')');
PRINT (G,0,4);
NEWLINE (2);
SPACE (20);
WRITETEXT ('('ALPHA%PARTICLE%COUNTS%BY MONITOR%=')');
PRINT (CM,0,4);
NEWLINE (2);
SPACE (20);
WRITETEXT ('('CORRECTION%FACTOR%=')');
PRINT (F,2,4);
NEWLINE(4);
SPACE(2);
WRITETEXT('('M')');
SPACE(5);
WRITETEXT('('COR')');
SPACE(5);
WRITETEXT('('C[M]')');
SPACE(3);
WRITETEXT('('CA[M]')');
SPACE(3);
WRITETEXT('('CB[M]')');
SPACE(3);
WRITETEXT('('EE[M]')');
SPACE(2);
WRITETEXT ('('DPDE[M]')');
SPACE(3);
WRITETEXT ('('A[M]')');
SPACE(3);
WRITETEXT ('('DDVA[M]')');
SPACE(2);
WRITETEXT ('('EFF[M]')');
SPACE(2);
WRITETEXT ('('EFFN[M]')');
SPACE(2);
WRITETEXT ('('EN[M]')');
SPACE(2);
WRITETEXT ('('NF[M]')');
SPACE(2);
WRITETEXT ('('NFC[M]')');
SPACE(2);
WRITETEXT ('('NFA[M]')');
NEWLINE(2);

```

```

JJ:=0;
'FOR' M:=I+1 'STEP' 3 'UNTIL' J-1 'DO'
'BEGIN'
NFA[M]:=(NFC[M-1]+NFC[M]+NFC[M+1])/3;
'IF' NFA[M] 'GT' 0.0 'THEN'
'BEGIN'
JJ:=JJ+1;
NFA2[JJ]:=NFA[M];
'END';
'END';

```

```

HGLOGSCALE(NFA2, JJ, 6.0, MIN, MAX, 1);
HGLOGAXIS (0.0, 0.0, N, J2, 6.0, 90.0, MIN, MAX);
HGPAxisV (0.0, 0.0, NEU, -J1, 9.0, 0.0, 0.0, 1.0, 0.6, 2);
HGPNUMBER(2.5, -1.0, 0.2, FLOT, 0.0, 0, 3, 0);
JJ:=0;
'FOR' M:=1+1 'STEP' 3 'UNTIL' J-1 'DO'
'BEGIN'
NEWLINE(1);
PRINT(M, 3, 0);
PRINT(COUNT[M], 5, 0);
PRINT(C[M], 5, 0);
PRINT (CA[M], 5, 0);
PRINT (CB[M], 5, 0);
PRINT(EE[M], 1, 2);
PRINT(DPDE[M], 1, 3);
PRINT (A[M], 4, 1);
PRINT(DDVA[M], 5, 1);
PRINT(EFF[M], 1, 4);
PRINT(EFFN[M], 1, 4);
PRINT(EP[M], 2, 2);
PRINT(NF[M], 5, 0);
PRINT (NFC[M], 5, 0);
PRINT (NFA[M], 5, 0);
'IF' NFA[M] 'GT' 0 'THEN'
'BEGIN'
JJ:=JJ+1;
PLOT CROSS(EP[M]*0.6, NFA2[JJ], 0.1);
'END';
'END';
'END';
HG PLOT(0.0, 0.0, 3, 0);
'IF' IROW=0 'THEN'
'BEGIN'
IROW:=1;
HG PLOT(0.0, 12.0, 0, 4);
'END' 'ELSE'
'BEGIN'
IROW:=0;
HG PLOT(-15.0, -12.0, 0, 4);
'END';
'GOTO' NEXT;
FINAL:
CLOSEPLOT;

```

REFERENCES

1. H. Goldstein.  
"Principles of Reactor Shielding",  
Addison-Wesley Publishing Co. (1959).
2. B.T. Price et al.  
"Radiation Shielding",  
Pergamon Press, (1957).
3. A.P. Beselkin et al.  
"Spectra of Fast Reactor Neutrons After Passing Through  
Graphite, Lead and Iron".  
Translated from Atomnaya Energya, Vol. 16, No. 1. (1964).
4. G.A. Vasilev et al.  
"Attenuation of Reactor Radiations by Serpentine Concrete".  
J. Nucl. Energy. Parts A & B. Vol. 20, pp 390-397, (1966).
5. V.A. Dulin et al.  
"Neutron Angular and Energy Distribution at the Boundary  
of Two Media".  
Soviet Atomic Energy Vol.17, No.6, (1964).
6. I.V. Goryachev et al.  
"Angular Distribution of Fast Neutrons Outside Iron  
Shielding".  
Soviet Atomic Energy, Vol. 20, No. 6, (1966).

7. Proceedings of the Conference on The Physics Problems of Reactor Shielding, held at The Atomic Energy Research Establishment, Harwell, Sept. 1967. Vol. 1,2,3,4 and 5.
8. "Engineering Compendium on Radiation Shielding". International Atomic Energy Agency, Vienna. Vol. 1, (1968).
9. R.J. Howerton.  
"Semi-Empirical Neutron Cross Sections: 0.5 to 15 MeV"  
Part II, UCRL-5531, (1958).
10. K. Shure.  
"P3 Multigroup Calculations of Neutron Attenuation".  
Nucl. Sci. and Eng. Vol. 19, 310, (1964).
11. Neutron Attenuation.  
Reactor Handbook, Vol. III, Part B, Shielding (1962).
12. S. Glasstone.  
"Principles of Nuclear Reactor Engineering".  
MacMillan & Co.Ltd., London, (1956).
13. J.R. Lamarsh.  
"Introduction to Nuclear Reactor Theory".  
Addison-Wesley, (1966).
14. S. Glasstone and M.C. Edlund.  
"The Elements of Nuclear Reactor Theory".  
MacMillan & Co.Ltd., London, (1952).

15. J.H. Ferziger et al.  
"The Theory of Neutron Slowing Down in Nuclear Reactors".  
Pergamon Press, (1966).
16. D.J. Hughes.  
"Neutron Cross-Sections."  
Pergamon Press, (1957).
17. S.J. Bame et al.  
 ${}^6\text{Li}(n,t){}^4\text{He}$  Reaction at Intermediate Energies".  
Phys. Rev., Vol. 114, No. 6, (1959).
18. R.B. Murry et al.  
"Cross Section for  ${}^6\text{Li}(n,\alpha){}^3\text{He}$  Reaction for  
 $1.2 \leq E_n \leq 8.0$  MeV".  
Phys. Rev. Letter. Vol. 3, No. 7, (1959).
19. J.B. Marion and J.L. Fowler.  
"Fast Neutron Physics, Part I."  
Interscience Publishers Inc. (1966).
20. W.J. Price.  
"Nuclear Radiation Detection."  
McGraw Hill Book Company, Second Ed. (1964).
21. W.D. Allen.  
"Neutron Detection".  
George Newnes Ltd., London, (1960).

22. F.D. Brooks.  
"Organic Scintillators".  
Prog. Nucl. Phys., Vol. 5, (1956).
23. R.B. Murray.  
"Use of  ${}^6\text{LiI(EU)}$  As a Scintillation Detector and  
Spectrometer for Fast Neutrons".  
Nucl. Instr. 2, (1958).
24. R. Batchelor et al.  
"The Interactions of Neutrons with  ${}^6\text{Li}$  and  ${}^7\text{Li}$   
Between 1.5 and 7.5 MeV".  
Nucl. Phys., 47, (1963).
25. R.B. Murray et al.  
"Scintillation Response of Activated Inorganic Crystals  
to Various Charged Particles".  
Phys. Rev. Vol. 122, No. 2, (1961).
26. J.R.P. Eaton et al.  
"The Response of  ${}^6\text{LiI(EU)}$  to Neutrons as a Function  
of Temperature".  
Proc. Phys. Soc. Vol. 83, (1964).
27. D.R. Johnson et al.  
"A Sensitive Spectrometer for Fast Neutrons Using  
 ${}^6\text{LiI(EU)}$ ".  
Nucl. Instr. and Meth. Vol. 75, (1969).

28. A.O. Hanson and J.L. McKibben.  
"A Neutron Detector Having Uniform Sensitivity  
From 10 KeV to 3 MeV".  
Phys. Rev. Vol. 72, (1947).
29. R. Batchelor et al.  
"Helium-3 Filled Proportional Counter for Neutron  
Spectroscopy".  
Rev. Sci. Instr., Vol. 26, No. 11, (1955).
30. T. Fuse et al.  
Neutron Spectroscopy with a  $^3\text{He}$  Proportional Counter".  
Nucl. Instr. and Meth., Vol. 74, (1969).
31. R.V. Babock et al.  
"Coated Semi-conductor is Tiny Neutron Detector".  
Nucleonics, Vol. 17, (1959).
32. K.G. McKay et al.  
"Electron Multiplication in Silicon and Germanium".  
Phys. Rev. Vol. 91, 1079, (1953).
33. F.D. Brooks.  
"A Scintillation Counter with Neutron to Gamma Ray  
Discriminator."  
Nucl. Instr. and Meth., Vol. 4, (1959).
34. V.V. Verbinski et al.  
"Radiation Measurements in Nuclear Power".  
Institute of Physics and Physical Society. Sept.(1966).

34. V.V. Verbinski et al.  
"Radiation Measurements in Nuclear Power".  
Institute of Physics and Physical Society. Sept. (1966).
35. T.A. Love et al.  
"Absolute Efficiency Measurements of NE-213 Organic  
Phosphors of Detecting 14.5 and 2.7 MeV Neutrons."  
Rev. Sci. Instr. Vol. 39, (1968).
36. T.G. Masterson.  
"Response of NE-218 to Fast Neutrons".  
Nucl. Instr. and Meth., Vol. 88, (1970).
37. M. Cambiaghi.  
"Fast Neutron Spectrometry with Identification of  
Recoil Protons".  
Nucl. Instr. and Meth. Vol. 82, (1970).
38. G.C. Bonazzola et al.  
"On the Measurement of Backward Scattering of  
14 MeV Neutrons".  
Nucl. Instr. and Meth. 87, (1970).
39. R.N. St. Onge et al.  
"A Simple High Resolution Pulse Shape Discriminator".  
Nucl. Instr. and Meth. Vol. 69, (1969).
40. H.J. Kellermann et al.  
"Neutron Detection Efficiency of Liquid Scintillator  
NE-214 in the MeV Range".  
Nucl. Instr. and Meth. Vol. 94, (1971).

41. S. Mubarakmand et al.  
"Neutron Detection Efficiency of an Organic Scintillator".  
Nucl. Instr. and Meth. Vol. 93, (1971).
42. M.E. Toms.  
"A Computer Analysis to Obtain Neutron Spectra From An  
Organic Scintillator."  
Nucl. Instr. and Meth. Vol. 92, (1971).
43. R.J. Schuttler.  
"Efficiency of Organic Scintillators for Fast Neutrons".  
ORNL-3888. July (1966).
44. R.B. Owen.  
"Pulse Shape Discrimination Identifies Particle Types".  
Nucleonics. Vol. 17, No. 9 (1959).
45. V.V. Verbinski et al.  
"Calibration of an Organic Scintillator for Neutron  
Spectrometry".  
Nucl. Instr. and Meth. Vol. 65, (1968).
46. M.E. Toms.  
"Stilbene and NE-213 Characteristics Related to Their  
Use for Neutron Spectroscopy".  
I.E.E.E. Trans. Nucl. Sci., NS17, 3, (1970).
47. T.K. Alexander et al.  
"An Amplitude-Insensitive System That Distinguishes  
Pulses of Different Shapes".  
Nucl. Instr. and Meth., Vol. 13, (1961).

48. Gy. Mathe et al.  
"Pulse Shape Discrimination Method for Particle Identification".  
Nucl. Instr. and Meth. Vol. 27, (1964).
49. G.W. McBeth et al.  
"A Simple Zero Crossing Pulse Shape Discrimination System".  
Nucl. Instr. and Meth. Vol. 93, (1971).
50. R.A. Winyard et al.  
"Pulse Shape Discrimination in Inorganic and Organic Scintillators".  
Nucl. Instr. and Meth. Vol. 95, (1971).
51. I.J. Taylor et al.  
"A High Speed Pulse Shape Discrimination".  
Nucl. Instr. and Meth., Vol. 88, (1970).
52. R.A. Tietsch et al.  
"A Zero Crossing Pulse Shape Discriminator For Space Application".  
I.E.E.E. Transaction on Nucl. Sci. Feb. (1967).
53. T.G. Miller.  
"Measurement of Pulse Shape Discrimination Parameters for Several Scintillators".  
Nucl. Instr. and Meth. Vol. 63, (1968).

54. M.L. Roush et al.  
"Pulse Shape Discrimination".  
Nucl. Instr. and Meth., Vol. 31, (1964).
55. G. Bellettini et al.  
"Determination of the Optimum Working Conditions of the  
Photomultiplier".  
Nucl. Instr. and Meth., Vol. 21, (1963).
56. G. Bellettini et al.  
"On the Voltage Distribution for Philips 56 and 58 AVP  
Photomultipliers".  
Nucl. Instr. and Meth. Vol. 27, (1964).
57. K.F. Flynn et al.  
"The Half-Height, At the Compton Edge of the Pulse  
Height Distribution".  
Nucl. Instr. and Meth., Vol. 27, (1964).
58. R. Batchelor et al.  
"The Response of Organic Scintillators to Fast Neutrons".  
Nucl. Instr. and Meth. Vol. 13, (1961).
59. Yu. Kazanski et al.  
English translation: "Soviet Atomic Energy".  
Atomnaya Energia, 20, 143, (1966).
60. J.R. Stehn et al.  
"Neutron Cross Sections".  
BNL-325, Second Edition, Vol. 1, May (1964).

61. D.L. Smith et al.  
"Measurement of the Response of Several Organic Scintillators to Electrons, Protons and Deuterons".  
Nucl. Instr. and Meth. Vol. 64, (1968).
62. W.W. Lindstrom et al.  
"Improved Computer Simulation of the Detection Process in NE-102 and NE-213 Scintillator for 0 to 4.8 MeV Neutrons".  
Nucl. Instr. and Meth., Vol. 98, (1972).
63. M.N. Thompson et al.  
"Neutron Spectra from Am- $\alpha$ -Be and Ra- $\alpha$ -Be Sources.  
Nucl. Instr. and Meth., Vol. 37, (1965).
64. A.D. Vijaya et al.  
"The Neutron Spectrum of Am- $\alpha$ -Be Neutron Sources".  
Nucl. Instr. and Meth. Vol.III, (1973).
65. R.B. Owen.  
I.R.E. Transactions on Nuclear Science.  
Vol. NS-5, (1958).
66. F.D. Brooks.  
"Organic Scintillators".  
Progress in Nuclear Physics, Vol. 5, pp.252, (1956).
67. V.A. Dulin et al.  
"Neutron Angular and Energy Distribution at the Boundary of Two Media".  
Soviet Atomic Energy. Vol. 17, No.6, (1964).

68. K.H. Maier et al.  
"Light Output of NE-213 for Protons".  
Nucl. Instr. and Meth. Vol. 59. (1968).
69. D. Kopsch et al.  
"Alpha-Proton Discrimination with NE-213 Liquid  
Scintillator Used for the Measurement of the  $(n, \alpha)$   
Reaction on  $^{12}\text{C}$ ".  
Nucl. Instr. and Meth. Vol. 54, (1967).
70. M. Forte et al.  
"Electronic Methods for Discriminating Shapes".  
Nuclear Electronics, 2. I.A.E.A., Vienna, (1962).
71. A. Huck et al.  
Nucl. Instr. and Meth., Vol. 59, (1968).
72. Technical Bulletin Societe Anonyme de Machines Electrostatiques,  
Grenoble, France, June, (1961).
73. A.H. Wapstra.  
"Isotropic Masses I. A. 34  
Physica 21, 367, (1955).
74. L. Blumberg et al.  
Atomic Energy Comm. Report. A.E.C.U. 3118, (1956).
75. J. Benveniste et al.  
"Information on the Neutrons Produced in the  $^3\text{He}(d,n)^4\text{He}$   
Reaction".  
U.C.R.L. 4266, (1964).

76. E.W. Saker et al.  
"Calculated Neutron Yield from Titanium Tritium Targets  
with Deuteron Bombardment".  
S.E.R.L. Technical Rept. No. M.61. Sept. (1958).
77. "Catalogue of Radioactive Products".  
The Radio-Chemical Centre, Amersham, England.  
p.p. 160, Oct., (1965).
78. J. Chadwick.  
The Radio-Chemical Centre, Amersham.  
Private Communication, Oct. (1968).
79. E.M. Gunnerson et al.  
"On the Efficiency of the Reaction  ${}^3\text{He}(d,n){}^4\text{He}$   
Titanium Tritide Bombarded with Deuterons".  
Nucl. Instr. and Meth., Vol. 8, (1960).
80. J. Benveniste et al.  
"The Problem of Measuring The Absolute Yield of  
14 MeV Neutrons by an Alpha Counter".  
U.C.R.L. 5619, (1959).
81. M.M. Wasson.  
"The Use of Stilbene with Decay Time Discrimination  
As a Fast Neutron Spectrometer".  
A.E.R.E. Rept. 4269, (1963).

82. H.W. Broek et al.  
"The Stilebene Scintillation Crystal as a Spectrometer  
for Continuous Fast Neutron Spectra".  
Rev. Sci. Instr. Vol. 31, 1063, (1960).
83. S. Yiftah et al.  
"Fast Reactor Cross Sections".  
Pergamon Press, New York. (1960).
84. S. Yiftah et al.  
"Nuclear Cross Sections for Fast Reactors".  
IAEC. Rept. IA-980, (1964).
85. L.P. Abagyan et al.  
"Group Constants for Nuclear Reactor Calculations".  
Phys. Energy Instr. U.S.S.R, (1962).  
Translated by Consultant Bureau, U.S.A. (1964).
86. B. Davison et al.  
"Neutron Transport Theory".  
Oxford University Press, (1957).
87. H. Clark.  
"Methods and Data for Reactor Shield Calculations  
Advances in Nuclear Science and Technology".  
Vol. 5. Chap. 4, (1969).
88. R.T. Carr et al.  
Gamma-ray Dosimetry with Organic Scintillators.  
Nucleonics. Vol. 11, 53, (1953).

89. L.S. Ornstein and Uhlenbeck.  
"Some Kinetic Problems Regarding the Motion of Neutrons  
through Paraffin".  
Physica. Vol. 4, 478, (1937).
90. E. Fermi.  
Ricerca Scientifica, Vol. 7. (2), (1936).
91. B.W. Roos et al.  
"Some Aspects of the Use of Digital Computers in  
Nuclear Reactor Design."  
Advances in Nuclear Science and Technology Vol.2.  
Chapt. 6, (1964).
92. G.I. Marchux (ed)  
"Numerical Methods for Reactor Calculation".  
Translated by Consultants Bureau, New York. (1959).
93. H. Greenspan et al. (ed).  
"Computing Methods in Reactor Physics."  
Gordon and Breach Science Publisher Inc.  
New York, (1968).
94. J.J. MacInerney.  
" A Solution of the Space-Energy Angle Dependent,  
Neutron Slowing-Down Problem".  
Nucl. Sci. and Eng. Vol. 22, 215, (1965).

95. C. Mark.  
"The Spherical Harmonics Methods, I - General Development of the Theory".  
Canadian Rept. CRT-340, Atomic Energy of Canada Ltd.,  
Chalk River Project. Nov. 30. (1944).
96. C. Mark.  
"The Spherical Harmonics Methods, II - Application to Problems with Plane and Spherical Symmetry."  
Canadian Rept. CRT-338, Atomic Energy of Canada Ltd.  
Chalk River Project. May. 31. (1945).
97. B. Davison.  
"Some Remarks on Application of the Spherical Harmonics Method in the Case of Complex Geometries".  
British Report. A.E.R.E. - T/R - 700 Great Britain  
Atomic Energy Research Establishment.
98. M.E. Mandl.  
"The Spherical Harmonics Method in Plane and Spherically Symmetric Geometry in Multi-Velocity Group Theory and its Application in the two Velocity-Group  $P_3$  - Approximation."  
British Rept. A.E.R.E. - T/R. 1295, Great Britain.  
Atomic Energy Research Establishment, Nov. (1953).
99. N. Tralli et al.  
"The  $P_3$  Approximation to the Transport Equation for Cylindrical Geometry."  
U.S.A.E.C. Rept. N40-3923, Walter Kidde.  
Nuclear Laboratories, Inc., May. 15, (1953).

100. B.G. Carlson.  
"Solution of The Transport Equation by the  $S_n$   
Approximations".  
LA-1599, (revised version, LA-189), (1953).
101. B.G. Carlson.  
"Numerical Solution of Transient and Steady State  
Neutron Transport Problems".  
LA-2260, (1959).
102. B.G. Carlson et al.  
"Solution of the Transport Equation by the  $S_n$  Method".  
Proc. Second. U.V. Inter. Conf. "Peaceful Uses of  
Atomic Energy, Geneva, 16. (1958).
103. G.C. Wick.  
Physics, 121, 702, (1973).
104. S. Chandrasekhar.  
Radiative Transfer.  
Oxford University Press, (1950).
105. R.T. Ackroyd et al.  
"Survey of Theoretical Calculation Methods".  
Karlshure Symposium on Criticality Control in Chemical  
and Metallurgical Plant. Published by the European  
Nuclear Energy Agency.

106. L.V. Spencer et al.  
"Penetration and Diffusion of X-ray Calculation of Spatial Distributions by Polynomial Expansion".  
Phys. Rev., Vol. 81, 464, (1951).
107. H. Goldstein et al.  
"Calculation of the Penetration of Gamma Rays."  
NYO-3075, (1954).
108. R.E. Marshak.  
"Theory of the Slowing Down of Neutrons by Elastic Collision with Atomic Nuclei".  
Rev. Mod. Phys. Vol. 19, 185, (1947).
109. P.R. Wallace et al.  
Canadian Report M.T., 12, (1943).
110. G. Goertzel et al.  
"Methods in Transport Problems".  
Progress in Nuclear Energy Series 1, Vol. 2.  
ed. by D.J. Hughes et al.  
New York. Pergamon Press (1958).
111. M.H. Kalos et al.  
"Reactor Problems".  
Nucleonics, Vol. 15, No. 5, 64, 1957.
112. K.T. Spinney.  
"Neutron Attenuation in Concrete".  
A.E.R.E. T/R. 2507, (1957).

113. A.F. Avery et al.  
"Methods of Calculations for Use in the Design of Shields for Power Reactors".  
A.E.R.E. - R. 3216, (1960).
114. K.D. Lathrop.  
"D.T.T. IV, A Fortran - IV Program for Solving the Multigroup Transport Equation with Anistropic Scattering".  
LA - 3373, (1963).
115. D.E. Bendall.  
"RASH-D, A Mercury Programme for Neutron Shielding Calculations".  
AEEW-M-261, (1962).
116. E.G. Peterson.  
"MAC, A Bulk Shileidng Code".  
HW-73381, (1962).
117. L. Hjarne.  
" A User Manual for the N.R.N. Shield Design Method".  
AE - 145, (1964).
118. R.V. Maghreblien et al.  
" Reactor Analysis".  
McGraw-Hill, New York. Ch.4., (1960).
119. A.M. Weinberg et al.  
"The Physical Theory of Neutron Chain Reactors".  
University of Chicago Press, Chicago, Ch.10., (1958).

120. J. Butler et al.  
"Removal - Diffusion Theory".  
Engineering Compendium on Radiation Shielding
121. A.F. Avery.  
"A Multigroup Method for Calculating Neutron Attenuation  
in Water".  
A.E.E.W. - R 125, (1962).
122. S.M. Kabir.  
"Measurements and Calculations of Spatial Distribution of  
Fast Neutron Spectra in Iron and Iron-Uranium Assemblies  
from a 14 MeV Source".  
A thesis submitted to the University of Aston in  
Birmingham, U.K., (1971).
123. R.D. Albert et al.  
"A Simplified Theory of Neutron Attenuation and its  
Application to Reactor Shield Design".  
U.S.A.E.C. Rept. W.A.P.D. - 15, (1950).
124. R.D. Chapman et al.  
"Effective Neutron Removal Cross Section for Shielding".  
U.S.A.E.C. Rept., A.E.C.D., 3978, (1955).
125. D.L. Broder et al.  
"Biological Shielding of Ships Reactors".  
Leningrad, Sudpromgiz, (1964).